Investigation on Molecular Self-Organisation in Peptide Systems: from Functional Assembly to Autonomous Replication

A Dissertation Submitted to the
Indian Institute of Technology Guwahati
As Partial Fulfillment for the Degree of

Doctor of Philosophy in Chemistry

Submitted by

Sukesh Shill

Roll No. 196122038

Department of Chemistry
Indian Institute of Technology Guwahati
Guwahati-781039, Assam, India

Dedicated

To

My family

INDIAN INSTITUTE OF TECHNOLOGY GUWAHATI

Department of Chemistry

STATEMENT

I do hereby declare that the matter embodied in this thesis entitled "**Investigation on Molecular Self-Organisation in Peptide Systems: from Functional Assembly to Autonomous Replication**" is the result of experiments carried out by me in the Department of Chemistry, Indian Institute of Technology Guwahati, India, under the supervision of Prof. Bhubaneswar Mandal.

In keeping with the general practice of reporting scientific observations, due acknowledgements have been made wherever the work described is based on the findings of other investigators.

Date: December, 2025
Place: IIT Guwahati

Sukesh Shill

Indian Institute of Technology Guwahati
Department of Chemistry
North Guwahati, Guwahati-781039, India
Phone: +91 (361) 258 2319 (O); Fax: +91 (361) 258 2349
e-mail: **bmandal@iitg.ac.in**

CERTIFICATE

This is to certify that **Mr. Sukesh Shill** (Roll No. 196122038) has been working under my supervision since July 2019 as a regular registered Ph.D. student. I am forwarding his thesis entitled "**Investigation on Molecular Self-Organisation in Peptide Systems: from Functional Assembly to Autonomous Replication**" to be submitted for the Ph.D. (Science) Degree of this Institute. I certify that he has fulfilled all the requirements according to the rules of this institute regarding the investigations embodied in his thesis, and this work has not been submitted elsewhere for a degree.

Date: December, 2025
Place: IIT Guwahati

Prof. Bhubaneswar Mandal
Thesis Supervisor
Department of Chemistry

Acknowledgements

The journey of the Ph.D. is not always a smooth one. However, along the way, I have encountered persons who helped to make this journey pleasurable. I would like to express sincere gratitude to those who directly or indirectly helped me throughout the Ph.D. journey and motivated me on the path to success.

First and foremost, I would like to express my sincere gratitude and thanks to my thesis supervisor, Prof. Bhubaneswar Mandal, for his invaluable guidance, encouragement, and inspiration throughout my Ph.D. program, which helped me to enhance my knowledge and inspired me to make the right decisions at crucial moments. I am also thankful to him for giving me the freedom to pursue my interests in his lab, and I find myself privileged to have worked under his kind guidance.

I would like to acknowledge my sincere gratitude to all my doctoral committee members, Prof. Chandan Mukherjee, Prof. Lal Mohan Kundu, and Dr. Sunanda Chatterjee, for their valuable advice and timely suggestions during my doctoral studies.

I am grateful to the Ministry of Human Resource and Development (MHRD), India, for financial support and to IIT Guwahati for all the facilities that were made available to me. I want to thank the Department of Chemistry, the Central Instrument Facility (CIF) and the North East Centre for Biological Sciences and Healthcare Engineering (NECBH), and IIT Guwahati for providing the instrumental facilities.

Further, I would like to thank all my past and present group members for their friendship and assistance. I especially want to thank my seniors, Dr. Sujan Kalita, Dr. Sourav Kalita, Dr. Tapasi Kalita, Dr. Gobinda Dolai, Dr. Sandip Mondal, Dr. Sayanta Roy and Mr. Altaf for their assistance and willing to discuss problems and ideas with me. I also thank my juniors for their help during my Ph.D. tenure. I thank the other lab mates, Avisek, Asmita, Baite and Tapas for their cooperation in my research work, without which it would not be easy to complete the Ph.D. thesis. I also want to thank all my M.Sc. and B.Tech juniors (especially Tuhin) for their cooperation in my research work. It was great to work and spend time with these lovely human beings, and I will always carry the memories of their jokes, laughter, and humour throughout my life. I am lucky to get such a type of research environment and lab mates.

I thank all of my Ph.D. batchmates (July 2019), the other research scholars from my senior and junior batches in the chemistry department, and all my IITG friends who have shared their thoughts and views with me. I also specially thank Raktim and Avishek for their significant help in Ph.D. thesis work and mental support. I also thank all my M.Sc. and Ph.D. friends at IIT Guwahati with whom I had a good time and shared many joyful moments during festivals, picnics and sports.

I would like to express my special gratitude to my school and college teachers, who enlightened my educational pursuits. I would also like to thank all my childhood friends, friends who supported me throughout my educational journey, from school to higher studies, for supporting me and providing such wonderful memories.

Finally, I want to thank all of my family members. Without their selfless love, care, support, and encouragement, the journey would not have been possible. Their contributions have been invaluable. I wish to express my sincere gratitude to my parents, wife, my little daughter, sister and other family members for their endless moral support and motivation, especially at difficult times. My Ph.D. endeavours would not have been completed without their blessings. They are the main soul and inspiration for every step that I achieve in my life.

Sukesh Shill

List of abbreviations

Aβ	Amyloid beta
Ac	Acetyl group
ACN	Acetonitrile
Ac_2O	Acetic anhydride
AD	Alzheimer's disease
AFM	Atomic force microscopy
AU	Arbitrary unit
BET	Brunauer-Emmett-Teller
BnBr	Benzyl bromide
Boc	*tert*-Butyloxycarbonyl
BOP	Benzotriazol-1-yloxy-tris(dimethylamino) phosphoniumhexafluorophosphate
CD	Circular dichroism
CHCA	α-Cyano-hydroxy-cinnamic acid
CP	Cyclic peptide
DCM	Dichloromethane
DIPEA	Diisopropylethylamine
DLS	Dynamic light scattering
DMF	N, N-dimethyl formamide
DMSO	Dimethyl sulfoxide
ESI-MS	Electrospray Ionization Mass Spectrometry
EtOAc	Ethyl acetate
Et_2O	Diethyl ether
Equiv	Equivalent

Fmoc	9-Fluorenylmethoxycarbonyl
FT-IR	Fourier Transformation Infra-red Spectroscopy
FESEM	Field Emission Scanning Electron Microscopy
FETEM	Field Emission Transmission Electron Microscopy
HCl	Hydrochloric acid
HFIP	1,1,1,3,3,3-hexafluoro-iso-propanol
HPLC	High-performance liquid chromatography
LiOH	Lithium hydroxide
LP	Linear peptide
MALDI	Matrix-assisted laser desorption ionization
MeOH	Methanol
MBHA	Methyl-benzhydryl-amine
Me	Methyl
mL	milliliter
mM	millimolar
µL	micro liter
µM	micro molar
MW	Molecular weight
nm	Nanometre
NMI	*N*-Methyl imidazole
NMR	Nuclear Magnetic Resonance
OMe	Methyl ester
o-NosylOXY	Ethyl 2-cyano-2-(2-nitrophenylsulfonyloxyimino)
OtBu	*tert*-butyl ester
Oxyma	Ethyl 2-cyano-2-(hydroxyimino)acetate
PBS	Phosphate buffer solution

RB	Round-bottom flask
RP	Reverse Phase
SPPS	Solid phase peptide synthesis
tBu	*tert*-Butyl
TGA	Thermogravimetric analysis
TFA	Trifluoroacetic acid
ThT	Thioflavin T
TLC	Thin-layer chromatography
R_t	Retention time
UV	Ultraviolet

Abbreviations for intensities of ^{1}H-NMR signals

s	singlet	q	quartet
d	doublet	m	multiplate
dd	doublet of doublet	Hz	Hertz
t	triplet	MHz	Mega-Hertz

List of natural amino acids

Amino acids	**Abbreviation**	
	Three letter code	***One letter code***
Alanine	Ala	A
Arginine	Arg	R
Asparagine	Asn	N
Aspartic acid	Asp	D
Cysteine	Cys	C
Glutamic acid	Glu	E
Glutamine	Gln	Q
Glycine	Gly	G
Histidine	His	H
Isoleucine	Ile	I
Leucine	Leu	L
Lysine	Lys	K
Methionine	Met	M
Phenylalanine	Phe	F
Proline	Pro	P
Serine	Ser	S
Threonine	Thr	T
Tryptophan	Trp	W
Tyrosine	Tyr	Y
Valine	Val	V

Abstract

The contents of the thesis entitled **"Investigation on Molecular Self-Organisation in Peptide Systems: from Functional Assembly to Autonomous Replication"** are divided into six chapters based on the results of the experimental work performed during the complete course of the doctoral studies.

Chapter 1: In this chapter, we have briefly introduced the supramolecular self-assembly of small peptides and the self-replication of peptides.

Chapter 2: In this chapter, we have discussed about the materials used for experimental purposes, the general methods of the synthetic procedures and instrumentations carried out during the thesis work.

Chapter 3: In this chapter, we have jotted down our work on forming well-ordered spherical dipeptide assemblies, which could bind Thioflavin T. This is special, as we know ThT to bind fibrils characteristically.

Chapter 4: In this chapter, we have reported supramolecular self-assembly of tripeptides, which undergoes morphological transformation from spherical to rod-like nanostructure with time, along with their applications.

Chapter 5: In this chapter, we have demonstrated the design and synthesis of a model cyclic peptide self-replicator, which mainly exists in random coil secondary conformation: a deviation from conventional peptide self-replicators.

Chapter 6: In this chapter, we have investigated the effect of backbone stereochemical modification via the incorporation of D-amino acids in the self-replication of cyclic peptides.

The chapter-wise summaries of the above-mentioned thesis works are described below.

Chapter 1: Introduction

In this chapter, we have delved into the supramolecular self-assembly behaviour exhibited by short peptides, such as dipeptides and tripeptides. Peptides have this unique ability to organise spontaneously into higher-order structures through non-covalent interactions. This inherent tendency to form assemblies often gives rise to supramolecular structures with remarkable functional properties. Some key properties include morphological transformations, gas adsorption, drug encapsulation, and interactions with fluorescent dyes. Moreover, small peptides can be readily modified to develop bio-responsive and functional nanomaterials due to their low molecular weight and economical synthesis.

Additionally, we have explored the concept of "self-replication of peptides", with a particular emphasis on cyclic peptides and how self-replication played a significant role in the context of origin of life studies. The ability of specific peptide systems to undergo template-assisted replication offers valuable insights into prebiotic chemistry and the emergence of molecular complexity. Peptides possess suitable characteristics, such as chemical versatility, ability to form stable secondary structures, and capacity to engage in non-covalent interactions essential for molecular recognition and templating. Cyclic peptides have the potential to emerge as an excellent candidate in the field of self-replication due to their constrained backbone and increased stability against enzymatic degradation. In prebiotic chemistry, such systems provide a plausible pathway for the emergence of informational and catalytic macromolecules under non-enzymatic conditions.

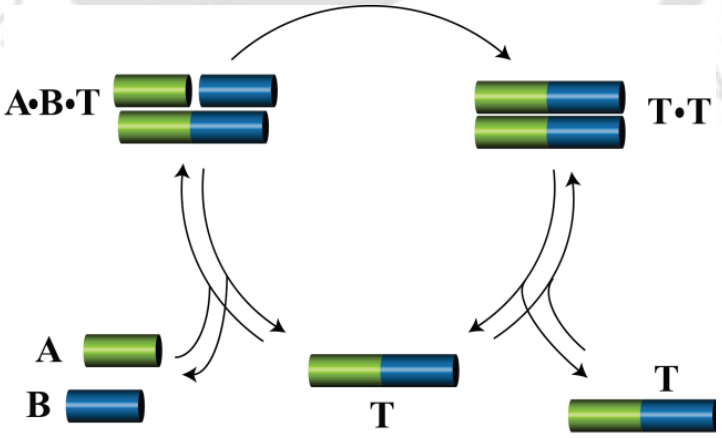

Figure 1. Representation of a self-replicating system described by an autocatalytic cycle. Where A and B represent the precursors, which are fragments of template T.

[Courtesy: This figure is taken from Dadon, Z.; Wagner, N.; Ashkenasy, G. The road to non-enzymatic molecular networks. *Angew. Chem. Int. Ed.,* **2008**, *47*, 6128-61.

Chapter 3: Unprecedented Binding of Thioflavin T with Well-Ordered Spherical Aggregates: a False Positive?

Due to its selective affinity toward amyloid fibrils, Thioflavin T (ThT), a benzothiazole dye, has long been utilized as a gold-standard fluorescent probe. This undergoes a significant enhancement in fluorescence intensity upon binding to the characteristic β-sheet-rich architecture of amyloid aggregates, making it an indispensable tool for diagnostic and research applications. However, ThT's binding properties extend beyond the characterization of amyloid fibrils. It can be utilized to analyse the interaction of various cellular components, such as nucleic acids, intracellular proteins, and other peptides without fibrous morphology, with different binding mechanisms and fluorescence outcomes.

In this current chapter, we explore an unusual and noteworthy observation of ThT binding with well-ordered spherical peptide aggregates formed by tryptophan-containing analogues of biologically relevant dipeptides, Boc-Phe-Trp-OMe (FW), Boc-Val-Trp-OMe (VW), Boc-Leu-Trp-OMe (LW), and Boc-Ile-Trp-OMe (IW). This represents a significant highlight of our research endeavour and deviation from the established paradigm that limits ThT interactions primarily to amyloid-like, fibrillar structures.

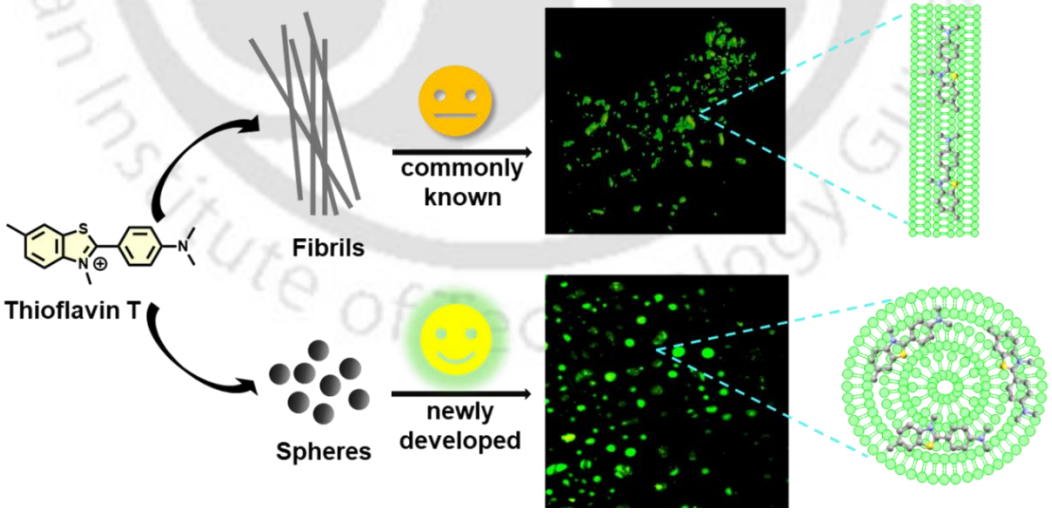

Figure 2. Schematic representation of the binding of Thioflavin T with spherical aggregates.

Chapter 4: Morphology Transition of Tripeptides from Porous Spherical to Rod-like Nanostructures for Small Molecule Adsorption

Peptides exhibit an amazing ability to self-organize into various nanostructures, ranging from simple amorphous aggregates to highly ordered and complex architectures such as fibrils and nanotubes. These morphological transformations are not arbitrary but are strongly influenced by the intrinsic physicochemical characteristics of the peptide sequences and external environmental parameters like pH, temperature, and solvent polarity.

In this chapter, we report the design and synthesis of a set of four tripeptides, Boc-LVL-OMe (LVL), Boc-IVI-OMe (IVI), Boc-LVI-OMe (LVI), and Boc-IVL-OMe (IVL), inspired by the molecular motifs associated with the hydrophobic core of peripheral myelin protein 22. The designed tripeptides undergo a direct morphological transformation (except for Boc-IVL-OMe), evolving spontaneously from one structural form to another under ambient conditions with time. The designed self-assembled tripeptides also possess N_2 gas adsorption, drug encapsulation, and subsequent release upon ionic stimuli.

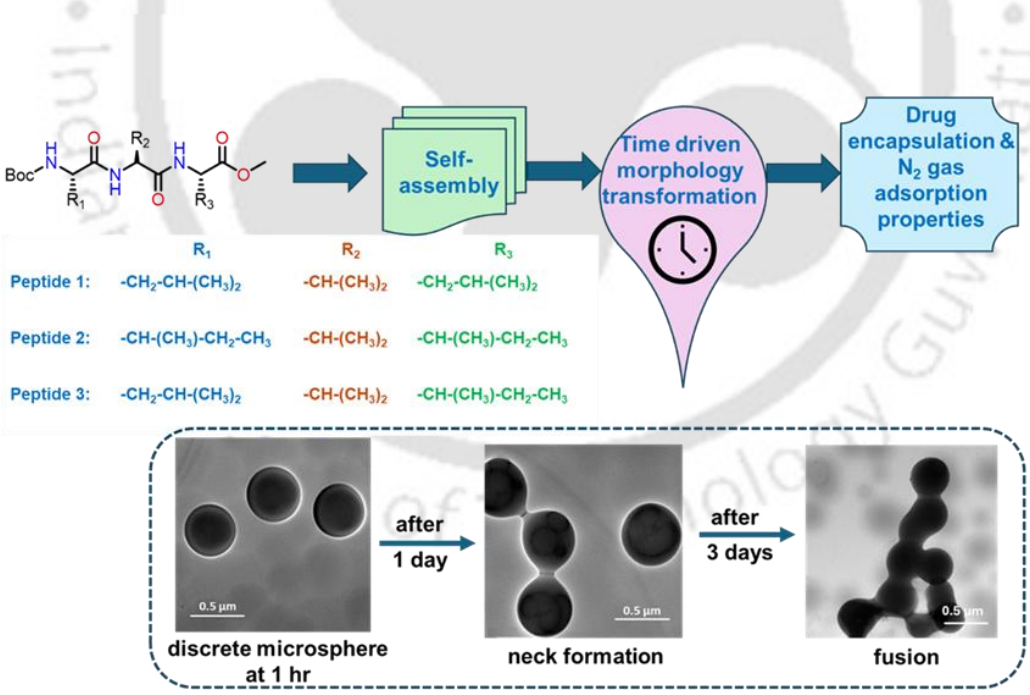

Figure 3. Time-dependent morphological transformation of tripeptides and their application.

Chapter 5: Self-Replication of Novel Cyclic Peptides under Conformationally Challenging Environment

Self-replication is a fundamental process in the emergence of biological complexity and a cornerstone in systems chemistry. Self-replication in peptides typically occurs through templating mechanisms, where a peptide or peptide assembly serves as a template for forming new molecules and accelerates the formation of more of the same molecule. Recently, the study and design of self-replicating peptides have been centred mainly around helical coiled coil structures and β-sheet forming peptides. Yet, the question remains: are stable secondary structures an absolute prerequisite for peptide self-replication? Moreover, cyclic peptides make them attractive candidates for novel replication pathways with their closed-loop topology, intrinsic stability against degradation, conformational restriction, and potential for highly selective intermolecular contacts. Despite these properties, no model system for cyclic peptide self-replication has yet been reported.

In this chapter, we report the design, synthesis, and characterisation of a self-replicating head-to-tail cyclic peptide (CP1), derived from the hydrophobic core of the Aβ peptide. Our designed self-replicating cyclic peptides do not form α-helical or β-sheet-rich conformations under the experimental conditions. Also, we have successfully implemented a new ligating strategy by using benzyl-ester mediated amide bond formation for the first time, offering an alternative to the widely used Kent's ligation.

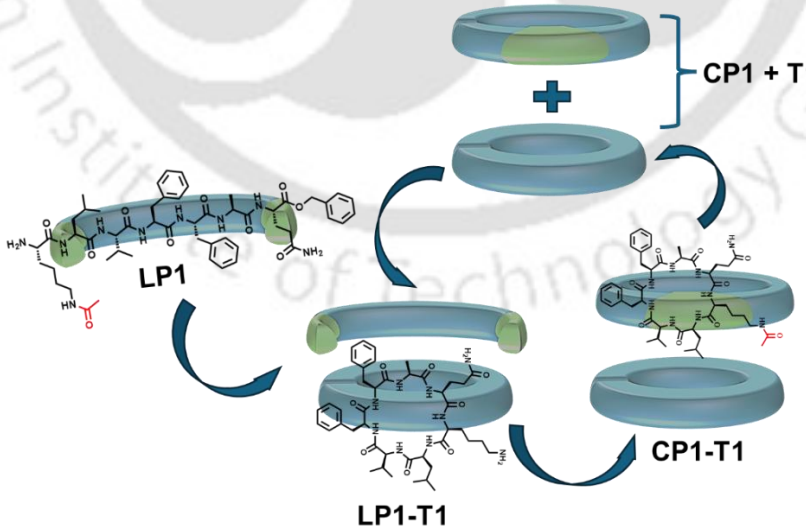

Figure 4. Schematic representation of self-replication of CP1 from its precursor LP1.

Chapter 6: Tuning the Self-Replication of Cyclic Peptides through Backbone Stereochemical Modification

It is a well-established tactic in peptidomimetic and cyclic peptide design. Incorporating a D-amino acid in the peptide backbone introduces a kink or turn, thereby bringing the N- and C-termini closer in 3D space. Thus, we have designed and synthesised two heterochiral self-replicating head-to-tail cyclic peptides, CP2 and CP3, utilizing this property of D-amino acids. These cyclic peptides show much better self-replicating ability and yield significantly more product than that discussed in Chapter 4. Introducing the D-amino acid reduces entropic penalties and increases effective molarity for cyclisation, making the intramolecular ligation reaction of the precursor molecules more favourable.

Similarly, as discussed in Chapter 4, the two designed heterochiral cyclic peptides also exist predominantly in random coil conformations under the experimental conditions. The designed cyclic peptide self-replicators exhibit remarkable sequence and spatiochiro selectivity. These findings contribute to understanding molecular self-organisation and highlight the role of supramolecular assembly, intermolecular recognition, and environmental conditions in developing minimalistic systems with life-like properties.

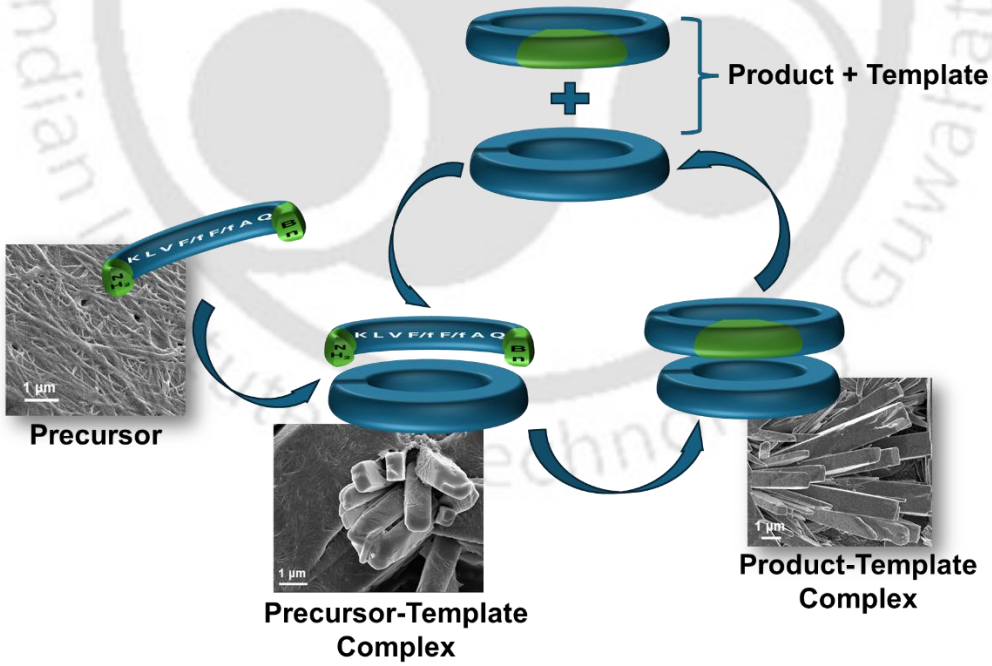

Figure 5. A minimalistic self-replicating system is represented by a structural transformation from a fibrous precursor to a rod-like product.

Summary of the thesis contents

We have unveiled a noteworthy and atypical characteristic of Thioflavin T (ThT), a benzothiazole dye. We observed that ThT has an affinity for and interacts with well-organized spherical aggregates formed by our designed self-assembled dipeptides. Additionally, we established a direct morphological transformation of the designed tripeptides with time from nano-spheres to rod-like structures through self-assembly. These self-assembled tripeptides have N_2 gas adsorption properties and can also encapsulate a powerful hydrophobic drug, curcumin. Furthermore, it also displays KCl-mediated salt-triggered disruption and release of encapsulated drug molecules. Moreover, we have successfully designed and synthesized the first-ever cyclic peptide-based model self-replicators. The designed self-replicating systems operate through templated autocatalysis while adopting random-coil conformations rather than conventional β-sheet or helical motifs. We have also successfully implemented a new ligating strategy by using benzyl-ester mediated amide bond formation, offering an alternative to the widely used Kent's ligation method.

Table of contents

Chapter 1

Introduction and Objectives

भारतीय प्रौद्योगिकी संस्थान गुवाहाटी
Indian Institute of Technology Guwahati

1.1. Introduction

This thesis explored the concept of "self-replication of peptides", with a particular emphasis on cyclic peptides and how self-replication played a significant role in the context of origin of life studies. With different molecular systems available to study, peptides offer a unique position due to their chemical versatility, ability to form stable secondary structures, and capacity to engage in non-covalent interactions essential for molecular recognition and templating.[1,2] Cyclic peptides, owing to their constrained backbone and increased stability against enzymatic degradation,[3,4] can act as promising candidates for investigating primitive self-replicating systems. Additionally, in this thesis, we demonstrated the supramolecular self-assembly of short peptides, such as dipeptides and tripeptides. Therefore, we have incorporated a brief discussion regarding amino acids, peptides, proteins, and their architecture in this section.

1.2. Amino acids, Peptides, and Proteins

Amino acids, peptides, and proteins are fundamental building blocks of life, playing vital roles in nearly all biological processes and functions of all living organisms (Figure 1.1). At the most basic level, amino acids are small organic molecules that share a common backbone structure- an amino group, a carboxyl group, a hydrogen atom, and a distinctive side chain, all bonded to a central, α-carbon atom. There are twenty standard amino acids in nature, all α- amino acids, each differing in its side chains, which contribute to their chemical diversity and influence how they interact with one another.[5]

When amino acids link together through covalent bonds known as peptide bonds, they form peptides. These can vary in length from short chains- often referred to as oligopeptides- to longer, more complex chains called polypeptides. Oligopeptides typically consist of 2 to around 20 amino acid residues, e.g., di-, tri-, tetra-peptide, etc., while polypeptides usually contain more than 20 amino acids. These peptides are more than just structural intermediates; many possess unique biological activities and can act as hormones, signalling molecules, or antimicrobial agents. Because of their relatively simple structures and tuneable properties, peptides have become valuable tools in biochemical research and therapeutic design.[6,7]

Proteins represent the highest level of structural organization in this group. They are composed of one or more long polypeptide chains that usually contain more than 50 amino acid residues, having their molecular masses in the range from 10 kDa to 100 kDa. Proteins can fold into specific three-dimensional shapes, driven by the sequence of their constituent amino acids. This folding is crucial, as the function of a protein is intimately linked to its structure. Proteins are remarkably versatile and can catalyze chemical reactions as enzymes, transport molecules across membranes, provide mechanical strength in tissues, and regulate gene expression, among countless other roles.[8,9]

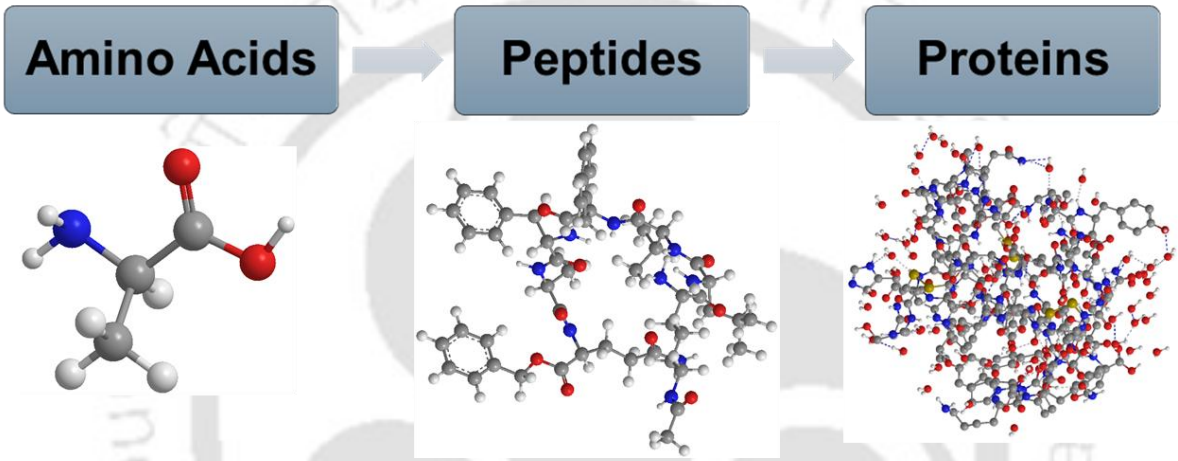

Figure 1.1. *The hierarchical organization of biomolecules from amino acids to proteins.*

1.3. Levels of Protein Organisation

Proteins are not just long chains of amino acids- they are intricately folded and precisely organized 3D molecules that carry out specific functions in living systems. To fully understand how a protein works, it is important to look at its structural architecture on different levels. Protein structure is typically described into four hierarchical levels: primary, secondary, tertiary, and quaternary. Each level builds on the previous one, ultimately contributing to the unique shape and function of a protein.

1.3.1. Primary Structure:

The primary structure of a protein is its most basic form, where a linear sequence of amino acids is linked together by peptide bonds. This linear arrangement of amino acids in a polypeptide chain is often referred to as the protein's "backbone." The primary structure is

the foundation for all higher levels of organisation, influencing how the protein will fold and function.

1.3.2. Secondary Structure:

The secondary structure of the protein can be referred to as the folding of an amino acid chain into a regular spatial arrangement without the involvement of the conformation of the side chains. These structures predominantly arise due to hydrogen bonding between NH and CO groups of the amino acids in a peptide chain. The most common types of secondary structures are α-helix, β-sheet, and β-turn conformations.

α-helix: The alpha helix is one of the most well-characterized secondary structures, first described by Linus Pauling and Robert Corey in the early 1950s. In this structure, the polypeptide chain coils around an imaginary axis with its backbone running longitudinally through it, and the side chain groups are directed outside the helical backbone, minimizing steric hindrance and making the structure favourable for interaction with the surrounding environment. Each amino acid in an alpha helix is involved in a hydrogen bond between the carbonyl oxygen (C=O) of one residue and the amide hydrogen (N-H) of the residue four positions ahead (i + 4) in the chain (Figure 1.2). This regular bonding pattern stabilizes the helical structure. On average, there are 3.6 amino acid residues per turn, and the separation between helical turns is 5.4 Å long along the long axis.[5,10]

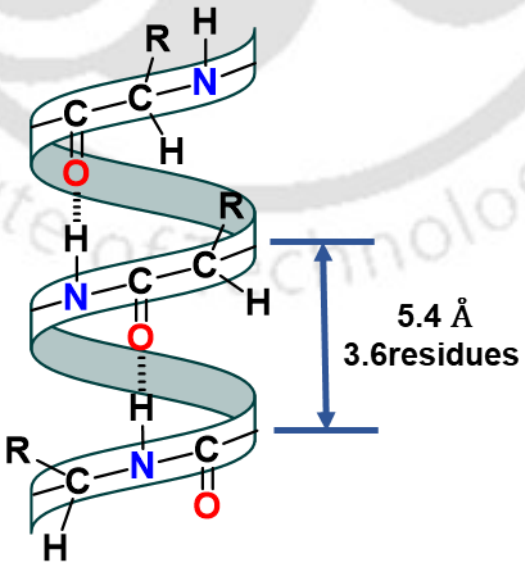

Figure 1.2. *Schematic representation of α-helix structure.*

β-sheet: The beta sheet is another fundamental secondary structure, consisting of extended strands of polypeptides aligned side-by-side and stabilized by inter-strand hydrogen bonds. Beta sheets can be arranged mainly in two ways: parallel, where the neighbouring strands run in the same direction, and antiparallel, where adjacent strands run in opposite directions. Antiparallel beta sheets tend to be more stable due to more linear hydrogen bonding. The distance between two adjacent β-strands in a β-sheet arrangement is 3.5 Å. Unlike the intra-chain hydrogen bonding in alpha helices, beta sheets are stabilized by inter-chain hydrogen bonding between the backbone atoms of adjacent strands (Figure 1.3). In three-dimensional space, beta sheets form pleated, sheet-like structures, which can be flat or slightly twisted. The side chains alternate between projecting above and below the sheet plane, contributing to sheet stability and interactions with other molecules.[11]

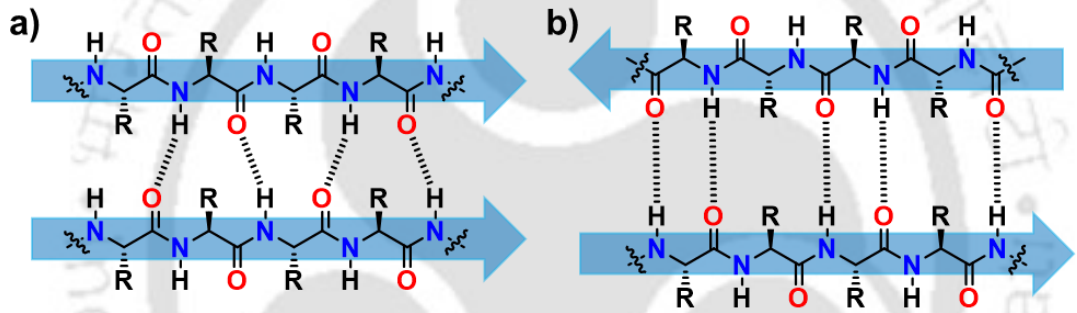

Figure 1.3. *Schematic representation of a). parallel β-sheet and b). antiparallel β-sheet structures.*

β-turn: The beta turn is a short, tight loop that reverses the direction of the polypeptide chain. It typically involves four amino acids, where the CO group of the i^{th} residue forms a hydrogen bond with the NH group of $(i+3)^{th}$ residue to stabilize the turn. The other two residues do not participate in any interaction but make a loop (Figure 1.4). Certain amino acids, like glycine and proline, are frequently found in beta turns. Glycine provides flexibility due to its small size, while proline introduces a natural kink that facilitates the tight turn.[12,13]

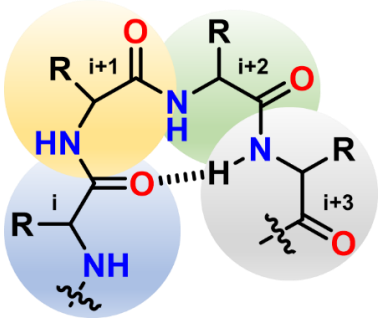

Figure 1.4. *Schematic representation of β-turn structure.*

1.3.3. Tertiary Structure:

The protein tertiary structure refers to the overall three-dimensional (3D) shape of a single polypeptide chain. It results from a variety of interactions between the side chains (R-groups) of the amino acids, including hydrophobic interactions, hydrogen bonds, ionic bonds, and disulfide bridges. This level of structure determines how the protein folds into its final, functional form. Tertiary structure is crucial because a protein's activity, whether it is binding to another molecule, catalyzing a reaction, or sending a signal, depends heavily on its shape. Misfolding of proteins at this level can lead to the onset of various diseases like Alzheimer's or Parkinson's disease, where protein misfolding and aggregation play a central role.[14,15]

1.3.4. Quaternary Structure:

Some proteins consist of a single polypeptide chain, but many functional proteins are made up of multiple subunits, each with its own tertiary structure. These subunits come together and interact to form the quaternary structure of the protein. The arrangement and interaction of these subunits are essential for the protein's overall stability and activity.

1.4. Supramolecular Self-assembly

Supramolecular self-assembly is a fundamental process through which individual molecules spontaneously organize into ordered structures through non-covalent interactions[16,17] such as hydrogen bonding, π–π stacking, van der Waals forces, electrostatic attractions, etc. (Figure 1.5). While covalent synthesis relies strongly on strong chemical bonds formation, supramolecular assembly, on the other hand, operates on reversible and dynamic interactions that allow the system to adapt and respond to its environment. In recent years, supramolecular self-assembly has emerged as a versatile tool for designing functional nanostructures, offering a bridge between molecular chemistry and materials science.[18-20]

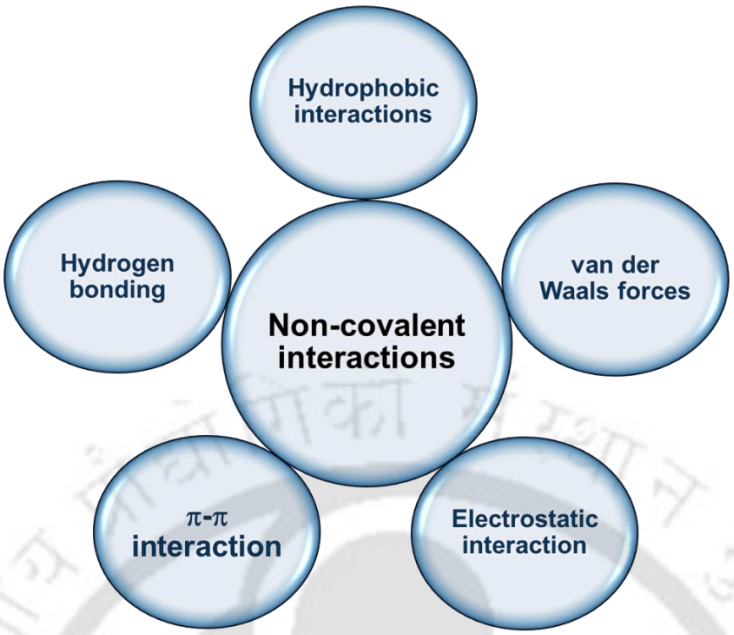

Figure 1.5. *Various kinds of noncovalent interactions in supramolecular chemistry.*

1.4.1. Self-assembly of Small Peptides:

Small peptides' self-assembly represents a powerful approach to construct well-defined nanostructures through spontaneous organization driven by non-covalent interactions. Short peptide sequences, unlike long polypeptides or proteins, due to their simplicity and tunability, allow precise control over molecular design and self-assembly behaviour. Even minimal sequences, such as dipeptides and tripeptides, can form diverse supramolecular architectures, including nanofibers, nanotubes, vesicles, sheets, etc. (Figure 1.6). The process of self-assembly in small peptides is highly sensitive to external factors such as pH, ionic strength, temperature, and solvent polarity. These environmental conditions can regulate intermolecular forces, which lead to the formation of distinct morphologies.

The versatility of small peptides arises from their modularity and biocompatibility, making them attractive candidates for applications in nanomedicine, biomaterials, and catalysis. Their ability to mimic natural motifs while remaining synthetically accessible enables the rational design of functional assemblies that can facilitate diverse applications.[21,22]

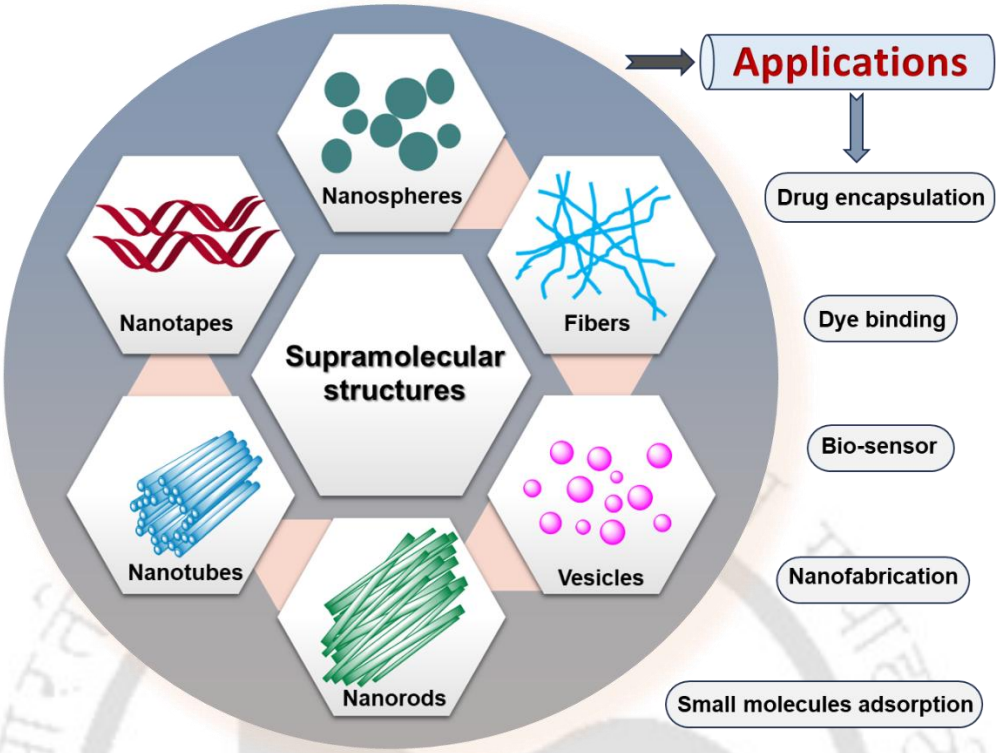

Figure 1.6. *Different kinds of supramolecular architecture and their applications.*

1.4.2. Implications of Self-assembly of Peptides:

The self-assembly of peptides holds profound implications for both fundamental science and practical applications. Their ability to undergo controlled morphological transformations and interact selectively with small molecules can be harnessed for the development of functional nanomaterials.

One of the most promising applications of such assemblies lies in drug encapsulation and delivery. Peptide-based supramolecular nanostructures possess inherent tunability and biocompatibility, which allow them to encapsulate or entrap hydrophobic (or amphiphilic) drug molecules through non-covalent interactions. The dynamic assembly and disassembly equilibrium also enables responsive drug release under physiological conditions, offering potential for targeted and controlled therapeutic applications.[23,24]

Similarly, the interaction of peptide assemblies with dye molecules such as Thioflavin T (ThT) or Congo Red reveals how supramolecular organization can create confined binding pockets or hydrophobic microenvironments. These features make peptide assemblies useful

as sensing platforms, where changes in fluorescence or absorbance signal indicate molecular binding or structural rearrangements. The same principles can extend to adsorption of other functional molecules, highlighting their relevance in bioimaging, pollutant removal, or molecular recognition studies.[25,26]

The structural characterization of peptide self-assemblies frequently employs small-molecule fluorescent probes to complement microscopic and spectroscopic analyses. Among these, Thioflavin T (ThT) is among the most widely used diagnostic markers of amyloid formation. ThT is a benzothiazole-based molecular rotor whose fluorescence intensity is weak in free solution due to rapid intramolecular rotation upon its aromatic rings. While binding to structurally ordered environments that restrict this free rotation, the fluorescence intensity increases significantly. This property has made ThT a standard tool for monitoring aggregation kinetics and detecting β-sheet-rich fibrillar structures.[27-31]

However, emerging studies suggest that ThT responsiveness may not depend solely on canonical amyloid structures (discussed in detail in Chapter 3, below). Instead, fluorescence enhancement fundamentally requires a sufficiently rigid, electronically compatible microenvironment that can restrict dye rotation. Factors such as hydrophobic confinement, aromatic π–π stacking, cation–π interactions, and supramolecular order may all contribute to this effect.

Short peptide systems are known to form structurally diverse assemblies, including spheres, rods, fibrils, etc. While fibrillar morphologies are frequently associated with amyloid behavior, well-ordered spherical aggregates can also exhibit significant nanoscale organization. In such cases, the interaction of ThT with non-fibrillar assemblies raises important questions regarding probe specificity. Addressing this distinction is critical to avoid over interpretation of fluorescence data.

1.5. Self-replicating Materials

Self-replicating materials: an emerging frontier represents a fascinating intersection of materials science, chemistry, and biology, where synthetic systems are engineered to auto-catalytically promote their own synthesis, and systems where autocatalysis co-occurs with information transfer and heredity are said to be self-replicating. This capability is crucial

because it represents a step toward understanding how life might have emerged from simple molecules on prebiotic Earth.

Self-replication in chemical systems is distinguished from simple self-assembly by the requirement that the product actively promotes its own formation via autocatalytic reaction and diversification. Establishing true self-replication, therefore, requires careful kinetic and mechanistic validation.[32]

Experimentally, demonstration of self-replication typically involves: (i) observation of product-dependent rate enhancement, (ii) kinetic signatures consistent with autocatalysis, such as sigmoidal growth profiles or concentration-dependent acceleration, and (iii) control experiments that distinguish template-assisted pathways from spontaneous background reactions. Beyond efficient self-propagation, self-replication should also be accompanied by molecular or supramolecular diversification, such diversity provides the basis for selection and evolutionary adaptation. Mechanistically, self-replication requires the assembled product to facilitate bond formation through molecular recognition and preorganization of reactive termini of the precursor molecules.[33,34]

In peptide-based systems, supramolecular assembly can provide a structural framework for templating by spatially organizing reactants and lowering the activation barrier for ligation. However, the dynamic nature of peptide aggregates requires rigorous kinetic analysis to confirm autocatalytic amplification. Therefore, demonstration of self-replication requires integrating structural characterization with quantitative kinetic evaluation.

1.5.1. Amyloidogenic Peptides:

Amyloidogenic peptides are short protein fragments or sequences within proteins that have the ability to self-assemble into highly ordered fibrillar structures known as amyloid fibrils. These insoluble protein aggregates, known as amyloids, are characterized by their highly ordered cross-β-sheet structures and are linked to a wide range of diseases, including Alzheimer's, Parkinson's, and prion-related disorders.[35-39] The process by which amyloid fibrils form is not uniform; rather, it can follow multiple pathways depending on the variety of amyloid-prone conformations present and the surrounding environment. Factors such as the amino acid sequence of the protein, the specific structure adopted by the amyloidogenic monomer, and experimental conditions like pH, temperature, protein concentration, and

solvent composition play significant roles in determining how aggregation occurs. As a result, researchers have observed different mechanisms and pathways for amyloid assembly under different scenarios.

Typically, the aggregation kinetics of amyloid-forming proteins follow a nucleation-dependent mechanism, which is often described by a characteristic sigmoidal (S-shaped) curve over time. The formation and accumulation of these amyloid fibrils underlie a group of human illnesses collectively known as "amyloidosis".[40,41] Till date, scientists have identified around 50 such disorders, often called protein misfolding or conformational diseases, all of which involve proteins losing their normal structure and aggregating into harmful deposits.

It has been proposed and experimentally shown that native amyloid fibrils are capable of self-replication, though their efficiency remains moderate.[42,43] Building on earlier investigations, researchers have intentionally designed peptide sequences that can assemble into amyloid-like fibrils, allowing them to function both as templates for self-assembly and as self-replicating entities. This design strategy takes advantage of the inherent recognition properties of amyloid-forming peptides. Specifically, amyloid fibrils can selectively bind polypeptide chains that share the same chemical composition. Once recognized, these peptides align along the fibril surface, adopting the characteristic amyloid conformation as they assemble. Through this process, the fibril extends its length while preserving active sites necessary to catalyse subsequent cycles of growth.[44]

Although the experiments did not achieve substantial amplification of replication, i.e., the reactions seeded with pre-formed fibrillar templates did not yield dramatically higher product amounts compared to unseeded controls, however, this work nonetheless represents the first demonstration that amyloid-like fibrillar assemblies can serve as macromolecular scaffolds with both molecular recognition capabilities and catalytic function.

1.5.2. Minimalistic Self-replicating System:

Self-replication is one of the most fascinating and fundamental hallmarks of life. While the natural world demonstrates extraordinarily complex forms of self-replication (like that of DNA replication within a living cell), researchers have long sought to refine this process

into the simplest possible terms. This effort has led to the concept of minimalistic self-replicating systems. A minimalistic self-replicating system consists of a small set of building blocks that can spontaneously assemble into a structure capable of templating or catalyzing its own formation. Unlike biological replication, which relies on intricate networks of enzymes and highly regulated processes, these systems aim to be as simple and autonomous as possible.[45-47]

Most minimalistic self-replicating systems are built on the idea of templating, where a molecule or assembly of molecules serves as a pattern to guide the arrangement of additional building blocks into a replica of itself. Several general strategies adopted by researchers to design such systems are based on molecular recognition, reversible assembly, and autocatalysis.

The search for minimal replicators began in the late 20th century. Orgel and coworkers were among the first to systematically explore template-directed ligation of oligonucleotides, demonstrating that short RNA strands could align complementary fragments to accelerate their own assembly. These studies provided an early experimental basis for the "RNA world" hypothesis.[48-51] von Kiedrowski in 1986, reported an autocatalytic system based on the self-replication of an oligomeric DNA analogue by template-directed chemical ligation. This was among the first clear demonstrations that a small synthetic molecule could catalyse its own production, marking a turning point in prebiotic chemistry.[52,53] Later, Rebek and co-workers in the 1990s developed minimalist replicators based on reversible imine formation between small organic fragments, showing that non-biological molecules can also be coaxed into self-replication cycles.[54]

The kinetic behaviour of minimal self-replicating systems can be effectively understood through a simplified mechanistic model, as represented by a basic set of chemical equations (Equation 1). The replication process begins with the association of precursor molecules (P) with an existing template strand (T), leading to the formation of a transient precursor-template complex (P·T). This complex serves as a reactive intermediate that facilitates the ligation reaction, ultimately generating a template-product complex, denoted as T·T. For the replication cycle to proceed efficiently, this T·T complex must subsequently dissociate, yielding two free template molecules (T). These liberated templates then act as new

catalytic entities, initiating further rounds of replication and thereby sustaining the autocatalytic cycle (Figure 1.7).

$$P + T \underset{k_2}{\overset{k_1}{\rightleftharpoons}} P \cdot T \qquad (1)$$

$$P \cdot T \overset{k_3}{\rightarrow} T \cdot T \qquad (2)$$

$$T \cdot T \underset{k_5}{\overset{k_4}{\rightleftharpoons}} T + T \qquad (3)$$

Equation 1. *Chemical equations describing a minimal self-replicating system.*

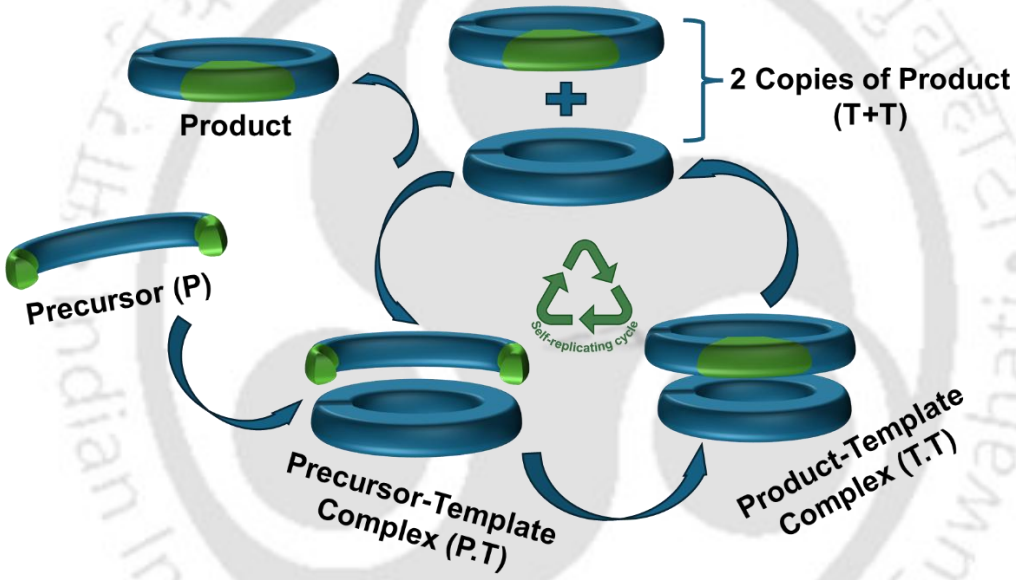

Figure 1.7. *Schematic representation of a minimalistic self-replicating system based on autocatalytic cycle.*

Comprehensive kinetic analyses of several minimal self-replicating systems have demonstrated a distinctive relationship between the initial rate of product formation and the concentration of the template present at the beginning of the reaction. Specifically, the rate of replication exhibits a linear dependence on the square root of the initial template concentration, rather than on the concentration itself. This observation implies that the kinetics of replication are governed by the nature and efficiency of the T·T complex dissociation step.[33,34]

Two characteristic kinetic regimes have been identified based on the dissociation rate of the template–product complex. In systems where T·T dissociates rapidly, the newly formed templates are quickly released, allowing each to participate in additional replication cycles. This scenario results in an autocatalytic amplification process that follows an exponential growth pattern. In contrast, when the dissociation of T·T occurs slowly, the product molecules remain transiently bound to their templates, hindering further replication events. This slow release of active templates imposes a kinetic constraint that manifests as product inhibition, producing a parabolic growth profile.

The distinction between these two kinetic behaviours can be quantitatively visualized using a log–log plot, where the logarithm of the initial rate of product formation is plotted against the logarithm of the initial template concentration. The slope of this plot defines the apparent reaction order (p), serving as a diagnostic parameter for the kinetic regime. A slope of 1 corresponds to exponential growth, characteristic of fast T·T dissociation and efficient replication, whereas a slope of 0.5 indicates parabolic growth, associated with slow dissociation and pronounced product inhibition.[55,56]

1.6. Peptides Self-replication

Self-replicating peptides are a remarkable class of biomolecules and hold immense significance due to their potential role in the fields of synthetic chemistry, molecular biology, and origin of life studies.[57-61] These small chains of amino acids possess the unique ability to undergo processes that mimic biological self-replication, a fundamental feature of life itself. Self-replication of peptides involves the study of mechanisms by which these molecules can copy their structural motifs and propagate, much like genetic material.[62,63] This capability is crucial because it represents a step toward understanding how life might have emerged from simple molecules on prebiotic Earth. The ability of peptides to replicate could provide insights into the minimal requirements for life, as well as a template for developing new bio-inspired materials with self-sustaining and adaptive properties.

1.6.1. Background:

Self-replication in peptides typically occurs through templating mechanisms, where a peptide or peptide assembly serves as a template for the formation of new molecules and accelerates the formation of more of the same molecule. In recent times, the study and

design of self-replicating peptides have been centered mainly around helical coiled coil structures and β-sheet-forming peptides.[32,64-69]

Ghadiri and co-workers[64] in 1996, presented the first experimental demonstration of self-replication of a 32-membered peptide system, establishing a molecular model for autocatalytic replication. The study designed an α-helical coiled-coil peptide that catalyzes its own formation from two complementary peptide fragments through a templated ligation process. The replication followed parabolic (second-order) kinetics, confirming the presence of an autocatalytic feedback loop. Structural investigations showed that molecular recognition between complementary helical domains was essential for replication, while mutations at key hydrophobic residues disrupted the self-replicating ability. This pioneering work provided a fundamental proof-of-concept that peptides can undergo self-replication, offering a chemical framework for understanding molecular evolution and prebiotic self-organization.

In 1997, Ghadiri and colleagues[65] reported an example of a minimal hypercyclic network formed by two coiled-coil peptide replicators based on the design previously studied by the same group, capable of both self- and cross-catalysis. Each peptide was generated from a common electrophilic fragment and distinct nucleophilic partners, leading to a mutually reinforcing system where the formation of one replicator accelerated the production of the other. Kinetic analyses revealed nonlinear autocatalytic behaviour, and mutation studies confirmed that replication was highly sequence specific. This study provided the first clear experimental evidence of a symbiotic molecular network, highlighting how cooperative interactions between self-replicating peptides could have contributed to early evolutionary processes and the emergence of life.

In 2001, Ghadiri and co-workers[66] developed a chiroselective self-replicating peptide system that demonstrated molecular recognition based on chirality. Using coiled-coil peptide templates, the study showed that replication occurred selectively between components of the same chirality, while the opposite enantiomers failed to cross-replicate. Kinetic studies confirmed that replication followed autocatalytic behavior with strong stereochemical fidelity. This work revealed that molecular self-replication can exhibit chiral discrimination, suggesting that such processes could have contributed to the emergence of biological homochirality during early chemical evolution.

Chmielewski and co-workers[67] in 1997 developed a pH-responsive self-replicating peptide system, demonstrating external control over molecular replication. The peptide was designed as a coiled-coil structure that templated its own formation from its corresponding nucleophilic and electrophilic fragments through covalent ligation. The replication efficiency was found to depend strongly on pH, as protonation states modulated the peptide's folding and recognition between complementary fragments. This study highlighted the possibility of environmentally regulated molecular self-replication, showing that replication processes can be dynamically controlled by simple physicochemical parameters.

In 1998, Chmielewski and co-workers[68] developed a self-replicating peptide system whose replication could be regulated by ionic conditions, introducing external control over autocatalytic behavior. The peptide was designed as a coiled-coil template that promoted its own synthesis through non-covalent recognition and ligation of its corresponding nucleophilic and electrophilic fragments. The study demonstrated that ionic strength and salt composition significantly influenced both the assembly and the replication rate, highlighting the role of electrostatic interactions in modulating molecular self-replication.

In 2009, Ashkenasy and co-workers[32] developed a self-replicating system based on amphiphilic β-sheet peptides, demonstrating that molecular self-replication can be driven by non-covalent assembly processes. In this design, peptide fragments assembled into β-sheet structures that brought reactive termini into proximity, facilitating templated ligation and the formation of new replicating species. The replication followed autocatalytic kinetics and was coupled with supramolecular organization, where β-sheet aggregation played a crucial role in promoting replication efficiency. This study highlighted the ability of structured peptide assemblies to sustain self-replication through cooperative assembly.

In 2017, Ashkenasy and co-workers[69] explored how sequence selectivity and evolutionary behaviour can emerge within prebiotic peptide replication networks. Using a synthetic system of short amphiphilic β-sheet driven peptides capable of template-assisted replication, they demonstrated that specific sequences could become enriched over multiple replication cycles due to differences in catalytic efficiency and self-assembly propensity. The study revealed that native-like peptide sequences could spontaneously arise from initially random mixtures through kinetic selection and feedback, mimicking early

evolutionary processes. These findings highlight how chemical self-replication coupled with molecular recognition could drive the emergence of biologically relevant peptides under prebiotic conditions.

In 2010, Otto and co-workers[70] investigated how mechanical forces influence molecular self-replication. Two peptide-based macrocycles, hexamer and heptamer, self-assemble into fibers via β-sheet interactions. Shaking favors hexamer formation, while stirring promotes heptamer growth due to differences in fiber fragmentation. This mechanosensitivity drives kinetic control over product selection. This study highlights how kinetic control and self-organization can drive molecular replication, offering insights into non-equilibrium processes relevant to the origin of life.

Otto and co-workers[71] in 2017 reported the structural and spectroscopic characteristics of self-replicating peptide macrocycles using a combination of experimental and computational methods. Their study revealed that these replicators form ordered supramolecular assemblies, where stacking interactions and β-sheet-like arrangements drive fiber formation and replication. Spectroscopic analyses, supported by molecular dynamics simulations, showed that aromatic and hydrogen-bonding interactions stabilize the assemblies and influence their optical signatures. The work provided detailed molecular-level insight into how structure and organization within peptide assemblies correlate with their self-replication behaviour, advancing the understanding of the physical basis of autocatalytic nanostructures.

1.6.2. Cyclic Peptides as Self-replicator:

Despite the progress in recent years on self-replicating systems, till now, no cyclic peptide-based self-replicating model peptide has been reported. Also, certain questions remain unclear, like whether stable secondary structures are strictly necessary for self-replication to occur. Could molecular replication also arise in the absence of conventional structural motifs such as helices and β-sheets? Unlike linear peptides, cyclic peptides' closed-loop topology confers enhanced stability against enzymatic degradation and promotes conformational restriction, which can support selective and stable intermolecular interactions.[3,4] This architectural rigidity often facilitates specific intermolecular contacts, such as stacking interactions or complementary surface recognition, which are essential for templated replication.

1.7. Knowledge gap

1. Thioflavin T (ThT) has long been utilized as a gold-standard fluorescent probe due to its selective affinity toward amyloid fibrils. However, ThT's binding properties extend beyond the characterization of amyloid fibrils and have remained unexplored.

2. In recent times, the morphology transformation of peptides has emerged as a pivotal area of research. Furthermore, the morphological transformation of peptides plays a crucial role in different aspects of science. One of the key drivers behind this morphological transformation is external stimuli, such as changes in pH, temperature, or solvent conditions. However, the direct transformation of peptide morphology has been explored less over time.

3. Among the many candidates for self-replicator design, peptides occupy a central position. Cyclic peptides possess several advantages, such as structural rigidity, reduced conformational flexibility, and enhanced stability, thus presenting a promising platform for exploring synthetic self-replicating systems. Despite these properties, no model system for cyclic peptide self-replication, consisting of standard amino acids, has yet been reported.

4. Recently, the study and design of self-replicating peptides have been centred mainly around helical coiled coil structures and β-sheet forming peptides. Yet, the question remains: are stable secondary structures an absolute prerequisite for peptide self-replication?

5. Nearly all previously reported self-replicating systems, except Otto's work (disulfide bridge formation) and Insua's oxime ligation, have relied on thioester-mediated Kent's ligation strategy, and no alternative has yet been reported.

1.8. Objectives of the thesis

The following objectives of my Ph.D. thesis work are formulated to address the problems mentioned earlier.

1. Investigation of the binding properties of Thioflavin T (ThT) with well-ordered spherical aggregates formed by the self-assembling dipeptides, using a diverse array of analytical techniques and theoretical calculations.

2. Investigation of direct morphological transformation of tripeptides with time and their application in gas adsorption and drug encapsulation.

3. Design and development of a novel cyclic peptide-based model cyclic peptide self-replicatory system utilising the self-assembly properties of the hydrophobic core motif of the Aβ peptide.

4. Investigation on the necessity of conventional helical or sheet-like characteristics for peptide self-replication. Design and development of self-replicating systems that operate through templated autocatalysis while adopting random-coil conformations rather than conventional β-sheet or helical motifs.

5. To develop a new synthetic toolkit for ligation reactions to construct cyclic peptide self-replicators. Demonstration of the first-time use of a benzyl ester-mediated ligating strategy for efficient amidation, as an alternative to the widely used Kent's ligation strategy.

1.9. References

1. Maury, C. P. J. Self-propagating β-sheet polypeptide structures as prebiotic informational molecular entities: the amyloid world. *Orig. Life Evol. Biosph.* **2009**, *39*, 141-150.
2. Rout, S. K.; Friedmann, M. P.; Riek, R.; Greenwald, J. A prebiotic template-directed peptide synthesis based on amyloids. *Nat. Commun.*, **2018**, *9*, 234.
3. Hill, T. A.; Shepherd, N. E.; Diness, F.; Fairlie, D. P. Constraining cyclic peptides to mimic protein structure motifs. *Angew. Chem. Int. Ed.* **2014**, *53*, 13020-13041.
4. Khatri, B.; Nuthakki, V. R.; Chatterjee, J. Strategies to enhance metabolic stabilities. *Methods Mol. Biol.* **2019**, 17-40.
5. Nelson, D. L.; Cox, M. M. *Lehninger's Principles of Biochemistry (4th edition) New York, W. H. Freeman and Company.* **2005**.
6. Berg, J.; Tymoczko, J.; Stryer, L. *Biochemistry. (5th edition) New York: W H Freeman and Company*. **2002**.
7. Priller, C.; Bauer, T.; Mitteregger, G.; Krebs, B.; Kretzschmar, H. A.; Herms, J. Synapse formation and function is modulated by the amyloid precursor protein. *J. Neurosci.* **2006**, *26*, 7212-7221.
8. Clamp, M.; Fry, B.; Kamal, M.; Xie, X.; Cuff, J.; Lin, M. F.; Kellis, M.; Lindblad-Toh, K.; Lander, E. S. Distinguishing protein-coding and noncoding genes in the human genome. *Proc. Natl. Acad. Sci. U.S.A.* **2007**, *104*, 19428-19433.
9. Petsko, G.; Ringe, D. *Protein structure and function. (1st edition) London: New Age Press*. **2004**.
10. Pauling, L.; Corey, R. B.; Branson, H. R. (1951) The structure of proteins: Two hydrogen-bonded helical configuration of the polypeptide chain. *Proc. Nat. Acad. Sci. U.S.A.* **1951**, *37*, 205-211
11. Pauling, L.; Corey, R. B. The pleated sheet, A new layer configuration of polypeptide chains. *Proc. Nat. Acad. Sci. U.S.A.* **1951**, *37*, 251-256.
12. Krieger, F.; Möglich, A.; Kiefhaber, T. Effect of proline and glycine residues on dynamics and barriers of loop formation in polypeptide chains. *J. Am. Chem. Soc.* **2005,** *127*, 3346-3352.
13. Jacob, J.; Duclohier, H.; Cafiso, D. S. (1999). The role of proline and glycine in determining the backbone flexibility of a channel-forming peptide. *Biophys. J.* **1999**, *76*, 1367-1376.
14. Takalo, M.; Salminen, A.; Soininen, H.; Hiltunen, M.; Haapasalo, A. Protein aggregation and degradation mechanisms in neurodegenerative diseases. *Am. J. Neurodegener. Dis.* **2013**, *2*, 1-14.
15. Ross, C. A.; Poirier, M. A. Protein aggregation and neurodegenerative disease. *Nat. Med.* **2004**, *10*, S10-S17.
16. Rehm, T. H.; Schmuck, C. Ion-pair induced self-assembly in aqueous solvents. *Chem. Soc. Rev.* **2010**, *39*, 3597-3611.
17. Whitesides, G. M.; Grzybowski, B. Self-Assembly at All Scales. *Science* **2002**, *295*, 2418-2421.
18. Gosline, J.; Lillie, M.; Carrington, E.; Guerette, P.; Ortlepp, C.; Savage, K. Elastic proteins: biological roles and mechanical properties. *Philos. Trans. R. Soc. Lond. B Biol. Sci.* **2002**, *357*, 121-132.

19. Knowles, T. P.; Fitzpatrick, A. W.; Meehan, S.; Mott, H. R.; Vendruscolo, M.; Dobson, C. M.; Welland, M. E. Role of intermolecular forces in defining material properties of protein nanofibrils. *Science* **2007**, *318*, 1900-1903.
20. Zhao, F.; Ma, M. L.; Xu, B. Molecular hydrogels of therapeutic agents. *Chem. Soc. Rev.* **2009**, *38*, 883-891.
21. Tsai, W. W.; Li, L. S.; Cui, H.; Jiang, H.; Stupp, S. I. Self-assembly of amphiphiles with terthiophene and tripeptide segments into helical nanostructures. *Tetrahedron* **2008**, *64*, 8504-8514.
22. Shao, H.; Nguyen, T.; Romano, N. C.; Modarelli, D. A.; Parquette, J. R. Self-assembly of 1-D n-type nanostructures based on naphthalene diimide-appended dipeptides. *J. Am. Chem. Soc.* **2009**, *131*, 16374-16376.
23. Simeoni, F.; Morris, M. C.; Heitz, F.; Divita, G. Insight into the mechanism of the peptide-based gene delivery system MPG: implications for delivery of siRNA into mammalian cells. *Nucleic Acids Res.* **2003**, *31*, 2717-2724.
24. Almeida, A. J.; Souto, E. Solid lipid nanoparticles as a drug delivery system for peptides and proteins. *Adv. Drug Delivery Rev.* **2007**, *59*, 478-490.
25. Naiki, H.; Higuchi, K.; Hosokawa, M.; Takeda, T. Fluorometric determination of amyloid fibrils in vitro using the fluorescent dye, thioflavine T. *Anal. Biochem.* **1989**, *177*, 244-249.
26. Levine, H. Thioflavine T interaction with amyloid β-sheet structures. *Amyloid* **1995**, *2*, 1-6.
27. Biancalana, M.; Koide, S. Molecular mechanism of Thioflavin-T binding to amyloid fibrils. *Biochim Biophys Acta* **2010**, *1804*, 1405-1412
28. Vassar, P. S.; Culling, C.F. Fluorescent stains, with special reference to amyloid and connective tissues. *Arch. Pathol.* **1959**, *68*, pp. 487-498.
29. Levine III, H. Thioflavine T interaction with synthetic Alzheimer's disease β-amyloid peptides: Detection of amyloid aggregation in solution. *Protein Sci.* **1993**, *2*, 404-410.
30. Levine III, H. Stopped-flow kinetics reveal multiple phases of thioflavin T binding to Alzheimer β (1-40) amyloid fibrils. *Arch. Biochem. Biophys.* **1997**, *342*, 306-316.
31. Levine, H. Thioflavine T interaction with amyloid β-sheet structures. *Amyloid* **1995**, *2*, 1-6.
32. Rubinov, B.; Wagner, N.; Rapaport, H.; Ashkenasy, G. Self-replicating amphiphilic β-sheet peptides. *Angew. Chem.* **2009**, *121*, 6811-6814.
33. von Kiedrowski, G. Minimal replicator theory I: Parabolic versus exponential growth. *Bioorganic chemistry frontiers* **1993**, 113-146.
34. Reinhoudt, D. N.; Rudkevich, D. M.; de Jong, F. Kinetic analysis of the Rebek self-replicating system: is there a controversy? *J. Am. Chem. Soc.* **1996**, *118*, 6880-6889.
35. Squires, A. M.; Devlin, G. L.; Gras, S. L.; Tickler, A. K.; MacPhee C. E.; Dobson, C. M. X-ray scattering study of the effect of hydration on the cross-β structure of amyloid fibrils. *J. Am. Chem. Soc.* **2006**, *128*, 11738-11739.
36. Zhang, R.; Hu, X.; Khant, H.; Ludtke, S. J.; Chiu, W.; Schmid, M. F.; Frieden C.; Lee, J.-M. Interprotofilament interactions between Alzheimer's Aβ_{1-42} peptides in amyloid fibrils revealed by cryoEM. *Proc. Natl. Acad. Sci. U. S. A.* **2009**, *106*, 4653-4658.

37. Makin, O. S.; Serpell, L. C. Structures for amyloid fibrils. *FEBS Journal* **2005**, *272*, 5950-5961.
38. Westermark, P.; Benson, M. D.; Buxbaum, J. N.; Cohen, A. S.; Frangione, B.; Ikeda, S.; Masters, C. L.; Merlini, G.; Saraiva, M. J.; and Sipe, J. D. A primer of amyloid nomenclature. *Amyloid* **2007**, *14*, 179-183.
39. Chiti, F.; Dobson, C. M. Protein misfolding, functional amyloid, and human disease. *Annu. Rev. Biochem*. **2006**, *75,* 333-366.
40. Jarrett, J. T.; Lansbury Jr, P. T. Seeding "one-dimensional crystallization" of amyloid: a pathogenic mechanism in Alzheimer's disease and scrapie? *Cell,* **1993***, 73,* 1055-1058.
41. Morris, A. M.; Watzky, M. A.; Finke, R. G. Protein aggregation kinetics, mechanism, and curve-fitting: A review of the literature. *Biochim. Biophys. Acta.* **2009**, *1794*, 375-397.
42. Brack, A.; Orgel, L. E. β structures of alternating polypeptides and their possible prebiotic significance. *Nature* **1975**, *256*, 383-387.
43. Carny, O.; Gazit, E. A model for the role of short self-assembled peptides in the very early stages of the origin of life. *FASEB Journal* **2005**, *19*, 1051-1055.
44. Dawson, P. E.; Muir, T. W.; Clark-Lewis, I.; Kent, S. B. Synthesis of proteins by native chemical ligation. *Science* **1994**, *266*, 776-779.
45. Eigen, M.; Schuster, P. *The hypercycle: a principle of natural self-organization*. *Springer Science & Business Media.* **2012**.
46. Paul, N.; Joyce, G. F. A self-replicating ligase ribozyme. *Proc. Nat. Acad. Sci. U.S.A.* **2002**, *99*, 12733-12740.
47. Crick, F. H. C. The origin of the genetic code. *J. Mol. Biol.* **1968**, *38*, 367-379.
48. Orgel, L. E.; Lohrmann R. Prebiotic chemistry and nucleic acid replication. *Acc. Chem. Res.* **1974**, *7*, 368-377.
49. Zielinski, W. S.; Orgel, L. E. Autocatalytic synthesis of a tetranucleotide analogue. *Nature* **1987**, *327*, 346-347.
50. Kim, D. E.; Joyce, G. F. Cross-catalytic replication of an RNA ligase ribozyme. *Chem. Biol.* **2004**, *11*, 1505-1512.
51. Lincoln, T. A.; Joyce, G. F. Self-sustained replication of an RNA enzyme. *Science* **2009**, *323*, 1229-1232.
52. von Kiedrowski, G. A self-replicating hexadeoxynucleotide. *Angew. Chem. Int. Ed.* **1986**, *25*, 932-935.
53. von Kiedrowski, G.; Wlotzka, B.; Helbing, J. Sequence dependence of template-directed syntheses of hexadeoxynucleotide derivatives with 3′–5′ pyrophosphate linkage. *Angew. Chem. Int. Ed.* **1989**, *28*, 1235-1237.
54. Wintner, E. A.; Rebek, J. Autocatalysis and the generation of self-replicating systems. *Acta Chem. Scand.* **1996**, *50*, 469-485.
55. Paul, N.; Joyce, G. F. Minimal self-replicating systems. *Curr. Opin. Chem. Biol.* **2004**, *8*, 634-639.
56. Dadon, Z.; Wagner, N.; Ashkenasy, G. The road to non-enzymatic molecular networks. *Angew. Chem. Int. Ed.* **2008**, *47*, 6128-6136.

57. Lifson, S. On the crucial stages in the origin of animate matter. *J. Mol. Evol.* **1997**, *44*, 1-8.
58. Kauffman, S. Question 1: origin of life and the living state. *Origins Life Evol. Biosphere* **2007**, *37*, 315-322.
59. Ruiz-Mirazo, K.; Briones, C.; de la Escosura, A. Prebiotic systems chemistry: new perspectives for the origins of life. *Chem. Rev.* **2014**, *114*, 285-366.
60. Ashkenasy, G.; Hermans, T. M.; Otto, S.; Taylor, A. F. Systems chemistry. *Chem. Soc. Rev.* **2017**, *46*, 2543-2554.
61. Mattia, E.; Otto, S. Supramolecular systems chemistry. *Nat. Nanotechnol.* **2015**, *10*, 111-119.
62. Patzke, V.; von Kiedrowski, G. Self replicating systems. *Arkivoc*, **2007**, *5*, 293-310.
63. Vidonne, A.; Philp, D. Integrating replication processes with mechanically interlocked molecular architectures. *Tetrahedron* **2008**, *64*, 8464-8475.
64. Lee, D. H.; Granja, J. R.; Martinez, J. A.; Severin, K.; Ghadiri, M. R. A self-replicating peptide. *Nature* **1996**, *382*, 525-528.
65. Severin, K.; Lee, D. H.; Martinez, J. A.; Ghadiri, M. R. Peptide self-replication via template-directed ligation. *Chem. Eur. J.* **1997**, *3*, 1017-1024.
66. Saghatelian, A.; Yokobayashi, Y.; Soltani, K.; Ghadiri, M. R. A chiroselective peptide replicator. *Nature* **2001**, *409*, 797-801.
67. Yao, S.; Ghosh, I.; Zutshi, R.; Chmielewski, J. A pH-modulated, self-replicating peptide. *J. Am. Chem. Soc.* **1997**, *119* (43), 10559-10560.
68. Yao, S.; Ghosh, I.; Zutshi, R.; Chmielewski, J. A self-replicating peptide under ionic control. *Angew. Chem. Int. Ed.* **1998**, *37*, 478-481.
69. Nanda, J.; Rubinov, B.; Ivnitski, D.; Mukherjee, R.; Shtelman, E.; Motro, Y.; Ashkenasy, G. Emergence of native peptide sequences in prebiotic replication networks. *Nat. Commun.* **2017**, *8*, 434.
70. Carnall, J. M.; Waudby, C. A.; Belenguer, A. M.; Stuart, M. C.; Peyralans, J. J. P.; Otto, S. Mechanosensitive self-replication driven by self-organization. *Science*, **2010**, *327*, 1502-1506.
71. Frederix, P.W.; Idé, J.; Altay, Y.; Schaeffer, G.; Surin, M.; Beljonne, D.; Bondarenko, A.S.; Jansen, T.L.; Otto, S.; Marrink, S. J. Structural and spectroscopic properties of assemblies of self-replicating peptide macrocycles. *ACS nano*, **2017**, *11*, 7858-7868.

Chapter 2

Materials, Methods, and Instrumentations

भारतीय प्रौद्योगिकी संस्थान गुवाहाटी
Indian Institute of Technology Guwahati

2.1. Materials and Methods

2.1.1. Reagents and Solvents

The mentioned Fmoc-protected amino acids, N-terminus Boc-protected amino acids, unprotected amino acid, Rink Amide MBHA resin (loading 0.7 mmol/g), and Benzotriazol-1-yloxy- tris(dimethylamino)phosphonium hexafluorophosphate (BOP) coupling reagent were purchased from GL Biochem (Shanghai). Ethyl 2-cyano-2-(2-nitrobenzenesulfonyloxyimino) acetate (*o*-NosylOXY), a coupling reagent, was synthesized in our laboratory starting from reagents Ethyl-hydroxyiminocyanoacetate (Oxyma) and 2-nitrobenzenesulphonyl chloride. Diisopropylethylamine (DIPEA), and silica gel (60-120 mesh) were purchased from Spectrochem. Pvt. Ltd. (India). Lithium hydroxide (LiOH), hexafluoroisopropanol (HFIP) and thioflavin T (ThT) were purchased from Sigma Aldrich. Trifluoroacetic acid (TFA), acetic anhydride (synthesis grade) and N-methylimidazole (NMI) of extra pure grade were purchased from SRL, India. Piperidine, acetonitrile of HPLC grade, dimethylformamide (DMF), dichloromethane (DCM), diethyl ether and chloroform-d ($CDCl_3$) of extra pure grade were purchased from Merck, India.

The coupling reagent was invented and synthesized in our lab according to the previous literature report.[1]

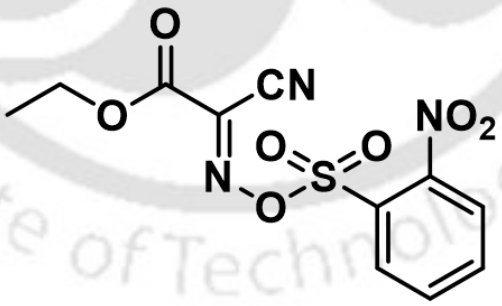

Figure 2.1. *Chemical structure of o-NosylOXY*

The rationale for using this coupling reagent is as follows:

It enables racemization free synthesis of peptides, thereby preserving the stereochemical purity of the products. In addition, it can be utilized in both solution and solid phase peptide synthesis, making it a versatile choice for wide range of synthetic applications. The reagent

is also effective under mild and ambient reaction conditions. Furthermore, it represents a cost effective and environmentally friendly approach to peptide synthesis, owing to its recyclability and reduced generation of chemical waste.

2.1.2. Dipeptides Sample Preparation

0.5 mg of all the dipeptides were taken in different Eppendorf vials and dissolved in 500 µL of PBS-ACN mixture (PBS/ACN = 3:2). The solutions were sonicated and vortexed properly for about 5 minutes and then immediately required amount of sample solutions were transferred into different vials and diluted further using PBS (pH 7.4) only, to get desired 300 µM solution. These sample solutions were then incubated at 37 ºC and used for different experimental purposes.

2.1.3. Tripeptides Sample Preparation

0.5 mg of all the tripeptides was dissolved in a 1:1 MeOH-H_2O mixture and was properly sonicated and vortexed. The prepared peptide sample solutions were then further diluted to obtain the desired concentration (500 µM) and kept in incubation at 37 ºC. The incubated sample solutions were then utilized for the different experiments carried out.

2.1.4. Sample Preparation for the Self-replication Studies

0.5 mg of all the synthesized peptides were taken in different Eppendorf vials and dissolved in 1 ml of PBS-ACN mixture (PBS: ACN = 3:2). The sample solutions were sonicated and vortexed properly for about 5 minutes and then required amount of sample solutions were transferred immediately into different vials and diluted further using PBS only (pH 7.4), to get the desired final concentration of sample solutions. The sample solutions were kept in incubation at 37 ºC and were utilized for different experimental purposes.

2.1.5. Detection Limit Calculation

The detection limit was calculated from the fluorescence titration study of ThT with the dipeptides. ThT's fluorescence emission spectra were measured ten times, and the standard deviation of the blank measurement was calculated at 485 nm. A plot of fluorescence emission intensity at 485 nm versus the concentration of peptides was used to determine the slope. The detection limit was calculated accordingly using the following Eq. (2.1).[2]

$$Detection\ limit\ =\ 3\sigma/k \qquad (2.1)$$

where σ is the standard deviation of the blank measurements, and k is the slope obtained from the plot as mentioned above.

2.1.6. Estimation of the Apparent Binding Constant

The apparent binding constants for each of the ThT-dipeptide complexes were estimated from the fluorescence titration study of ThT with the dipeptides utilizing the Benesi-Hildebrand (B-H) plot as shown below, Eq. (2.2).[3,4]

$$1/(I - I_0)\ =\ 1/\{K(I_{max} - I_0)\ C\}\ +\ 1/(I_{max} - I_0) \qquad (2.2)$$

I_0 is the emission intensity of ThT at maxima (λ = 485 nm), I is the emission intensity recorded in the presence of the different concentrations of the peptides (at λ = 485 nm), and I_{max} is the maximum emission intensity value obtained during the titration experiment. K is the apparent binding constant (M^{-1}) obtained from the slope of the linear plot.

2.1.7. Relative Quantum Yield Calculation

The quantum yield was estimated utilizing both the fluorescence and UV-VIS spectroscopy and compared with respect to fluorescein. Fluorescein, having a literature Φ = 0.92, was dissolved in 0.1 M NaOH solution in distilled water (η = 1.33), ThT and the ThT-dipeptide complexes were dissolved in PBS buffer (η = 1.33). The relative quantum yields were then calculated using the following Eq. (2.3).

$$\Phi = \Phi_R \times \frac{I}{I_R} \times \frac{A_R}{A} \times \frac{\eta^2}{\eta_R^2} \qquad (2.3)$$

Where Φ is the quantum yield, I symbolize the area under the emission spectra, A represents the absorbance at the excitation wavelength (445 nm), and η is the refractive index. The subscript R refers to the reference fluorophore of known quantum yield.

2.1.8. Computational Details

We conducted a detailed theoretical analysis to gain better insights into the non-covalent interactions (NCI). The initial structures of the species were taken from the crystal

structures **FW** (CCDC No: 2144263), **VW** (CCDC No: 2144259), and **IW** (CCDC No: 2144261).[5] The structure for **LW** was obtained from its isomer **IW**. A detailed conformational search of the adduct was performed using CREST.[6] The appropriate and lowest energy conformation is considered for DFT calculation. The implicit solvation model SMD[7] was applied to account for solvation effects without explicitly including solvent molecules. All DFT calculations were performed using Gaussian 16,[8] with visualization done via GaussView 6.0.[9] Geometry optimization and frequency calculations were performed using the dispersion corrected Becke, 3-parameter, Lee–Yang–Parr functional (B3LYP-D3)[10] with 6-31++G[11] basis set. The NCIs were confirmed through isosurface and RDG scatter plots generated using Multiwfn[12] and visualized with VMD software.[13] For the EDA, we have implemented the zeroth order Symmetry-adapted perturbation theory (SAPT0),[14] incorporated in the PSI4 code[15] with jun-cc-pVDZ basis set,[16] to get a clear idea of the interactions involved in the complex.

2.2. Instrumentations

2.2.1. Nuclear Magnetic Resonance (NMR) Spectroscopy:

Samples were prepared by dissolving peptides in 0.5 mL CDCl3 solvent to perform NMR. The Bruker Ascend 600 MHz and 400 MHz instrument was employed to collect the NMR data, and the data were analyzed using MestReNova software. The reported chemical shift (δ) and coupling constants (*J*) values were measured in ppm and Hz units, respectively.

2.2.2. Mass Spectrometry:

Samples were prepared by dissolving peptides in a required volume of acetonitrile-water solvent mixture to perform HRMS. The Agilent-Q-TOF 6546 LC instrument and Electrospray ionization (ESI) technique ('+'ve mode) were adopted to get HRMS data. The data was analyzed by mass Hunter workstation software.

2.2.3. MALDI-TOF Mass Spectrometry:

For MALDI-TOF characterization of the purified peptides, the peptide solutions were dissolved in an ACN-H2O mixture and mixed with CHCA (α-cyano-hydroxy-cinnamic acid) matrix solution in a 1:1 ratio. The prepared sample was then analyzed using Bruker Daltonics FlexControl software on a BRUKER autoflex speed instrument. The mass of the

individual peaks of the purified peptides was assigned using the FlexAnalysis software. $[M+H]^+$, $[M+Na]^+$ and $[M+K]^+$ peaks were observed for the purified peptides.

2.2.4. High-performance liquid chromatography (HPLC):

The purity of the synthesized peptides was examined using analytical HPLC. Thermo Scientific instrument was utilized for the purpose, along with a reverse-phase Poroshell 120 EC, C18 column (4.6 × 100 mm). A linear solvent gradient with 5-95% ACN/H_2O and 15 minutes (in some cases, 10 minutes) runtime at 1 mL/min flow rate was set to carry out the experiment.

2.2.5. Field Emission Scanning Electron Microscopy (FE-SEM):

10 µL of each of the incubated peptide sample solutions at 37 ºC was taken out, and drop-cast on an Al-foil wrapped glass slide at required time intervals. The prepared samples were then dried in an incubator overnight and kept in a desiccator at room temperature prior to imaging. FESEM images were captured on FE-SEM Gemini-300 (ZEISS) and SIGMA-300 (ZEISS) instruments.

2.2.6. Field Emission Transmission Electron Microscopy (FE-TEM):

10 µL of each of the incubated peptide sample solutions at 37 ºC was taken out at required time intervals and spotted on the dark side of the carbon-coated copper grid. 2 mins after the spotting, the excess solution was removed using a blotting paper and the grid was allowed to dry. 10 µL of 2% uranyl acetate solution was then added on the same side of the grid as the staining agent and kept for another 2 mins; the excess solution was again removed using blotting paper. The samples were dried in an incubator overnight and kept in a desiccator at room temperature prior to imaging. TEM images were captured on a JEOL (Model: JEM-2100F Field Emission Electron Microscope) at 200 kV.

2.2.7. Dynamic Light Scattering (DLS) Measurements:

200 µL of each of the incubated peptide sample solutions at 37 ºC were taken in a 1 mL cuvette at required time intervals, and the DLS study was carried out at 25 °C using a 633 nm He-Ne laser on a Zetasizer Nano series Nano-ZS90 (Malvern Instruments). The system was equilibrated for 120 seconds prior to scanning, and each measurement obtained was an average of three scans. The software data were then processed and plotted on OriginPro 8

software, and the intensity percentage vs size distribution of the particles was reported in the provided DLS experiment.

2.2.8. Circular Dichroism (CD) Spectroscopy:

Incubated peptide sample solutions at 37 ºC of specific concentrations at required time intervals were used to record CD spectra. Each of the sample solutions was taken in a cuvette of bandwidth 1 mm, and three scans were recorded for each sample on a JASCO J-1500 spectropolarimeter. The processed software data were then plotted on OriginPro 8 software, and mean residue molar ellipticity θ (deg. $cm^2.dmol^{-1}$) vs wavelength (nm) was reported in the provided CD spectra.

Observed ellipticity (mdeg) was converted to mean residue molar ellipticity using the following equation:

θ (deg. $cm^2.dmol^{-1}$) = Ellipticity (mdeg). 10^6 / (Pathlength (mm). [Protein] (μM). N

Where [Protein] is the concentration of the peptide samples (in μM), and N represents the number of amide bonds in the peptide sequence.

2.2.9. Fourier-Transform Infrared (FT-IR) Spectroscopy:

Incubated peptide sample solutions of specific concentrations were lyophilized at required time intervals to get the solid samples. FT-IR spectra of the solid peptide samples were then recorded using a PerkinElmer UATR Two FT-IR spectrometer. (KBr pellet technique was not used).

2.2.10. N_2 Gas Adsorption Experiment:

N_2 gas adsorption and desorption studies were analyzed using Quantachrome Instruments at STP. For this experiment, the peptide sample solutions were first incubated for the required time interval at 37 °C and then lyophilized to get the solid samples. These solid samples were then used for further analysis. Initially, all the solid peptide samples were degassed for 3 hrs at 70 °C. BET surface areas were measured using the Brunauer-Emmett-Teller (BET) equation.

2.2.11. Fluorescence Spectroscopy and Fluorescence Microscopy:

For the Thioflavin T fluorescence assay, ThT having concentration of 50 μM was prepared in PBS (pH 7.4). For the dose-dependent study, $A\beta_{1-40}$ (20 μM) and the purified peptide

samples were dissolved in PBS and mixed to obtain the desired different molar ratios (1:5, 1:15, 1:30). For the fluorescence titration study for peptides with ThT (50 μM), peptide solutions of desired concentrations (10 μM to 600 μM) were prepared as mentioned above, and all the samples mentioned above were kept for incubation at 37 ºC.

To perform the fluorescence experiment, 40 μL of the peptide solutions were taken from the incubated sample solution and mixed with 160 μL of PBS and 200 μL of the ThT solution at each time interval. The excitation wavelength was set at 445 nm for the experiment, and the emission was recorded at 485 nm.

For the drug encapsulation study, 500 μM of each of the peptide solutions was co-incubated with 30 μM curcumin solution, and fluorescence emission spectra (wavelength 450−700 nm) were recorded on a Fluoromax-4 Horiba Fluorospectrometer at different time intervals. For this experiment, a total of 400 μL of the incubated mixture sample solutions was taken in a 1 mL quartz cuvette, and a slit of 5 nm was used. Each scan was repeated three times.

For the ThT dye binding study, 10 μL of each of the incubated dipeptide sample solutions (300 μM), after 4 days of incubation, were taken in an Eppendorf and mixed with 10 μL ThT solution (50 μM). The mixture solution was then drop-cast on a clean microscopic glass slide and kept in an incubator for drying.

For the curcumin drug encapsulation study, 10 μL of each of the curcumin mixed peptide solutions after 36 hr of incubation were taken out and drop cast on a clean glass slide. It was kept for drying at room temperature. For the salt-mediated disruption study, KCl solution (1.5 mM) was added to the 2-day incubated curcumin mixed peptide solution and then kept for further incubation at 37 °C up to 36 hr. Fluorescence microscopic imaging was then conducted for each case on an Olympus BX 51 fluorescence microscope with 50× and 100× magnification.

2.2.12. Thermogravimetric analysis (TGA):

Incubated peptide solution at 37 °C were first lyophilized at the required time interval to get the dry solid samples. The obtained solid samples were subjected to thermogravimetric analysis using a PerkinElmer TGA analyzer (TGA 4000). The parameters used for this experiment are as follows. The heating rate of the sample = 10 °C/min in an alumina crucible, and the flow rate of dynamic atmospheric N_2 = 30 cm^3/min.

2.2.13. Melting Point

Melting points were recorded on the Buchi melting point apparatus.

2.2.14. UV-Vis Spectroscopy

UV/Vis spectra of the compounds analyzed were recorded in a PerkinElmer Lambda 365+ spectrometer at room temperature.

2.3. Solid Phase Peptide Synthesis (SPPS) Protocol

All the above-mentioned solid-phase peptide syntheses were done manually inside a frit-fitted plastic syringe. A Stuart tube rotator with 40 rpm was used following standard protocols of solid phase peptide synthesis (SPPS).[17,18] The Rink Amide MBHA resin (200 mg) of loading 0.7 mmol/g was taken inside a 5 mL frit-fitted plastic syringe and swollen in DCM for 3 h, followed by DMF for another 1h.

2.3.1. Peptide coupling

All peptide couplings were performed at room temperature. For a standard coupling, 3 equivalents of Fmoc-amino acid, 3.5 equivalents of BOP or o-NosylOxy as coupling reagent and 7 equivalents of DIPEA as base were dissolved in DMF and added to the resin inside the syringe. The coupling time varied from 3 h to 12 h, depending on the environment and nature of the amino acids being coupled. In case of any incomplete coupling, the coupling reaction was repeated. After each coupling, resin was washed thoroughly with DMF and DCM, respectively, for 5 mins each.

2.3.2. Fmoc deprotection

After each coupling, N_{α}-Fmoc was deprotected using 20% piperidine in DMF for 21 mins (7 mins × 3). After deprotection, the resin was washed thoroughly with DMF for 5 mins prior to the next coupling.

2.3.3. Kaiser test

Successful coupling of each amino acid was monitored by performing the Kaiser test.[19] For the test, a few beads of resin (should be in DCM medium) were taken out of the syringe in a fusion tube, and to it, 1:1 Kaiser A solution and Kaiser B solution were added. In another fusion tube, only Kaiser A and B solutions (1:1) were taken, and both the tubes were heated over a sand bath at 80 °C for 5 mins. The appearance of blue/purple colour in the tube

containing resin beads indicated a positive Kaiser test, whereas the fusion tube containing only Kaiser solutions remained red/brown in colour. The composition of the Kaiser solutions is mentioned below:

Kaiser A: 0.5 g ninhydrin in 10 mL ethanol

Kaiser B: 0.4 mL of 0.001 M KCN (aq) in 20 mL pyridine

2.3.4. Acetylation (capping)

Acetylation or capping was performed when, even after repeated coupling, some free NH_2 groups remained. In such cases, after coupling, the resin was washed with DCM for 5 times. Thereafter, a 1:1 mixture of acetic anhydride (Ac_2O) and N-methyl imidazole (NMI) was dissolved in DCM and added to the resin. The reaction was carried out for 1h to 2h and then thoroughly washed with DCM.

2.3.4. Final cleavage of peptide from resin

After complete synthesis of the peptide sequence, the resin was treated with a mixture of TFA/DCM/H2O (9/0.5/0.5) solution for 3h. Approximately 2.5-3 mL of the cocktail solution was used for 200 mg of resin. After completion of the final cleavage of the peptide from resin, the crude peptide was precipitated in cold diethyl ether. The precipitate was then washed thoroughly with diethyl ether and centrifuged to obtain the crude solid product. The crude peptide was first dried and then purified by semi-preparative HPLC.

2.4. Synthetic Procedure of the Designed Peptides

2.4.1. Procedure for the Synthesis of Dipeptides

The dipeptides **FW**, **VW**, **LW** and **IW** (discussed in Chapter 3, below) were synthesized as follows:

For **FW**, Boc-Phe-OH (400 mg, 1.5 mmol), DIPEA (193.5 mg, 1.5 mmol), and *o*-NosylOXY (490.5 mg, 1.5 mmol) were taken in 50 ml R.B. and dissolved in DCM. The whole reaction mixture was stirred at room temperature for 15 min for pre-activation. After that, neutralized H_2N-Trp-OMe (392 mg, 1.8 mmol) solution in DCM was added to the reaction mixture and stirred for 4 h continuously. Then, the diluted reaction mixture in DCM was treated separately for workup with 10% citric acid (3 times) and 10% NaHCO3

solution (3 times). The crude reaction mixture is concentrated with the assistance of a rotary evaporator. Finally, column chromatography was performed to obtain the pure dipeptide, **FW**. The peptide was characterized using 1D ^{1}H and ^{13}C NMR spectroscopy and Mass spectrometry.

The other dipeptides, **VW**, **LW** and **IW** were synthesized using the same protocol as mentioned above.

2.4.2. Procedure for the Synthesis of Tripeptides

The tripeptides **LVL**, **IVI**, **LVI** and **IVL** (discussed in Chapter 4, below) were synthesized as follows:

For **LVL**, the solution of Boc-L-Val-OH (300 mg, 1.38 mmol), *o*-NosylOXY (451 mg, 1.38 mmol), and DIPEA (178 mg, 1.38 mmol) in 50 mL DCM were stirred for 10 minutes for pre-activation of the acid. After that, neutralized H_2N-L-Leu-OMe (304 mg, 2.1 mmol) in DCM was gradually added to the reaction mixture, and the whole solution was kept stirring for 4 h at room temperature for successful coupling of the amino acid. Then, the reaction mixture was washed three times individually with 10% citric acid and sodium bicarbonate solution, respectively. The organic layer was concentrated to obtain protected dipeptide Boc-L-Val-L-Leu-OMe by using a rotary evaporator. After that, the Boc protecting group was cleaved by trifluoroacetic acid in DCM and neutralized by the required amount of DIPEA, which was monitored by pH check. The amine-free di-peptide was combined with Boc-L-Leu-OH to obtain the intended tripeptide, **LVL**. At last, the crude tripeptide was purified by column chromatography (stationary phase: silica gel, mobile phase: EtOAc/Hexane). The reversed-phase analytical HPLC was performed to verify the purity of the tripeptide.

The other tripeptides, **IVI**, **LVI** and **IVL** were synthesized using the same protocol as mentioned above.

2.4.3. Procedure for the Synthesis of Fmoc-Glu-OMe and Fmoc-Glu-OBn.

The acid, Fmoc-Glu(OtBu)-OH (850 mg, 1 equiv), was dissolved in ACN, followed by the addition of DIPEA (516 mg, 2 equiv). The solution was stirred for 2-3 mins for thorough mixing, followed by the addition of MeI (1128 mg, 4 equiv)/BnBr (1368 mg, 4 equiv) to obtain the required ester of glutamic acid. The reaction mixture was stirred for 12-15 h at

room temperature. After completion of the reaction, acetonitrile was evaporated completely, and the reaction mixture was diluted with ethyl acetate; the organic layer was washed thoroughly with 5% citric acid and 5% $NaHCO_3$ solution, dried with anhydrous Na_2SO_4, and the product was purified by silica gel column chromatography to obtain the methyl/benzyl ester product. The product thus obtained was dissolved in a 1:1 TFA-DCM mixture solution and was stirred at room temperature for 1.5 h for the removal of the -OtBu group. After completion of the reaction, TFA was evaporated completely by purging nitrogen gas and then by rotary evaporator. The reaction mixture was washed thoroughly with DCM several times to ensure complete removal of TFA, followed by the addition of hexane to obtain the solid products of Fmoc-Glu-OMe and Fmoc-Glu-OBn.

2.4.4. Procedure for the Synthesis of Linear Peptides

The linear peptides **LP1**, **A-LP1, G-LP1, LP2, A-LP2, G-LP2, LP3, A-LP3 and G-LP3** (discussed in Chapters 5 & 6, below) were synthesized as follows:

All the linear peptides were synthesized first by anchoring Fmoc-Glu-OBn through the C-terminus of its side chain on 200 mg Rink amide MBHA resin (loading 0.7 mmol/g). Each coupling was carried out with 3 equivalents of Fmoc-amino acid, 3.5 equivalents of *o*-NosylOXY as coupling reagent and 7 equivalents of DIPEA as base. After each coupling, the resin was washed with DMF and DCM and the Kaiser test was performed. Fmoc-deprotection was performed using 20% piperidine in DMF for (7 mins × 3). After deprotection, the resin was washed thoroughly with DMF and proceeded for next coupling. After completion of the linear sequences, the peptides were cleaved from the resin using 3 mL solution of a mixture of TFA/DCM/H2O (9/0.5/0.5) for 3h. The crude peptides after cleavage were precipitated in cold diethyl ether. The precipitate was washed thoroughly with ether and centrifuged to obtain the crude solid products. The crude peptides were then dried and dissolved in CH_3CN/H_2O solvents. The purification was performed using a semi-preparative RP-HPLC (Thermo Fisher Scientific) using C18 µ-Bondapak column (dimensions 250 × 10 mm, particle size 12 µm, pore size 175 Å) at a flow rate of 5 mL/min using a binary solvent system of A (0.1% TFA in H_2O) and solvent B (0.1% TFA in CH_3CN) and a linear gradient from 5 to 100% CH_3CN till 25 mins, followed by 100% CH_3CN till 30 mins and finally lyophilized to obtain the pure peptides.

2.4.5. Procedure for the Synthesis of Cyclic Peptides

The cyclic peptides **T1**, **T2** and **T3** (as discussed in Chapters 4 & 5) were synthesized as follows:

All the cyclic peptides were synthesized first by anchoring Fmoc-Glu-OMe through the C-terminus of its side chain on 200 mg Rink amide MBHA resin, and proceeded further as discussed above. After completion of the linear sequences, the methyl ester at the C-terminus was cleaved using 5 equivalents of LiOH in a minimal amount of H_2O along with DMF for 4 h, followed by Fmoc-cleavage at the N-terminus using 20% piperidine in DMF. Thereafter, on-resin head-to-tail cyclisation were carried out using 3.5 equiv of BOP as the coupling reagent and 7 equiv of DIPEA as base for 24 h. Finally, the cyclic peptides were cleaved from the resin using the above-mentioned cocktail solution and purified.

2.5. References

1. Dev, D.; Palakurthy, N. B.; Thalluri, K.; Chandra, J.; Mandal, B. Ethyl 2-Cyano-2-(2-nitrobenzenesulfonyloxyimino)acetate (o-NosylOXY): A Recyclable Coupling Reagent for Racemization-Free Synthesis of Peptide, Amide, Hydroxamate, and Ester. J. Org. Chem. 2014, 79, 5420-5431.
2. Pandit, S. K.; Das, G. Fluorescent detection of tryptophan in physiological media: Potential applications in environmental samples and living systems. *Sens Actuators B-Chem*. **2024**, *417*, 136131.
3. Benesi, H. A.; Hildebrand, J. H. A spectrophotometric investigation of the interaction of iodine with aromatic hydrocarbons. *J. Am. Chem. Soc*. **1949,** *71*, 2703-2707.
4. Basak, M.; Das, G. Amine-incorporated quinoxaline based fluorescent sensor for detection of trace water: Solvent influenced self-assembly. *Spectrochim. Acta A Mol. Biomol*. **2022,** *280*, 121521.
5. Dolai, G.; Shill, S.; Roy, S.; & Mandal, B. Atomic Insight on Inhibition of Fibrillization of Dipeptides by Replacement of Phenylalanine with Tryptophan. *Langmuir* **2023**, *39*, 9367-9383.
6. Pracht, P.; Bohle, F.; & Grimme, S. Automated exploration of the low-energy chemical space with fast quantum chemical methods. *Phys. Chem. Chem. Phys*. **2020**, *22*, 7169-7192.
7. Marenich, A. V.; Cramer, C. J.; Truhlar, D. G. Universal solvation model based on solute electron density and on a continuum model of the solvent defined by the bulk dielectric constant and atomic surface tensions. *J. Phys. Chem*. **2009,** *113*, 6378-6396.
8. Gaussian 16, Revision C.01, M. J. Frisch.; G. W. Trucks.; H. B. Schlegel.; G. E. Scuseria.; M. A. Robb.; J. R. Cheeseman.; G. Scalmani.; V. Barone.; G. A. Petersson.; H. Nakatsuji.; X. Li. M. Caricato.; A. V. Marenich.; J. Bloino.; B. G. Janesko.; R. Gomperts.; B. Mennucci.; H. P. Hratchian.; J. V. Ortiz.; A. F. Izmaylov.; J. L. Sonnenberg.; D. Williams-Young.; F. Ding.; F. Lipparini.; F. Egidi.; J. Goings.; B. Peng.; A. Petrone.; T. Henderson.; D. Ranasinghe.; V. G. Zakrzewski.; J. Gao.; N. Rega.; G. Zheng.; W. Liang.; M. Hada.; M. Ehara.; K. Toyota.; R. Fukuda.; J. Hasegawa.; M. Ishida.; T. Nakajima.; Y. Honda.; O. Kitao.; H. Nakai.; T. Vreven.; K. Throssell.; J. A. Montgomery.; J. E. Peralta.; F. Ogliaro.; M. J. Bearpark.; J. J Heyd.; E. N. Brothers.; K. N. Kudin.; V. N. Staroverov.; T. A. Keith.; R. Kobayashi.; J. Normand.; K. Raghavachari.; A. P. Rendell.; J. C. Burant.; S. S. Iyengar.; J. Tomasi.; M. Cossi.; J. M. Millam.; M. Klene.; C. Adamo.; R. Cammi.; J. W. Ochterski.; R. L. Martin.; K. Morokuma.; O. Farkas.; J. B. Foresman.; D. J. Fox.; *Gaussian, Inc., Wallingford CT*, **2016**.
9. GaussView, Version 6, R. Dennington.; T. A. Keith.; J. M. Millam.; *Semichem Inc., Shawnee Mission, KS*, **2016**.
10. Becke, A. D. Density-functional thermochemistry. I. The effect of the exchange-only gradient correction. *J. Chem. Phys.* **1992,** *96*, 2155-2160.
11. Clark, T.; Chandrasekhar, J.; Spitznagel, G. W.; Schleyer, P. V. R. Efficient diffuse function-augmented basis sets for anion calculations. III. The 3-21+ G basis set for first-row elements, Li–F. *J. Comput. Chem*. **1983**,*4*, 294-301.

12. Lu, T.; Chen, F. Multiwfn: A multifunctional wavefunction analyzer. *J. Comput. Chem.* **2012,** *33*, 580-592.
13. Humphrey, W.; Dalke, A.; Schulten, K. VMD: visual molecular dynamics. *J. Molec. Graphics* **1996**, *14*, 33-38.
14. Parker, T. M.; Burns, L. A.; Parrish, R. M.; Ryno, A. G.; Sherrill, C. D. Levels of symmetry adapted perturbation theory (SAPT). I. Efficiency and performance for interaction energies. *J. Chem. Phys.* **2014**, *140*.
15. Parrish, R. M.; Burns, L. A.; Smith, D. G.; Simmonett, A. C.; DePrince III, A. E.; Hohenstein, E. G.; Sherrill, C. D. Psi4 1.1: An open-source electronic structure program emphasizing automation, advanced libraries, and interoperability. *J. Chem. Theory Comput*. **2017**, *13*, 3185-3197.
16. Papajak, E.; Truhlar, D. G. Convergent partially augmented basis sets for post-hartree− fock calculations of molecular properties and reaction barrier heights. *J. Chem. Theory Comput.* **2011,** *7*, 10-18.
17. Coin, I.; Beyermann, M.; Bienert, M.; Solid-phase peptide synthesis: from standard procedures to the synthesis of difficult sequences. *Nat*. *Protoc*. **2007**, *2*, 3247-3256.
18. Amblard, M.; Fehrentz, J. A.; Martinez, J.; Subra, G. Methods and Protocols of Modern Solid Phase Peptide Synthesis. *Mol. Biotech.* **2006**, *33*, 239-254.
19. Kaiser, E.; Colescot, R. L.; Bossinge, C. D.; Cook, P. I. Color test for detection of free terminal amino groups in solid phase synthesis of peptides. *Anal. Biochem*. **1970**, *34*, 595-598.

Chapter 3

Unprecedented Binding of Thioflavin T with Well-Ordered Spherical Aggregates: a False Positive?

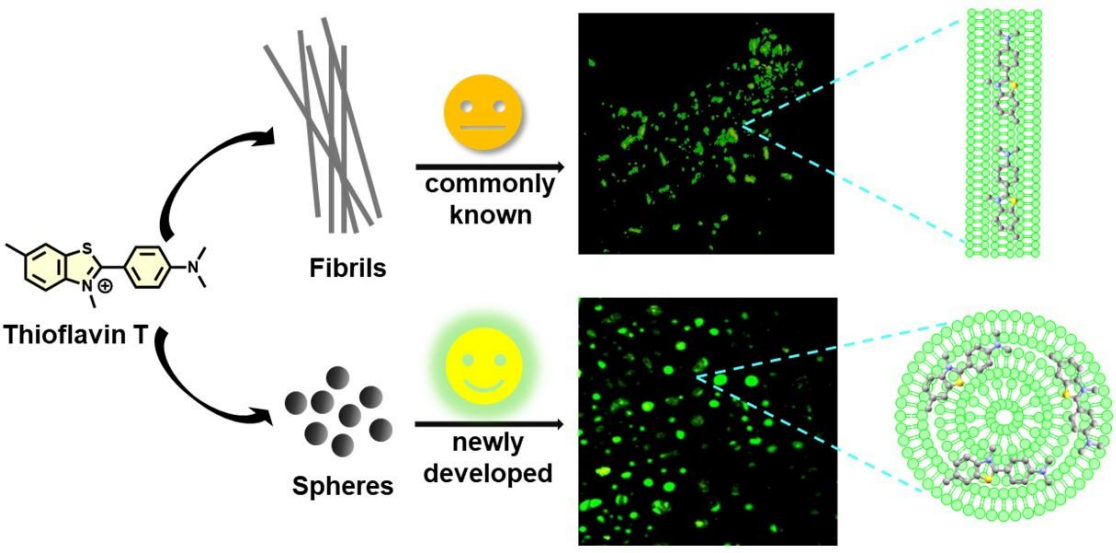

भारतीय प्रौद्योगिकी संस्थान गुवाहाटी
Indian Institute of Technology Guwahati

3.1. Background

Thioflavin T (ThT), a benzothiazole-based fluorescent dye, has long served as a sensitive probe for identifying and characterizing amyloid fibrils; insoluble protein aggregates implicated in various neurodegenerative disorders such as Alzheimer's and Parkinson's diseases. Beyond its classical role in amyloid detection, ThT has recently gained attention for its broader binding versatility. Several studies have demonstrated that ThT can also interact with peptides and biomolecules lacking the characteristic β-sheet-rich fibrillar organization typically associated with amyloids.[1-4]

Notably, the interaction of ThT with non-fibrillar systems has revealed alternative binding mechanisms and diverse fluorescence behaviors. For instance, Rosenberry et al.[5] discovered that ThT selectively binds to the peripheral anionic site (P-site) of human acetylcholinesterase (AChE), a region devoid of amyloid-like β-sheet structure could induce a significant ~1000-fold increase in fluorescence emission. Similarly, Dzwolak and co-workers[6] showed that ThT can form ordered complexes with α-helical poly-L-glutamic acid (PLGA), suggesting that β-sheet stacking and π–π interactions are not the only structural prerequisites for ThT-protein association. In addition, Ranjan et al.[2] demonstrated that ThT can act as a powerful fluorescence reporter for non-canonical nucleic acid conformations, including duplexes, triplexes, and G-quadruplexes, thereby broadening its scope to monitor DNA conformational transitions, enzymatic processes, and cellular binding events. Moreover, Sulatskaya et al.[7] reported that under highly acidic conditions (pH 2), proteins and peptides possessing a net positive charge exceeding +0.18 fail to exhibit ThT staining. Consequently, amyloid detection under such conditions may yield false negatives, as increasing acidity was found to suppress ThT fluorescence intensity even upon fibril binding.[8,9] In this study, we aim to explore how Thioflavin T (ThT) interacts with peptide structures that do not exhibit fibrillar morphology and neither remain in β-sheet-rich conformations.

3.2. Design, Synthesis & Characterization of the Peptides

The design of the dipeptides was inspired by the hydrophobic core motif of the Aβ-peptide. Recently, our group has investigated on the atomic-level molecular arrangement, self-assembly, and morphology of **FW** (Boc-FW-OMe) and **VW** (Boc-VW-OMe), tryptophan-

containing analogs of biologically relevant VF and FF dipeptides.[10] It was observed that, just by replacing Phe with Trp, the morphology of the dipeptides changes from fiber to nanosphere.

Therefore, we designed four dipeptides, namely, Boc-Phe-Trp-OMe (**FW**), Boc-Val-Trp-OMe (**VW**), Boc-Leu-Trp-OMe (**LW**), and Boc-Ile-Trp-OMe (**IW**), which gave rise to distinct nano-spherical morphologies. The N-terminus and C-terminus of the peptides were protected using Boc and OMe groups, respectively, ensuring that any variations in their self-assembly behaviour arise solely from differences in the peptide side chains, and with these designed dipeptides, we aimed to evaluate their ability to inhibit $A\beta_{1\text{-}40}$ fibril formation under near-physiological conditions.

The designed dipeptides were synthesized in the solution phase using a standard synthetic protocol (Scheme 3.1).[11,12]

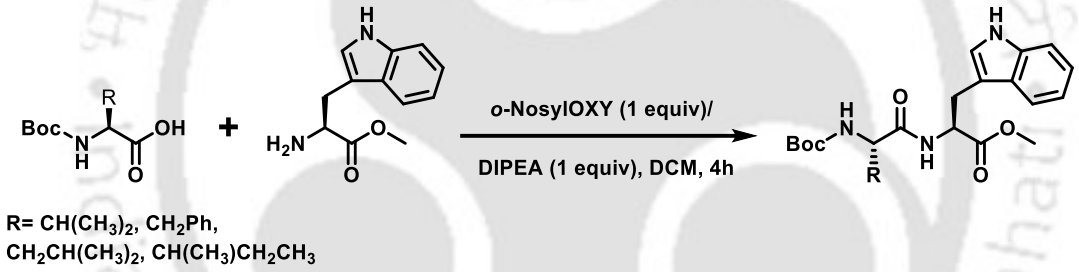

Scheme 3.1*. Schematic representation of the synthesis of dipeptides in solution.*

The protected dipeptides were synthesized in solution phase using *o*-NosylOXY, a recently developed modern coupling reagent, with DCM serving as the reaction solvent. For the synthesis, one amino acid contained a Boc (tert-butyloxycarbonyl) group protecting at the N-terminus, while the other was used in its methyl ester-protected C-terminal form. Following successful coupling, the crude products were purified through column chromatography to obtain the desired pure dipeptides. The characterisation of the synthesized compounds was achieved using 1D ^{1}H and ^{13}C NMR spectroscopy and Mass spectrometry.

3.3. Fluorescence Spectroscopic & Microscopic Study

In order to examine how tryptophan-containing dipeptides influence the aggregation process of $A\beta_{1\text{–}40}$ under conditions that closely mimic physiological environments, we

performed the following experiments. Initially, $A\beta_{1-40}$ (20 μM) was incubated alone in phosphate-buffered saline (PBS, 50 mM, pH 7.4) at 37 °C, and its aggregation was monitored using Thioflavin T (ThT) fluorescence. As expected, the fluorescence intensity gradually increased over time, reaching its highest value after approximately 48 hours, indicating the progressive formation of amyloid fibrils. When $A\beta_{1-40}$ (20 μM) was co-incubated with a fivefold molar excess of the dipeptides FW (100 μM) and VW (100 μM), only a slight or negligible reduction in fluorescence intensity was observed, suggesting that at this concentration, the dipeptides had little to no impact on fibril formation (Figure 3.1a). To further explore their potential inhibitory capacity, we increased the dipeptide concentrations. Interestingly, rather than suppressing amyloid formation, higher concentrations of FW and VW corresponding to 15- and 30-fold molar excess (300 μM and 600 μM, respectively), produced an even greater increase in ThT fluorescence compared to $A\beta_{1-40}$ alone (Figure 3.1b). This observation was contrary to our initial expectation that the dipeptides would interfere with or reduce fibril formation.

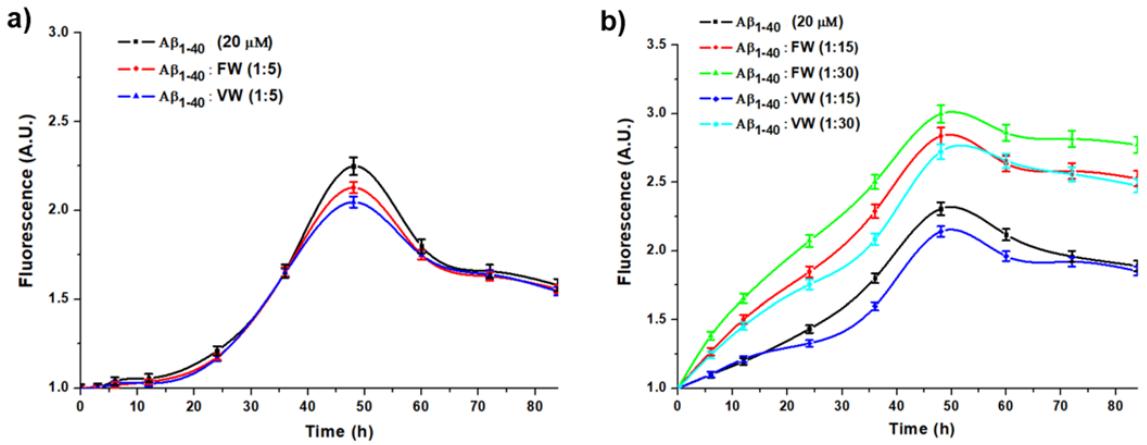

Figure 3.1. *Time-dependent ThT fluorescence assay of a). $A\beta_{1-40}$ in the absence and the presence of 5- fold molar excesses of FW and VW. b). $A\beta_{1-40}$ in the absence and the presence of 15- and 30- fold molar excess of FW and VW.*

To gain insights into the structural consequences of this co-incubation, field emission transmission electron microscopy (FETEM) was conducted on the samples containing $A\beta_{1-40}$ (20 μM) incubated with FW (300 μM) and VW (300 μM) for 48 hours under identical conditions. The microscopic images revealed that both components retained their characteristic morphologies: the fibrous structures of $A\beta_{1-40}$ and the spherical assemblies of the dipeptides were clearly visible and coexisted without any noticeable disruption (Figure

3.2). These findings imply that the dipeptides do not interfere with the fibrillation of $A\beta_{1-40}$ nor alter its morphology. Instead, the unexpected increase in ThT fluorescence can be rationalized as an additive effect, most likely arising from the independent interaction of ThT with both the $A\beta_{1-40}$ fibrils and the self-assembled dipeptide nanostructures.

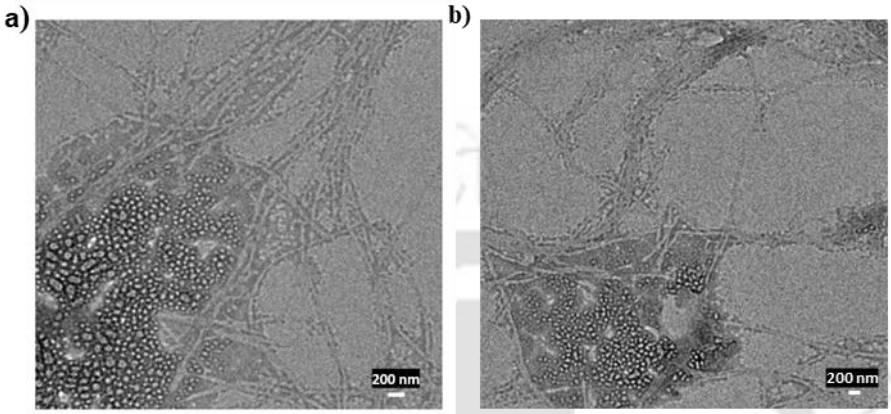

Figure 3.2. *FETEM images of $A\beta_{1-40}$ (20 μM) co-incubated with (a) FW (300 μM), (b) VW (300 μM) after 4 days of incubation in PBS, pH 7.4 at 37 ℃.*

To further understand the unexpected fluorescence enhancement observed in the co-incubation studies, we examined the intrinsic interaction of the dipeptides with ThT through time-dependent fluorescence assays. Interestingly, even in the absence of $A\beta_{1-40}$, the fluorescence intensity of ThT gradually increased when incubated with the dipeptides alone, indicating that the dipeptides themselves are capable of binding to ThT. Moreover, the intensity of fluorescence was found to rise gradually with increasing concentrations of the dipeptides, suggesting a concentration-dependent association between ThT and these peptide assemblies.

To determine whether this interaction was specific to the dipeptides FW and VW or reflected a broader phenomenon, two additional dipeptides, LW and IW, were synthesized following the same design strategy (Scheme 3.1). ThT fluorescence assays conducted under identical conditions demonstrated that LW and IW, both of which self-assemble into distinct spherical nanostructures, also exhibited a time-dependent and concentration-dependent increase in ThT fluorescence (Figure 3.3). These results imply that ThT binding is not unique to a particular dipeptide sequence but may represent a more general property of peptides that organize into spherical morphologies with heterogeneous conformational characteristics.

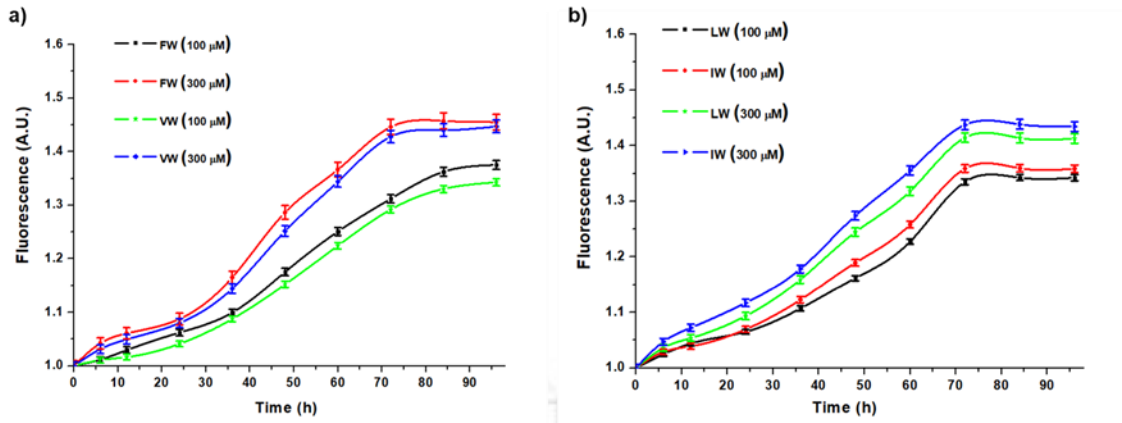

Figure 3.3. *Time-dependent ThT fluorescence assay of the dipeptides alone.*

Comparable findings have been reported by Zhang et al.,[13] who investigated a series of fluorinated dipeptides constructed from fluorinated phenylalanine (Z) linked with natural amino acids such as phenylalanine (F), tyrosine (Y), and tryptophan (W). Their study revealed that while FZ, ZF, and ZY formed ribbon-like nanofibers that strongly interacted with ThT, the dipeptides YZ, WZ, and ZW self-assembled into spherical nanoparticles that also bound ThT, albeit with comparatively weaker fluorescence enhancement. This correlation between molecular architecture and ThT response highlights how supramolecular organization can influence the extent of dye binding. Although the fluorescence intensity associated with spherical aggregates is generally lower than that produced by amyloid-like fibrils, such observations provide important clues regarding the structural and chemical factors that modulate ThT association.

To further validate the ThT-dipeptide interaction, fluorescence microscopy was employed. Samples of the dipeptides (300 μM), incubated for four days, were mixed with ThT (50 μM) in a 1:1 ratio and drop-cast onto glass slides for imaging. Upon microscopic examination, the spherical structures displayed bright green fluorescence, offering clear visual confirmation of ThT binding to the dipeptide assemblies (Figure 3.4). This direct observation complements the fluorescence assay data and establishes that the self-assembled dipeptide nanostructures possess distinct affinity toward the ThT molecule.

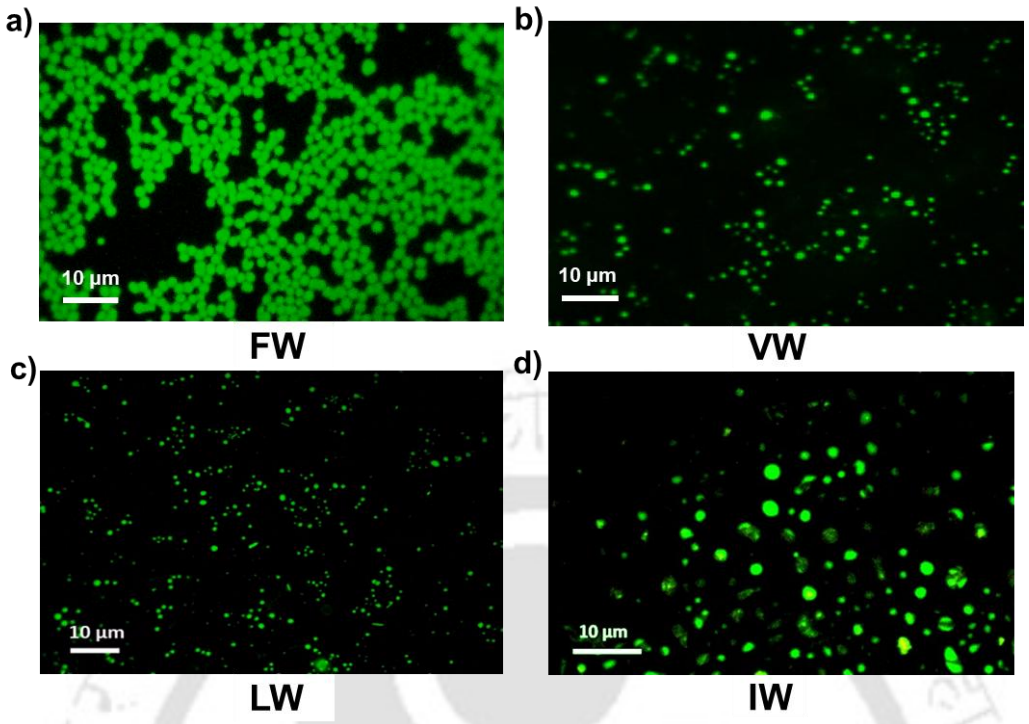

Figure 3.4. *Thioflavin T (50 µM) mixed dipeptides (300 µM each) displaying bright green, fluorescent images on binding with a) FW, b) VW, c) LW, and d) IW.*

3.3.1. Fluorescence Titration Analysis:

To gain deeper insight into the fluorescence enhancement behaviour observed upon increasing the concentration of the dipeptides and to extract relevant quantitative parameters, fluorescence titration experiments were carried out using ThT and the dipeptide assemblies. In this study, peptide solutions of FW, VW, LW, and IW, each pre-incubated for three days, were prepared at varying concentrations ranging from 10 µM to 600 µM. Upon performing a fluorescence assay using these peptide solutions of different concentrations with ThT, a progressive enhancement in fluorescence intensity was observed with increasing peptide concentration (Figure 3.5). The fluorescence signal continued to rise until it reached a plateau near 400 µM, indicating saturation of the binding sites.

From this titration analysis, important parameters such as the limit of detection (LOD) and apparent binding constants were determined (Figure 3.6). The binding constants were calculated using the Benesi–Hildebrand method, where emission intensity values at 485 nm were employed to construct double reciprocal plots of $(I_{max} - I_{min}) / (I - I_{min})$ versus 1/

[peptide]. Each plot exhibited a strong linear relationship with correlation coefficients ($r^2 \approx 0.99$), confirming the formation of a 1:1 complex between ThT and the respective dipeptides.[14]

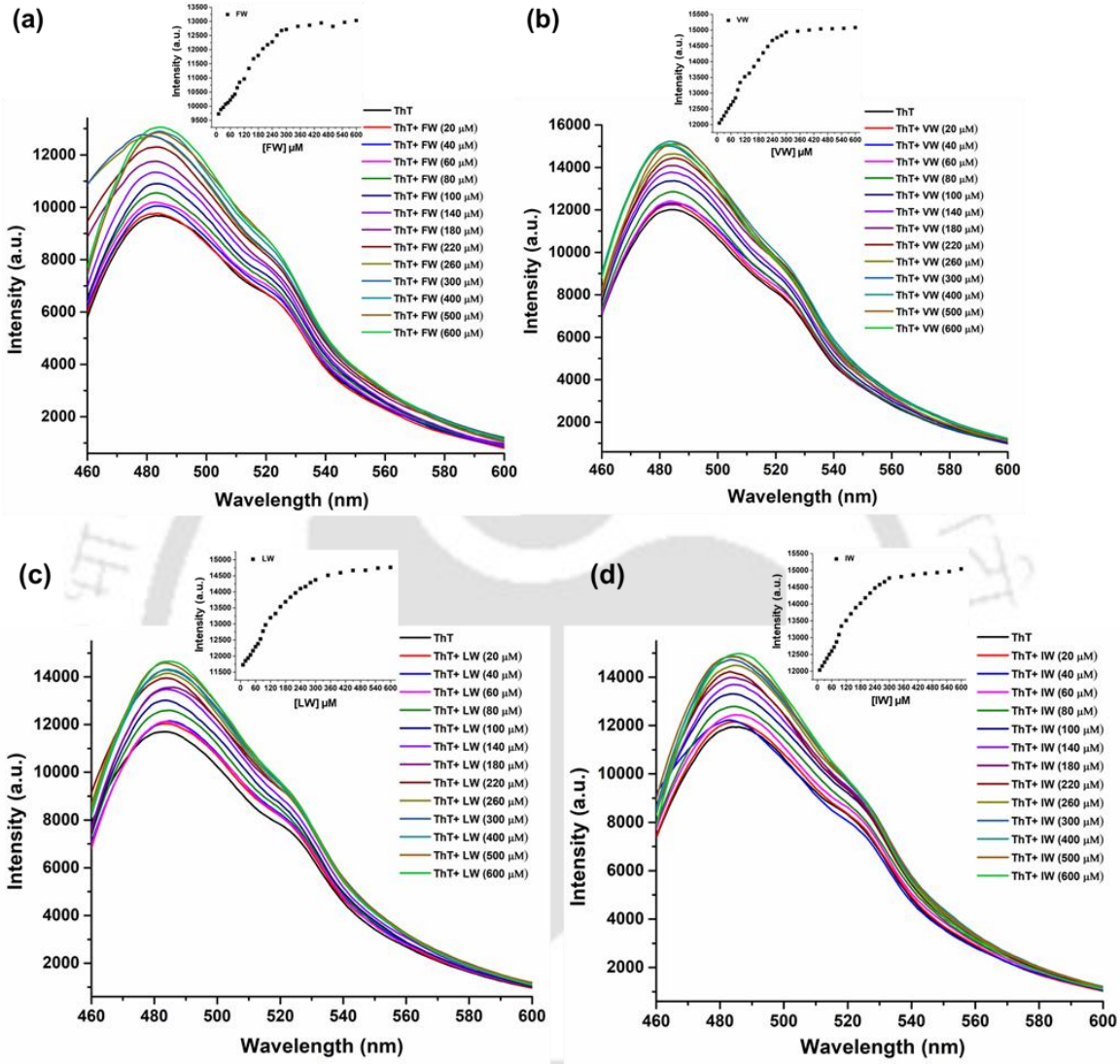

Figure 3.5. *Fluorescence titration spectra of ThT (50 μM) with varying concentrations of a) FW, b) VW, c) LW, and d) IW. [Inset: Fluorescence intensity at 485 nm vs. concentration of dipeptides, λ_{ex} = 445 nm].*

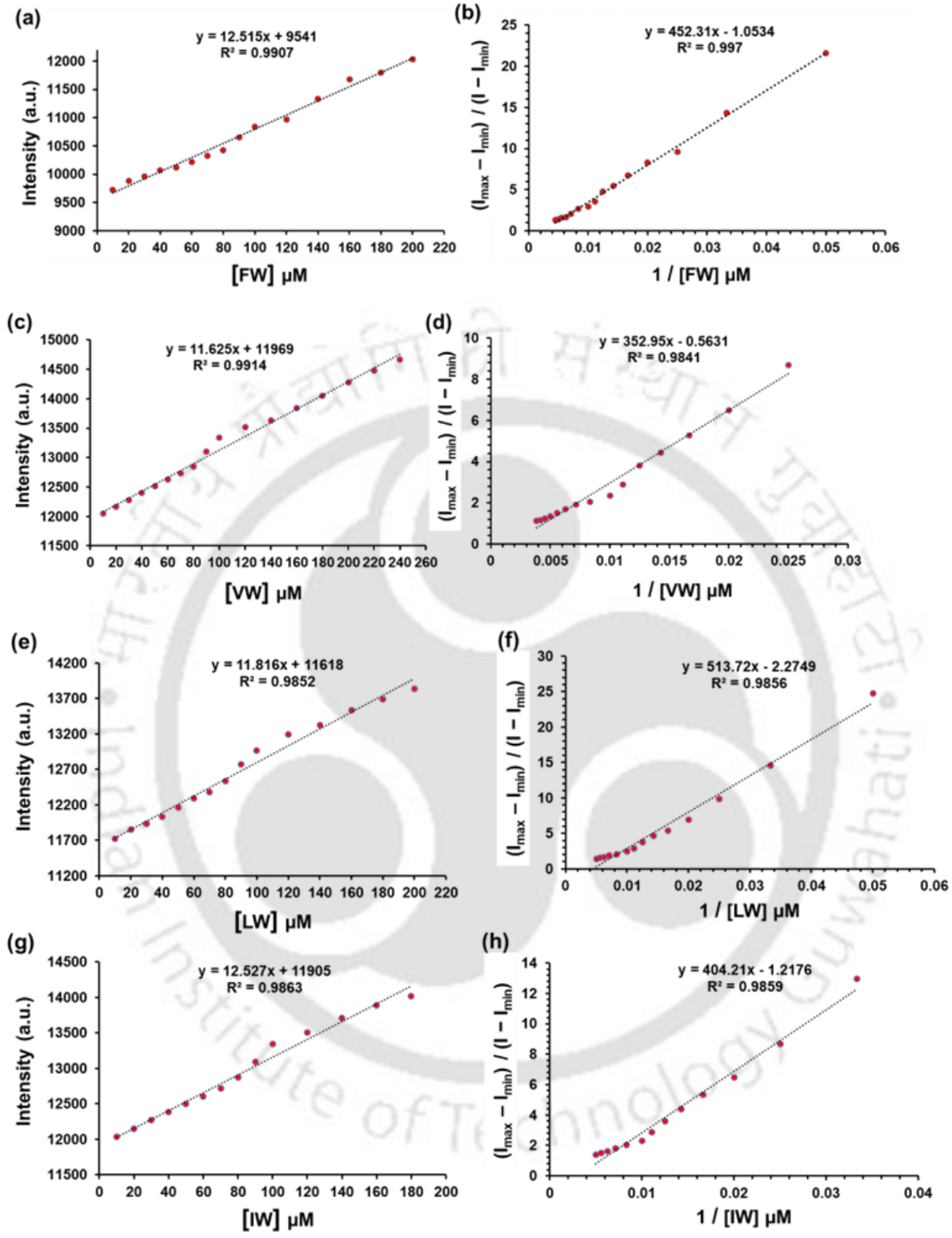

Figure 3.6. *Determination of detection limit and binding constants for a,b) ThT-FW complex, c,d) ThT-VW complex, e,f) ThT-LW complex, and g,h) ThT-IW complex, respectively.*

The calculated LOD and binding constant (K) values were tabulated below (Table 3.1). These K values indicate a moderate but definite binding affinity between ThT and the dipeptides. Moreover, the observed binding constants were lower than those reported for

ethidium bromide (1.6×10^6 M^{-1})[15], implying that the interaction between ThT and the dipeptide assemblies is not of an intercalative nature.[16]

Table 3.1. Calculated Limit of Detection and Binding constant values for ThT-dipeptide complexes.

Sample	Solvent system	Limit of detection (LOD)	Binding constant, K (M^{-1})
ThT-FW complex	PBS (pH 7.4)	9.2 µM	0.22 × 10^4
ThT-VW complex	PBS (pH 7.4)	14.4 µM	0.28 × 10^4
ThT-LW complex	PBS (pH 7.4)	15.3 µM	0.19 × 10^4
ThT-IW complex	PBS (pH 7.4)	14.3 µM	0.24 × 10^4

3.3.2. Quantum Yield Calculations:

The relative quantum yields of free ThT and its complexes with the dipeptide assemblies were evaluated using fluorescein as the reference standard. Interestingly, the ThT–dipeptide complexes exhibited significantly higher quantum yield values than the free dye, which showed a comparatively low quantum yield (Φ = 0.006) (Table 3.2). This enhancement indicates that upon association with the dipeptide aggregates, the photophysical properties of ThT are altered in a way that promotes greater fluorescence efficiency. Such an effect can be attributed to the stabilization of the dye's excited state through its interaction with the peptide matrix. The binding likely restricts the rotational and vibrational degrees of freedom of the ThT molecules, thereby suppressing nonradiative relaxation pathways and enhancing radiative emission processes.[17] As a result, the ThT–dipeptide complexes display enhanced fluorescence emission relative to the unbound dye.

Table 3.2. Calculated relative quantum yield values for ThT and ThT-dipeptide complexes.

Sample	Area under emission spectra	Abs at 445 nm	Refractive Index	Relative Quantum Yield
Fluorescein	1.6 × 10^7	0.0098	1.33	92 % (Known)
ThT	4.77 × 10^5	0.0427	1.33	0.6 %

ThT-FW complex	7.02 × 10^5	0.0219	1.33	1.8 %
ThT-VW complex	6.63 × 10^5	0.0254	1.33	1.4 %
ThT-LW complex	5.68 × 10^5	0.0277	1.33	1.1 %
ThT-IW complex	5.82 × 10^5	0.0355	1.33	1.0 %

3.4. Theoretical Study

To further validate the experimental findings and understand the atypical interaction between ThT and the designed dipeptides, density functional theory (DFT) calculations were carried out. DFT was chosen as it offers valuable insights into the electronic structure, spatial orientation, and reactivity of molecular systems, thereby enabling a deeper understanding of intermolecular associations. In particular, non-covalent interaction (NCI) analysis combined with reduced density gradient (RDG) mapping was employed to characterize the nature and strength of the weak forces governing the ThT–dipeptide complexes. These computational tools are particularly useful for visualizing non-covalent regions and distinguishing among hydrogen bonding, van der Waals, and steric interactions within a molecular system.[18-20]

3.4.1. NCI-RDG Analysis:

The NCI plot serves as an efficient means to locate and interpret regions of weak interactions in molecular assemblies. This method utilizes RDG values to identify interaction zones based on electron density and its derivatives. In the corresponding scatter plots, blue regions denote attractive hydrogen-bonding interactions, green regions represent van der Waals forces, and red areas correspond to steric repulsion between molecular fragments. The RDG is plotted against the product of electron density (ρ) and the sign of the second-largest eigenvalue of the Hessian matrix (λ_2), according to the following Equation (3.1).[21-23]

$$RDG(r) = \frac{1}{2(3\pi^2)^{\frac{1}{3}}} \times \frac{|\nabla\rho(r)|}{\rho(r)^{\frac{4}{3}}} \qquad (3.1)$$

Positive values of sign (λ_2) ρ indicate repulsive (steric) interactions, negative values correspond to attractive interactions such as hydrogen bonding, and values near zero represent weak van der Waals interactions arising from dispersion and dipole-induced effects.[24,25]

The 2D scatter plots and RDG isosurfaces for the ThT–dipeptide complexes (Figure 3.7) reveal distinct interaction profiles. For the ThT–FW complex, the sign (λ_2) ρ values range from approximately −0.02 to 0.03 a.u., whereas for the ThT–VW, ThT–LW, and ThT–IW complexes, the values fall within the range of −0.015 to 0.03 a.u. All complexes exhibit similar steric repulsive interactions in the positive region of the plots. However, comparison of the left (negative) region of the scatter plots, which represents attractive forces, shows that the ThT–FW complex exhibits relatively stronger van der Waals interactions, with sign (λ_2) ρ around −0.02 a.u., compared to the slightly weaker interactions observed for the other three dipeptides (around −0.015 a.u.).

These observations suggest that ThT interacts with all the studied dipeptides predominantly through non-covalent interactions such as van der Waals forces and π–π stacking. The relatively enhanced interaction in the ThT–FW complex may originate from the additional aromatic π-system in FW, which facilitates stronger π–π interactions with ThT. Moreover, FW displays a higher degree of β-sheet content compared to VW, LW, and IW (as shown in Table 3.6), which may further stabilize its interaction with ThT molecules. Overall, the computational analysis strongly supports the experimental results obtained from fluorescence spectroscopy and microscopy, reinforcing that the ThT–dipeptide association is governed mainly by non-covalent forces, with FW showing a slightly higher affinity due to its aromatic character and secondary structural features.

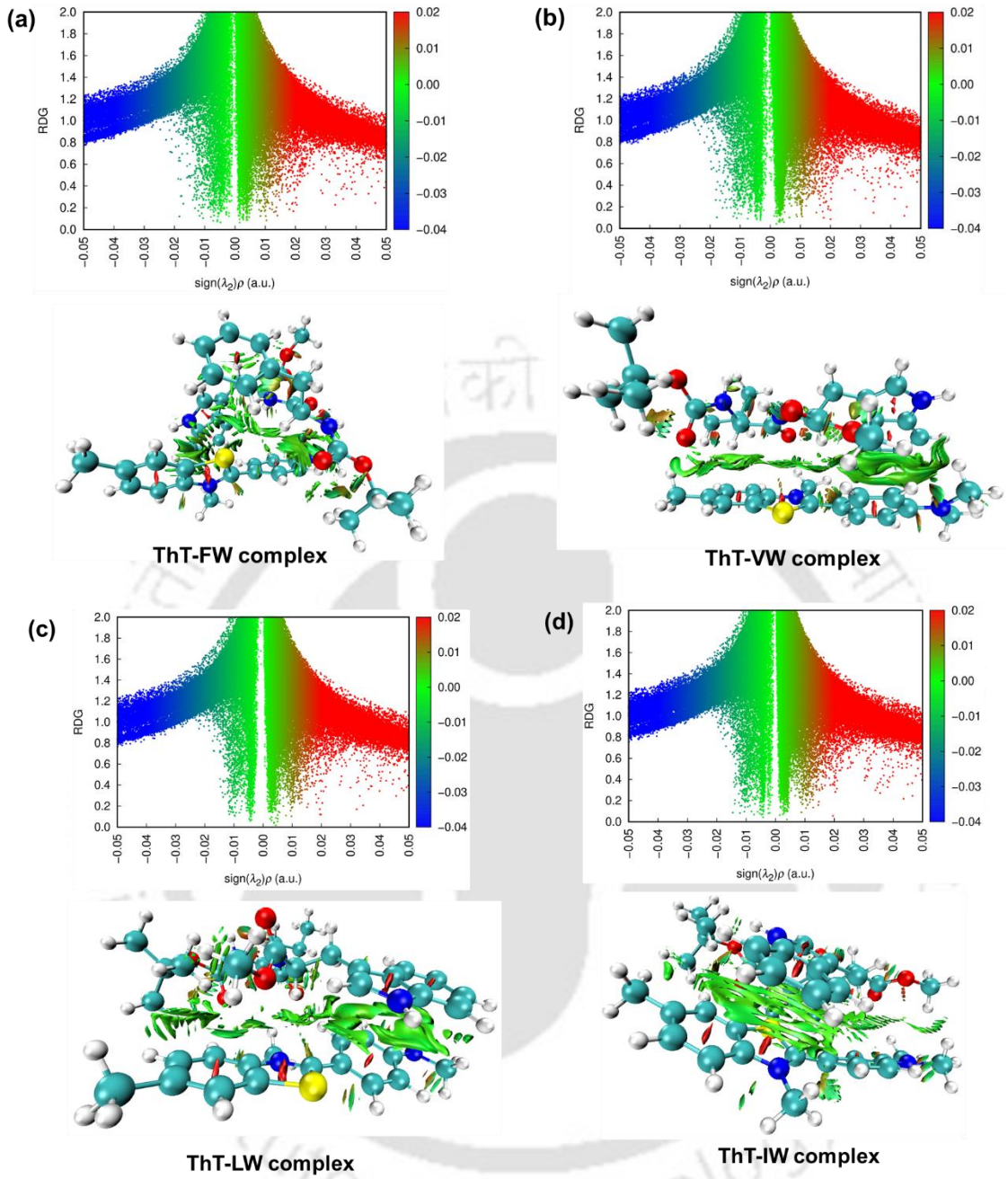

Figure 3.7. *2D scatter graph and reduced gradient density surface analysis for (a) FW-ThT complex, (b) VW-ThT complex, (c) LW-ThT complex, and (d) IW-ThT complex.*

3.4.2. EDA Analysis:

To gain deeper insight into the nature of interactions between Thioflavin T (ThT) and the dipeptides, computational studies were performed using the zeroth-order symmetry-adapted perturbation theory (SAPT0) approach.[26] In this method, ThT and each dipeptide were treated as separate molecular fragments interacting within a singlet electronic state

framework. The total interaction energy, [ΔE_{int} (SAPT0)], was divided into four primary components: electrostatic (E_{elst}), exchange (E_{exch}), induction (E_{ind}), and dispersion (E_{disp}) terms[27,28]. The electrostatic term (E_{elst}) represents the classical Coulombic attraction between the charge distributions of the interacting fragments, while the exchange term (E_{exch}) arises from the Pauli exclusion principle, accounting for repulsive interactions due to electron density overlap. The induction component (E_{ind}) corresponds to the interaction between the permanent and induced multipoles, and the dispersion term (E_{disp}) reflects the electron correlation effects responsible for London dispersion or van der Waals forces. The overall interaction energy can therefore be expressed as the sum of these four contributions, as shown in Equation (3.2).

$$\Delta E_{int}(SAPT0) = E_{elst} + E_{exch} + E_{ind} + E_{disp} \qquad (3.2)$$

The results of the energy decomposition analysis (EDA) revealed that the dispersion term (E_{disp}) contributes most significantly to the total interaction energy (Table 3.3). This indicates that weak non-covalent interactions, particularly van der Waals forces, are the primary stabilizing factor in the ThT–dipeptide complexes. Such dominance of dispersion interactions suggests that ThT binding to the dipeptide assemblies is largely governed by these weak but pervasive attractive forces.

Table 3.3. Energy decomposition analysis (EDA) displaying the contribution of different factors in the total interaction energy (kcal/mol) for the ThT-dipeptide complexes.

Complex	E_{elst}	E_{exch}	E_{ind}	E_{disp}	$\Delta E_{int}(SAPT0)$
THT-FW	−13.82	26.11	−6.33	−32.92	−26.85
THT-VW	−17.28	25.00	−5.39	−31.36	−29.04
THT-LW	−20.58	26.33	−7.67	−31.38	−33.31
THT-IW	−15.74	29.11	−7.69	−34.69	−29.02

3.4.3. Thermodynamic Parameters Study:

The optimized energies of all systems, including Thioflavin T (ThT), the individual dipeptides, and their corresponding ThT–dipeptide complexes, were evaluated using density functional theory (DFT) at the B3LYP-D3/6-31++G level of theory. The computed parameters, namely, the corrected zero-point energies (EE + ZPE), enthalpies (H), and Gibbs free energies (G), are summarized (Table 3.4). Based on these values, the thermodynamic parameters such as the change in Gibbs free energy (ΔG^o), enthalpy (ΔH^o), and entropy (ΔS^o) associated with the complex formation were subsequently determined and are presented (Table 3.5). The entropy change was calculated using Equation (3.3).

$$\Delta G^\circ = \Delta H^\circ - T\Delta S^\circ \qquad (3.3)$$

Thermodynamic quantities provide valuable insights into the nature of non-covalent interactions that stabilize molecular complexes. Generally, positive values of both ΔH^o and ΔS^o are indicative of hydrophobic interactions, while a negative ΔH^o coupled with a positive ΔS^o reflects electrostatic forces. Conversely, when both ΔH^o and ΔS^o exhibit negative values, the dominant interactions are attributed to hydrogen bonding and van der Waals forces.[29,30] In the present study, the calculated Gibbs free energy changes (ΔG^o) for all ThT–dipeptide complexes were negative, signifying that the binding process occurs spontaneously. Moreover, the simultaneous negative values of ΔH^o and ΔS^o suggest that the association between ThT and the dipeptides is primarily driven by van der Waals interactions. The exothermic nature of all the ThT–dipeptide complexes formation was reflected by the negative ΔH^o values.

Table 3.4. The corrected zero-point energies (EE+ZPE), enthalpies (H), and Gibbs free energies (G) of the species were computed at the B3LYP-D3/6-31++G level. All energies are in Hartree.

Species	EE+ZPE	Enthalpy, H	Gibbs Free Energy, G
THT	−1166.321483	−1166.301662	−1166.369380
FW	−1549.090698	−1549.056794	−1549.159613
VW	−1396.712707	−1396.680492	−1396.776971
LW	−1435.987969	−1435.954451	−1436.055487
IW	−1435.990114	−1435.956396	−1436.058294

THT-FW	–2715.447962	–2715.393822	–2715.539327
THT-VW	–2563.063845	–2563.011599	–2563.151445
THT-LW	–2602.339120	–2602.285474	–2602.428359
THT-IW	–2602.341980	–2602.288275	–2602.431404

Table 3.5. Thermodynamic parameters for the interaction between ThT and the dipeptide molecules at temperature, T = 298 K, computed at the B3LYP-D3/6-31++G level.

Complexes	**ΔG°** **(kcal/mol)**	**ΔH°** **(kcal/mol)**	**ΔS°** **(cal/mol.K)**
THT-FW	–6.4845	–22.1921	–52.6219
THT-VW	–3.1964	–18.4767	–51.2700
THT-LW	–2.1912	–18.4240	–54.4724
THT-IW	–2.3405	–18.9611	–55.7738

3.5. Morphology Study

To examine the morphological characteristics of the designed peptides, we employed field emission scanning electron microscopy (FE-SEM) and field emission transmission electron microscopy (FE-TEM). For these analyses, 300 μM solutions of each peptide (FW, VW, LW, and IW) were prepared in phosphate-buffered saline (PBS, pH 7.4) and incubated at 37 °C for four days to allow self-assembly. The FE-SEM images revealed that all four peptides self-assembled into well-defined spherical nanostructures with diameters ranging between 400 and 600 nm (Figure 3.8).

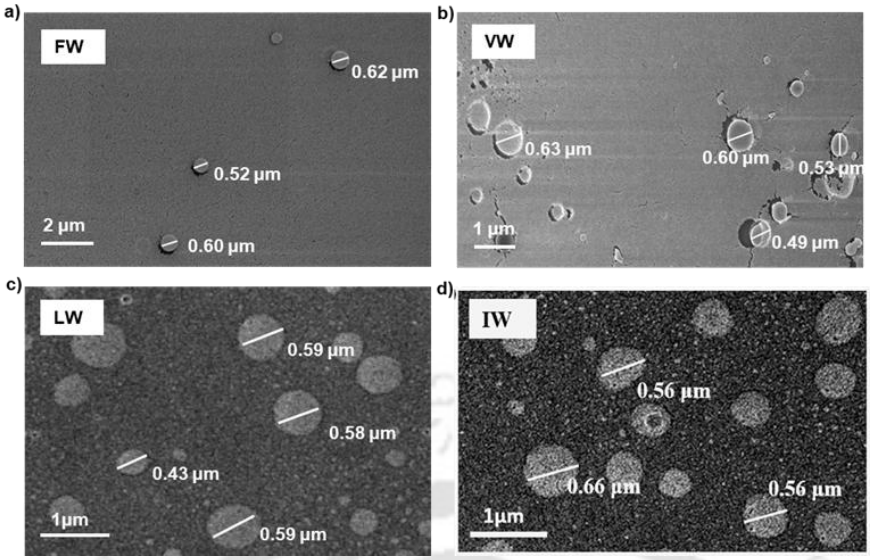

Figure 3.8. *FESEM images displaying the spherical morphology of the dipeptides (a) FW, (b) VW, (c) LW, and (d) IW and their respective diameters.*

To gain a more detailed understanding of their morphology, FE-TEM measurements were also carried out under similar conditions. Consistent with the FE-SEM observations, the FE-TEM images confirmed that each peptide formed uniform nano-spherical assemblies within the same size range of approximately 400-600 nm (Figure 3.9). The close agreement between the FE-SEM and FE-TEM results indicates the reproducibility and structural stability of these spherical nanostructures formed by the Trp-containing dipeptides.

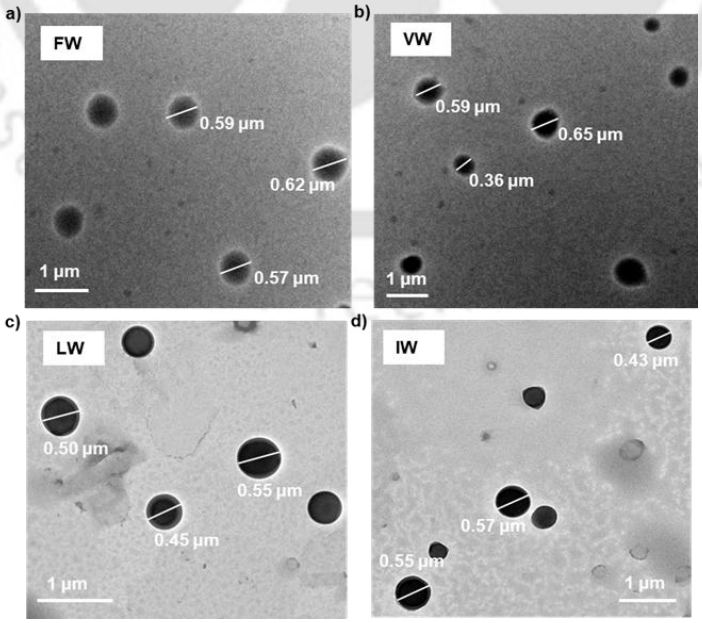

Figure 3.9. *FETEM images displaying the spherical morphology of the dipeptides (a) FW, (b) VW, (c) LW, and (d) IW and their respective diameters.*

3.6. DLS Study

The particle size distribution of the spherical assemblies was further analyzed using dynamic light scattering (DLS) to complement the morphological observations obtained from FE-SEM and FETEM analyses. For this measurement, peptide solutions (300 μM) that had been incubated in PBS buffer for four days were used. The DLS results revealed that the hydrodynamic diameters of the spherical assemblies formed by FW, VW, LW, and IW were approximately 615.5 nm, 650.0 nm, 501.0 nm, and 523.1 nm, respectively (Figure 3.10). These values are in good agreement with the dimensions observed in the electron microscopy studies, thereby confirming the formation of well-defined spherical nanostructures in solutions.

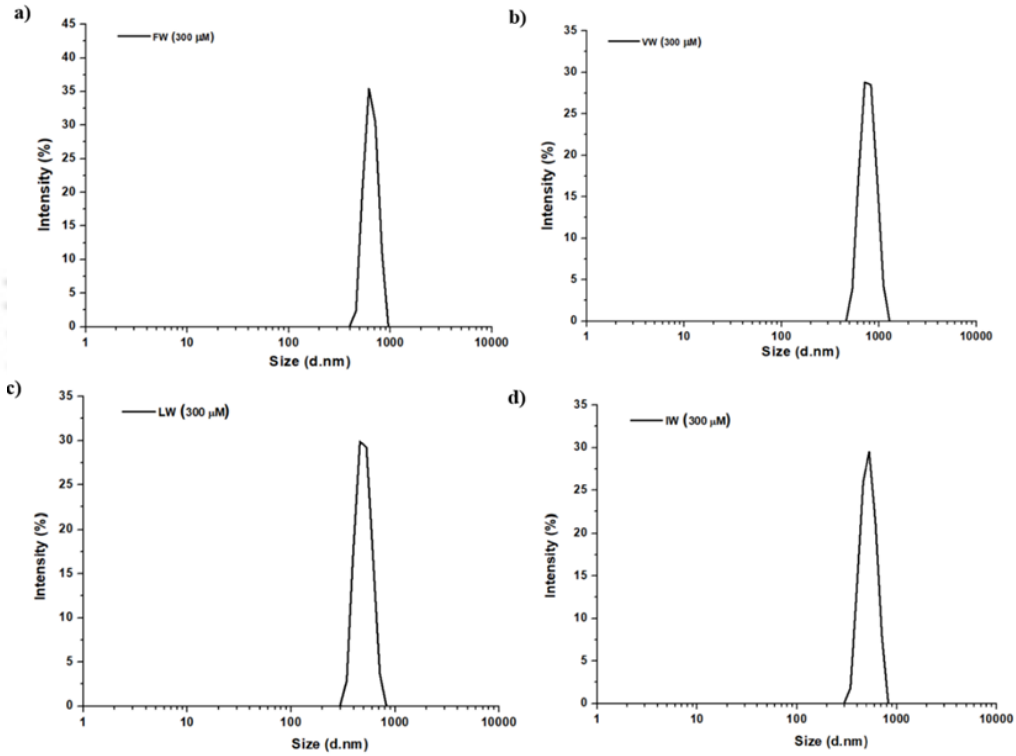

Figure 3.10. *Size distribution plot in DLS experiment of dipeptides (a) FW, (b) VW, (c) LW, and (d) IW exhibiting hydrodynamic diameters of 615.5 nm, 650 nm, 501 nm, and 523.1 nm, respectively, with polydispersity index of 0.372, 0.441, 0.638, and 0.603, respectively.*

3.7. Conformational Analysis

To gain insight into the conformational characteristics of the dipeptides, circular dichroism (CD) and solid-state Fourier-transform infrared (FTIR) spectroscopy analyses were carried

out. All sample solutions were prepared following the same procedure described earlier, and those incubated for four days were used for CD measurements. For FTIR analysis, the corresponding four-day-old solutions were lyophilized to obtain solid samples.

The CD spectra of all Trp-containing dipeptides, FW, VW, LW, and IW, displayed a distinct positive band around 230 nm, a characteristic feature of the tryptophan moiety.[31,32] In addition, each dipeptide exhibited a negative band in the 200–220 nm region, indicative of a combination of random coil and β-sheet conformations.[33,34] Among them, the FW dipeptide, which consists of two aromatic residues, showed a pronounced negative band near 217 nm, signifying the presence of both β-turn and β-sheet structural elements. In contrast, VW, LW, and IW, composed of aliphatic–aromatic amino acid residues, displayed two negative bands around 200 and 217 nm, suggesting the coexistence of random coil and β-sheet conformations (Figure 3.11). The relative contributions of different secondary structural motifs were further quantified using Reed's reference spectra, and the estimated values are summarized (Table 3.6).

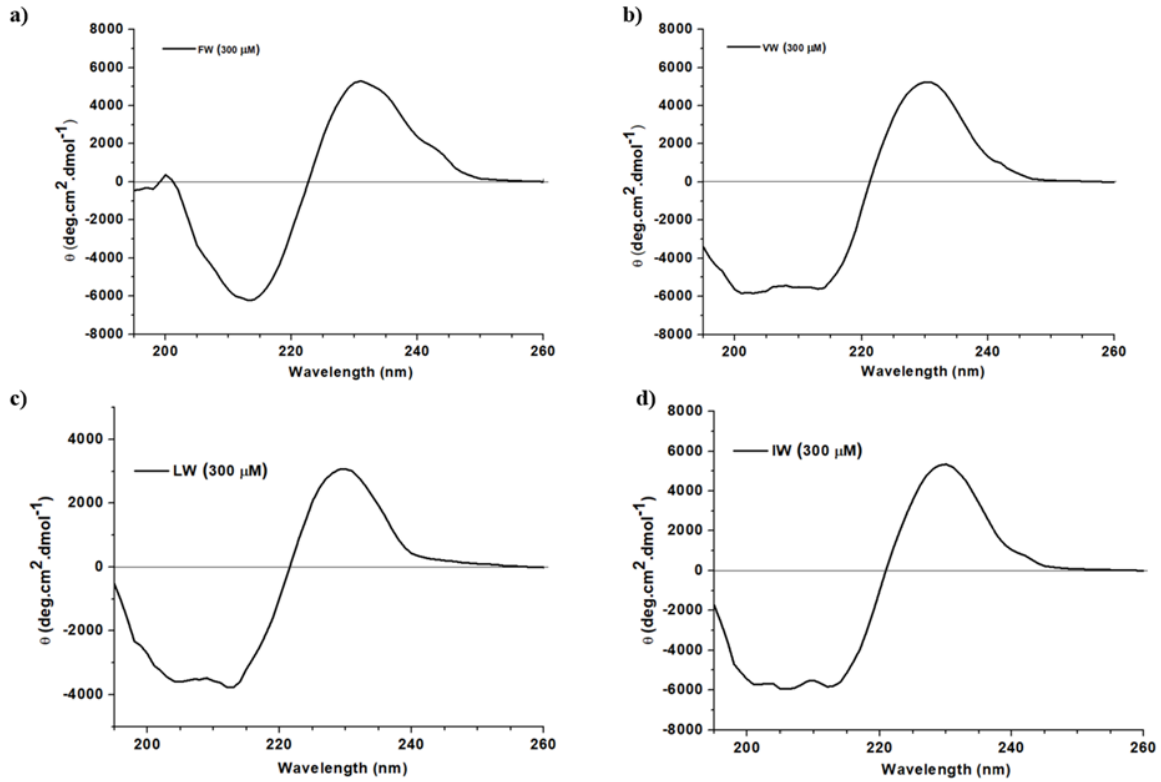

Figure 3.11. *CD spectra of 4-days old, incubated sample solution of (a) FW, (b) VW, (c) LW, and (d) IW (300 μM each) in PBS buffer, pH 7.4 at 37 ºC.*

Table 3.6. Estimation of % of Secondary Structure for the analyzed Dipeptides.

Peptide	Beta (%)	Turn (%)	Random (%)
FW	27.3	23.3	49.4
VW	23.8	24	52.2
LW	25.5	23.5	51.1
IW	26.5	21.2	52.3

Complementary solid-state FTIR measurements were conducted to substantiate the CD observations. The amide I region (1600–1700 cm^{-1}), primarily arising from C=O stretching vibrations, and the amide II region (1510–1580 cm^{-1}), corresponding to N–H bending and C–N stretching, provide crucial information about peptide backbone conformations. All four dipeptides exhibited similar spectral features, with amide I bands appearing between 1651 and 1694 cm^{-1} and amide II bands near 1519–1521 cm^{-1}. Specifically, FW showed amide I peaks at 1668 and 1688 cm^{-1} and an amide II band at 1519 cm^{-1}; VW exhibited amide I peaks at 1651 and 1689 cm^{-1} and an amide II band at 1521 cm^{-1}; LW displayed amide I bands at 1658 and 1694 cm^{-1}; and IW showed peaks at 1653 and 1688 cm^{-1} with an amide II band at 1520 cm^{-1}. These spectral signatures are consistent with the coexistence of β-turns, hydrogen-bonded antiparallel arrangements, and disordered structures[35-37] (Figure 3.12). Overall, the results indicate that the dipeptides do not adopt a single well-defined conformation but rather exist as a dynamic mixture of secondary structural motifs.

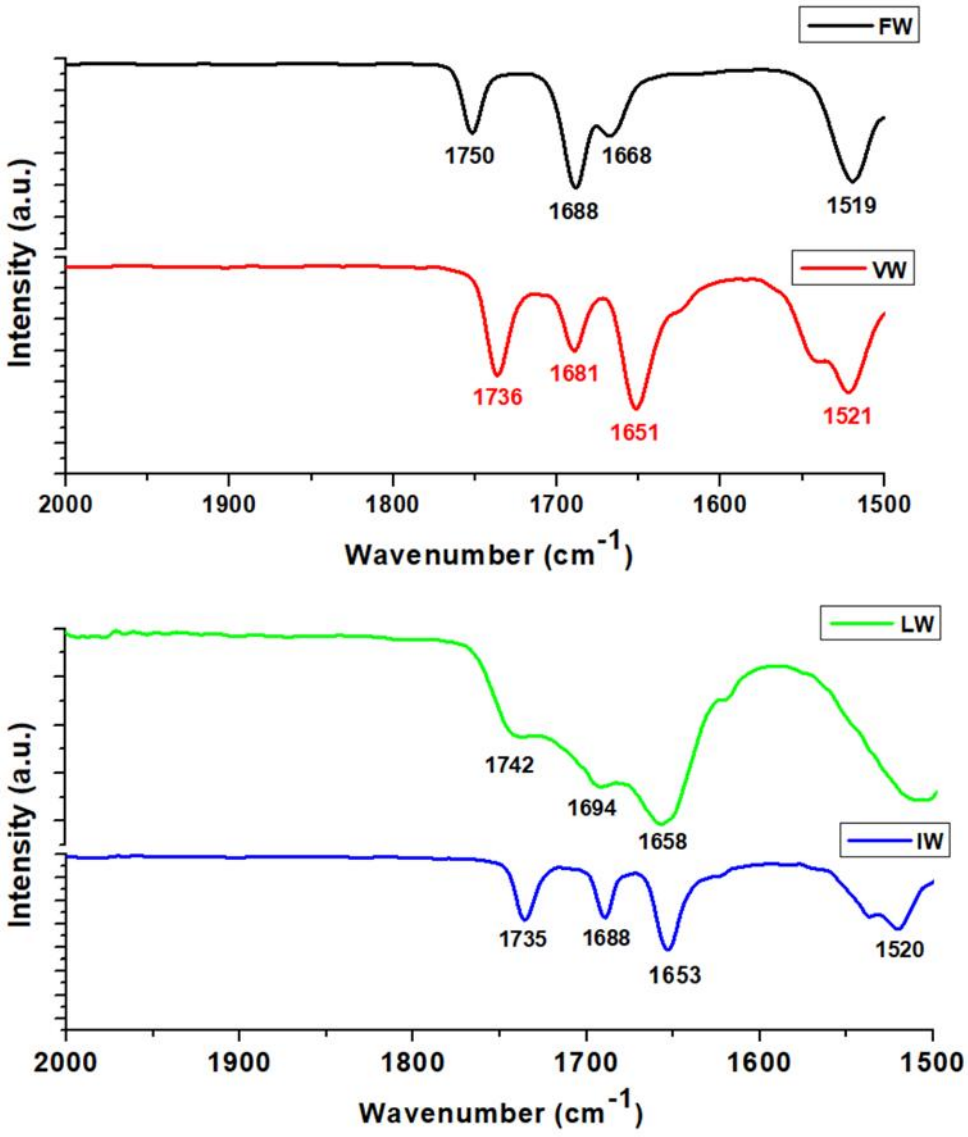

Figure 3.12. *FTIR spectra of 4-day incubated peptide aggregate of FW, VW, LW, and IW, respectively, (300 μM each) in solid state.*

3.8. Probable Binding Mechanism

The affinity of Thioflavin T (ThT) towards the nanoparticles formed by the designed dipeptides can largely be explained by the interplay of van der Waals and hydrophobic interactions. Although ThT carries a positive charge, it also contains a hydrophobic benzothiazole ring system that readily associates with nonpolar regions on the peptide nanoparticle surface through London dispersion forces. The spherical assemblies of these dipeptides are characterized by exposed hydrophobic surfaces, providing favourable

binding sites for ThT molecules. Such weak, non-covalent interactions play a key role in stabilizing the association between ThT and the peptide assemblies.

In addition to these hydrophobic contacts, π–π stacking and cation–π interactions further enhance the binding affinity. Each of the designed dipeptides includes a tryptophan residue, whose aromatic indole ring can engage in π–π stacking with the aromatic system of ThT. Moreover, the electron-rich nature of the indole ring makes it well suited for cation–π interactions with the positively charged benzothiazole moiety of the dye. The partial β-sheet organization exhibited by these dipeptides (Table 3.6) may also contribute by providing ordered domains that support stable ThT attachment.

Taken together, these multiple non-covalent forces, namely, hydrophobic, van der Waals, π–π, and cation–π interactions, collectively anchor ThT molecules onto the peptide nanoparticle surface. This immobilization restricts the internal rotational freedom of ThT's molecular framework, thereby enhancing its fluorescence emission, a phenomenon commonly known as the "molecular rotor" effect.[1,38]

3.9. Conclusion

In conclusion, this study highlights a distinctive property of Thioflavin T (ThT), showing its strong interaction with the well-organized spherical assemblies formed by designed Trp-containing dipeptides. Unlike its typical association with fibrillar or β-sheet-rich structures, ThT binding to these spherical aggregates represents an unusual phenomenon. Microscopic and fluorescence analyses confirmed the formation of stable ThT–dipeptide complexes, characterized by enhanced fluorescence and good binding affinity. Computational studies further supported these results, revealing that the interaction is spontaneous and predominantly stabilized by dispersion and van der Waals forces. Overall, this work expands the current understanding of ThT's binding behavior and opens up new possibilities for its use in peptide-based materials, sensing, and diagnostic applications.

3.10. Characterization data

Boc-Phe-Trp-OMe (FW)

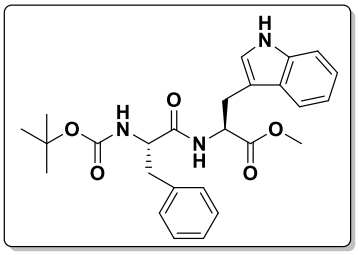

White solid, (560 mg, 80%), **^{1}H NMR (CDCl$_3$; 600 MHz)** δ 1.37 (9H, s); 3. 06-3.01 (2H, m); 3.30-3.23 (2H, m); 3.64 (3H, s); 4.37 (1H, s); 4.90-4.87 (1H, m); 4.96 (1H, s); 6.41 (1H, s); 6.88 (1H, s); 7.08 (1H, t, *J* = 7.8 Hz); 7.19 (3H, t, *J* = 7.2 Hz); 7.25-7.22 (1H, m); 7.29-7.26 (2H, m); 7.34 (1H, d, *J* = 8.4 Hz); 7.38 (1H, d, *J* = 7.8 Hz); 8.21 (1H, s); **^{13}C NMR (CDCl$_3$; 150 MHz)** δ 27.8, 28.3, 38.5, 52.5, 53.1, 55.8, 80.2, 109.9, 111.5, 118.6, 119.8, 122.4, 123.1, 127.1, 127.6, 128.7, 129.6, 136.2, 136.7, 155.4, 171.0, 171.9. HRMS (ESI): calculated $[M+H]^+$ 466.2297, found m/z. 466.2351.

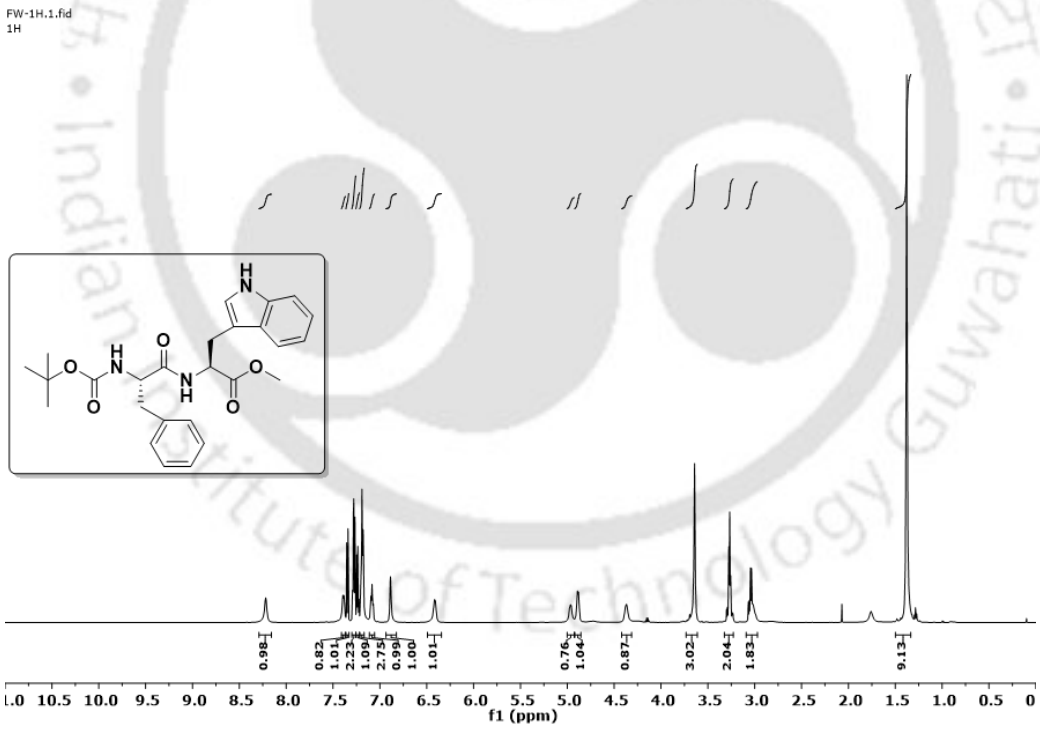

Figure 3.13. ^{1}H NMR spectra of peptide **Boc-Phe-Trp-OMe (FW).**

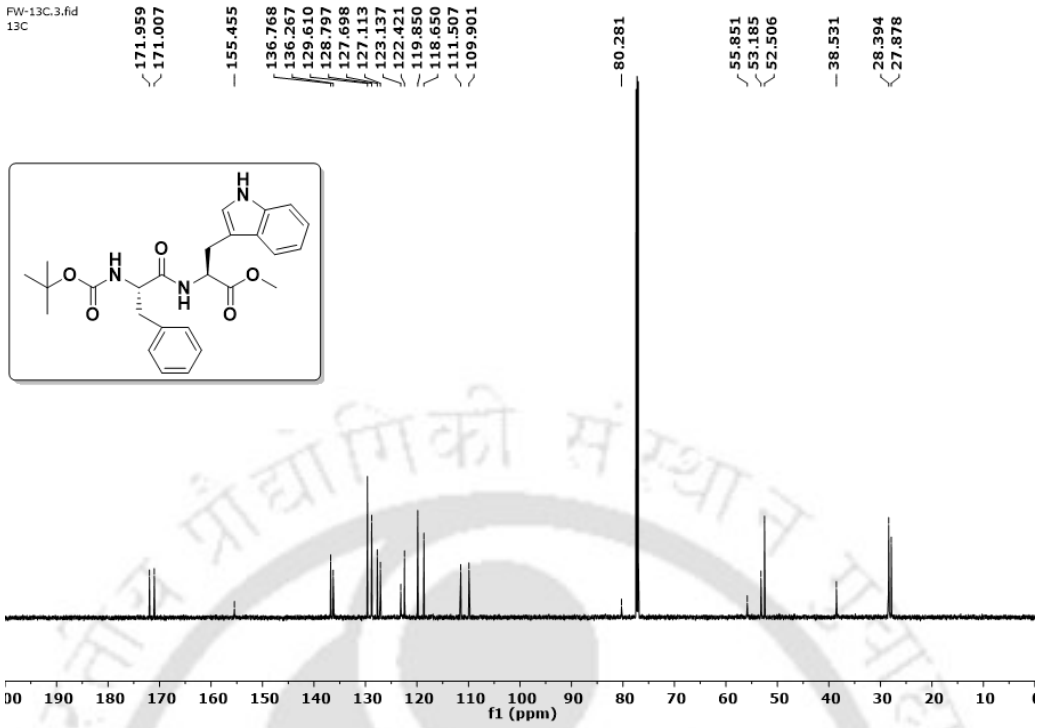

Figure 3.14. *^{13}C NMR spectra of peptide* ***Boc-Phe-Trp-OMe (FW).***

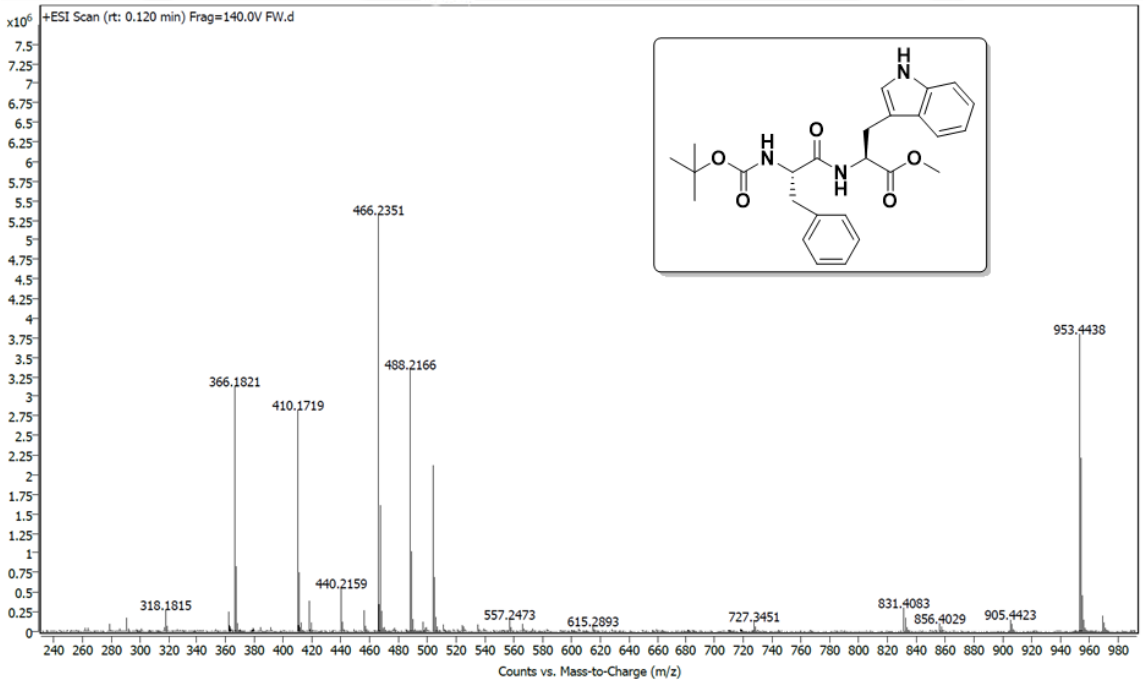

Figure 3.15. *MS spectra of peptide* ***Boc-Phe-Trp-OMe (FW).***

Boc-Val-Trp-OMe (VW)

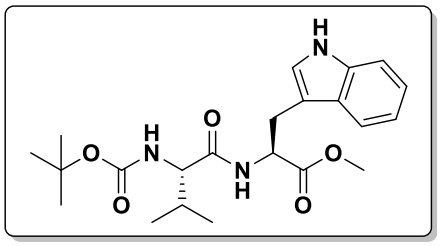

White solid, (652 mg, 85%), **^{1}H NMR (CDCl$_3$; 600 MHz)** δ 0.83 (3H, d, *J* = 6.6 Hz); 0.90 (3H, d, *J* = 6.6 Hz); 1.42 (9H, s); 2.08-2.03 (1H, m); 3.34-3.25 (2H, m); 3.64 (3H, s); 3.94 (1H, s); 4.93-4.89 (1H, m); 5.07 (1H, s); 6.42 (1H, s); 7.00 (1H, s); 7.11 (1H, t, *J* = 7.2 Hz); 7.17 (1H, t, *J* = 7.2 Hz); 7.33 (1H, d, *J* = 7.8 Hz); 7.52 (1H, d, *J* = 7.8 Hz); 8.27 (1H, s); **^{13}C NMR (CDCl$_3$; 150 MHz)** δ 17.7, 19.2, 27.8, 28.5, 31.2, 52.5, 52.9, 59.9, 80.0, 109.8, 111.5, 118.6, 119.9, 122.4, 123.2, 127.6, 136.3, 156.0, 171.5, 172.2. HRMS (ESI): calculated $[M+H]^+$ 418.2297, found m/z. 418.2353.

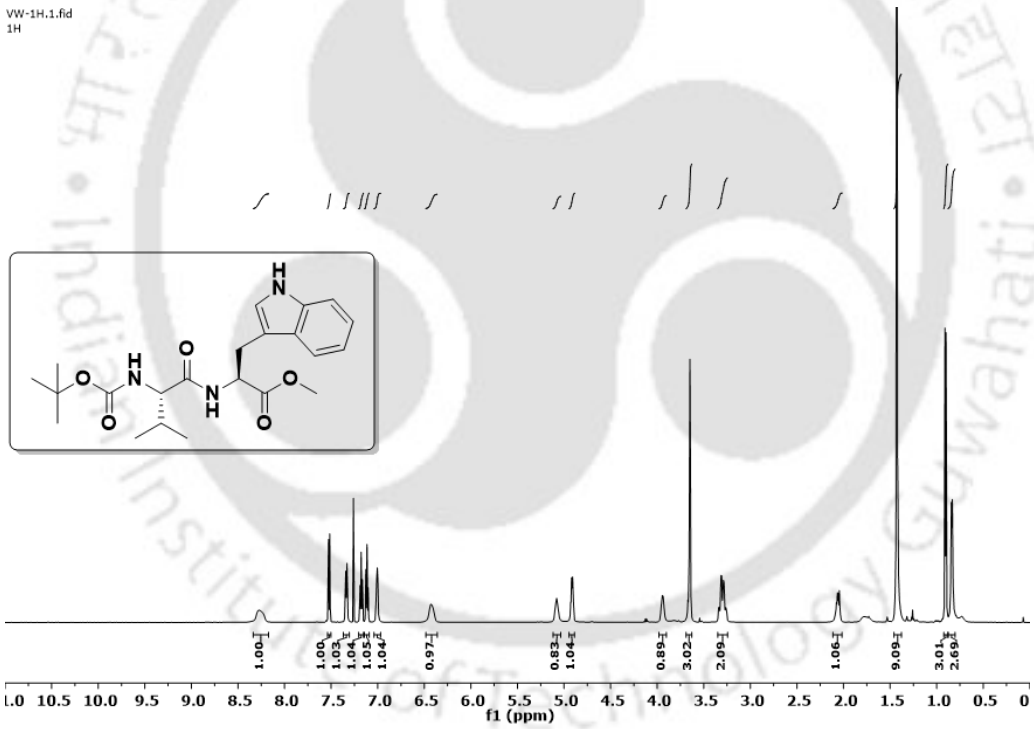

Figure 3.16. *^{1}H NMR spectra of peptide* ***Boc-Val-Trp-OMe (VW).***

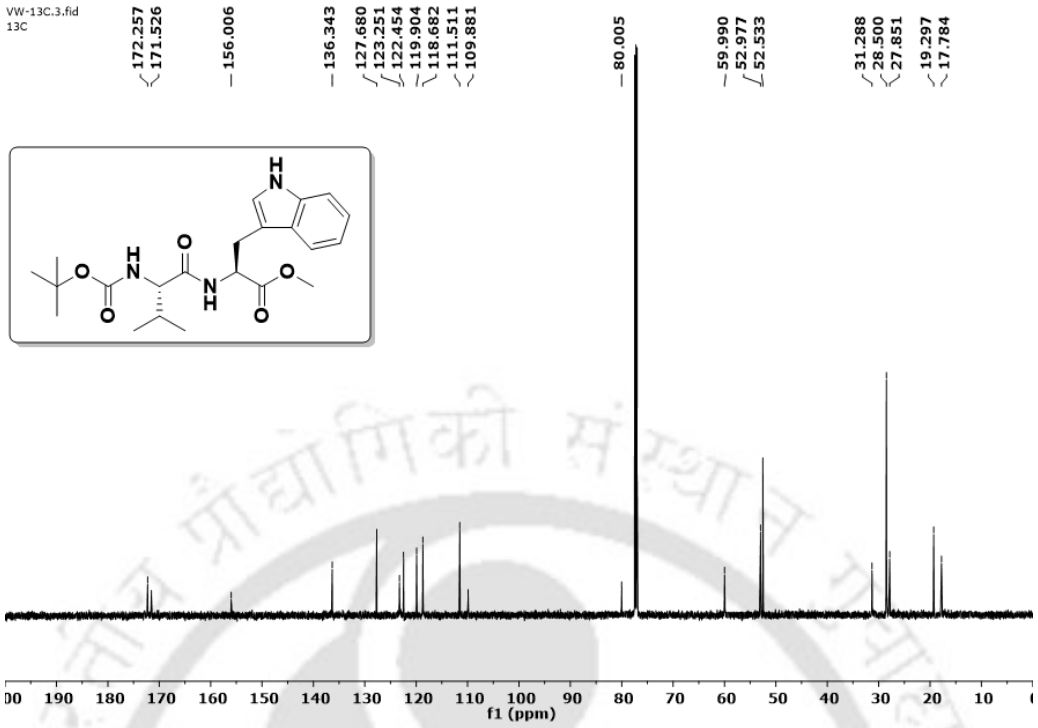

Figure 3.17. *^{13}C NMR spectra of peptide* ***Boc-Val-Trp-OMe (VW).***

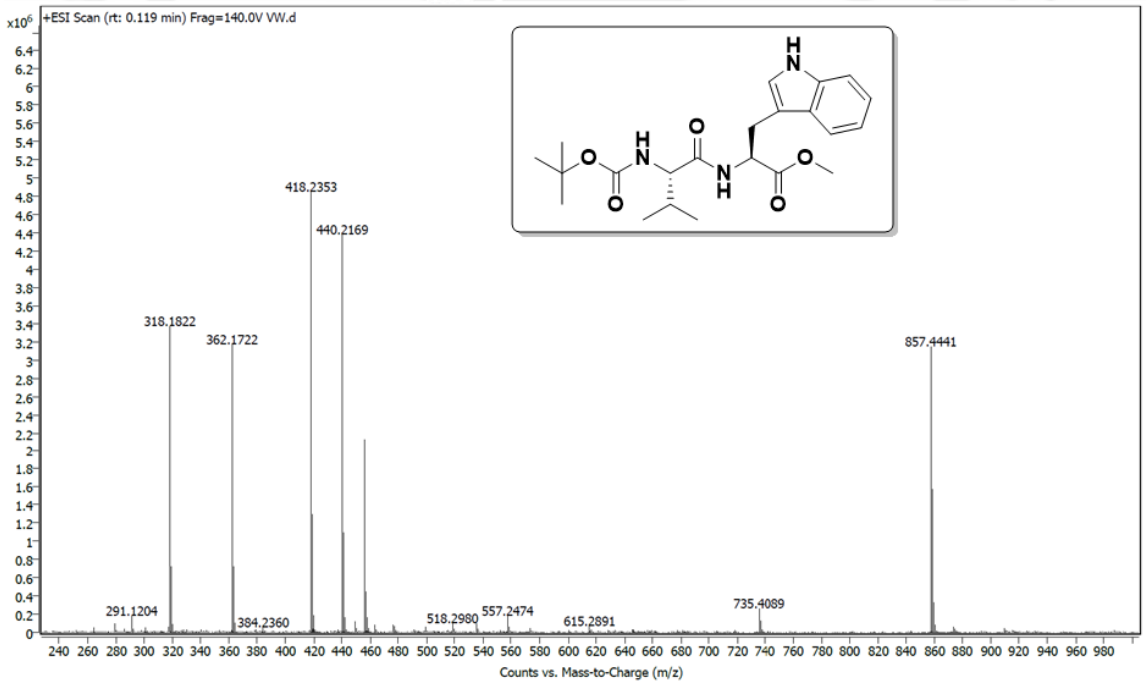

Figure 3.18. *MS spectra of peptide* ***Boc-Val-Trp-OMe (VW).***

Boc-Leu-Trp-OMe (LW)

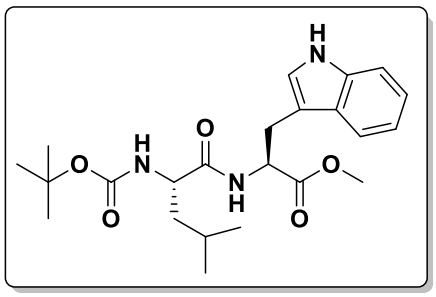

White solid, (581 mg, 84%), **^{1}H NMR (CDCl$_3$; 600 MHz)** δ 0.89-0.87 (6H, m); 1.31-1.21 (1H, m); 1.41 (9H, s); 1.64-1.55 (2H, m); 3.34-3.27 (2H, m); 3.64 (3H, s); 4.12-4.08 (1H, m); 4.90-4.85 (2H, m,); 6.62-6.60 (1H, m); 7.03 (1H, s); 7.10 (1H, t, *J* = 7.2 Hz); 7.17 (1H, t, *J* = 7.2 Hz); 7.33 (1H, d, *J* = 8.4 Hz); 7.51 (1H, d, *J* = 7.8 Hz); 8.26 (1H, s); **^{13}C NMR (CDCl$_3$; 150 MHz)** δ 22.0, 23.1, 24.8, 27.7, 28.4, 41.5, 52.5, 53.0, 53.3, 80.1, 109.9, 111.4, 118.7, 119.7, 122.3, 123.3, 127.7, 136.2, 155.7, 172.2, 172.4. HRMS (ESI): calculated $[M+H]^+$ 432.2454, found m/z. 432.2496.

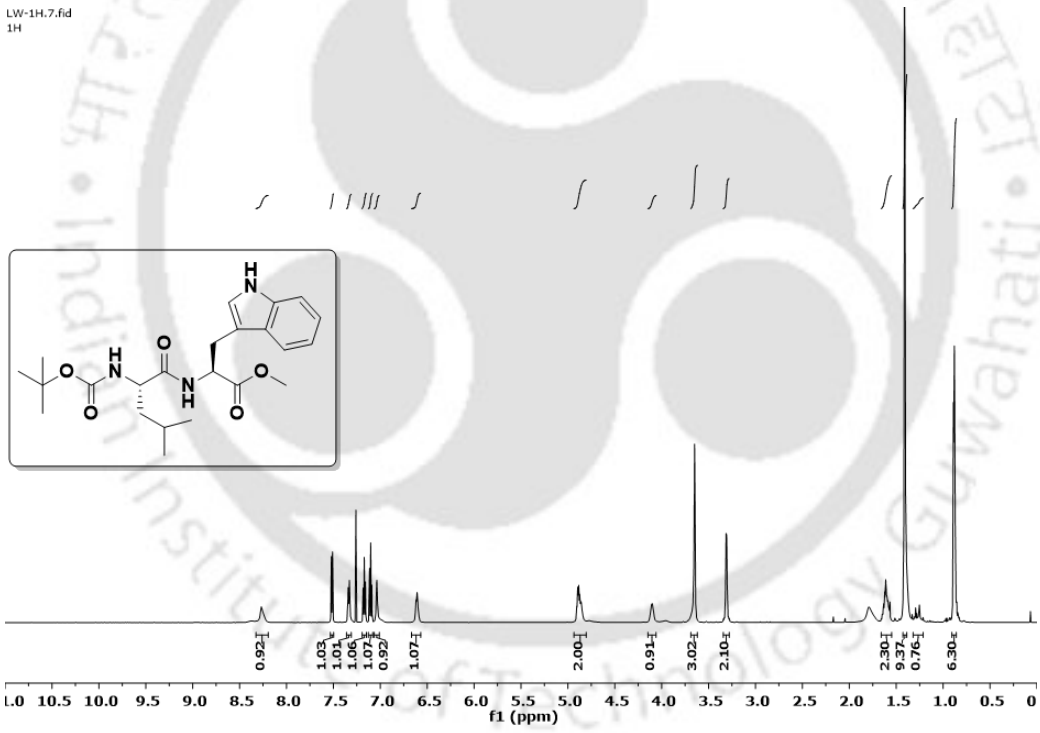

Figure 3.19. *^{1}H NMR spectra of peptide* ***Boc-Leu-Trp-OMe (LW).***

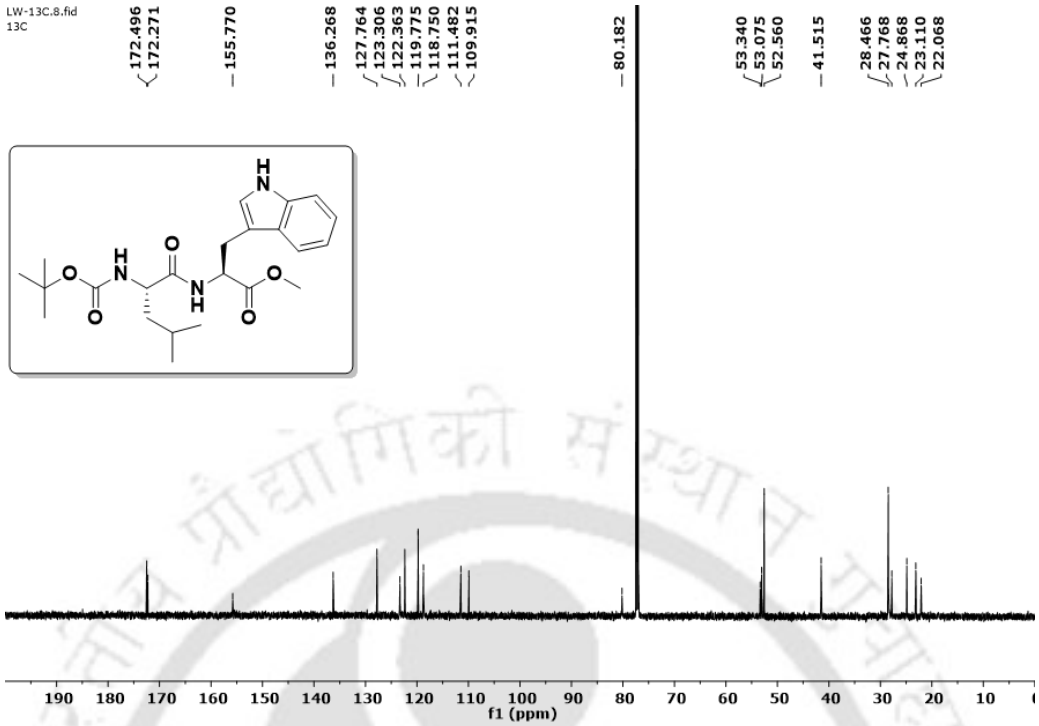

Figure 3.20. *^{13}C NMR spectra of peptide* ***Boc-Leu-Trp-OMe (LW).***

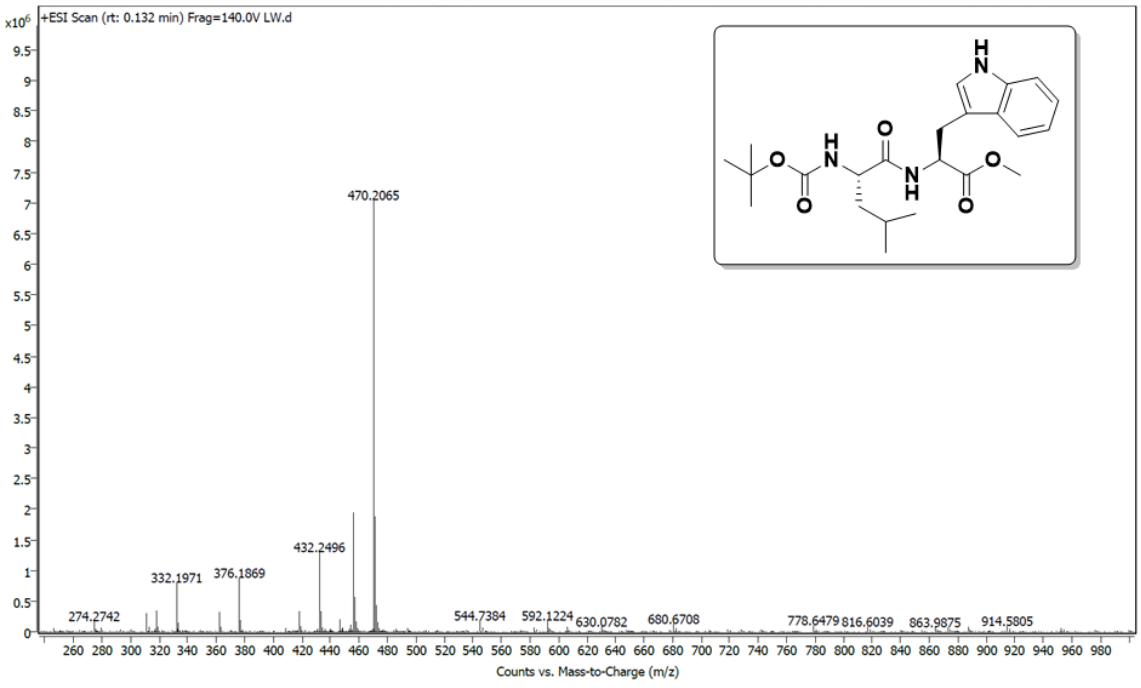

Figure 3.21. *MS spectra of peptide* ***Boc-Leu-Trp-OMe (LW).***

Boc-Ile-Trp-OMe (IW)

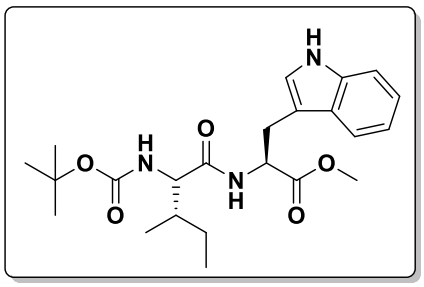

White solid, (574 mg, 83%), **^{1}H NMR (CDCl$_3$; 600 MHz)** δ 0.87-0.82 (6H, m); 1.06-0.99 (1H, m); 1.42 (9H, s); 1.82-1.72 (2H, m); 3.35-3.25 (2H, m); 3.64 (3H, s); 3.95 (1H, t, *J* = 7.8 Hz); 4.92-4.89 (1H, m); 5.06 (1H, d, *J* = 7.2 Hz); 6.40 (1H, s); 7.03 (1H, s); 7.11 (1H, t, *J* = 7.8 Hz); 7.17 (1H, t, *J* = 7.2 Hz); 7.34 (1H, d, *J* = 8.4 Hz); 7.52 (1H, d, *J* = 7.8 Hz); 8.23 (1H, s); **^{13}C NMR (CDCl$_3$; 150 MHz)** δ 11.6, 15.5, 24.7, 27.8, 28.5, 37.6, 52.5, 52.9, 59.3, 80.0, 109.8, 111.4, 118.6, 119.9, 122.4, 123.2, 127.6, 136.3, 155.8, 171.4, 172.2. HRMS (ESI): calculated $[M+H]^+$ 432.2454, found m/z. 432.2493.

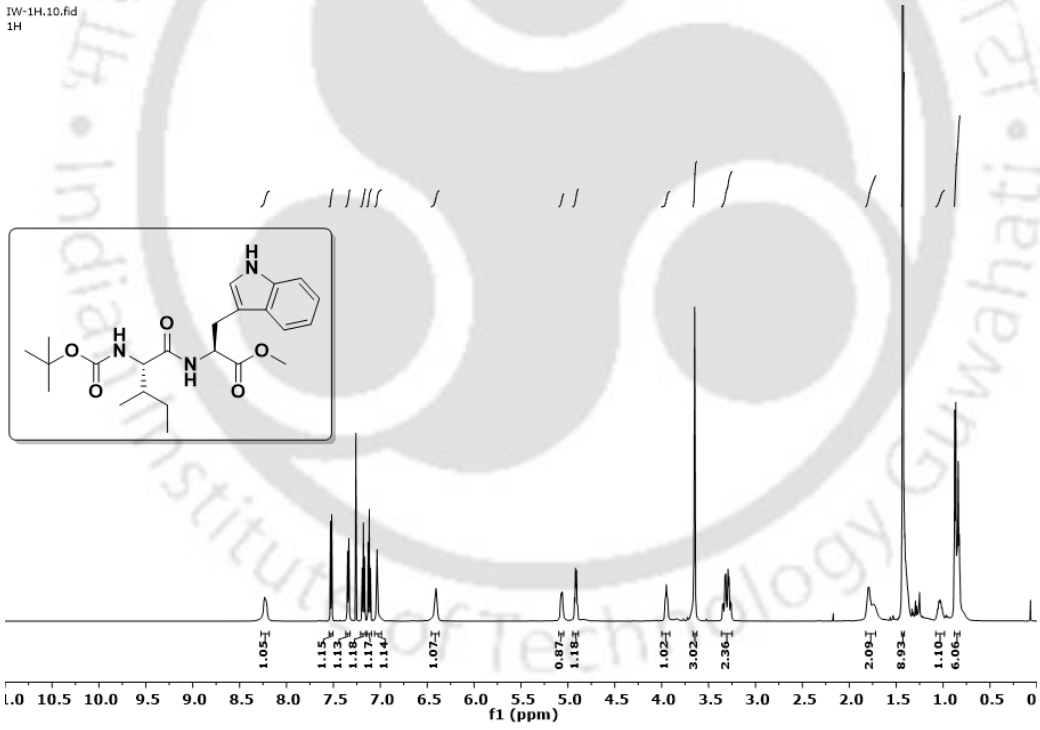

Figure 3.22. *^{1}H NMR spectra of peptide* ***Boc-Ile-Trp-OMe (IW).***

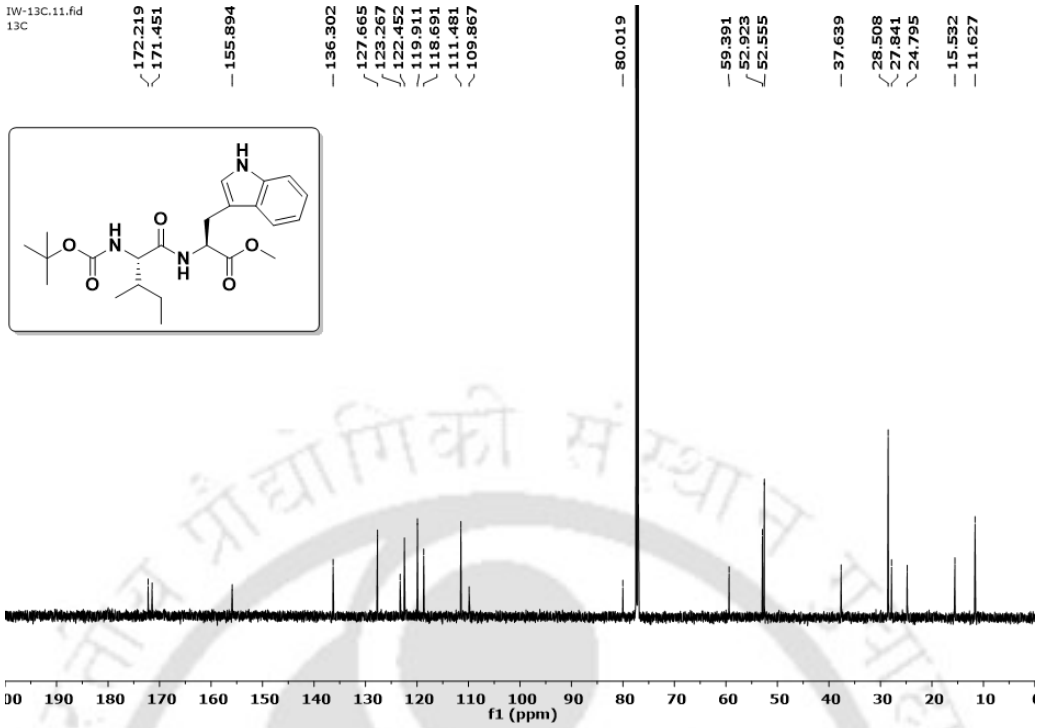

Figure 3.23. *^{13}C NMR spectra of peptide* ***Boc-Ile-Trp-OMe (IW).***

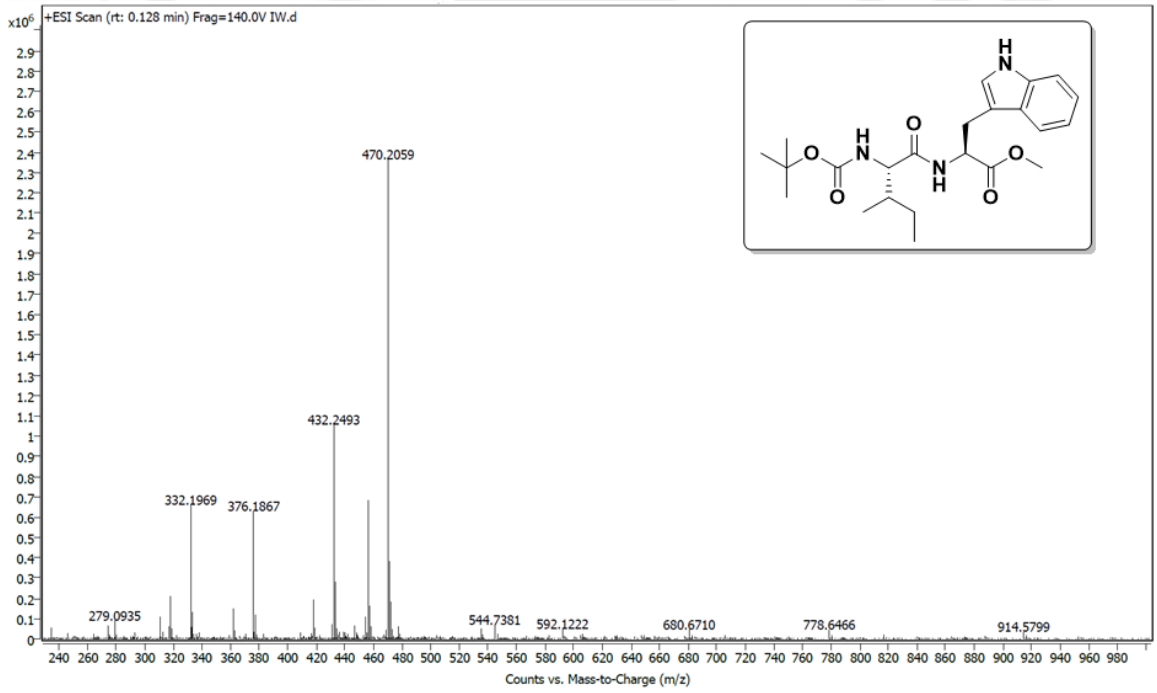

Figure 3.24. *MS spectra of peptide* ***Boc-Ile-Trp-OMe (IW).***

3.11. References

1. Groenning, M.; Olsen, L.; van de Weert, M.; Flink, J. M.; Frokjaer, S.; Jørgensen, F. S. Study on the binding of Thioflavin T to β-sheet-rich and non-β-sheet cavities. *J. Struct. Biol.* **2007**, *158*, 358-369.
2. Verma, S.; Ravichandiran, V.; Ranjan, N. Beyond amyloid proteins: Thioflavin T in nucleic acid recognition. *Biochimie*. **2021,** *190*, 111-123.
3. Khusbu, F. Y.; Zhou, X.; Chen, H.; Ma, C.; Wang, K. Thioflavin T as a fluorescence probe for biosensing applications.*Trends Anal. Chem.* **2018**, *109*, 1-18.
4. Singh, P. K.; Pettiwala, A. M.; Mudliar, N. H. Thioflavin T: A versatile optical probe for chemo and biosensing. Proc. Natl. Acad. Sci. **2019**, 85, 517-535.
5. Harel, M.; Sonoda, L. K.; Silman, I.; Sussman, J. L.; Rosenberry, T. L. Crystal structure of thioflavin T bound to the peripheral site of Torpedo californica acetylcholinesterase reveals how thioflavin T acts as a sensitive fluorescent reporter of ligand binding to the acylation site. *J.Am.Chem.Soc*. **2008,** *130*, 7856-7861.
6. Babenko, V.; Dzwolak, W. Thioflavin T forms a non-fluorescent complex with α-helical poly-l-glutamic acid. *Chem. Commun.* **2011**, *47*, 10686-10688.
7. Sulatsky, M. I.; Stepanenko, O. V.; Stepanenko, O. V.; Kuznetsova, I. M.; Turoverov, K. K.; Sulatskaya, A. I. Prediction of the Feasibility of Using the≪ Gold Standard≫ Thioflavin T to Detect Amyloid Fibril in Acidic Media. *Anal. Chem*. **2024**, *96*, 2158-2164.
8. Arad, E.; Green, H.; Jelinek, R.; Rapaport, H. Revisiting thioflavin T (ThT) fluorescence as a marker of protein fibrillation–The prominent role of electrostatic interactions. *J. Colloid Interface Sci*. **2020,** *573*, 87-95.
9. Sabaté, R.; Lascu, I.; Saupe, S. J. On the binding of Thioflavin-T to HET-s amyloid fibrils assembled at pH 2. J. *Struct. Biol*. **2008,** *162*, 387-396.
10. Dolai, G.; Shill, S.; Roy, S.; Mandal, B. Atomic Insight on Inhibition of Fibrillization of Dipeptides by Replacement of Phenylalanine with Tryptophan. *Langmuir* **2023**, *39*, 9367-9383.
11. Dev, D.; Palakurthy, N. B.; Thalluri, K.; Chandra, J.; Mandal, B. Ethyl 2-Cyano-2-(2-nitrobenzenesulfonyloxyimino) acetate (o-NosylOXY): a recyclable coupling reagent for racemization-free synthesis of peptide, amide, hydroxamate, and ester. *J. Org. Chem*. **2014**, *79*, 5420-5431.
12. Giri, R. S.; Manne, S. R.; Dolai, G.; Paul, A.; Kalita, T.; Mandal, B. FeCl3-mediated side chain modification of aspartic acid-and glutamic acid-containing peptides on a solid support. *ACS omega* **2017,** *2*, 6586-6597.
13. Zhang, H.; Lou, S.; Yu, Z. Polar− π interactions promote self-assembly of dipeptides into laminated nanofibers. *Langmuir* **2019**, *35*, 4710-4717.
14. Das, M.; Brahma, M.; Krishnamoorthy, G. Host-guest interaction aided Zinc carry and delivery by ESIPT active 2-(2′-hydroxyphenyl) benzoxazole. Spectrochim. Acta A Mol. Biomol. **2022**, *281*, 121474.
15. Chaveerach, U.; Meenongwa, A.; Trongpanich, Y.; Soikum, C.; Chaveerach, P. DNA binding and cleavage behaviors of copper (II) complexes with amidino-O-methylurea and N-methylphenyl-amidino-O-methylurea, and their antibacterial activities. *Polyhedron* **2010**, *29*, 731-738.

16. Behroozi, R.; Dehghanian, E.; Mansouri-Torshizi, H. A mechanism–based perspective on the interplay of new drug candidate with biomolecules. *J. Mol. Str.* **2025***, 1321*, 139700.
17. Sulatskaya, A. I.; Maskevich, A. A.; Kuznetsova, I. M.; Uversky, V. N.; Turoverov, K. K. Fluorescence quantum yield of thioflavin T in rigid isotropic solution and incorporated into the amyloid fibrils. *PloS one* **2010**, *5*, e15385.
18. Hohenberg, P.; Kohn, W. Inhomogeneous electron gas. *Phys. Rev.* **1964**, *136*, B864.
19. Kohn, W.; Sham, L. J. Self-consistent equations including exchange and correlation effects. *Phys. Rev.* **1965**, *140*, A1133.
20. Vengatesh, G.; Vinushya, N.; Jeyaprakash, G. M.; Mohini, A.; Mondal, P.; Reddy, R.; Shriram, Z. O. Crystal structures, NCI-RDG, Hirshfeld surface and energy framework analysis of tetra aryl substitute bispidine and oxaquinuclidine core containing derivatives: A potential COVID-19 drug candidate. *J. Mol. Str.* **2025,** *1321*, 140202.
21. Sunny, S. A.; Thomas, R. Exploring non-covalent interactions: A computational study of Methyl acetate in chloroform and Hexafluoroisopropanol. *Chem. Phys. Impact* **2024**, *8*, 100514.
22. Smati, S.; Djafri, A.; Menad, K.; Boukabcha, N.; Rahmani, R.; Goudjil, M.; Djafri, A. Synthesis, molecular structure, Hirshfeld surface analysis, NCI-RDG, spectral characterization analysis, nonlinear optical properties, and in silico molecular docking of (E)-3-(3-(2-methoxyphenyl)-4-methylthiazol-2 (3H)-ylidene) benzo [4, 5] imidazo [1, 2-c] thiazole-1 (3H)-thione. *J. Mol. Str.* **2024,** *1318*, 139157.
23. Johnson, E. R.; Keinan, S.; Mori-Sánchez, P.; Contreras-García, J.; Cohen, A. J.; Yang, W. Revealing noncovalent interactions. *J. Am. Chem. Soc.* **2010**, *132*, 6498-6506.
24. Ponnuchamy, V.; Sandak, A.; Sandak, J. Multiscale modelling investigation of wood modification with acetic anhydride. *Phys. Chem. Chem. Phys*.**2020**, *22*, 28448-28458.
25. Wang, Z.; Song, R.; Chen, W.; Wang, J.; Wang, P.; Zhang, Z.; Wan, F. Vibrational spectra and molecular vibrational behaviors of dibenzyl disulfide, dibenzyl sulphide and bibenzyl. *Int. J. Mol. Sci.* **2022***, 23*, 1958.
26. Parker, T. M.; Burns, L. A.; Parrish, R. M.; Ryno, A. G.; Sherrill, C. D. Levels of symmetry adapted perturbation theory (SAPT). I. Efficiency and performance for interaction energies. *J. Chem. Phys.* **2014**, *140*.
27. Sarma, M.; Sarmah, M. P.; Sarma, M. End group effects on anion binding in tetraglycine peptide: a computational study. *Chem. Asian J.* **2025**, *20*, e202400880.
28. Morokuma, K.; Kitaura, K. Energy decomposition analysis of molecular interactions. In *Chemical Applications of Atomic and Molecular Electrostatic Potentials: Reactivity, Structure, Scattering, and Energetics of Organic, Inorganic, and Biological Systems*. *Boston, MA: Springer US.* **1981**, 215-242.
29. Ross, P. D.; Subramanian, S. Thermodynamics of protein association reactions: forces contributing to stability. *Biochemistry* **1981**, *20*, 3096-3102.
30. Saeidifar, M.; Mansouri-Torshizi, H.; Palizdar, Y.; Eslami-Moghaddam, M.; Divsalar, A.; Saboury, A. A. Synthesis, characterization, cytotoxicity and DNA binding studies of a novel anionic organopalladium (II) complex. *Acta Chim. Slov*. **2014**, *61*, 126-136.

31. Myer, Y. P.; MacDonald, L. H. Circular dichroism of L-tryptophan by an improved dichrograph. *J. Am. Chem. Soc*. **1967**, *89*, 7142-7144.
32. Buczkowski, A.; Urbaniak, P.; Belica, S.; Sekowski, S.; Bryszewska, M.; Palecz, B. Formation of complexes between PAMAM-NH2 G4 dendrimer and L-α-tryptophan and L-α-tyrosine in water. *Spectrochim. Acta A Mol. Biomol. Spectrosc.* **2014,** *128*, 647-652.
33. Bera, S.; Jana, P.; Maity, S. K.; Haldar, D. Inhibition of fibril formation by tyrosine modification of diphenylalanine: crystallographic insights. *Cryst. Growth Des.* **2014,** *14*, 1032-1038.
34. Roy, S.; Giri, R. S.; Dolai, G.; Mandal, B. Role of side-chain and chirality of the amino acids on the supramolecular assemblies of dipeptides. *J. Mol. Str.* **2020,** *1221*, 128877.
35. Toniolo, C.; Palumbo, M. Solid-state infrared absorption spectra and chain arrangement in some synthetic homooligopeptides in the intermolecularly hydrogen-bonded pleated-sheet β-conformation. *Biopolymers* **1977**, *16*, 219-224.
36. Vass, E.; Hollósi, M.; Besson, F.; Buchet, R. Vibrational spectroscopic detection of beta-and gamma-turns in synthetic and natural peptides and proteins. *Chem. Rev.* **2003**, *103*, 1917-1954.
37. Dado, G. P.; Gellman, S. H. Intramolecular hydrogen bonding in derivatives of. beta.-alanine and. gamma.-amino butyric acid; Model studies for the folding of unnatural polypeptide backbones. *J. Am. Chem. Soc.***1994**, *116*, 1054-1062.
38. Biancalana, M.; Koide, S. (2010). Molecular mechanism of Thioflavin-T binding to amyloid fibrils. *Biochim Biophys Acta* **2010**, *1804*, 1405-1412.

Chapter 4

Morphology Transition of Tripeptides from Porous Spherical to Rod-like Nanostructures for Small Molecule Adsorption

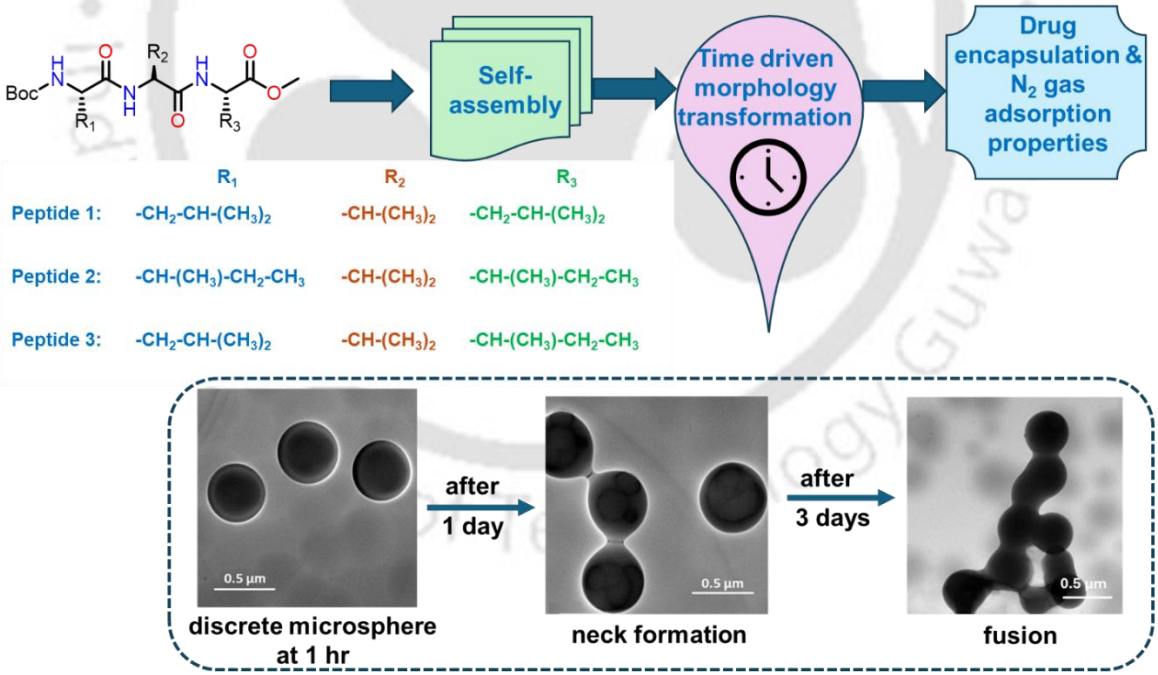

4.1. Background

The ability of peptides to self-assemble into ordered structures has become an exciting and rapidly growing focus in biomolecular science, offering vast potential for creating new materials with unique functions. Among the many aspects of this phenomenon, the transformation of peptide morphology over time has emerged as a particularly intriguing subject. Such transformations are not only relevant to material design but also play a central role in biological systems. For instance, in various neurodegenerative diseases, specific peptides undergo abnormal structural rearrangements, leading to the accumulation of toxic aggregates.[1-3] Studying how these peptides change shape and organize provides valuable insight into the mechanisms behind disease progression, helping to identify possible therapeutic approaches. The shift in peptide morphology is often governed by a delicate balance between the peptide's own molecular features and the surrounding environmental factors. Slight variations in conditions such as pH, temperature, or solvent composition can dramatically influence peptide conformation, driving the formation of distinct architectures and assemblies.[4-9]

In this regard, several studies have explored how variations in environmental or molecular factors can influence peptide morphology. Zhang *et al.*[10] investigated amphiphilic, surfactant-like peptides that exhibited structural transitions between nanovesicles and nanotubes. Gazit and co-workers[11] demonstrated that incorporating a thiol functionality into the diphenylalanine motif induces a morphological shift from tubular assemblies to spherical nanoparticles. Similarly, Li *et al.*[12,13] observed that the dipeptide FF transforms from nanotubular structures to vesicle-like morphologies when its concentration is altered. Shellnut and co-workers[14] reported a comparable transition in D-Phe-D-Phe assemblies, where dilution prompted a change in their morphology from nanotubes to vesicles. Matsui and Holtman[15] further revealed that benzoic diacid diamide molecules display a pH-dependent structural reorganization, evolving from microspheres to nanotubes. Consistent with these findings, Zhang *et al.*[16] also examined pH-responsive morphological transitions in peptide systems. Halder and co-workers[17] described a dilution-driven change in peptide assemblies, where spherical aggregates elongated into rod-like structures. Parquette *et al.*[8] demonstrated that peptide-dendron hybrids can reversibly interconvert between fibrillar and tubular nanostructures in response to pH variations or salt concentration. Kimura and

colleagues[7] reported a transformation from nanotubes to vesicular assemblies through the fusion of helically ordered segments via stereo-complex formation. In another study, Yao *et al.*[6] achieved controlled morphological switching in bipyridine-tripeptide assemblies by applying external stimuli such as temperature changes and ultrasound. Ulijn and co-workers[5] presented an enzyme-mediated mechanism that drives morphological transitions in aromatic peptide amphiphiles. Interestingly, unlike most of these examples where external triggers govern the transformation, Stupp *et al.*[4] observed a spontaneous temporal evolution of morphology from short, twisted ribbons to extended helical ribbons, occurring naturally over time.

4.2. Design, Synthesis & Characterization of the Peptides

The design of the tripeptides was inspired by the structural insights from Charcot–Marie–Tooth (CMT) disease, a prevalent inherited neuropathy. Alteration in the first transmembrane segment (TM1) of peripheral myelin protein 22 (PMP22) plays a central role in CMT type 1A disease. While Yamada and co-workers[18] previously synthesized the putative TM1 sequence (Boc-IVLH(Bom)VAVLVLLFVSTIV-OMe) and examined the impact of a proline mutation, our work focuses on the hydrophobic core region of the TM1 fragment. By reducing the segment to minimal tripeptide motifs, we aimed to investigate how subtle changes, particularly the exchange of leucine and isoleucine residues, impact the self-assembly pathways.

Therefore, we designed four fully protected hydrophobic tripeptides, namely, Boc-LVL-OMe (LVL), Boc-IVI-OMe (IVI), Boc-LVI-OMe (LVI), and Boc-IVL-OMe (IVL), and explored their time-dependent morphological transformation through supramolecular self-associations.

The designed tripeptides were synthesized using a conventional solution-phase method (Scheme 4.1), employing *o*-NosylOXY as the coupling reagent.

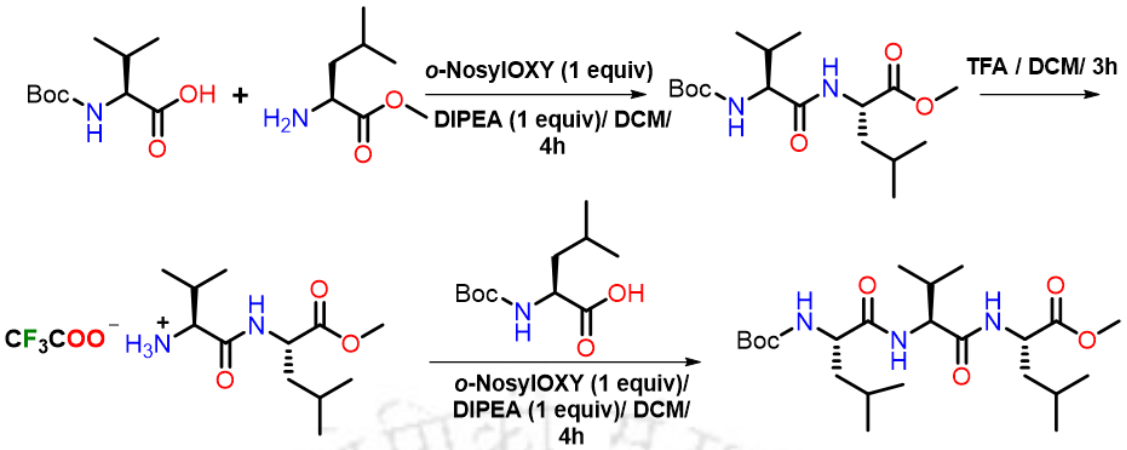

Scheme 4.1. *A schematic representation of the synthesis of a tripeptide in solution.*

The protected tripeptides were synthesized in solution phase using *o*-NosylOXY, a recently developed modern coupling reagent, with DCM serving as the reaction solvent. For the synthesis, initially, Boc-L-Val-OH was used, followed by coupling with the required methyl ester-protected C-terminal amino acid. After successful coupling, the Boc group from the valine moiety was removed, followed by coupling with the required Boc (tert-butyloxycarbonyl) group, protecting the N-terminal amino acid. The crude products were purified through column chromatography to obtain the desired pure tripeptides. The characterisation of the synthesized compounds was achieved using 1D ^{1}H and ^{13}C NMR spectroscopy and Mass spectrometry. The reversed-phase analytical HPLC was performed to verify the purity of the tripeptide.

4.3. Morphological Transformation Study

The time-dependent morphological evolution of the designed tripeptides through molecular self-assembly was examined using field-emission scanning electron microscopy (FESEM, Figure 4.1) and field-emission transmission electron microscopy (FETEM, Figure 4.2). The observations obtained from these microscopic analyses were further corroborated by dynamic light scattering (DLS) measurements, which showed consistent results with the proposed transformation behaviour (Figure 4.3).

4.3.1. Time-dependent FESEM & FETEM Study

For both sets of experiments, peptide solutions of 500 µM were prepared using a 1:1 methanol-water solvent system. The samples were then incubated at 37 °C, and

morphological studies were performed at specific time intervals using FESEM and FETEM. Remarkably, all tripeptides except IVL displayed a noticeable evolution in morphology over time. Within the initial hour of incubation, both FESEM and FETEM images revealed the formation of uniformly distributed spherical assemblies with diameters ranging between 400 and 600 nm. After 24 hours, distinct changes became apparent: for all tripeptides except IVL, the initially formed nanospheres appeared to interact and connect with each other, as observed by the formation of visible neck-like junctions, suggesting fusion between neighbouring spheres. By the fourth day, this fusion process had progressed significantly, resulting in elongated, rod-like nanostructures that seemed to arise from the merging of multiple spherical units. The transition from spherical to rod-shaped morphology was particularly pronounced in the LVL and IVI peptides, less evident in LVI, and completely absent in IVL.

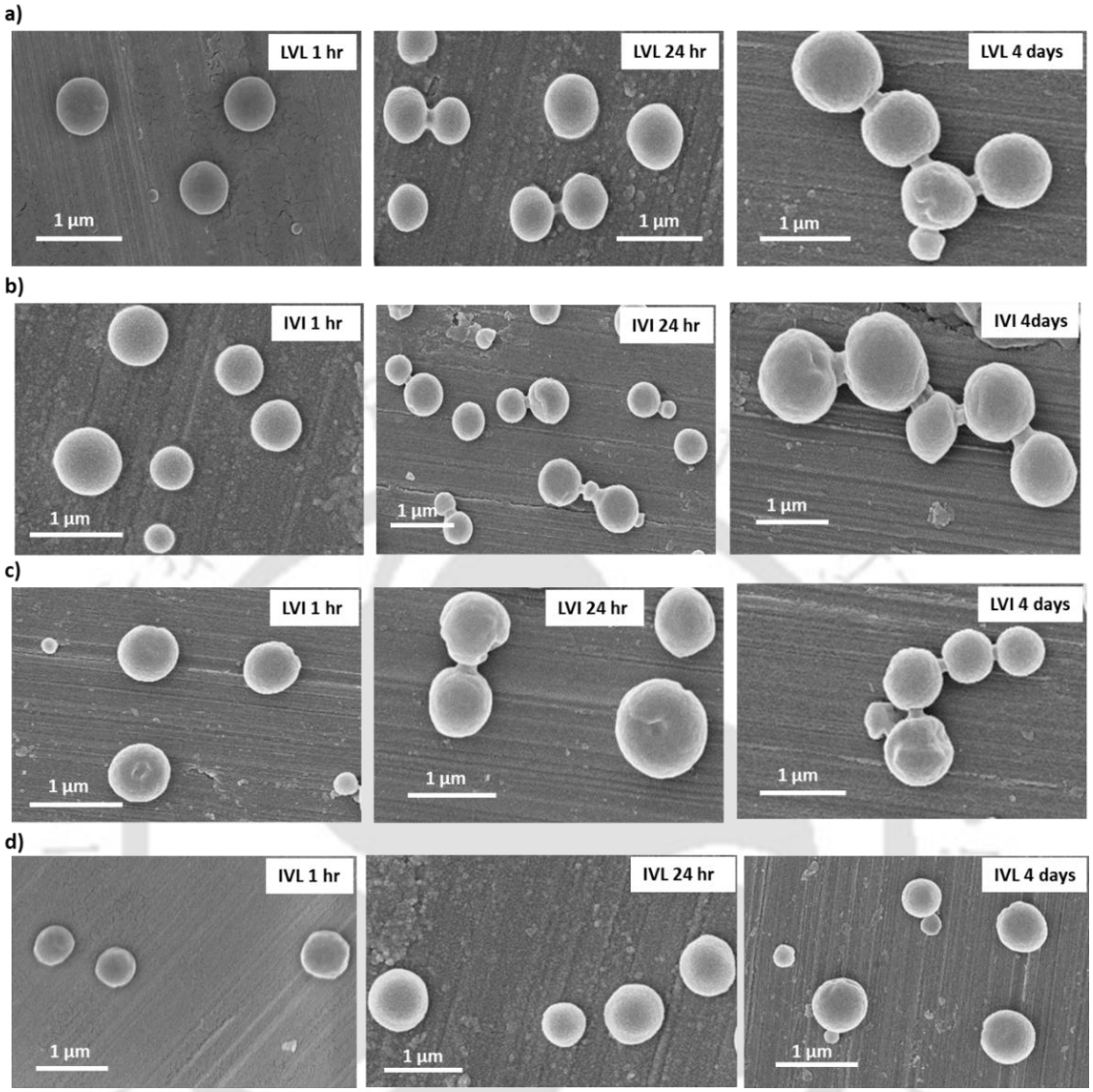

Figure 4.1. *FESEM images displaying morphological transformations of the tripeptides a) LVL, b) IVI, c) LVI, and d) IVL, at different time intervals.*

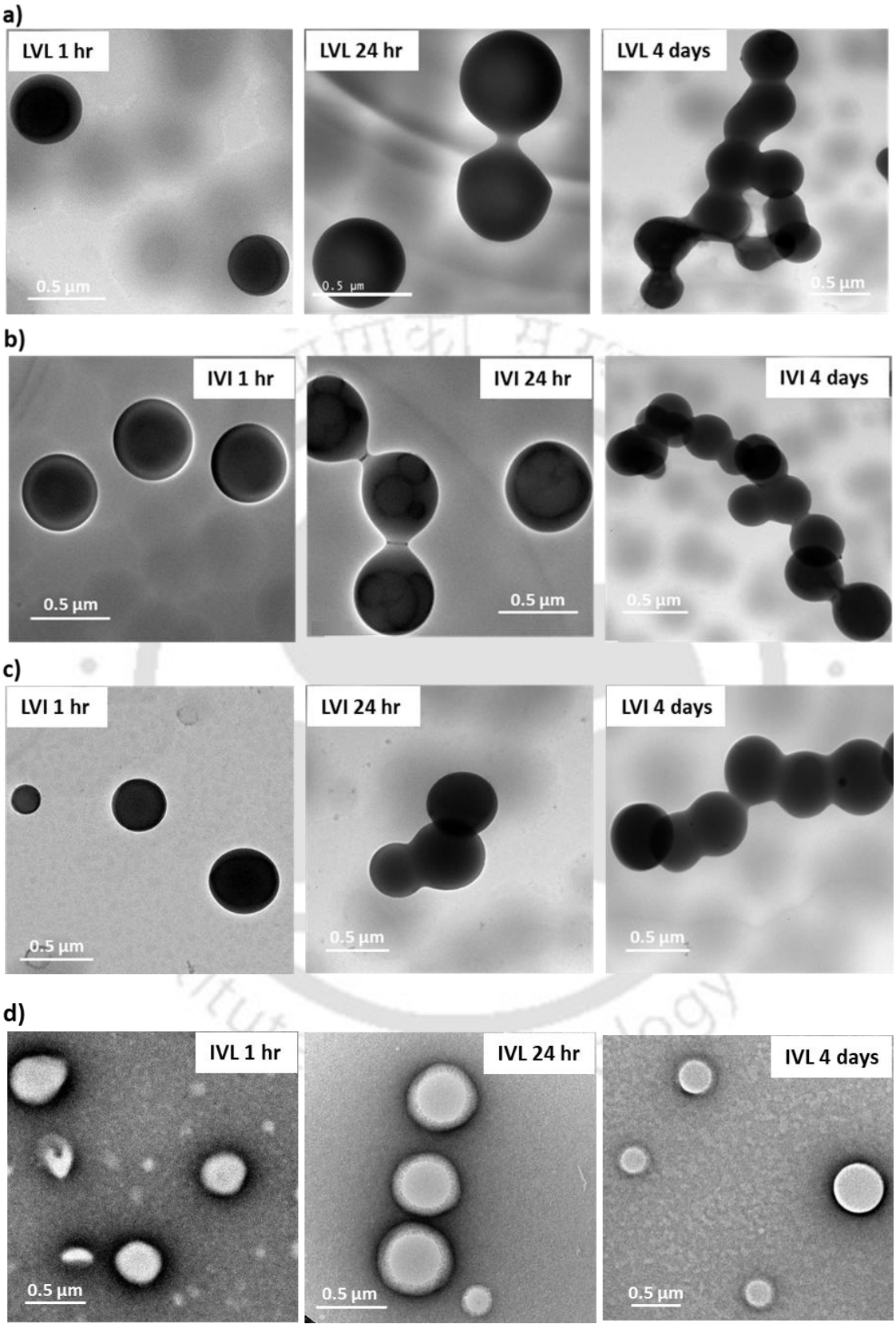

Figure 4.2. *FETEM images displaying morphological transformations of the tripeptides a) LVL, b) IVI, c) LVI, and d) IVL, at different time intervals.*

4.3.2. Time-dependent DLS Study

Dynamic light scattering (DLS) measurements were performed at the same time intervals corresponding to those used in the FESEM and FETEM analyses, employing the same incubated peptide solutions. At the initial time point of 1 hour, the DLS results indicated the formation of uniform nanoparticles for all tripeptides, with hydrodynamic diameters ranging from approximately 400 to 600 nm. After 24 hours of incubation, a noticeable increase in particle size distribution was observed, suggesting the coexistence of self-assembled structures of varying lengths. This growth in particle size is likely attributed to the gradual fusion or aggregation of nanospheres, resulting in the emergence of larger assemblies. By the fourth day, the samples exhibited even broader size distributions with significantly higher hydrodynamic diameters across all tripeptides, except in the case of IVL, which consistently showed particles of nearly the same size throughout the incubation period. The DLS findings are in strong agreement with the morphological evolution observed in FESEM and FETEM studies, further confirming the transformation in the self-assembled structures over time.

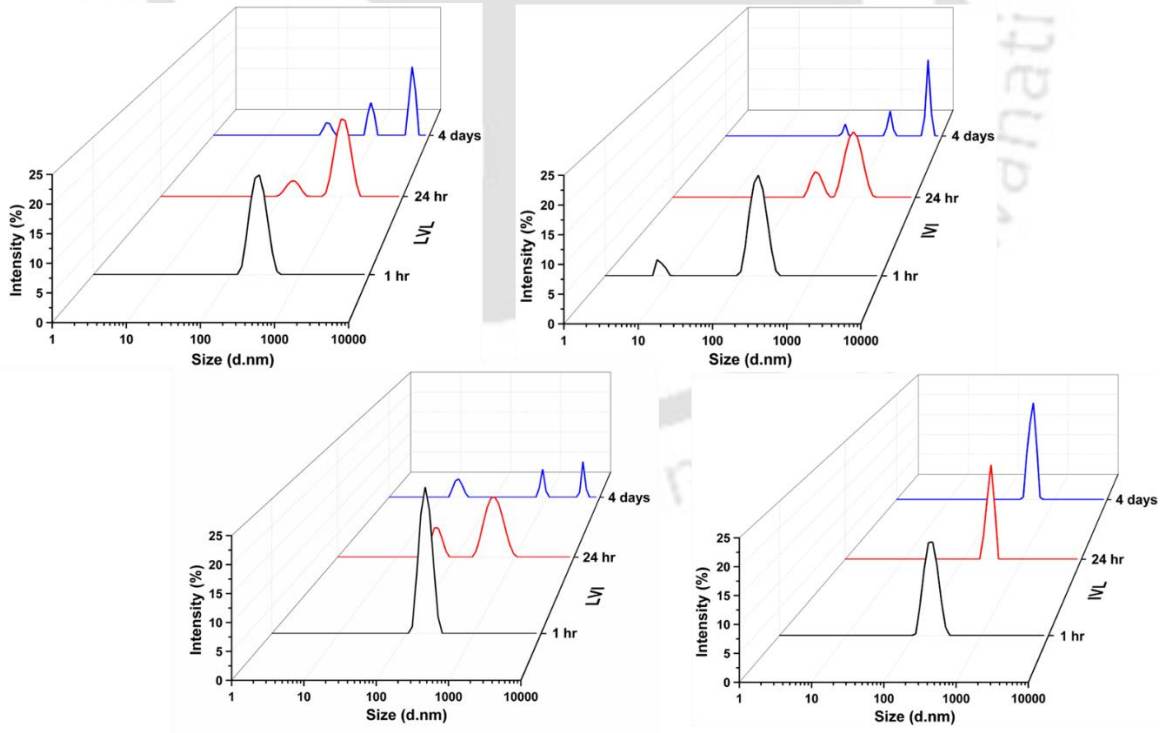

Figure 4.3. *Size distribution plot in DLS experiment of the tripeptides a) LVL, b) IVI, c) LVI, and d) IVL, at different time intervals.*

4.3.3. Plausible Mechanism

The gradual transformation of self-assembled tripeptides from spherical nanostructures to elongated, rod-like assemblies is an intriguing process. However, the underlying mechanism is often intricate and not yet completely understood. Several factors can influence this morphological evolution. For instance, the specific arrangement and position of amino acids within a peptide sequence can determine the nature and pattern of both intramolecular and intermolecular hydrogen bonding interactions. These hydrogen bonds play a crucial role in defining the overall architecture of the assembly: while hydrogen bonds formed along the peptide backbone typically favour linear, longitudinal growth, those involving side chains often facilitate the formation of more complex and ordered nanostructures.[19,20]

A plausible explanation for the observed transition can be proposed as follows. Initially, the tripeptides may rapidly organize into nanospheres, representing a kinetically trapped, metastable state formed during the early stages of self-assembly. These spherical aggregates correspond to a local energy minimum under the prevailing conditions. As time progresses, hydrophobic interactions among adjacent nanospheres may drive them closer together, leading to their fusion as a means to minimize the overall surface energy. With continued molecular rearrangement, additional non-covalent interactions, such as hydrogen bonding and π–π stacking, can further stabilize the growing assemblies, promoting their alignment and elongation into rod-like morphologies. In many peptide-based systems, such elongated structures are energetically more favourable than spherical ones, as their reduced curvature and surface free energy contribute to a more thermodynamically stable configuration.[21]

4.4. Conformational Study

For the conformational analysis, circular dichroism (CD) spectroscopy and solid-state Fourier-transform infrared (FTIR) spectroscopy were employed. Peptide samples of 500 μM were prepared in a 1:1 mixture of methanol and water, as described earlier, and incubated at 37 °C for four days. The CD measurements were performed using aliquots taken directly from the incubated solutions after four days. For FTIR analysis, the four-day-incubated samples were first lyophilized to obtain the solid material, which was then used for the solid-state spectral measurements.

4.4.1. Analysis by CD Spectroscopy

Circular dichroism (CD) analysis (Figure 4.4) revealed distinct spectral features for the LVL and IVI tripeptides, both of which displayed a pronounced negative band near 220 nm. In comparison, the intensity of this band was noticeably weaker for LVI and even more subdued for IVL. This trend suggests that LVL and IVI predominantly adopt β-sheet-rich conformations, while LVI and IVL exhibit a comparatively lower degree of β-sheet character. In addition, a subtle negative shoulder observed between 195 and 200 nm for all four tripeptides indicates the coexistence of some random coil components within their overall secondary structure.[22,23]

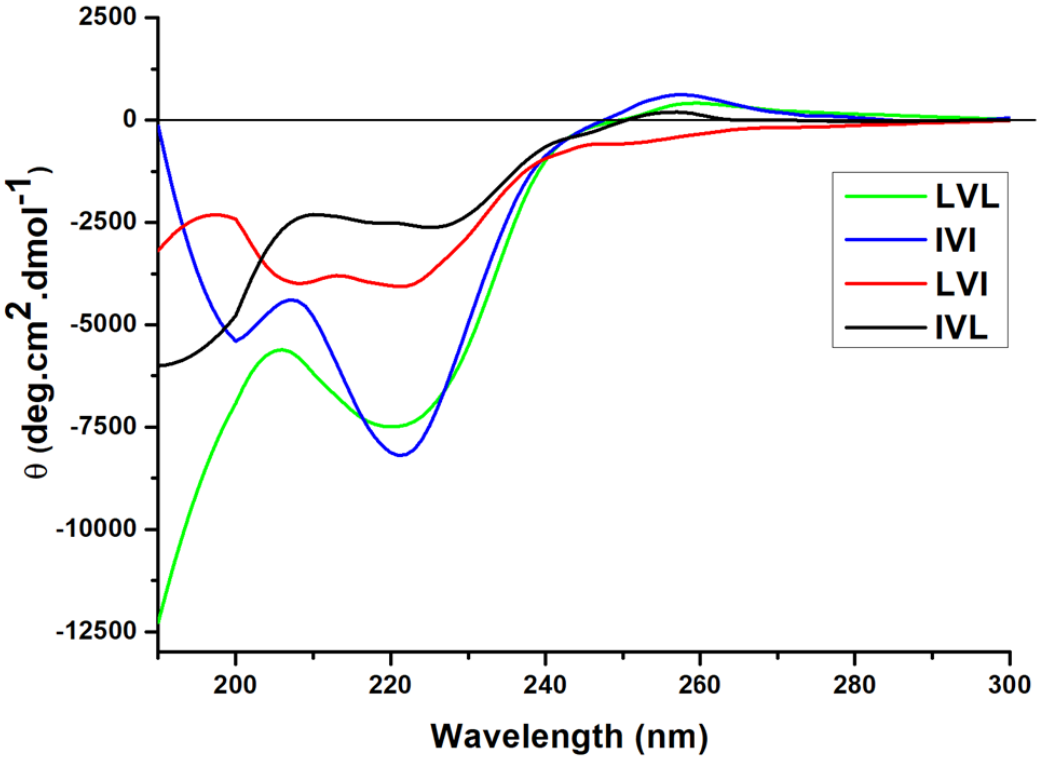

Figure 4.4. *CD spectra of 4 a 4-day-old, incubated sample solution (500 μM) of LVL, IVI, LVI, and IVL in 50% MeOH/H_2O at 37 ℃.*

4.4.2. Analysis by FTIR Spectroscopy

To complement the CD spectroscopy findings, FT-IR analysis was performed (Figure 4.5). The amide I region (1600–1700 cm^{-1}), primarily corresponding to C=O stretching vibrations, and the amide II region (1510–1580 cm^{-1}), associated with N–H bending and

C–N stretching, provide valuable insights into the secondary structural features of peptides. All four tripeptides exhibited an amide I absorption within the range of 1640–1692 cm^{-1}, along with a comparable amide II band appearing between 1516–1518 cm^{-1}. The amide I peaks observed at 1642 cm^{-1} for LVL and IVL, and at 1641 cm^{-1} for IVI and LVI, are characteristic of random coil conformations. In contrast, the bands located near 1692 cm^{-1} (LVL and LVI), 1691 cm^{-1} (IVL), and 1690 cm^{-1} (IVI) indicate the presence of antiparallel β-sheet structures. Furthermore, the appearance of the amide II bands at 1517 cm^{-1} for LVL and IVL, 1518 cm^{-1} for IVI, and 1516 cm^{-1} for LVI further supports the existence of β-sheet arrangements in these tripeptides.[24-27]

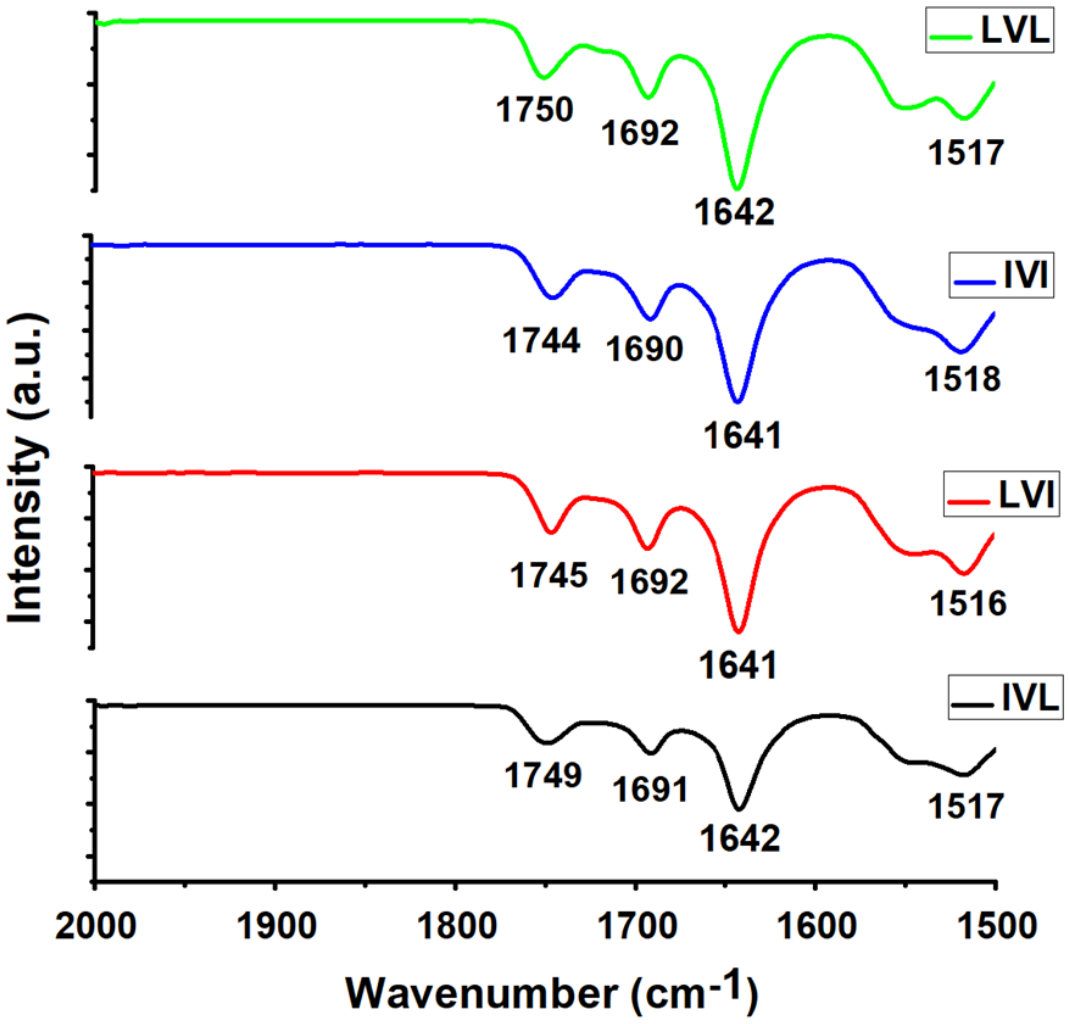

Figure 4.5. FTIR spectra of 4-day incubated peptide aggregate of LVL (green), IVI (blue), LVI (red), and IVL (black), respectively, (500 μM each) in a solid state.

4.5. N_2 Gas Adsorption Study

As the designed self-assembled tripeptides exhibited hollow nanostructures, clearly observed in the FESEM micrographs, their porosity characteristics were subsequently investigated. To assess this, nitrogen adsorption-desorption experiments were performed for all four tripeptides. The analysis revealed that, except for IVL, the other three sequences, namely, LVL, IVI, and LVI, displayed mesoporous behavior and followed type-III isotherm patterns (Figure 4.6). It is essential to note that purely organic mesoporous frameworks are typically characterized by relatively low surface areas.[28-35] In contrast, the N_2 sorption profiles of our peptide-based materials demonstrated appreciable adsorption capacities, with Brunauer-Emmett-Teller (BET) surface areas of 111.5 m^2/g for IVI, and 58.5 and 44.7 m^2/g for LVL and LVI, respectively, whereas IVL showed no adsorption activity.

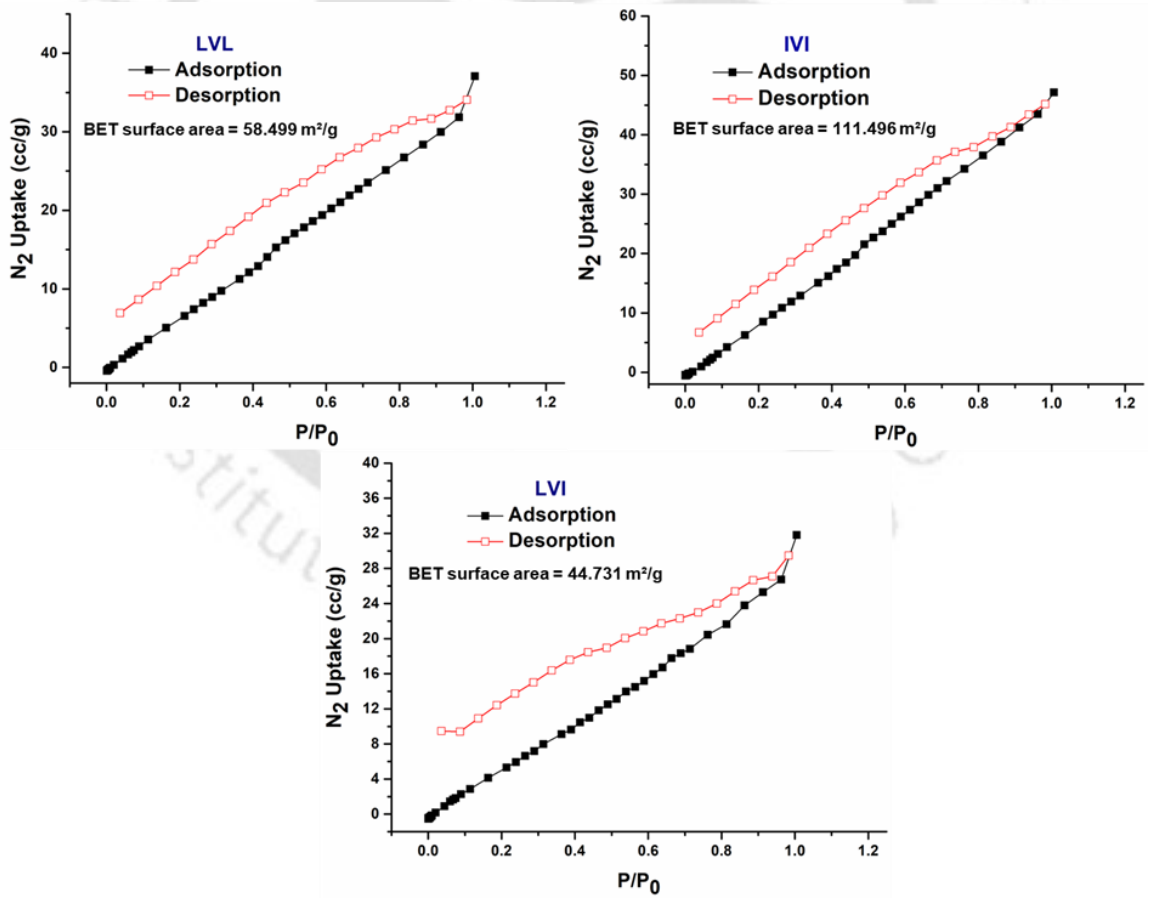

Figure 4.6. N_2 gas sorption isotherm of tripeptides LVL, IVI, and LVI, respectively.

4.6. Drug Encapsulation and Release Study

Another promising application of these nano-porous, hollow peptide-based assemblies lies in their potential use as carriers for targeted drug delivery. The encapsulation of small, biologically active drug molecules within peptide-based materials has rarely been documented.[36-39]

In this study, we investigated the encapsulation behaviour of curcumin, a hydrophobic fluorescent molecule known for its anticancer properties, within self-assembled tripeptide structures. To achieve this, 500 µM peptide solutions were prepared as previously described and co-incubated with 30 µM curcumin in a methanol–water (1:1) mixture at 37 °C. The encapsulation process was monitored using time-dependent fluorescence emission spectroscopy. Free curcumin (30 µM) displayed strong fluorescence intensity upon excitation at 435 nm; however, when incubated with the tripeptides, its fluorescence intensity gradually decreased over time, indicating encapsulation within the peptide assemblies. The monitoring was carried out for 36 hours, after which no notable change in intensity was observed. Among the samples, the curcumin–IVI mixture exhibited the most pronounced quenching (approximately 62% reduction in fluorescence intensity), followed by the curcumin–LVL mixture (around 50% reduction). Comparatively, the curcumin–LVI and curcumin–IVL mixtures showed very minimal inhibition (Figure 4.7).

Further confirmation of drug encapsulation was obtained through fluorescence microscopy. After 36 hours of co-incubation at 37 °C, each peptide–curcumin mixture (30 µM curcumin with 500 µM peptide) was drop-cast on clean glass slides and air-dried at room temperature before imaging. The emergence of distinct green fluorescence in the micrographs confirmed the successful entrapment of curcumin within the hollow, self-assembled architectures of the tripeptides (Figure 4.8). Also, the optical microscopy images for the tripeptide assemblies in the presence and absence of curcumin reveals that the overall morphology remained largely similar (Figure 4.8.e).

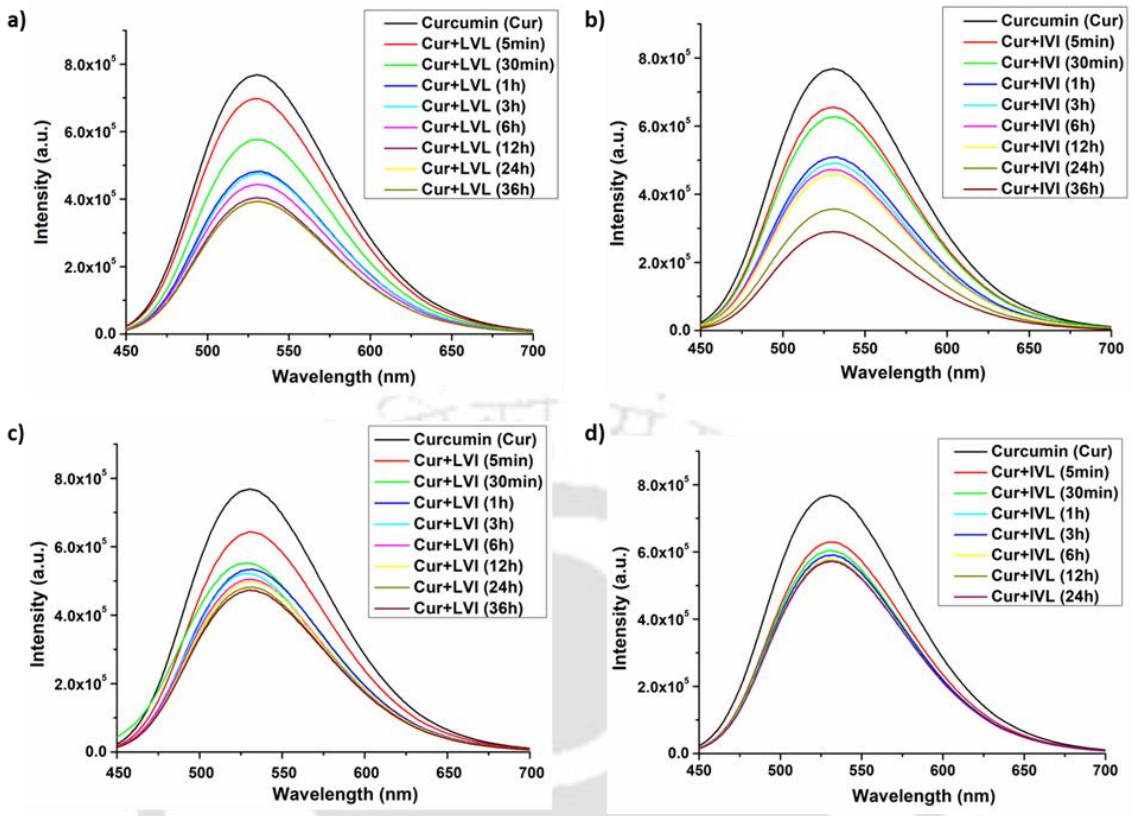

Figure 4.7. Time-dependent fluorescence emission spectra displaying curcumin encapsulation property of the peptides: a) LVL, b) IVI, c) LVI, and d) IVL.

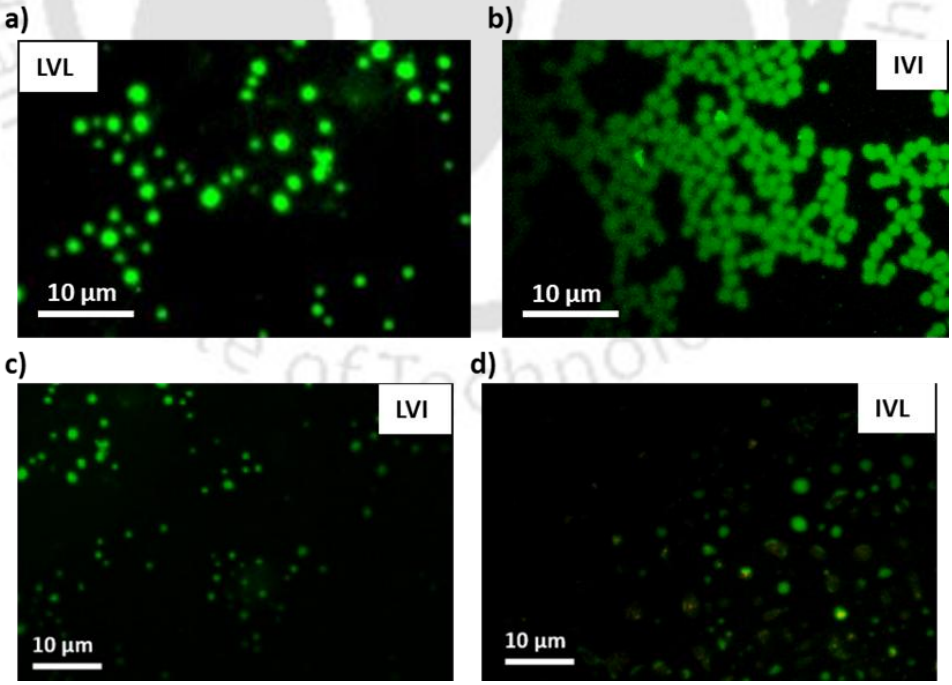

Figure 4.8. *Fluorescence microscopic images of curcumin (30 µM) mixed tripeptide solutions of a) LVL, b) IVI, c) LVI, and d) IVL (500 µM each) after 36 hr incubation at 37 ℃.*

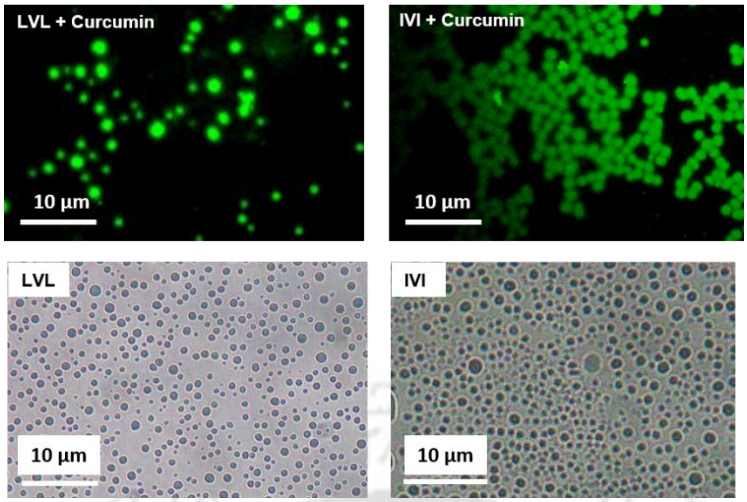

Figure 4.8. *e). Optical microscopy images of LVL and LVI tripeptides in presence and absence of curcumin.*

To explore the release behaviour of the encapsulated drug, we examined the disruption of peptide assemblies triggered by salt treatment. 1.5 mM KCl solution was added to 2-day-old incubated curcumin–IVI and curcumin–LVL for this purpose, followed by an additional incubation of 12 hours under the same experimental conditions. This led to an increase in fluorescence intensity of the curcumin molecule, suggesting the release of curcumin from the peptide framework (Figure 4.9). Microscopic analysis (Figure 4.10) and FESEM imaging (Figure 4.11) further confirmed the salt-induced disintegration of the hollow nanostructures, validating the release mechanism. As the encapsulation efficiency of the curcumin–LVI and curcumin–IVL systems was comparatively low, their salt-mediated release behaviour was not further examined.

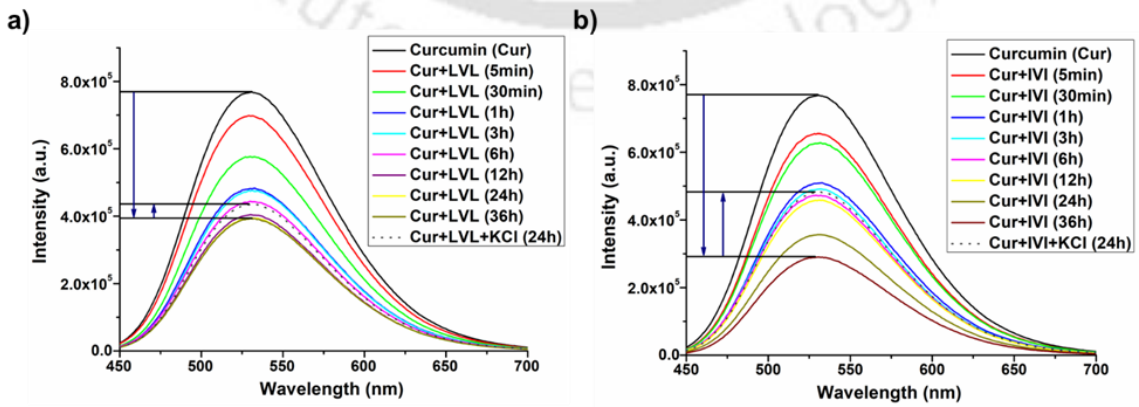

Figure 4.9. *Fluorescence emission spectra displaying the release of the encapsulated curcumin molecule for a) LVL, and b) IVI, when treated with KCl solution (1.5 mM).*

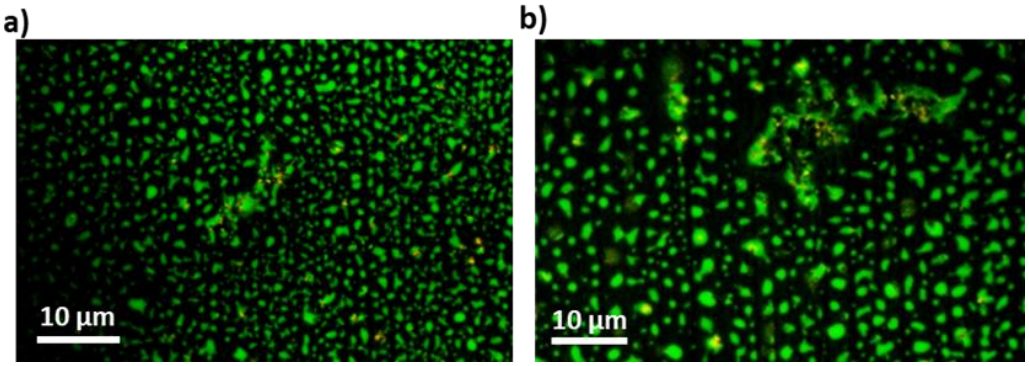

Figure 4.10. *Fluorescence microscopic images displaying disruption of curcumin mixed peptide morphology, a) LVL, and b) IVI, on being treated with KCl solution (1.5 mM).*

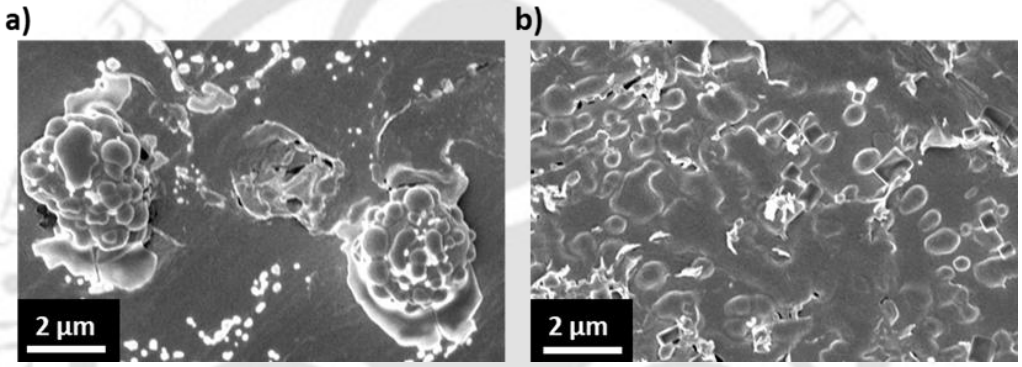

Figure 4.11. *FESEM images displaying disruption of peptide morphology: a) LVL and b) IVI when treated with KCl solution (1.5 mM).*

To further probe how curcumin is encapsulated within the self-assembled tripeptide, FTIR analysis was carried out on peptide-curcumin mixtures prepared at the same concentration ratios as described above. Their spectra were then compared with those of the corresponding peptide assemblies recorded under identical experimental conditions. Although FTIR is not highly sensitive to the quantitative extent of encapsulation, qualitative differences between the spectra can still reveal how the guest molecule interacts with the peptide framework. Notably, the spectra of the curcumin-loaded samples (Figure 4.12) retain the overall band shapes and positions seen for the peptide assemblies alone. This close similarity suggests that predominantly hydrophobic interactions govern the incorporation of curcumin into the nanostructures. Free curcumin typically displays a distinct and prominent C=O stretching band near 1622 cm^{-1}, the aromatic ring vibration around 1600 cm^{-1}, and mixed C=O/C=C vibrations near 1504 cm^{-1}. The absence of these characteristic signals suggests that curcumin got sequestered within the hollow interiors of

the self-assembled peptide assemblies. This interpretation is consistent with previous observations reported by Paramera and co-workers.[40]

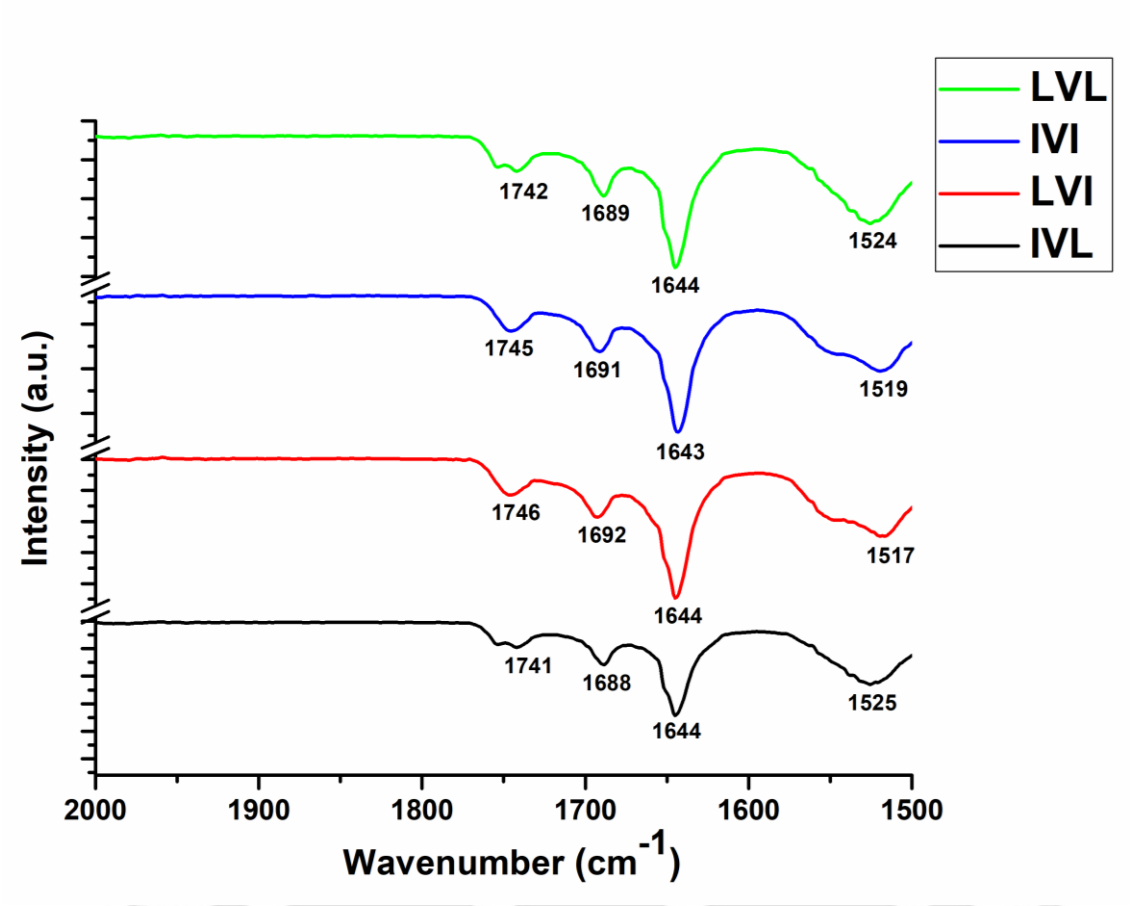

Figure 4.12. *FTIR spectra of 4-day incubated curcumin mixed peptide aggregate of LVL, IVI, LVI, and IVL, respectively, in solid state.*

A comparison of the TGA profiles of the curcumin mixed tripeptides with those of the individual peptides under identical compositions and conditions (Figure 4.13) showed a modest increase in thermal stability upon addition of curcumin. This enhancement is consistent with the encapsulation of curcumin within the peptide assemblies. A similar stabilizing effect of curcumin incorporation has been noted previously by Park and co-workers, aligning well with our findings.[41]

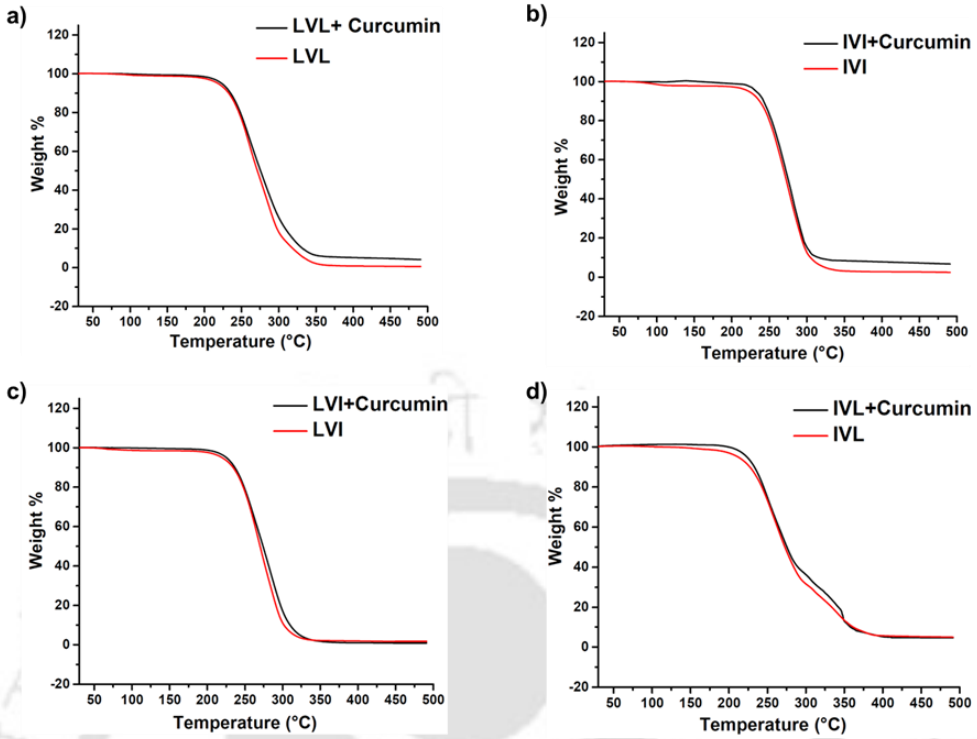

Figure 4.13. *TGA profile of 4-day incubated curcumin mixed peptide aggregate: a) LVL, b) IVI, c) LVI, and d) IVL.*

A probable mechanism for the encapsulation of the curcumin molecule co-incubated with the tripeptide solutions can be discussed as follows:

Our designed self-assembled tripeptides spontaneously organize into hollow nanostructures. During this assembly process, curcumin becomes integrated into the growing architecture rather than attempting to penetrate an already formed shell. Such co-assembly enables curcumin to be efficiently confined within the developing internal cavity. The resulting hollow spaces provide a hydrophobic interior that is well-suited to accommodate the highly hydrophobic curcumin molecule. The inclusion of curcumin is primarily driven by hydrophobic interactions between the drug and the peptide-rich core, which help retain the molecule within the structure as it forms. These interactions are likely complemented by short-range van der Waals contacts that further stabilize the encapsulated drug molecule. Through this mechanism, the self-assembling peptides create nanoscale compartments that not only entrap the drug molecule but also shield it from the surrounding environment. This confinement not only improves curcumin's stability and bioavailability but also supports a more gradual and controlled release profile. Overall, the co-assembly

pathway offers a more effective and robust mode of incorporation compared to simple surface adsorption.

4.7. Thermal Stability Study

To evaluate the thermal stability of the designed tripeptides, thermogravimetric analysis (TGA) was performed. The tripeptide samples were incubated for four days in a 1:1 methanol–water mixture, followed by lyophilization to obtain the aggregated solids used for analysis. Typically, in a TGA profile, the initial weight loss observed between 25 and 200 °C corresponds to the evaporation of surface-adsorbed or bound water molecules. At the same time, the subsequent decrease in mass within the 200–500 °C range is attributed to the breakdown of peptide bonds.[67] In the present study, all tripeptide assemblies exhibited the onset of weight loss only above 200 °C, indicating that the self-assembled structures possess considerable thermal stability. Furthermore, the absence of any noticeable mass loss below 200 °C suggests that no residual water or solvent molecules were trapped within the dried peptide aggregates (Figure 4.14).

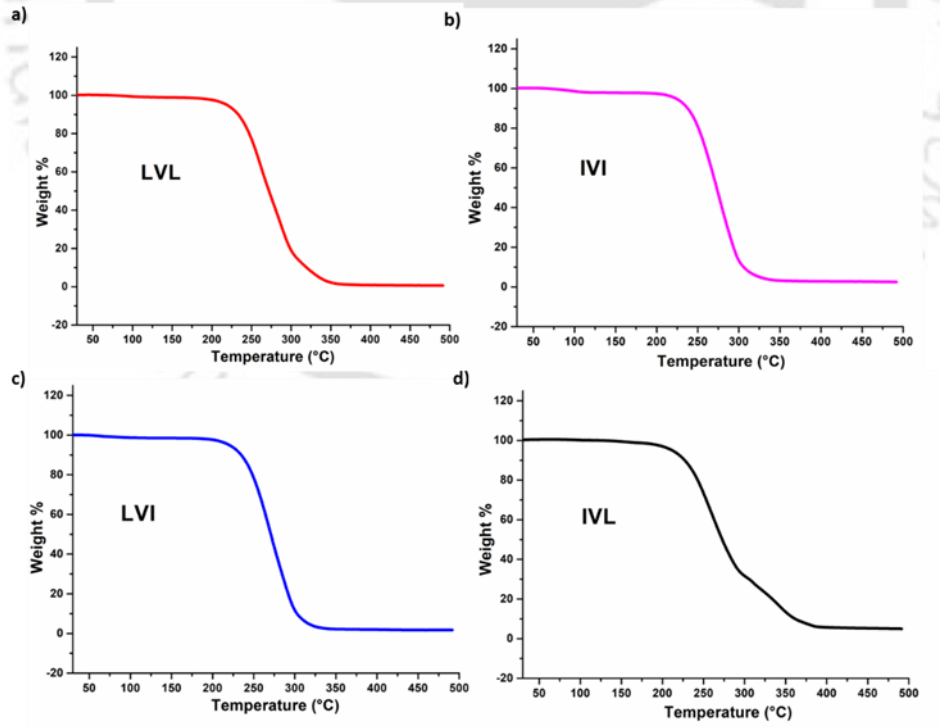

Figure 4.14. *TGA profile of the aggregated mass obtained from the peptides: a) LVL, b) IVI, c) LVI, and d) IVL.*

4.8. Conclusion

In summary, our study demonstrates a distinct time-dependent morphological transformation of tripeptides from nanospherical to rod-like structures through self-assembly. Among the investigated sequences, the fully protected hydrophobic tripeptides with identical terminal residues (LVL and IVI) exhibited the most pronounced morphological transitions, while the change was less evident for LVI and absent in IVL. These structural variations were further correlated with their surface properties and functional behaviour: LVL and IVI showed enhanced nitrogen adsorption capacities and superior curcumin encapsulation efficiencies, resulting in 50% and 62% fluorescence quenching, respectively. The temporal evolution of morphology was confirmed using FESEM and FETEM analyses, and the results were further supported by a DLS study. CD and FTIR studies indicated the coexistence of random coil and β-sheet conformations within the self-assembled architectures. Moreover, the porous peptide nanostructures showed reversible KCl-triggered release of encapsulated curcumin, underscoring their potential as time-responsive biomaterials. Collectively, these findings highlight the significance of molecular design in controlling peptide self-assembly, and they pave the way for the development of controllable, peptide-based nanocarriers for drug delivery applications.

4.9. Characterization data

Boc-Leu-Val-Leu-OMe (LVL)

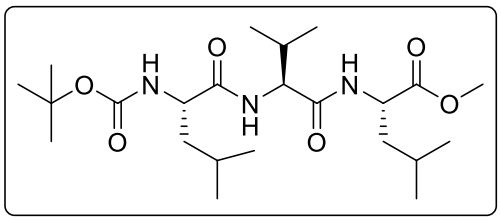

White solid, M.P 140-143 °C, (^{1}H NMR ($CDCl_3$; 600 MHz) δ in ppm 0.94-0.88 (18H, m); 1.40 (9H, s); 1.65-1.57 (4H, m); 2.10-2.06 (1H, m); 2.47 (1H, s); 3.70 (3H, s); 4.21-4.17 (1H, m); 4.37-4.34 (1H, t, *J* = 8.4 Hz); 4.58-4.55 (1H, m); 5.43 (1H, s); 7.09 (1H, s); 7.28 (1H, s). ^{13}C NMR ($CDCl_3$; 150 MHz) δ in ppm 18.3, 19.2, 21.9, 22.3, 22.9, 24.9, 28.4, 31.0, 41.1, 50.8, 52.3, 53.3, 58.6, 79.8, 155.8, 171.4, 172.9, 173.3. HRMS (ESI): calculated $[M+H]^+$ =458.3230, observed m/z = 458.3225. HPLC: retention time (t_R) = 12.621 min. The purified tripeptide 480 mg (Yield = 76% w.r.t. initial substrate Boc-L-Val-OH).

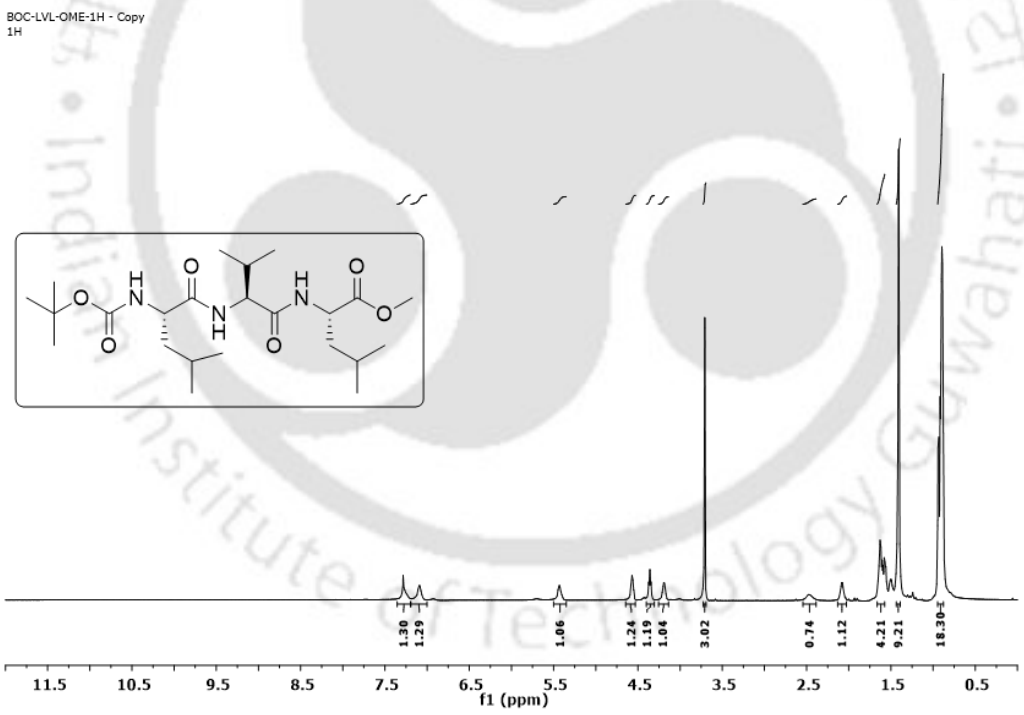

Figure 4.15. *^{1}H NMR spectra of peptide* ***Boc-Leu-Val-Leu-OMe (LVL)****.*

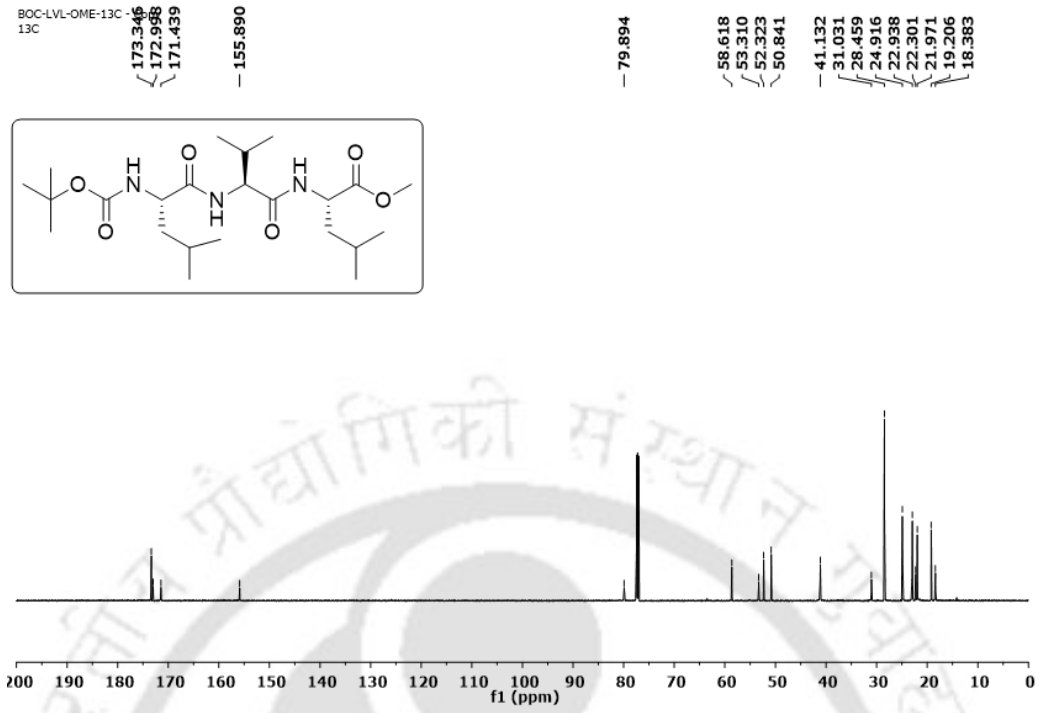

Figure 4.16. *^{13}C NMR spectra of peptide* ***Boc-Leu-Val-Leu-OMe (LVL)****.*

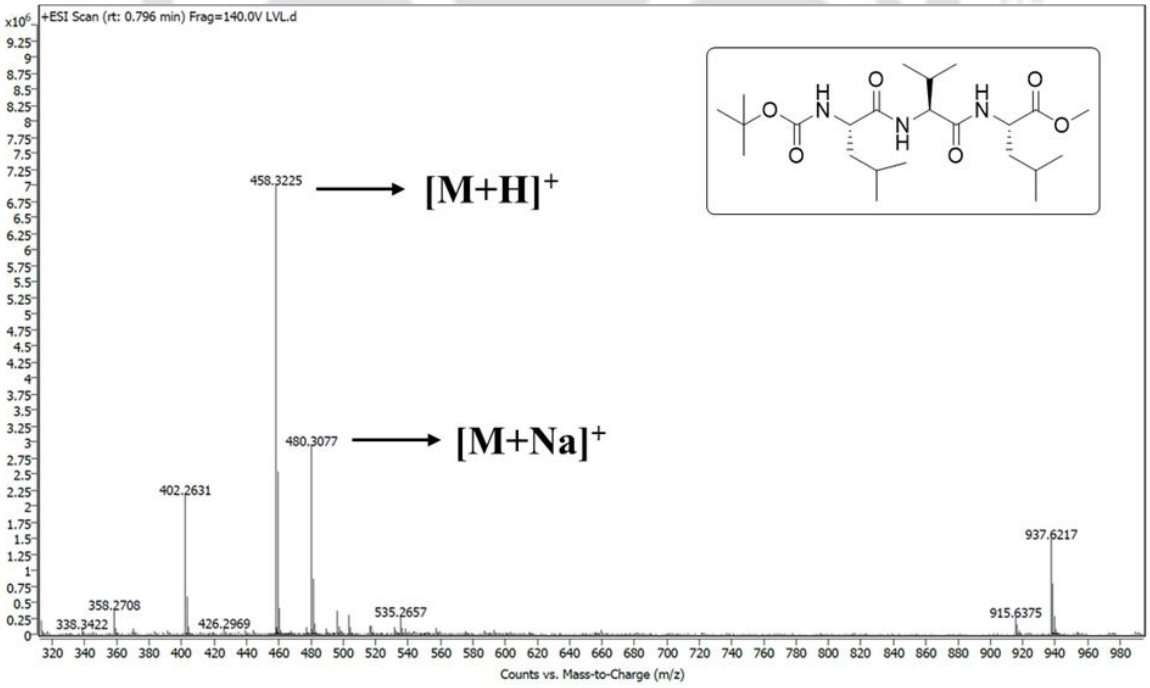

Figure 4.17. *MS spectra of peptide* ***Boc-Leu-Val-Leu-OMe (LVL).***

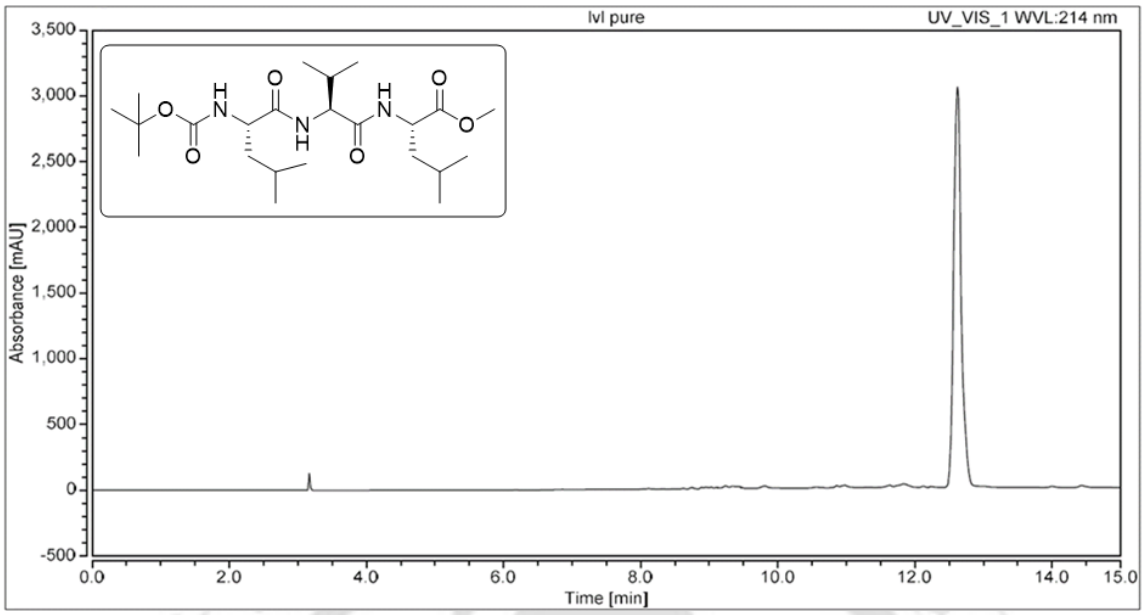

Figure 4.18. *HPLC profile picture of purified peptide* ***Boc-Leu-Val-Leu-OMe (LVL)****.*

Boc-Ile-Val-Ile-OMe (IVI)

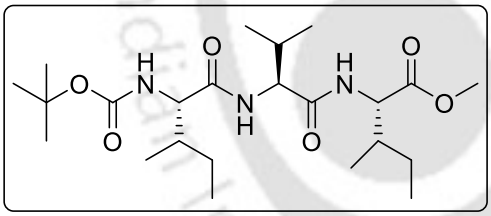

White solid, **M.P** 165-167 ºC, (**^{1}H NMR (CDCl$_3$; 600 MHz)** δ in ppm 0.86-0.82 (12H, m); 0.89 (6H, s); 1.18-1.07 (2H, m); 1.38 (9H, s); 1.54-1.53 (1H, m); 1.81-1.76 (1H, m); 1.91-1.85 (1H, m); 2.04-2.00 (1H, m); 3.69 (3H, s); 4.01-3.98 (1H, t, *J* = 9.0 Hz); 4.47-4.45 (1H, t, *J* = 7.8 Hz); 4.58-4.55 (1H, t, *J* = 6.0 Hz); 5.76 (1H, s); 7.28-7.21 (1H, m); 7.54-7.52 (1H, m). **^{13}C NMR (CDCl$_3$; 150 MHz)** δ in ppm 11.2, 11.5, 15.5, 18.6, 19.1, 25.0, 25.1, 28.4, 30.9, 36.8, 37.5, 52.0, 56.5, 58.7, 59.4, 79.4, 156.0, 171.7, 172.4. HRMS (ESI): calculated $[M+H]^+$ = 458.3230, observed m/z = 458.3226. HPLC: retention time (t_R) = 12.703 min. The purified tripeptide 498 mg (Yield = 78% w.r.t. initial substrate Boc-L-Val-OH).

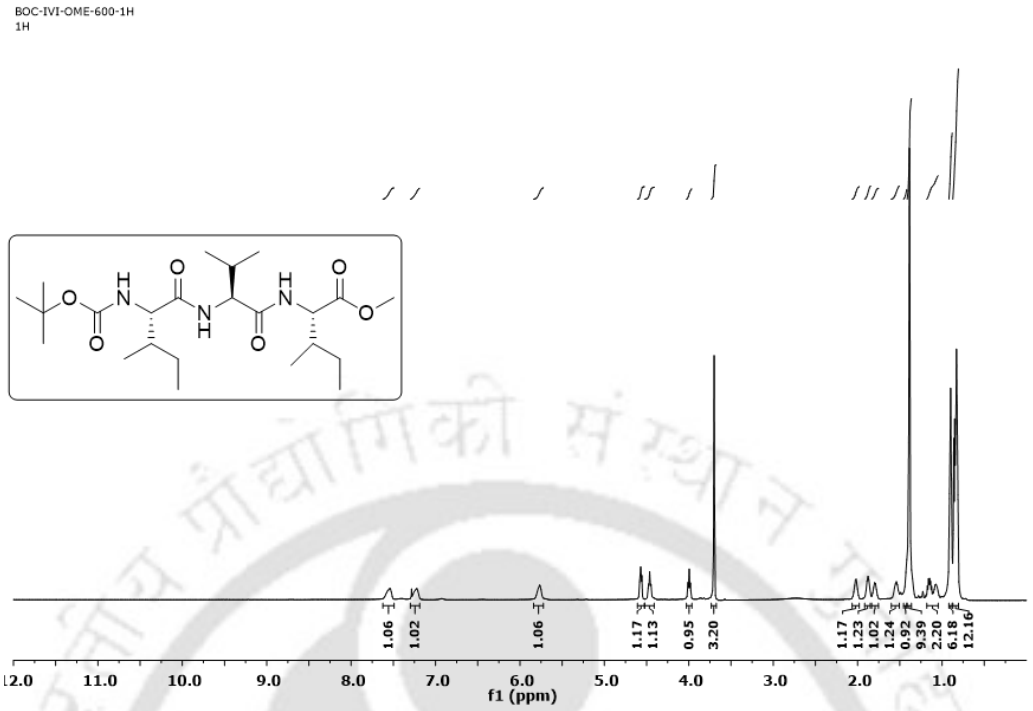

Figure 4.19. *[1]H NMR spectra of peptide* ***Boc-Ile-Val-Ile-OMe (IVI).***

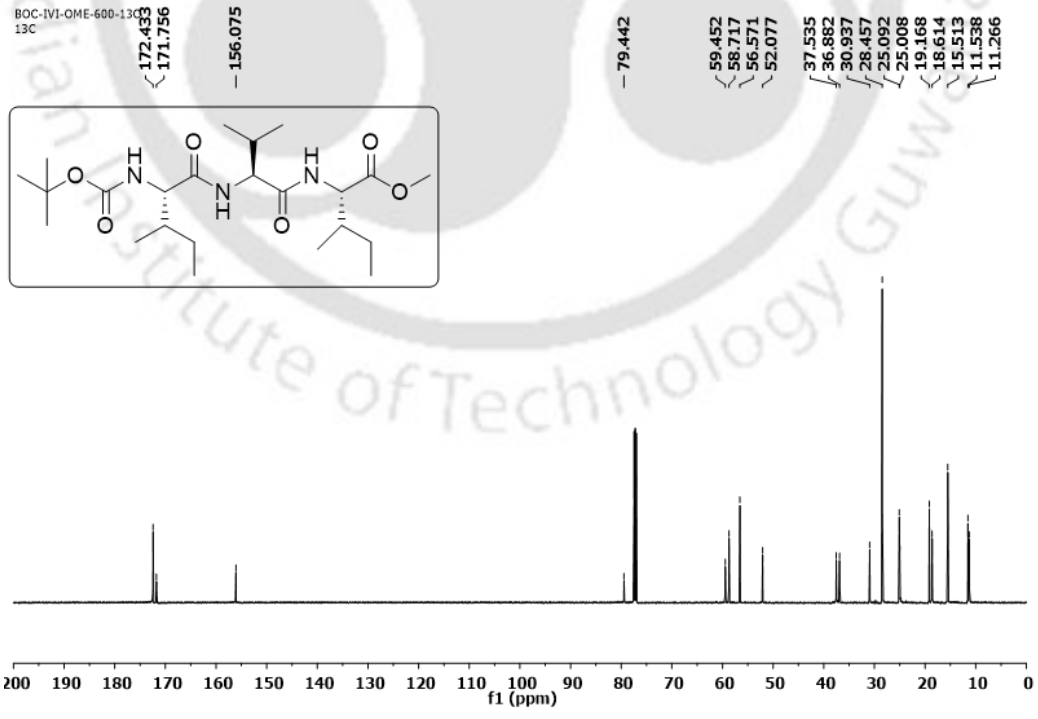

Figure 4.20. *[13]C NMR spectra of peptide* ***Boc-Ile-Val-Ile-OMe (IVI).***

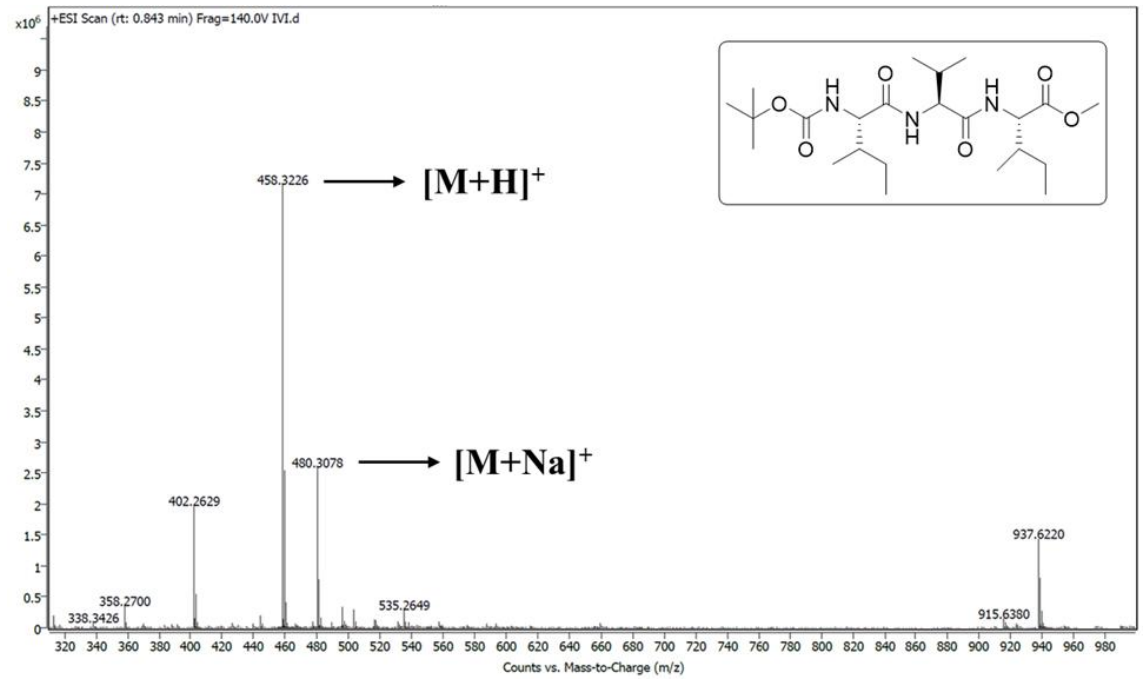

Figure 4.21. *MS spectra of peptide* ***Boc-Ile-Val-Ile-OMe (IVI).***

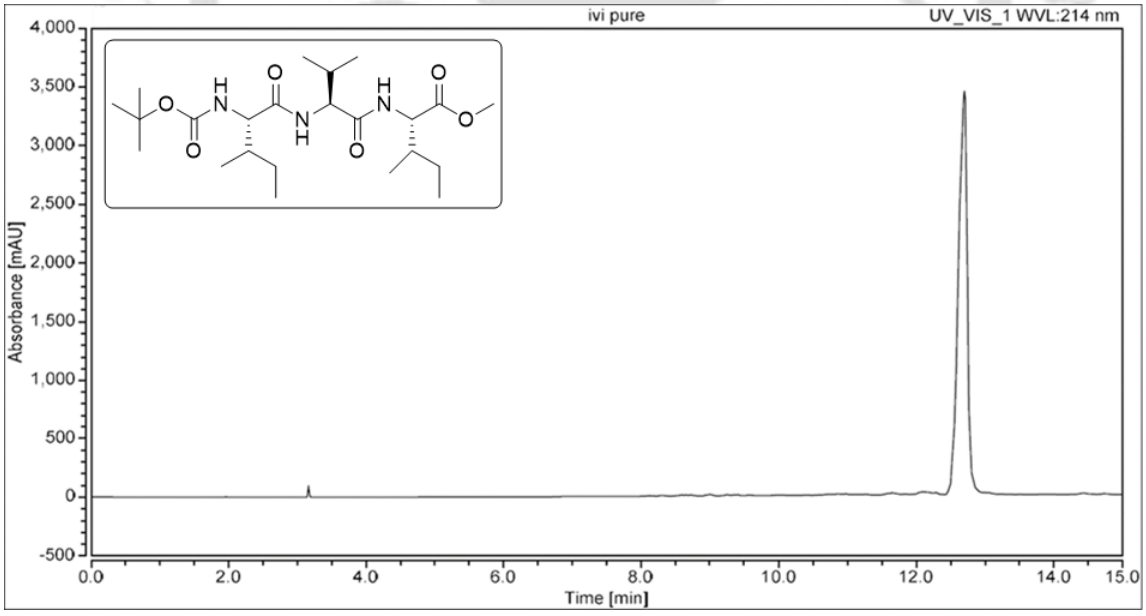

Figure 4.22. *HPLC profile picture of purified peptide* ***Boc-Ile-Val-Ile-OMe (IVI).***

Boc-Leu-Val-Ile-OMe (LVI)

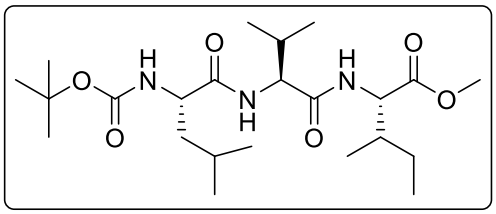

White solid, **M.P** 143-145 ºC, (**^{1}H NMR (CDCl$_3$; 600 MHz)** δ in ppm 0.92-0.86 (18H, m); 1.18-1.12 (1H, m); 1.40 (9H, s); 1.51-1.48 (1H, m); 1.65-1.61 (1H, m); 1.90-1.87 (1H, m); 2.08-2.03 (1H, m); 2.51 (1H, s); 3.71 (3H, s); 4.20-4.16 (1H, m); 4.41-4.39 (1H, t, *J* = 7.2 Hz); 4.56-4.54 (1H, m); 5.46 (1H, s); 7.06 (1H, s); 7.28 (1H, s). **^{13}C NMR (CDCl$_3$; 150 MHz)** δ in ppm 11.6, 15.5, 18.3, 19.2, 22.2, 23.0, 24.8, 25.1, 31.0, 37.6, 41.0, 52.1, 53.2, 56.6, 58.6, 79.8, 155.8, 171.5, 172.3, 173.0. HRMS (ESI): calculated $[M+H]^+$ = 458.3230, observed m/z = 458.3218. HPLC: retention time (t_R) = 12.653 min. The purified tripeptide 475 mg (Yield = 75% w.r.t. initial substrate Boc-L-Val-OH).

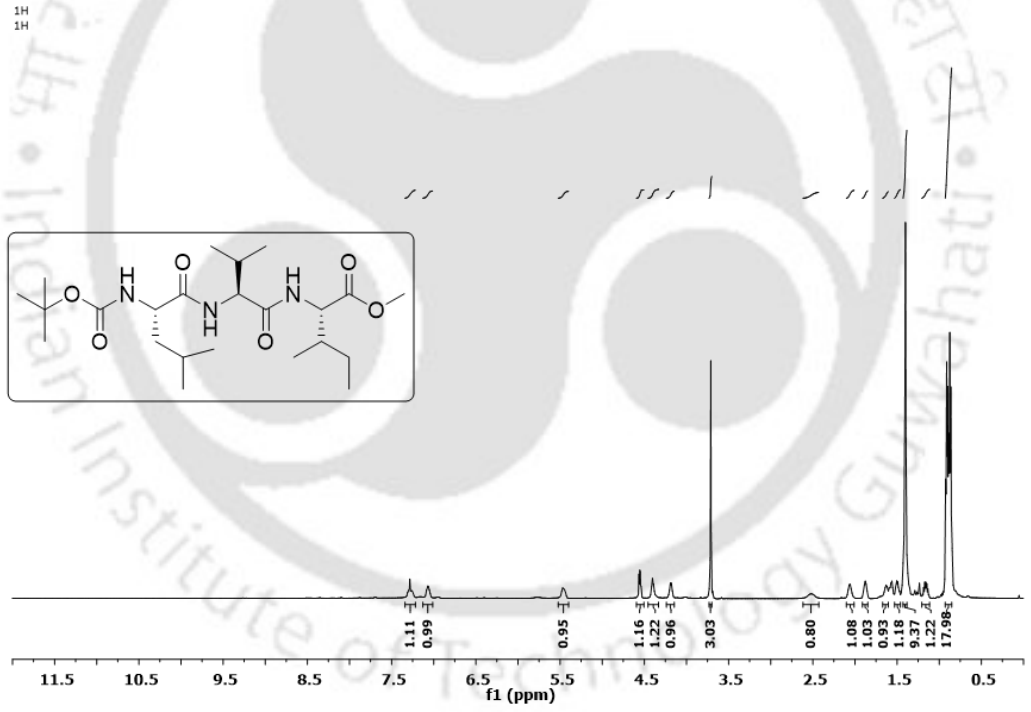

Figure 4.23. *^{1}H NMR spectra of peptide* ***Boc-Leu-Val-Ile-OMe (LVI).***

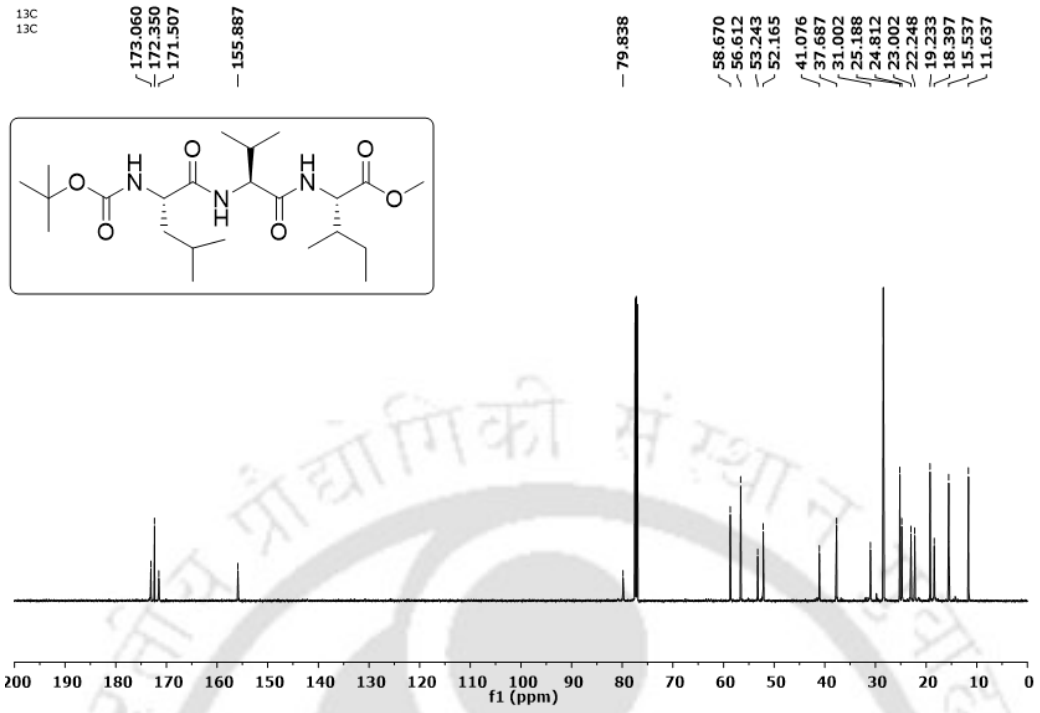

Figure 4.24. *^{13}C NMR spectra of peptide* ***Boc-Leu-Val-Ile-OMe (LVI).***

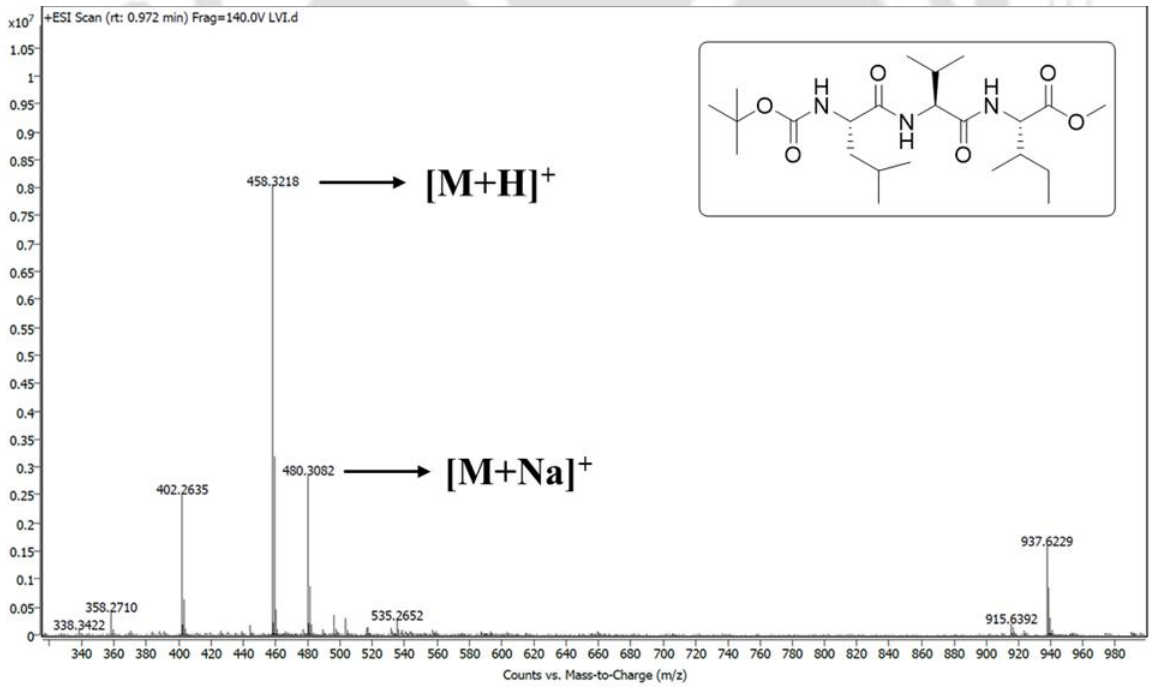

Figure 4.25. *MS spectra of peptide* ***Boc-Leu-Val-Ile-OMe (LVI).***

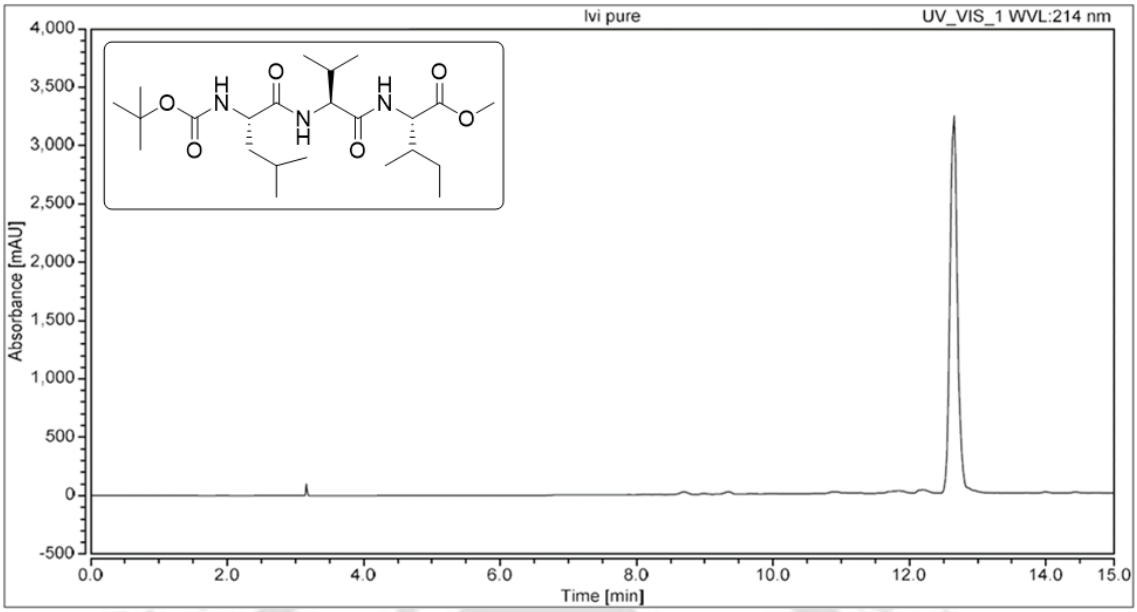

Figure 4.26. *HPLC profile picture of purified peptide* ***Boc-Leu-Val-Ile-OMe (LVI).***

Boc-Ile-Val-Leu-OMe (IVL)

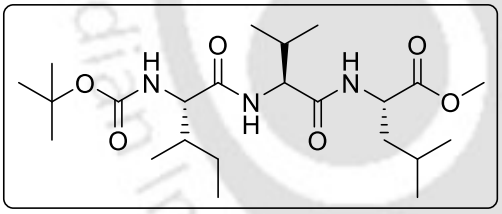

White solid, **M.P** 169-172°C, (**^{1}H NMR (CDCl$_3$; 600 MHz)** δ in ppm 0.94-0.83 (18H, m); 1.11-1.06 (1H, m); 1.40 (9H, s); 1.43 (1H, s); 1.63-1.60 (2H, m); 1.82-1.78 (1H, m); 2.09-2.03 (1H, m); 3.70 (3H, s); 4.02-3.99 (1H, t, *J* = 8.4 Hz); 4.40-4.37 (1H, t, *J* = 8.4 Hz); 4.59-4.56 (1H, m); 5.66 (1H, s); 7.28 (1H, s); 7.41 (1H, s). **^{13}C NMR (CDCl$_3$; 150 MHz)** δ in ppm 11.3, 15.5, 18.5, 19.1, 21.7, 23.0, 24.8, 25.0, 28.4, 30.9, 37.0, 40.9, 50.8, 52.3, 58.6, 59.5, 79.6, 156.0, 171.6, 172.4, 173.3. HRMS (ESI): calculated $[M+H]^+$ = 458.3230, observed m/z = 458.3225. HPLC: retention time (t_R) = 12.560. The purified tripeptide 473 mg (Yield = 74% w.r.t. initial substrate Boc-L-Val-OH).

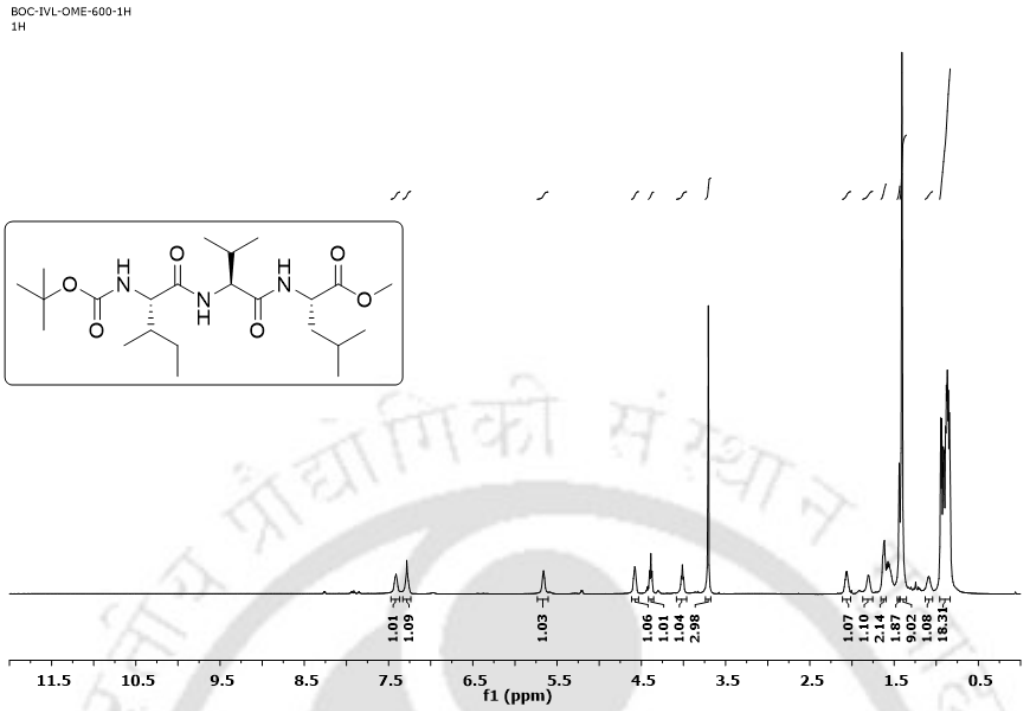

Figure 4.27. *[1]H NMR spectra of peptide* ***Boc-Ile-Val-Leu-OMe (IVL).***

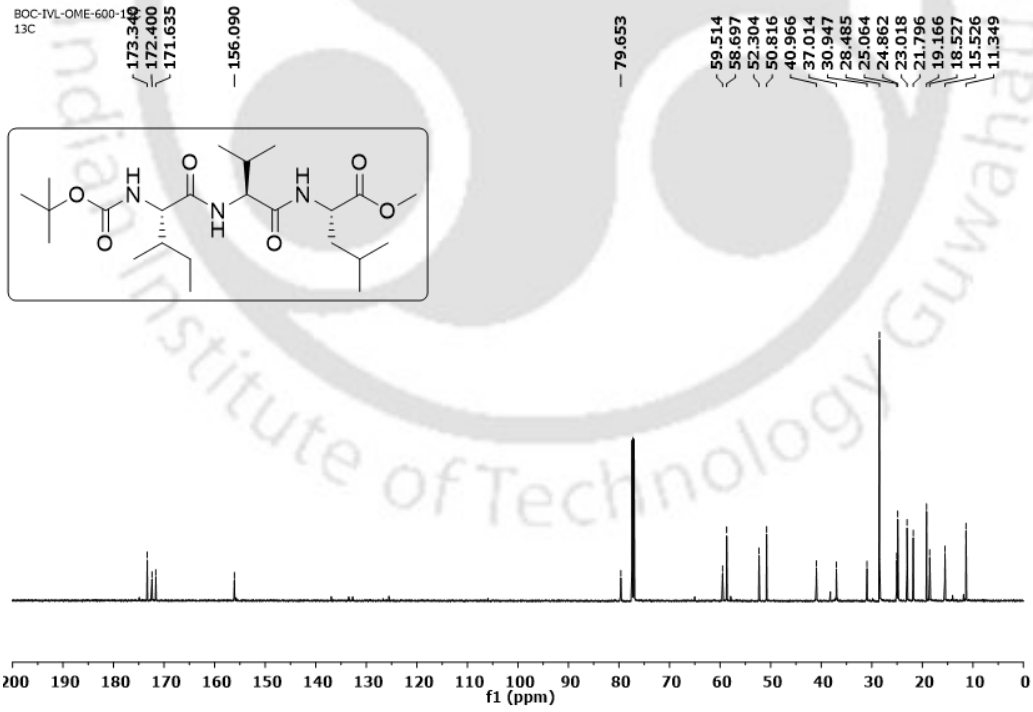

Figure 4.28. *[13]C NMR spectra of peptide* ***Boc-Ile-Val-Leu-OMe (IVL).***

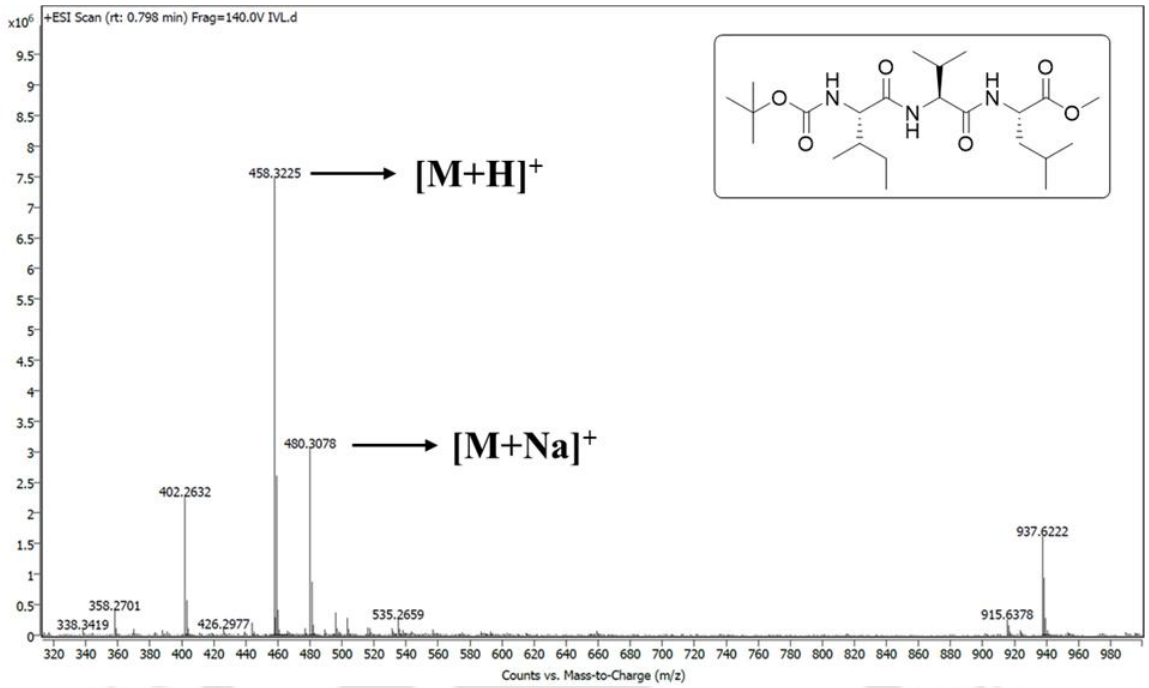

Figure 4.29. *MS spectra of peptide* ***Boc-Ile-Val-Leu-OMe (IVL).***

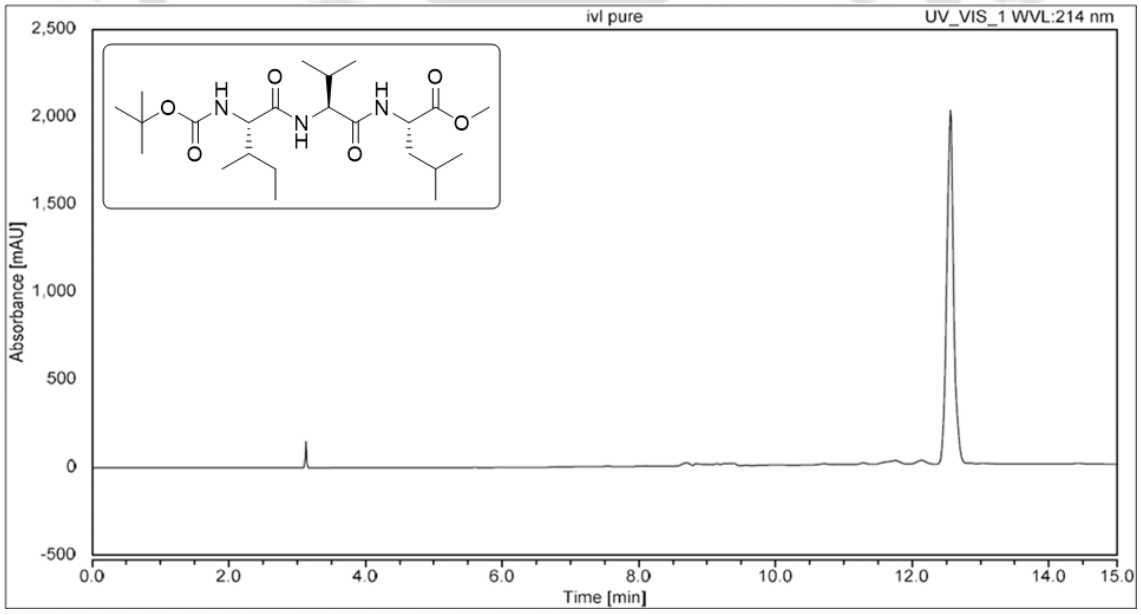

Figure 4.30. *HPLC profile picture of purified peptide* ***Boc-Ile-Val-Leu-OMe (IVL)****.*

4.10. References

1. Castelletto, V.; Hamley, I. W.; Harris, P. J. F. Self-assembly in aqueous solution of a modified amyloid beta peptide fragment. *Biophys. Chem.* **2008**, *138*, 29-35.
2. Balbach, J. J.; Ishii, Y.; Antzutkin, O. N.; Leapman, R. D.; Rizzo, N. W.; Dyda, F.; Tycko, R. Amyloid fibril formation by Aβ16-22, a seven-residue fragment of the Alzheimer's β-amyloid peptide, and structural characterization by solid state NMR. *Biochem.* **2000**, *39*, 13748-13759.
3. Kalita, S.; Kalita, S.; Kawa, A. H.; Shill, S.; Gupta, A.; Kumar, S.; Mandal, B. Copper chelating cyclic peptidomimetic inhibits Aβ fibrillogenesis. *RSC Med. Chem.* **2022**, *13*, 761-774.
4. Pashuck, E. T.; Stupp, S. I. Direct observation of morphological tranformation from twisted ribbons into helical ribbons. *J. Am. Chem. Soc.* **2010**, *132*, 8819-8821.
5. Sadownik, J. W.; Leckie, J.; Ulijn, R. V. Micelle to fibre biocatalytic supramolecular transformation of an aromatic peptide amphiphile. *Chem. Commun.* **2011**, *47*, 728-730.
6. Ke, D.; Zhan, C.; Li, A. D.; Yao, J. Morphological Transformation between Nanofibers and Vesicles in a Controllable Bipyridine–Tripeptide Self-Assembly. *Angew. Chem.* **2011**, *123*, 3799-3803.
7. Ueda, M.; Makino, A.; Imai, T.; Sugiyama, J.; Kimura, S. Transformation of peptide nanotubes into a vesicle via fusion driven by stereo-complex formation. *Chem. Commun.* **2011**, *47*, 3204-3206.
8. Shao, H.; Parquette, J. R. Controllable Peptide–Dendron Self-Assembly: Interconversion of Nanotubes and Fibrillar Nanostructures. *Angew. Chem.* **2009**, *121*, 2563-2566.
9. Qin, S. Y.; Chu, Y. F.; Tao, L.; Xu, S. S.; Li, Z. Y.; Zhuo, R. X.; Zhang, X. Z. Controllable micro/nanostructures via hierarchical self-assembly of cyclopeptides. *Soft Matter* **2011**, *7*, 8635-8641.
10. Vauthey, S., Santoso, S., Gong, H., Watson, N., & Zhang, S. Molecular self-assembly of surfactant-like peptides to form nanotubes and nanovesicles. *Proc. Natl. Acad. Sci.* **2002**, *99*, 5355-5360.
11. Reches, M.; Gazit, E. Formation of closed-cage nanostructures by self-assembly of aromatic dipeptides. *Nano Lett.* **2004**, *4*, 581-585.
12. Yan, X.; Cui, Y.; He, Q.; Wang, K.; Li, J.; Mu, W.; Ou-yang, Z. C. Reversible transitions between peptide nanotubes and vesicle-like structures including theoretical modeling studies. *Chem. Eur. J.* **2008**, *14*, 5974-5980.
13. Yan, X.; He, Q.; Wang, K.; Duan, L.; Cui, Y.; Li, J. Transition of cationic dipeptide nanotubes into vesicles and oligonucleotide delivery. *Angew. Chem. Int. Ed.* **2007**, *46*, 2431-2434.
14. Song, Y.; Challa, S. R.; Medforth, C. J.; Qiu, Y.; Watt, R. K.; Peña, D.; Shelnutt, J. A. Synthesis of peptide-nanotube platinum-nanoparticle composites. *Chem. Commun.* **2004,** 1044-1045.
15. Matsui, H.; Holtman, C. Organic nanotube bridge fabrication by controlling molecular self-assembly processes between spherical and tubular formations. *Nano Lett.* **2002**, *2*, 887-889.
16. Qin, S. Y.; Xu, S. S.; Zhuo, R. X.; Zhang, X. Z. Morphology transformation via pH-triggered self-assembly of peptides. *Langmuir* **2012**, *28*, 2083-2090.
17. Maity, S.; Jana, P.; Maity, S. K.; Haldar, D. Fabrication of hollow self-assembled peptide microvesicles and transition from sphere-to-rod structure. *Langmuir* **2011**, *27*, 3835-3841.

18. Yamada, K.; Sato, J.; Oku, H.; Katakai, R. Conformation of the transmembrane domains in peripheral myelin protein 22. Part 1. Solution-phase synthesis and circular dichroism study of protected 17-residue partial peptides in the first putative transmembrane domain. *J. Peptide Res*. **2003**, *62*, 78-87.
19. Han, S.; Cao, S.; Wang, Y.; Wang, J.; Xia, D.; Xu, H.; Zhao, X.; Lu, J. R. Self-Assembly of Short Peptide Amphiphiles: The Cooperative Effect of Hydrophobic Interaction and Hydrogen Bonding. *Chem.Eur. J.* **2011**, *17*, 13095-13102.
20. Ma, X.; Zhao, Y.; He, C.; Zhou, X.; Qi, H.; Wang, Y.; Chen, C.; Wang, D.; Li, J.; Ke, Y.; Wang, J.; Xu, H. Ordered Packing of β-Sheet Nanofibrils into Nanotubes: Multi-hierarchical Assembly of Designed Short Peptides. *Nano Lett.* **2021**, *21*, 10199-10207.
21. Levin, A.; Mason, T. O.; Adler-Abramovich, L.; Buell, A. K.; Meisl, G.; Galvagnion, C.; Bram, Y.; Stratford, S. A.; Dobson, C. M.; Knowles, T. P. J.; Gazit, E. Ostwald's rule of stages governs structural transitions and morphology of dipeptide supramolecular polymers. *Nat. Commun.* **2014**, *5*, 5219.
22. Dolai, G.; Shill, S.; Roy, S.; Mandal, B. Atomic Insight on Inhibition of Fibrillization of Dipeptides by Replacement of Phenylalanine with Tryptophan. *Langmuir* **2023**, *39*, 9367-9383.
23. Roy, S.; Giri, R. S.; Dolai, G.; Mandal, B. Role of side-chain and chirality of the amino acids on the supramolecular assemblies of dipeptides. *J. Mol. Str.* **2020**, *1221*, 128877.
24. Di Foggia, M.; Taddei, P.; Torreggiani, A.; Dettin, M.; Tinti, A. Self-assembling peptides for biomedical applications: IR and Raman spectroscopies for the study of secondary structure. *J. Proteome Res*. **2011**, *2*, 231.
25. Fink, A. L.; Calciano, L.J.; Goto, Y.; Nishimura, M.; Swedberg, S. A. Characterization of the stable, acid-induced, molten globule-like state of staphylococcal nuclease. *Protein Sci.* **1993**, *2*, 1155-1160.
26. Pelton, J. T.; McLean, L. R. Spectroscopic methods for analysis of protein secondary structure. *Anal. Biochem.* **2000**, *277*, 167-176.
27. Vass, E.; Hollósi, M.; Besson, F.; Buchet, R. Vibrational spectroscopic detection of beta-and gamma-turns in synthetic and natural peptides and proteins. *Chem. Rev*. **2003**, *103*, 1917-1954.
28. H. Mao.; M. A. Hillmyer. Macroscopic samples of polystyrene with ordered three-dimensional nanochannels. *Soft Matter* **2006**, *2*, 57-59.
29. W. M. Qiao.; Y. Song.; S. H. Hong.; S. Y. Lim.; S. H. Yoon.; Y. Korai.; I. Mochida. Development of Mesophase Pitch Derived Mesoporous Carbons through a Commercially Nanosized Template. *Langmuir* **2006**, *22*, 3791-3797.
30. Y. Lu. Surfactant-Templated Mesoporous Materials: From Inorganic to Hybrid to Organic. Angew. Chem. Int. Ed. **2006**, *45*, 7664-7667.
31. Y. Yan.; F. Zhang.; Y. Meng.; B. Tu.; D. Zhao. One-step synthesis of ordered mesoporous carbonaceous spheres by an aerosol-assisted self-assembly. *Chem. Commun.* **2007**, 2867-2869.
32. D. Chandra.; B. K. Jena.; C. R. Raj.; A. Bhaumik. Functionalized Mesoporous Cross-Linked Polymer As Efficient Host for Loading Gold Nanoparticles and Its Electrocatalytic Behavior for Reduction of H_2O_2. *Chem. Mater.* **2007**, *19*, 6290-6296.
33. M.M. Titirici.; A. Thomas.; M. Antonietti. Aminated hydrophilic ordered mesoporous carbons. *J. Mater. Chem.* **2007**, *17*, 3412-3418.

34. M. Nandi.; R. Gangopadhyay.; A. Bhaumik. Mesoporous polyaniline having high conductivity at room temperature. *Microporous Mesoporous Mater* **2008**, *109*, 239-247.
35. Chandra, D.; Bhaumik, A. A new functionalized mesoporous polymer with high efficiency for the removal of pollutant anions. *J. Mater. Chem.* **2009**, *19*, 1901-1907.
36. Yan, X.; He, Q.; Wang, K.; Duan, L.; Cui, Y.; Li, J. Transition of cationic dipeptide nanotubes into vesicles and oligonucleotide delivery. *Angew. Chem.* **2007**, *119*, 2483-2486.
37. Koley, P.; Pramanik, A. Nanostructures from Single Amino Acid-Based Molecules: Stability, Fibrillation, Encapsulation, and Fabrication of Silver Nanoparticles. *Adv. Funct. Mater.* **2011**, *21*, 4126-4136.
38. Dolai, G.; Giri, R. S.; Mandal, B. Protecting Group-Directed Diversity in the Morphology of Self-Assembled Ant-Aib Dipeptides: Garland-Like Architecture and Nanovesicle Formation. *ACS Appl. Bio Mater.* **2021**, *4*, 8343-8355.
39. Whitesides, G. M.; Grzybowski, B. Self-assembly at all scales. *Science* **2002**, *295*, 2418-2421.
40. Paramera, E.I.; Konteles, S.J.; Karathanos, V.T. Microencapsulation of curcumin in cells of Saccharomyces cerevisiae. *Food Chem.* **2011**, *125*, 892-902.
41. Park, I.; Kim, Y.K.; Kim, B.H.; Moon, T.W. Encapsulated amylosucrase-treated starch with enhanced thermal stability: Preparation and susceptibility to digestion. *Starch Stärke* **2014**, *66*, 216-224.

Chapter 5

Self-Replication of Novel Cyclic Peptides under Conformationally Challenging Environment

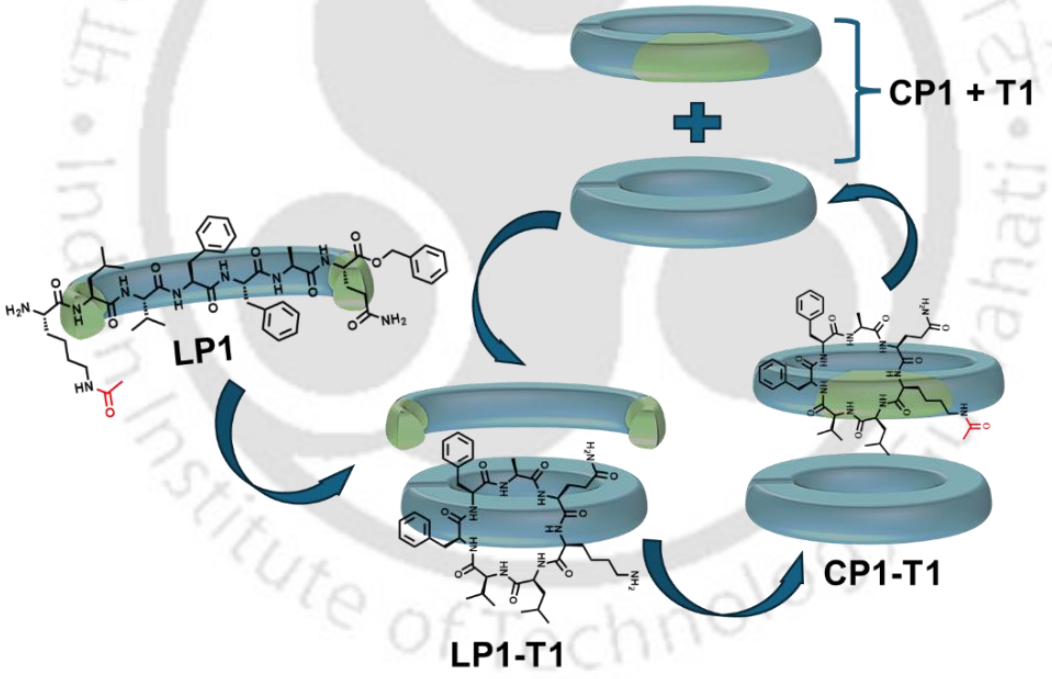

5.1. Background

Cyclic peptides possess unique structural features that make them promising candidates for synthetic self-replicating systems. Unlike linear peptides, they exhibit enhanced resistance to enzymatic degradation and spontaneous hydrolysis due to the absence of free termini and their conformational rigidity.[1,2] These characteristics provide a stable framework for investigating molecular self-replication under various conditions. However, no self-replicating system based on cyclic peptides has yet been demonstrated. Previous studies have primarily focused on linear peptides, particularly those that form α-helical or β-sheet structures, which facilitate template-assisted replication.[3-9] In this work, we examine how cyclic peptides, despite lacking conventional secondary structures, can undergo template-directed self-replication through non-covalent interactions and catalytic processes. It offers new insights into peptide-based molecular replication, advantageous for prebiotic chemistry models and long-term functional systems.

5.2. Proposed Hypothesis

Amyloid-β (Aβ) peptide is widely studied for its characteristic ability to self-assemble into fibrillar aggregates, a hallmark of Alzheimer's disease pathology. This self-assembling behaviour is largely driven by the hydrophobic core region ($A\beta_{16-20}$) of Aβ.[10,11] However, sequence cyclization significantly alters its self-assembling properties and effectively suppresses fibrillogenesis.[12,13] Our study leverages the self-assembling properties of Aβ by designing cyclic peptides that incorporate its hydrophobic core motif with the aim of constructing a minimalist, self-assembling system capable of templated self-replication.

5.3. Design of the Cyclic Peptides

The design of the peptides used in this study was inspired by the hydrophobic core motif of the Aβ peptide (Table 5.1). The precursor molecule (LP1) was designed so that its C-terminal is benzyl ester-protected and the N-terminal has a free $-NH_2$ group, i.e., the electrophilic and nucleophilic sites are located within the same molecule. An intramolecular ester condensation will give rise to the desired self-replicating cyclic product. As for the template molecule (T1), it was head-to-tail cyclized utilizing the synthetic procedure explained below. Also, we intentionally acetylated the $-NH_2$ group of

the lysine side chain in the precursor molecules so that it does not interfere or compete with the main chain -NH_2 group while the cyclization reaction occurs. This brings in a slight structural difference between the cyclic products formed (where the lysine side chain is acetylated) and the template molecules (where the -NH_2 group of the lysine side chain is kept free). This ingenious move not only helps us distinguish the template molecule from the cyclic product by a mass difference of 42 but also generates HPLC peaks at different retention times, which, in turn, helps in proper monitoring of the ligation reactions.

Table 5.1. Sequence of the peptides synthesized along with their codes, molecular weights, and specific roles.[a]

Peptide code	Sequence	Mol. Wt.	Role
LP1	**H_2N-K(Ac)-L-V-F-F-A-Q-COOBn**	983.54	Precursor (Feed stock)
T1	**K-L-V-F-F-A-Q** **└HNOC┘**	833.48	Template (Self-replicator)
A-LP1	**H_2N-A-L-V-F-F-A-Q-COOBn**	884.47	Mutated precursor (Feed stock)
G-LP1	**H_2N-G-L-V-F-F-A-Q-COOBn**	870.46	Mutated precursor (Feed stock)

[a]Standard amino acids are represented by their one-letter code, Ac= acetyl group, Bn= benzyl group.

5.4. Synthesis and Characterization of the Peptides

The cyclic and linear peptides were synthesized manually using a standard Fmoc/tBu solid-phase peptide synthesis (SPPS) protocol on a Stuart tube rotator, using Rink Amide MBHA resin as the solid support. The solid phase peptide syntheses were carried out first by anchoring Fmoc-Glu-OMe/Fmoc-Glu-OBn to Rink Amide resin through its side chain, and the peptide sequences were continued to obtain the sets of linear and cyclic peptides as mentioned in Table 5.1. For the cyclic peptides, methyl ester at the C-terminus was first cleaved using 5 equiv of LiOH dissolved in a minimal amount of H_2O along with DMF for 4 h, followed by Fmoc-cleavage at the N-terminus using 20% piperidine in DMF. Thereafter, head-to-tail cyclization was carried out using 3.5 equiv of BOP as the coupling reagent and 7 equiv of DIPEA as base for 24 h.

After completion of the synthesis, the peptides were cleaved from resin using 80% TFA, 15% DCM, and 5% H_2O for 3 h. After cleavage from the amide resin, glutamic acid at the C-terminus was converted to glutamine. The crude peptides were precipitated with cold

diethyl ether, washed thoroughly with diethyl ether three times, centrifuged, and then characterized by mass spectrometry and RP-HPLC.

5.5. Monitoring of the progress of self-replication reactions

Precursor, LP1 solution (400 µM) was prepared in PBS (50 mM) of pH 7.4. The prepared sample solution was incubated at 37 °C, and the intramolecular ester condensation reaction was monitored by analytical HPLC and CD at different time points (Figure 5.1).

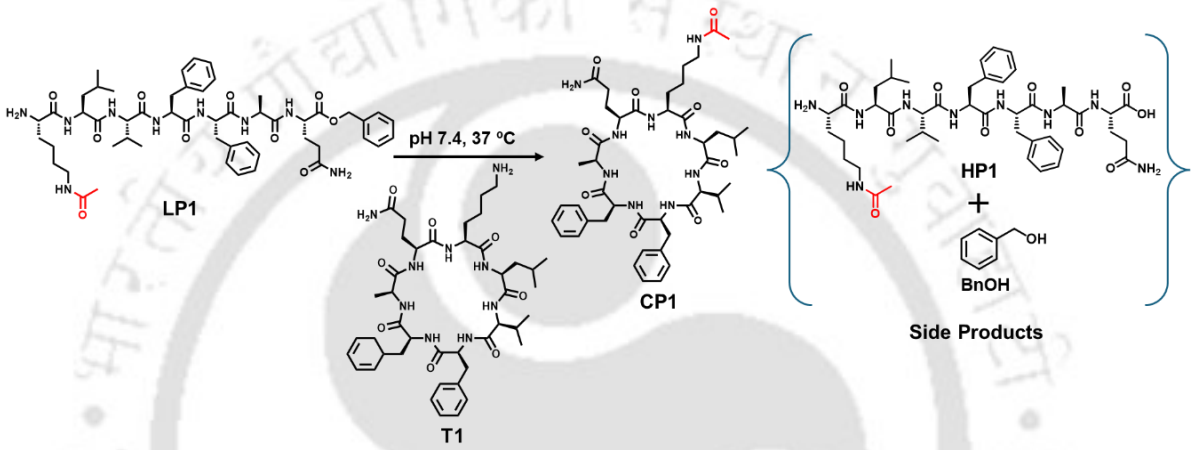

Figure 5.1. *Schematic representation of the proposed self-replication mechanism of the designed cyclic peptide.*

5.5.1. Time-dependent RP analytical HPLC

The time-dependent HPLC study reveals that, in the absence of any template, the ligation reaction proceeded very slowly, producing a very small amount of the cyclized product. After 24 hours of careful monitoring of the ligation reaction, a slight increase in the product (CP1) formation was observed; however, the formation of the hydrolyzed product (side product) also increased significantly compared to the product formation (Figure 5.2).

For a system to be called self-replicating, the reaction product should autocatalytically promote its own synthesis. To address this concern, we have performed additional experiments using the product (CP1) itself as the template (at various concentrations) for ligation with LP1. Under these conditions, we observed a significant enhancement in product formation under templated conditions compared to a non-templated reaction. These results indicate that the product CP1 can promote its own formation by promoting favorable

interactions between the reactants and are therefore consistent with an autocatalytic pathway of self-replication (Figure 5.3).

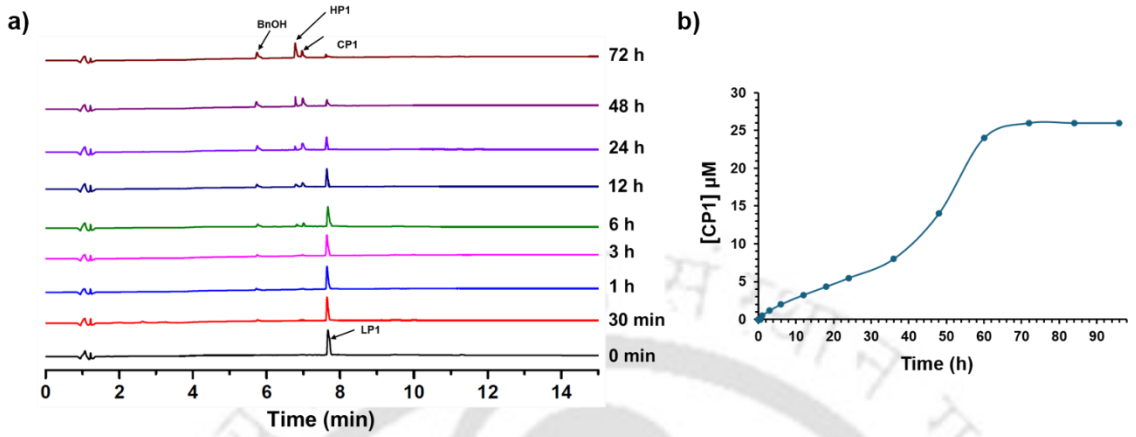

Figure 5.2. *a). Time-resolved HPLC chromatograms for the ligation reaction of LP1 (400 µM) in the absence of template. [HP1 represents the hydrolyzed product]. b). Kinetic plot for the quantity of CP1 produced over time in the absence of template (T1).*

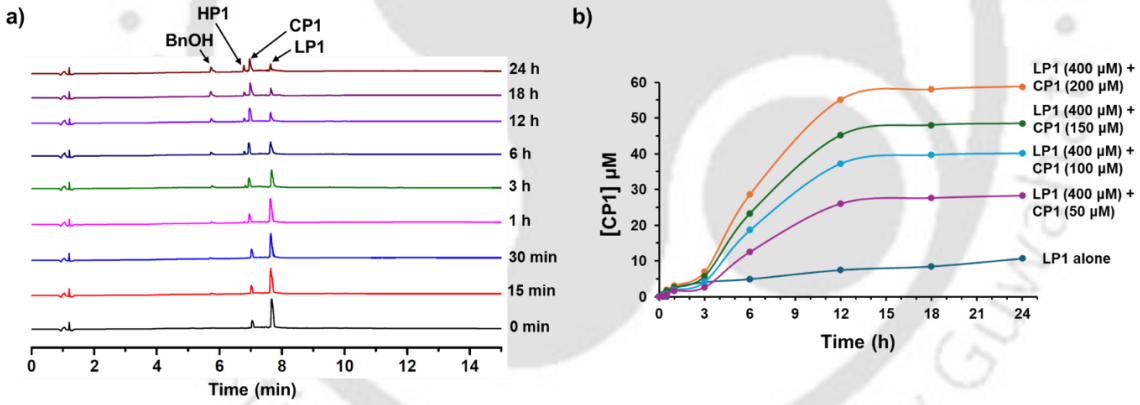

Figure 5.3. *a). Time-resolved HPLC chromatograms for the ligation reaction of LP1 (400 µM) in the presence of CP1 (200 µM). b). Kinetic plots for the quantity of CP1 produced over time in the presence and absence of different amounts of template (CP1) concentration. [The amount of CP1 produced in the ligation reaction was calculated by subtracting the initial concentration of CP1 taken as template from the final amount.*

Next, to simplify the monitoring and analysis of the ligation reaction, we performed the same reaction with template molecule (T1) at different concentrations (200, 150, 100, and 50 µM). The amount of product formed was increased by many folds compared to unseeded condition and also the amount of side product (HP1) formed was decreased significantly. The ligation reaction, when seeded, occurs faster than in unseeded conditions, and the

amount of product formation increases with increasing template concentration (Figure 5.4). In the ligation reaction under seeded conditions, after a lag phase of about 3 h, the rate of product formation increased significantly, monitored for up to 24 h. Beyond that time, the formation of the product reached a plateau, and a small amount of hydrolyzed product started to form. The ligation reaction, which was initially seeded with 200 µM template, produced 10-fold more product than that of the unseeded condition.

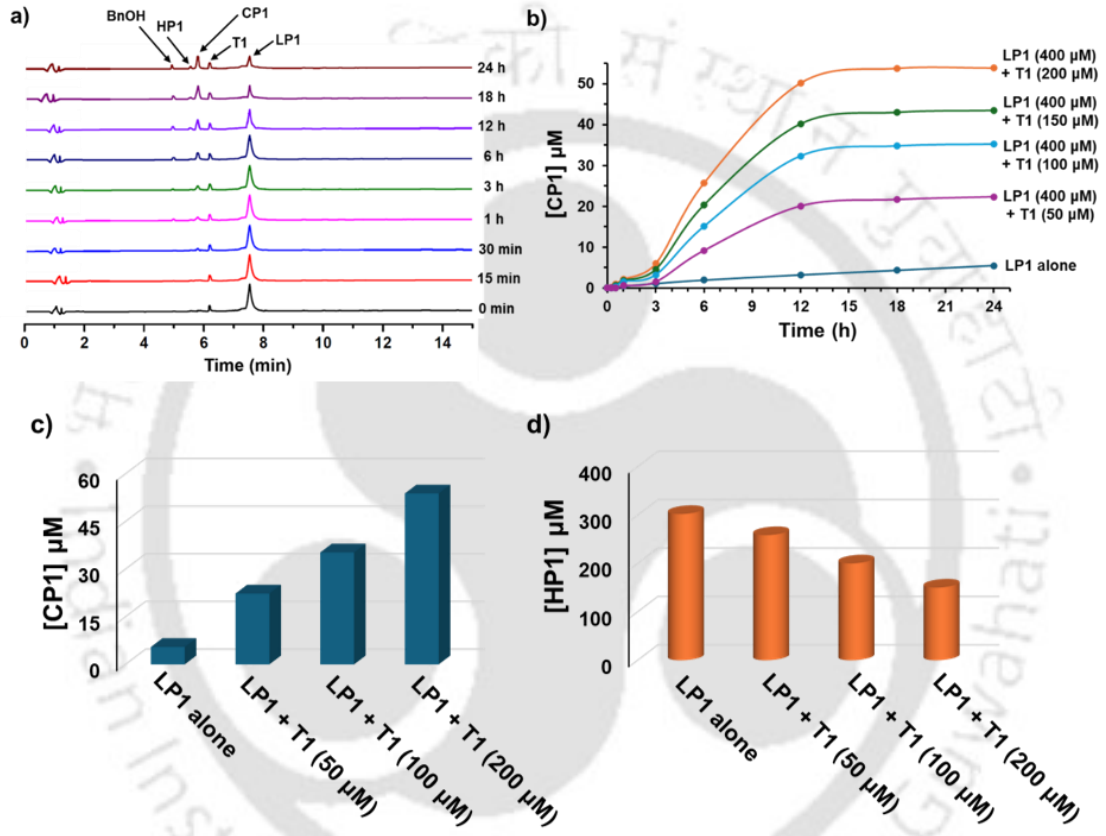

Figure 5.4. *a). Time-resolved HPLC chromatograms for the ligation reaction of LP1 (400 µM) in the presence of T1 (200 µM) were monitored up to 24 h. b). Kinetic plots for the quantity of CP1 produced over time in the presence and absence of different amounts of template (T1) concentration. c). Increase in product formation for the ligation reaction of LP1 (400 µM) in the presence of different T1 concentrations. d). Decrease in the hydrolyzed product formed for the ligation reaction of LP1 (400 µM) in the presence of different T1 concentrations.*

In Figure 5.3.b and 5.4.b, the kinetic profile for the quantity of CP1 produced during the ligation of LP1 in the absence of any template was monitored up to 24 h, where the product formation displayed a near-linear kinetic trajectory. The kinetic profiles were plotted up to 24 h to facilitate a direct comparison between the quantity of product formed under seeded

and unseeded conditions. However, the kinetic profile for the amount of product formed upon the complete course of the ligation reaction in the absence of template is shown in Figure 5.2.b. Comparing the kinetic profiles in Figure 5.3.b/5.4.b and Figure 5.2.b, it was evident that the ligation reaction carried out in the absence of the template was much slower, with a lag phase of around 24 h, compared to that under seeded conditions (lag phase of 3 h).

The presence of a lag phase in the kinetic profiles of both Figure 5.3.b and 5.4.b, even in the presence of a template, strongly indicates that the reaction is not a simple intramolecular cyclization process but rather involves an initial association step preceding catalytic acceleration. Thus, during this initial phase, supramolecular organization between the cyclic template and the linear precursor occurs, generating a structured microenvironment in which reactive termini are properly aligned. Once such precursor-template co-assemblies form, accelerated cyclization proceeds and ceases when the precursor molecules are exhausted, giving rise to the observed sigmoidal kinetics.

Notably, the reaction kinetics in the presence of CP1 closely resemble those obtained with T1. Despite the slight structural difference between T1 and CP1, the comparable kinetic profiles observed for both T1- and CP1-mediated ligation reactions suggest that the templating effect is primarily governed by the precise cyclic backbone and overall supramolecular organization, rather than the presence or absence of a free lysine side chain.

5.5.2. Time-dependent CD study

To further investigate the conformational changes throughout the course of the ligation reaction and the production of CP1 over time from the precursor LP1 in the presence of T1, we performed a time-dependent CD spectroscopy. The time-dependent CD spectroscopic study suggests that, initially (after 5 minutes), the solution displays a weak negative band around 200 nm, probably due to the formation of an unordered structure, consistent with early-stage, non-specific peptide interactions prior to the formation of more ordered assemblies. However, after 12 h, the appearance of prominent negative bands around 230 nm and 220 nm signifies the presence of both β-sheet and random coil conformations.[14,15] LP1 solution contributes to the formation of β-sheet conformation and presence of T1solution, and generation of in-situ CP1 contributes to the observed random coil

conformation. This observation is further backed and aligns with the CD spectroscopy of the individual species discussed below (section **5.6**). After 24 h, the appearance of a single prominent negative band around 200 nm indicates the conversion of LP1 to CP1 in the presence of T1, and both the template and product molecule contribute to the observed random coil conformation (Figure 5.5). To further support the findings from the time-dependent CD analysis, we conducted a FESEM study of the reaction mixture at 12 h. The microscopic image revealed the co-existence of fibrous and rod-like morphologies, indicating the simultaneous presence of both LP1 (contributing to the fibrous morphology) and CP1 + T1 (contributing to the rod-like morphology) in the reaction mixture. These results are consistent with the morphological observation discussed below.

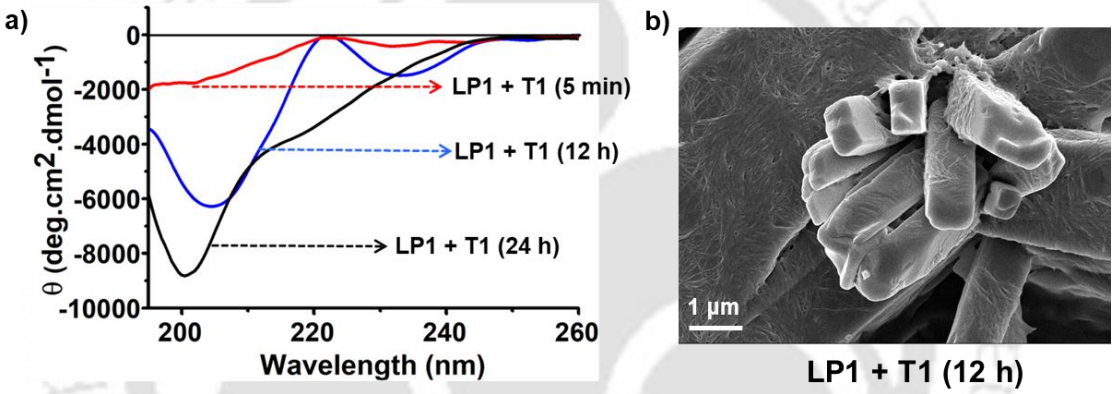

Figure 5.5. *a). CD spectra of the reaction mixture LP1 (400 µM) and T1 (200 µM) at different time intervals. b). FESEM image of the reaction mixture at 12 h, displaying the morphology of both fiber and rod-like structures.*

5.6. Morphology & Conformational Analysis

Morphology studies using both FESEM and FETEM reveal that the designed precursor molecule (LP1) displays long fibrillar morphology, whereas both the template molecule (T1) and the product molecule (CP1) exhibit highly organized rod-type structures under both microscopic analyses. Conformational studies suggest that LP1 adopts a β-sheet conformation, as evidenced by a negative band at around 220-230 nm and a positive band at around 190-200 nm. For both T1 and CP1, a prominent negative band around 190-200 nm indicates that these peptides exist mainly in random coil conformations (Figure 5.6). Thus, a change in morphology and conformation occurs when LP1 reacts to form self-replicating CP1.

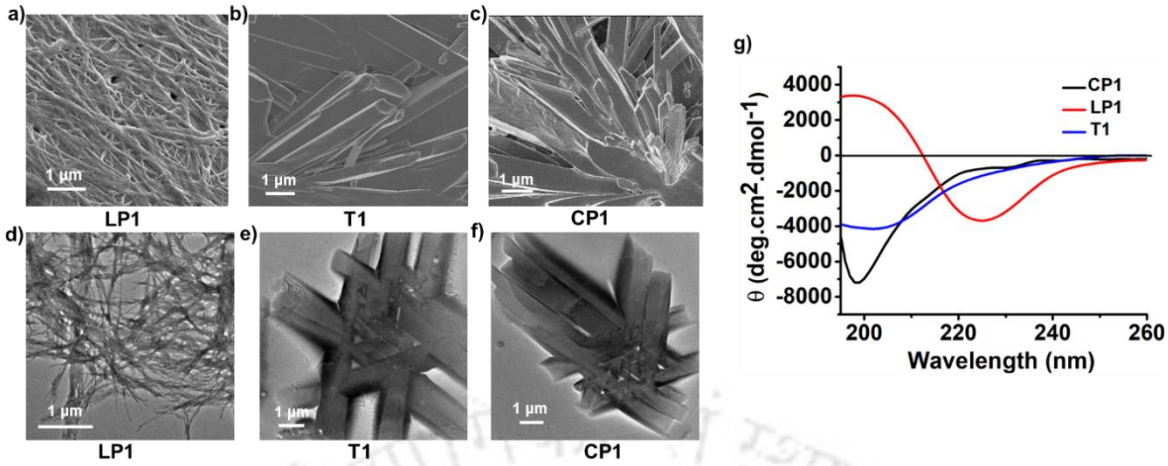

Figure 5.6. *a), b), c). FESEM images, d), e), f). FETEM images displaying morphologies, and g). CD spectra displaying the conformations of LP1, T1, and CP1.*

5.7. Sequence Selectivity

As a control reaction, we synthesized two additional linear peptides, A-LP1 and G-LP1 (Table 5.1), which differ from our original precursor molecule LP1 only at the N-terminus. A-LP1 contains alanine, and G-LP1 possesses a more flexible glycine moiety in place of lysine in LP1. With the aim of demonstrating that even a subtle mutation in the precursor molecule can significantly disrupt the efficiency of templated reactions, we set up two additional experimental designs. Both the A-LP1 and G-LP1 molecules (400 µM) were seeded with T1 (200 µM) and incubated under the same experimental conditions as described above. The ligation reactions were then monitored using time-dependent analytical HPLC. This study reveals that a very small amount of ligating products was formed during the ligation reaction. The quantity of products formed was negligible when compared to that of the product formed when LP1 was used as precursor, and its production proceeded linearly over the entire 24-hours of monitoring (Figure 5.7).

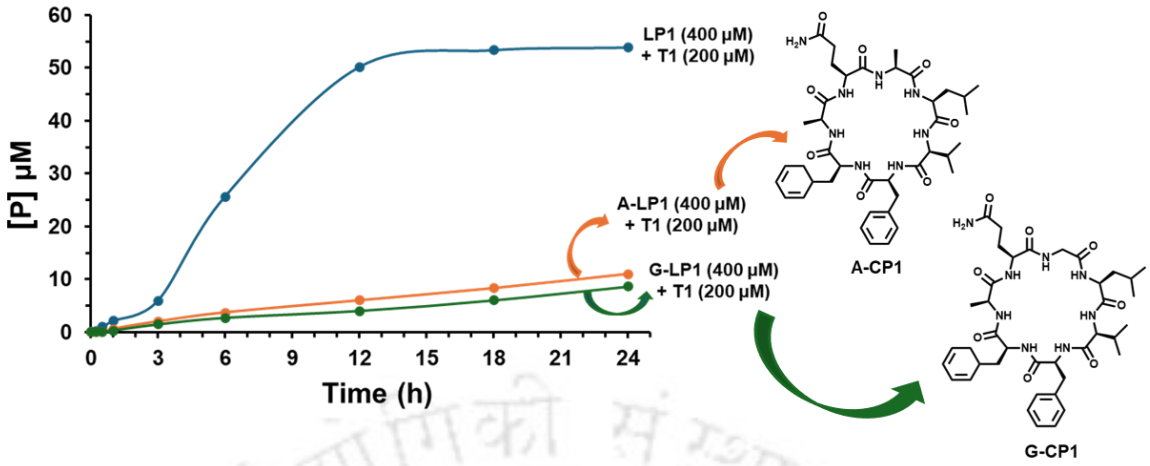

Figure 5.7. *Production of corresponding cyclic products (P) over time with mutated precursors A-LP1 and G-LP1 in the presence of T1. [Formation of P over time for LP1 + T1 is shown for comparison. The cyclic products other than CP1 are the ligating products of A-LP1 and G-LP1 formed under the experimental conditions. The concentration for all the cyclic products (P) was calculated by comparing it with the HPLC peak of the same molecule with a known concentration.]*

This experiment concludes that the significant enhancement of ligation when LP1 was used as a precursor in the presence of template T1 is not simply due to the crowding effect but rather a result of molecular recognition. Thus, peptide self-replication relies on precise, sequence-specific molecular recognition between the template and the precursor molecules. This is a case where sequence fidelity is required for functional molecular recognition. Even a single point mutation (K → A or G) abolishes the specific interactions required for templating, much like a missense mutation disrupting protein-protein interactions.

5.8. Kinetic Study

The kinetics of the self-replicating system can be described by the following set of chemical equations shown below. At first, the linear/precursor peptide (LP) binds reversibly with the template molecule (T) to form a precursor-template ($LP \cdot T$) complex. The presence of the pre-formed cyclic template molecule brings the reactive ends of the LPs into closer proximity, facilitating ligation to form the product-template ($CP{\cdot}T$) complex. In the last step, the product-template complex dissociates, producing two copies of product molecules ($CP\ and\ T$) each of CP and T can re-enter the next self-replicating cycle and continue it.

$$LP + T \rightleftharpoons LP \cdot T \quad (1)$$

$$LP \cdot T \rightarrow CP \cdot T \quad (2)$$

$$CP \cdot T \rightleftharpoons CP + T \quad (3)$$

$$LP \cdot CP \rightarrow CP \cdot CP \quad (4)$$

$$CP \cdot CP \rightleftharpoons CP + CP \quad (5)$$

The proposed mechanism is further supported by kinetic analysis using a logarithmic plot of initial reaction rates versus seeded template concentration (Figure 5.8). This analysis demonstrates exponential growth, with a catalytic reaction order of $p \approx 1$. This value suggests an efficient self-replication process in which each ligation step generates a new catalytic site that retains the original functionality. In the context of synthetic self-replicating systems, demonstrating exponential growth in the concentration of the replicator is essential to establish its potential for Darwinian-like evolution. Exponential amplification is a hallmark of systems capable of selective propagation. The reaction order (p) serves as an important indicator of replication efficiency: as p approaches 1, the system exhibits behavior closer to ideal exponential growth.[16,17] This, in turn, enhances the system's ability to selectively amplify the most efficient replicators, effectively mimicking natural selection.

We have further investigated the early events of the conformational transformation for both the precursor (LP1) and the hydrolyzed product (HP1) using time-dependent CD spectroscopy (Figure 5.8 c-f). A consistent change in the CD spectra was observed for both species as they transitioned from a random coil to a β-sheet conformation. A similar time-dependent cooperative conformational transition has been reported previously for many peptide systems[18,19] and is consistent with our observation. This change in conformation over time exhibited sigmoidal behavior, characterized by a lag phase followed by a cooperative growth phase, similar to the curve obtained for the product formation of the self-replicating cyclic peptides discussed above. This suggests that the conformational mutation of the peptides is also self-replicatory in nature, and for linear peptides (such as LP1 and HP1) it evolves to β -sheets followed by fibril formation.

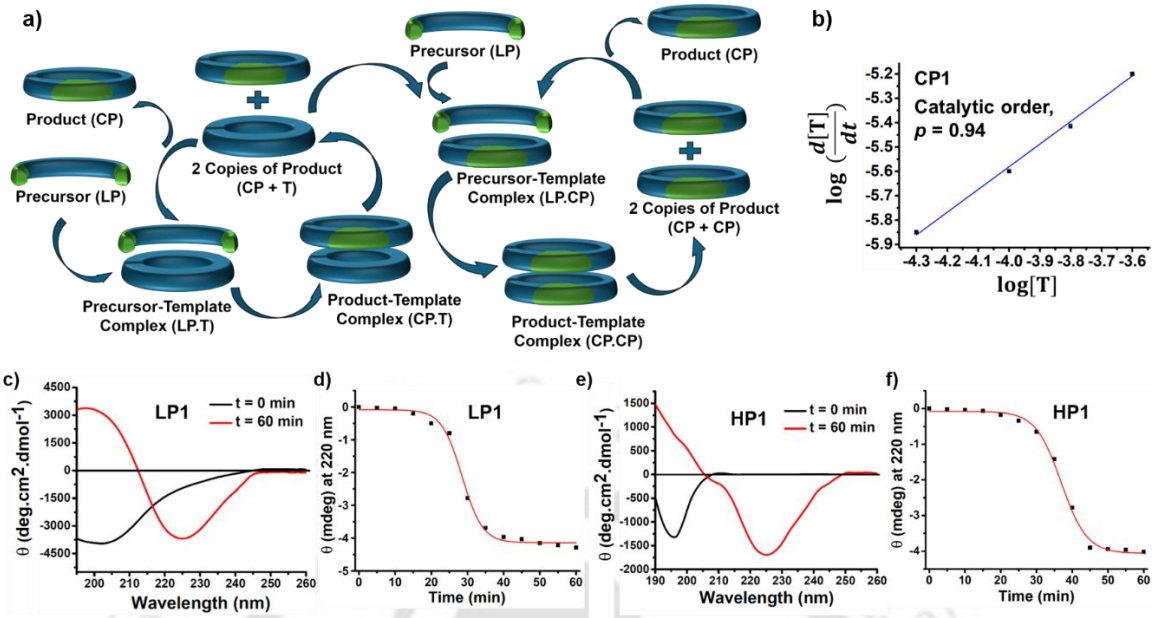

Figure 5.8. *a). Schematic representation of the self-replicatory process generating copies from the parent structure. b). Logarithmic plot of the initial rates extracted from the graph (Figure 5.4.b) as a function of seeded template concentrations. c) CD spectra, d) Time course measurement, of the random coil to β-sheet transformation of LP1. e) CD spectra, f). Time course measurement of the random coil to β-sheet transformation of HP1 (400 μM each, pH 7.4 at 37 °C (sigmoidal fit, R^2 = 0.99, each).*

We acknowledge the fact that, in previously studied systems, the term self-replication was applied to the synthesis of a larger molecule from its smaller building blocks. In contrast, our system does not involve covalent bond formation between separate fragments but rather involves intramolecular cyclization of a single precursor of identical length. However, the criteria that define self-replication are not the specific synthetic route but rather the ability of the product to catalyze or template the formation of additional copies of itself. The present system fulfills the defining criteria of self-replication and is thus termed "self-replication".

The advantages of the new system over multicomponent fragment-condensation replicators are that the templated cyclization strategy involves a single precursor-to-product transformation, potentially reducing competing side reactions and improving replication fidelity. Furthermore, the new self-replicating system does not rely on the conventional secondary structures for templating. Also, the benzyl ester-mediated ligation approach reduces hydrolytic degradation (under templated conditions) and undesired side reactions. The lower intrinsic reactivity of the benzyl ester suppresses background reactivity and

improves the signal-to-noise ratio of self-replication experiments, facilitating experimental handling and mechanistic investigation.

One of the disadvantages/shortages of the new system is that it is strongly dependent on templating interactions, and therefore, spontaneous background reactions remain limited under these conditions. Therefore, generation of variation in the next generation becomes limited. However, in the absence of the template, hydrolysis competes effectively with cyclization, leading to the formation of a significant quantity of hydrolyzed product.

5.9. Conclusion

In the present study, we have successfully designed, synthesized, and characterized a novel head-to-tail cyclic peptide capable of undergoing self-replication through templated autocatalytic mechanisms. Unlike traditional peptide-based self-replicators that rely heavily on structured motifs such as helical coiled coil and β-sheet assemblies, our designed self-replicating cyclic peptides exist predominantly in random coil conformations, having a rod-like architecture. We have also successfully implemented a new ligating strategy by using benzyl-ester mediated amide bond formation, offering an alternative to the widely used Kent's ligation method.[20] Benzyl-esters are generally more stable toward hydrolysis and undesired side reactions, whereas thioesters are more reactive under neutral and mildly basic aqueous conditions.[21,22] We acknowledge the fact that in our system (at pH 7.4), in the absence of a template, a substantial quantity of hydrolyzed product was formed, and the hydrolysis accelerated after 24 h in the reaction medium. However, such benzyl ester hydrolysis was significantly decreased when the ligation reactions were carried out in the presence of various template concentrations. HPLC analysis revealed that the self-replicating efficiency of the cyclic peptide under seeded conditions was many-fold higher than under unseeded conditions, and product formation increased with increasing template concentration. The designed self-replicating cyclic peptides exhibit exceptional molecular selectivity, including sequence selectivity, where sequence fidelity is strictly required between the precursor and the template for effective self-recognition and templated replication. Even a single point mutation is sufficient to disrupt the critical interactions required for successful templating. This exploration of self-replicating peptides combines disciplines such as chemistry, biology, and materials science, and continues to inspire researchers to uncover the molecular principles that enable these fascinating molecules to replicate.

5.10. Characterization data

Prior to the synthesis of the cyclic and linear peptides discussed above, Fmoc-Glu(OtBu)-OH was first converted into its methyl ester and benzyl ester derivatives using methyl iodide (MeI) and benzyl bromide (BnBr), respectively (Scheme 5.1 and 5.2). (Detailed synthetic procedure is discussed in Chapter 2).

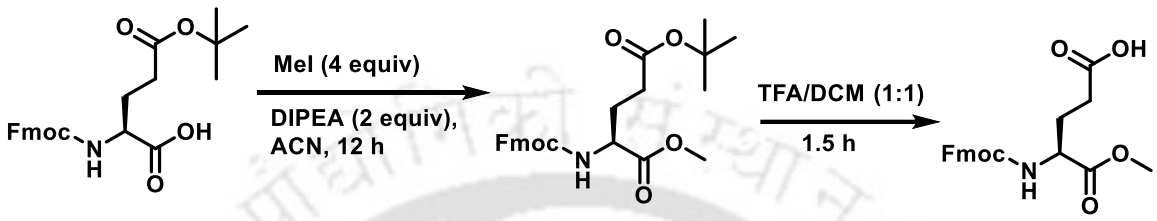

Scheme 5.1. *Schematic representation of the synthesis of Fmoc-Glu-OMe.*

White solid (650 mg, 85%), **^{1}H NMR (CDCl$_3$; 600 MHz)** δ 7.76 (d, *J* = 7.5 Hz, 2H), 7.59 (s, 2H), 7.40 (td, *J* = 7.5, 2.6 Hz, 2H), 7.31 (td, *J* = 7.5, 3.1 Hz, 2H), 5.49 (d, *J* = 8.2 Hz, 1H), 4.46 - 4.37 (m, 3H), 4.21 (t, *J* = 6.9 Hz, 1H), 3.75 (s, 3H), 2.44 (qt, *J* = 16.6, 7.1 Hz, 2H), 2.22 (dq, *J* = 13.5, 6.8 Hz, 1H), 1.97 (dq, *J* = 14.7, 8.1, 7.4 Hz, 1H). **^{13}C NMR (CDCl$_3$; 151 MHz)** δ 177.88, 172.67, 156.40, 144.13, 144.00, 141.66, 128.09, 127.43, 125.42, 125.38, 120.35, 120.34, 67.46, 53.49, 52.99, 47.48, 30.13, 27.77.

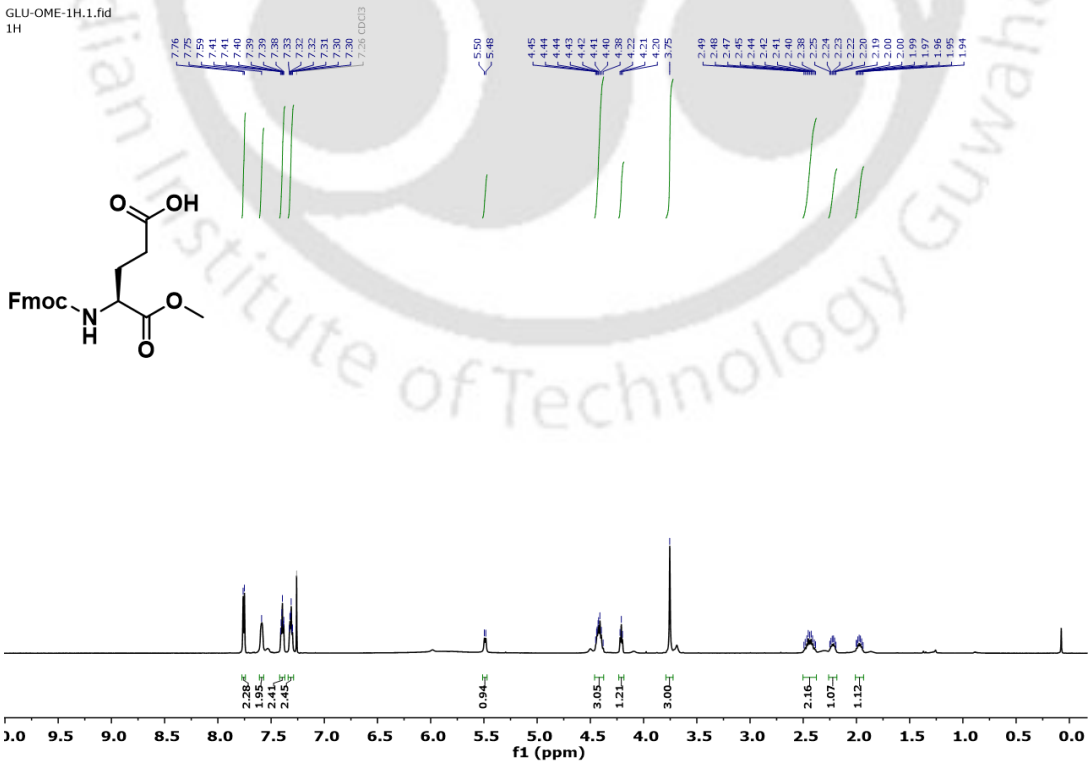

Figure 5.9. *^{1}H NMR spectra of Fmoc-Glu-OMe.*

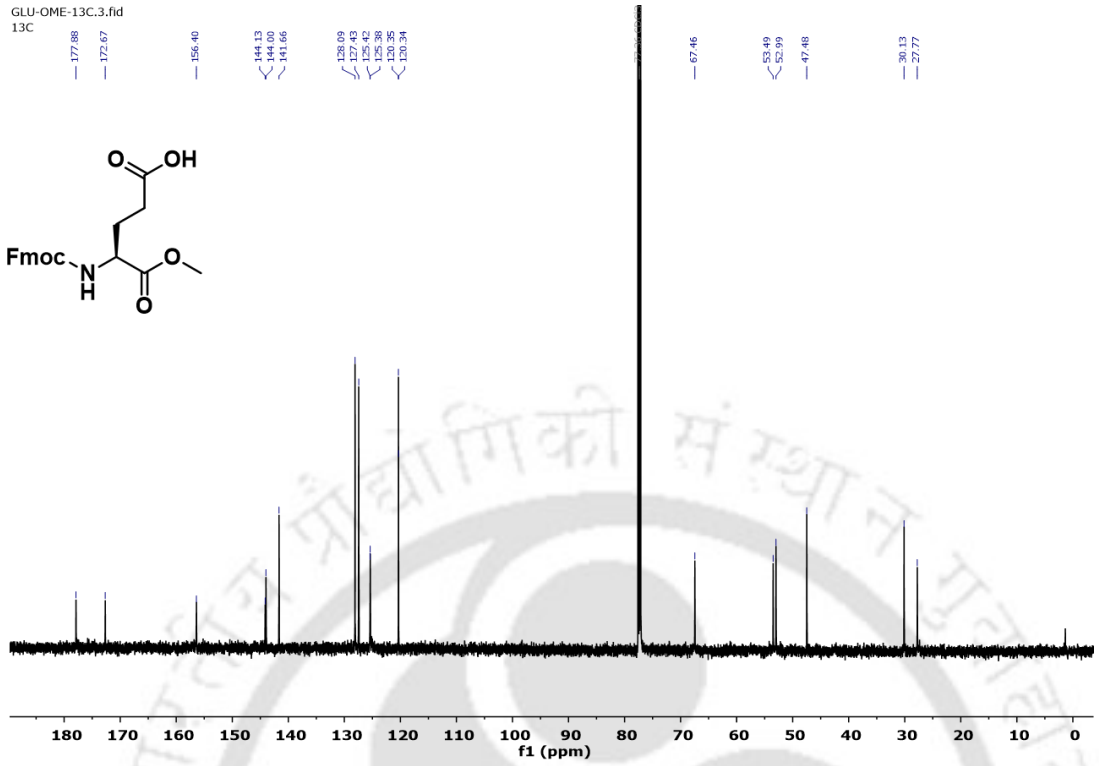

Figure 5.10. *^{13}C NMR spectra of Fmoc-Glu-OMe.*

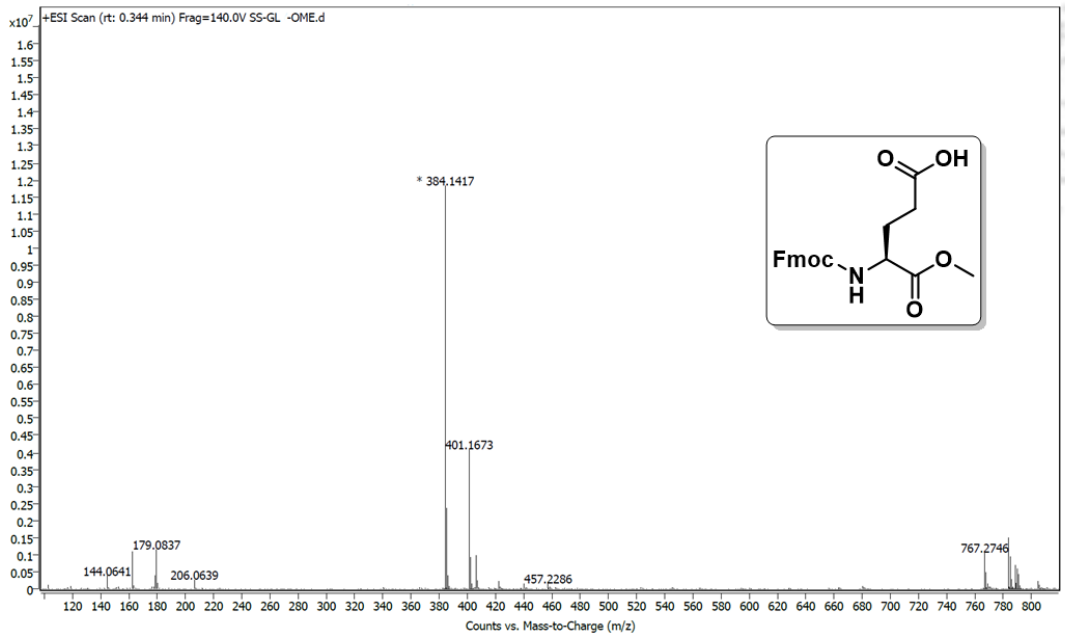

Figure 5.11. *ESI mass spectra of Fmoc-Glu-OMe. Calculated mass is 383.1369, observed mass is 384.1417 $[M+H]^+$, 401.1673 $[M+Na]^+$.*

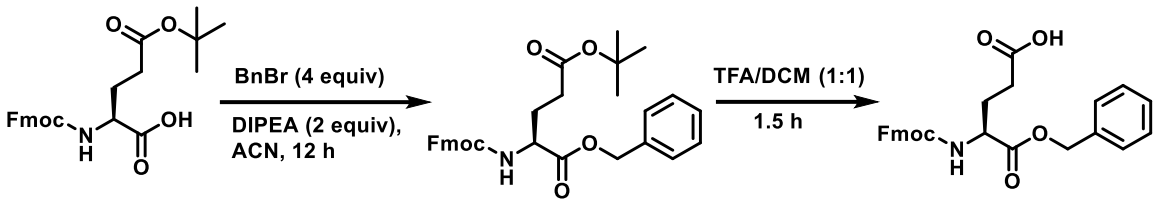

Scheme 5.2. *Schematic representation of the synthesis of Fmoc-Glu-OBn.*

White solid (760 mg, 83%), **^{1}H NMR (CDCl$_3$; 400 MHz)** δ 7.75 (d, *J* = 7.6 Hz, 3H), 7.58 (d, *J* = 7.5 Hz, 2H), 7.39 (t, *J* = 7.4 Hz, 3H), 7.35-7.33 (m, 5H), 5.48 (d, *J* = 8.5 Hz, 1H), 5.18 (s, 2H), 4.41 (dd, *J* = 7.1, 2.8 Hz, 2H), 4.20 (s, 1H), 2.48-2.18 (m, 5H). **^{13}C NMR (CDCl$_3$; 151 MHz)** δ 177.47, 172.03, 156.43, 144.13, 143.98, 141.65, 135.35, 129.02, 128.99, 128.95, 128.92, 128.69, 128.09, 127.44, 125.40, 120.35, 120.33, 67.87, 67.49, 53.60, 47.47, 30.04, 27.78.

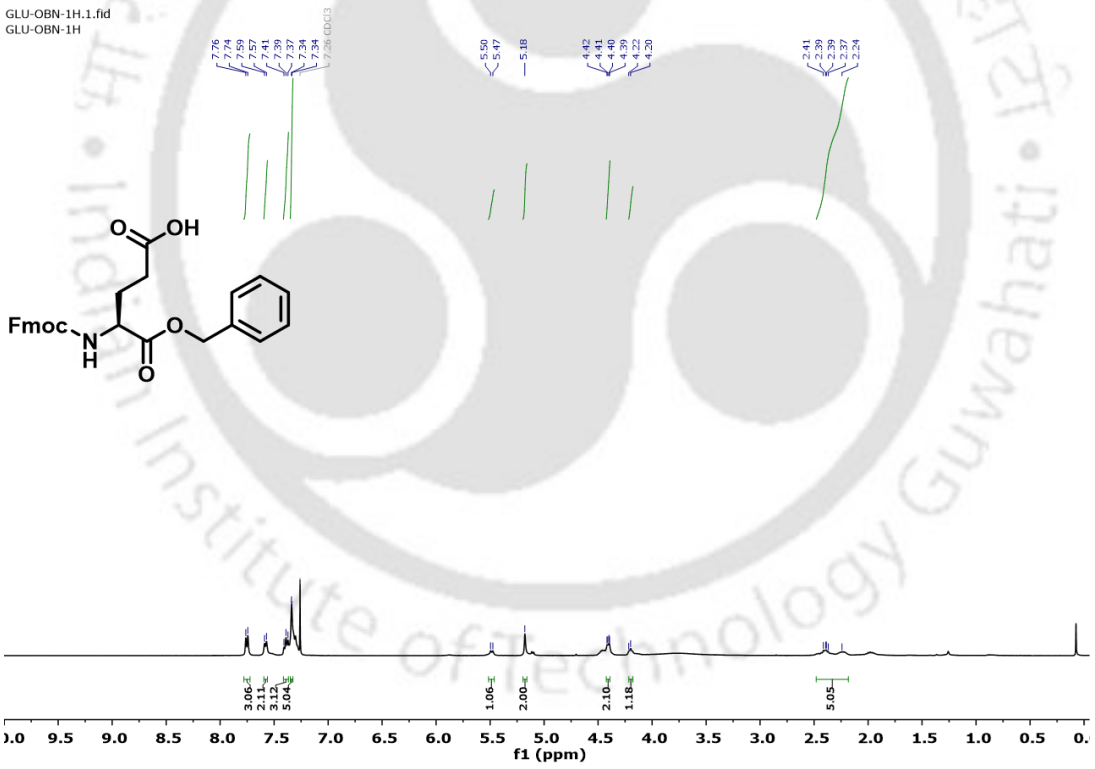

Figure 5.12*. ^{1}H NMR spectra of Fmoc-Glu-OBn.*

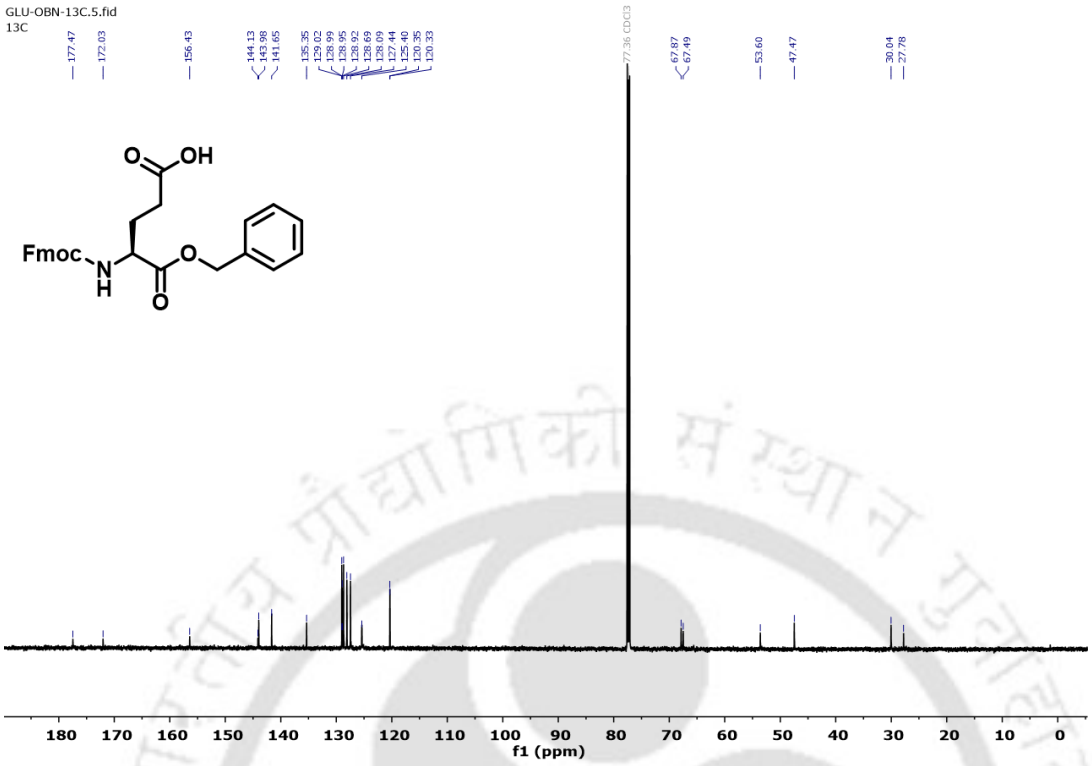

Figure 5.13. *^{13}C NMR spectra of Fmoc-Glu-OBn.*

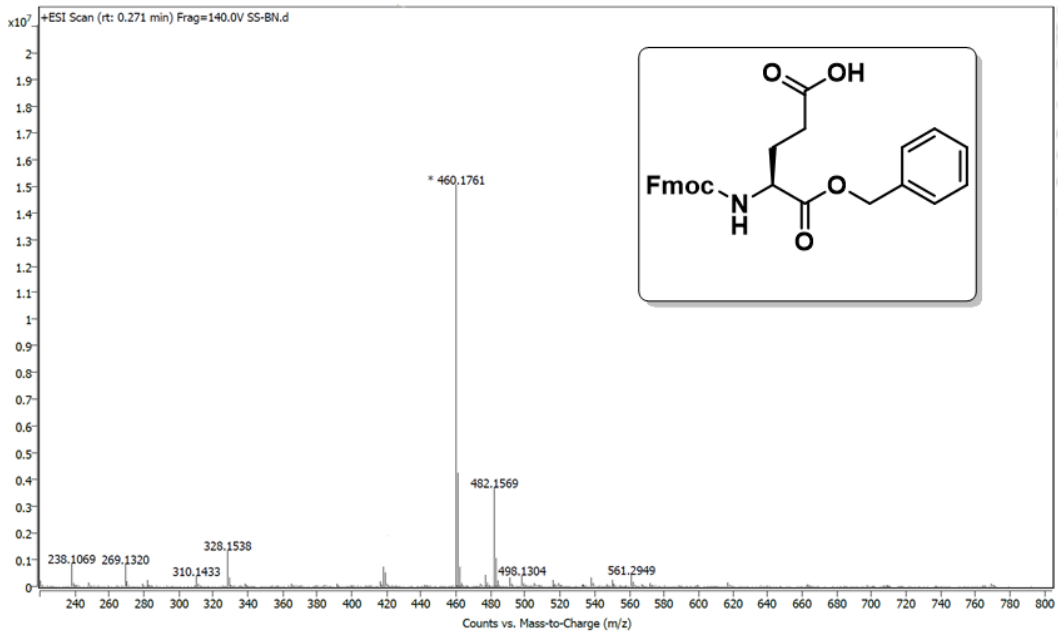

Figure 5.14. *ESI mass spectra of Fmoc-Glu-OBn. Calculated mass is 459.1682, observed mass is 460.1761 $[M+H]^+$, 482.1569 $[M+Na]^+$.*

H_2N-K(Ac)-L-V-F-F-A-Q-COOBn (LP1): (White fluffy powder, yield = 15.5 mg, 11.3% w.r.t the resin loading. Calculated mass is 983.548, observed mass is 985.077 $[M+2H]^+$, 1007.081 $[M+Na+H]^+$, 1023.101 $[M+K+H]^+$. HPLC retention time (t_R) = 6.9 min).

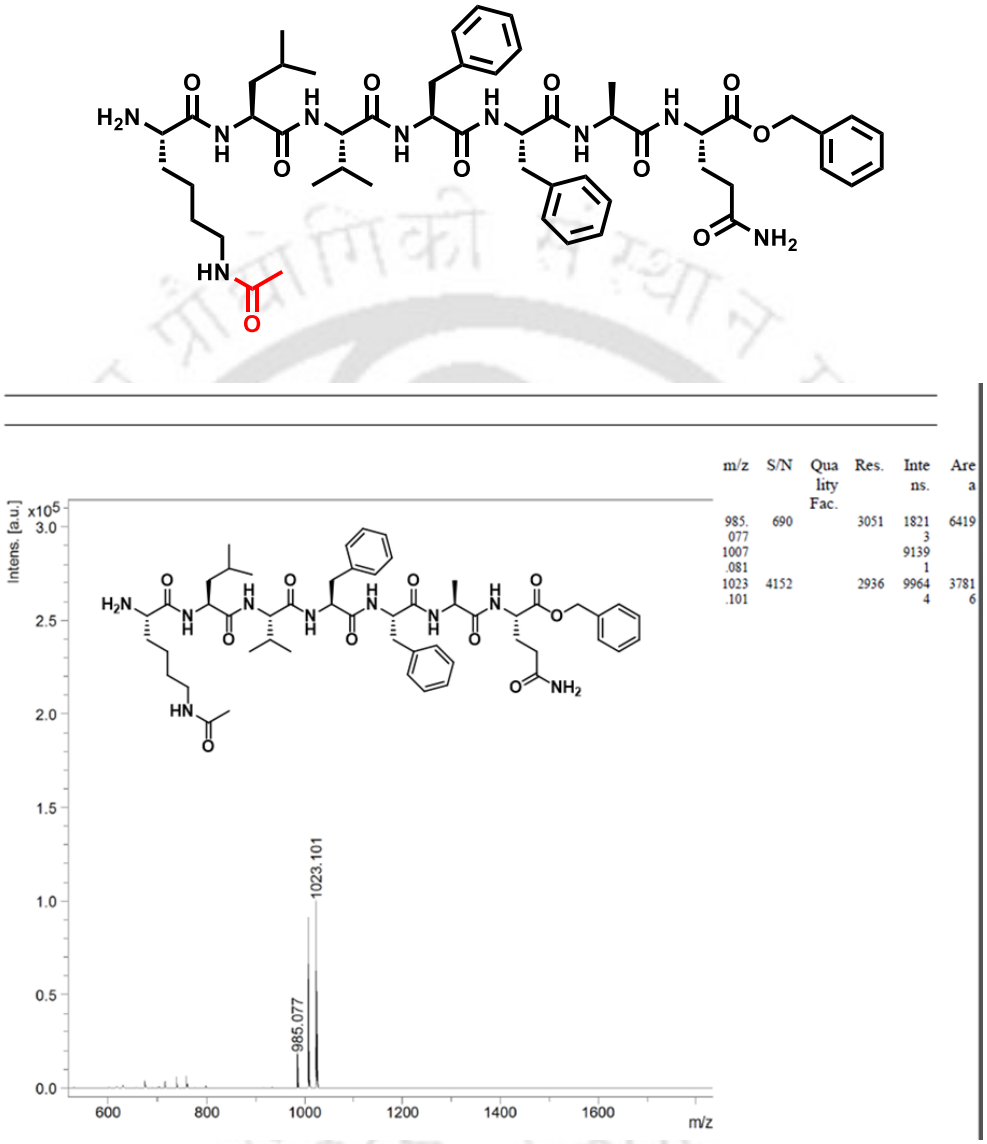

Figure 5.15. *MALDI-TOF mass spectrum of purified peptide LP1.*

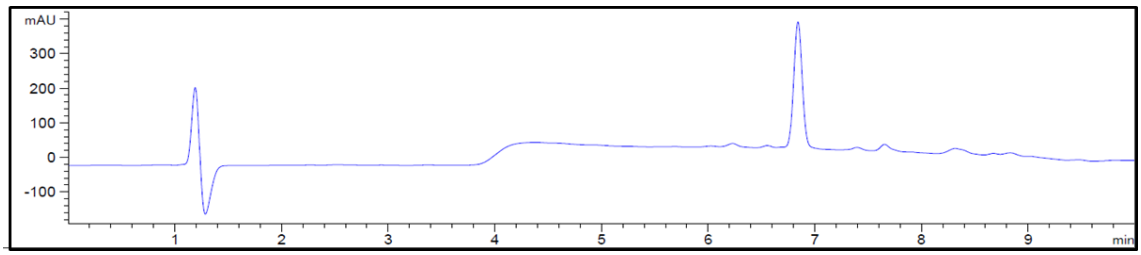

Figure 5.16. *HPLC profile of purified peptide LP1.*

K-L-V-F-F-A-Q (T1)
HNOC

: (White fluffy powder, yield = 8.5 mg, 7.3% w.r.t the resin loading. Calculated mass is 833.480, observed mass is 834.967 $[M+H]^+$ and 856.896 $[M+Na]^+$. HPLC retention time (t_R) = 7.4 min).

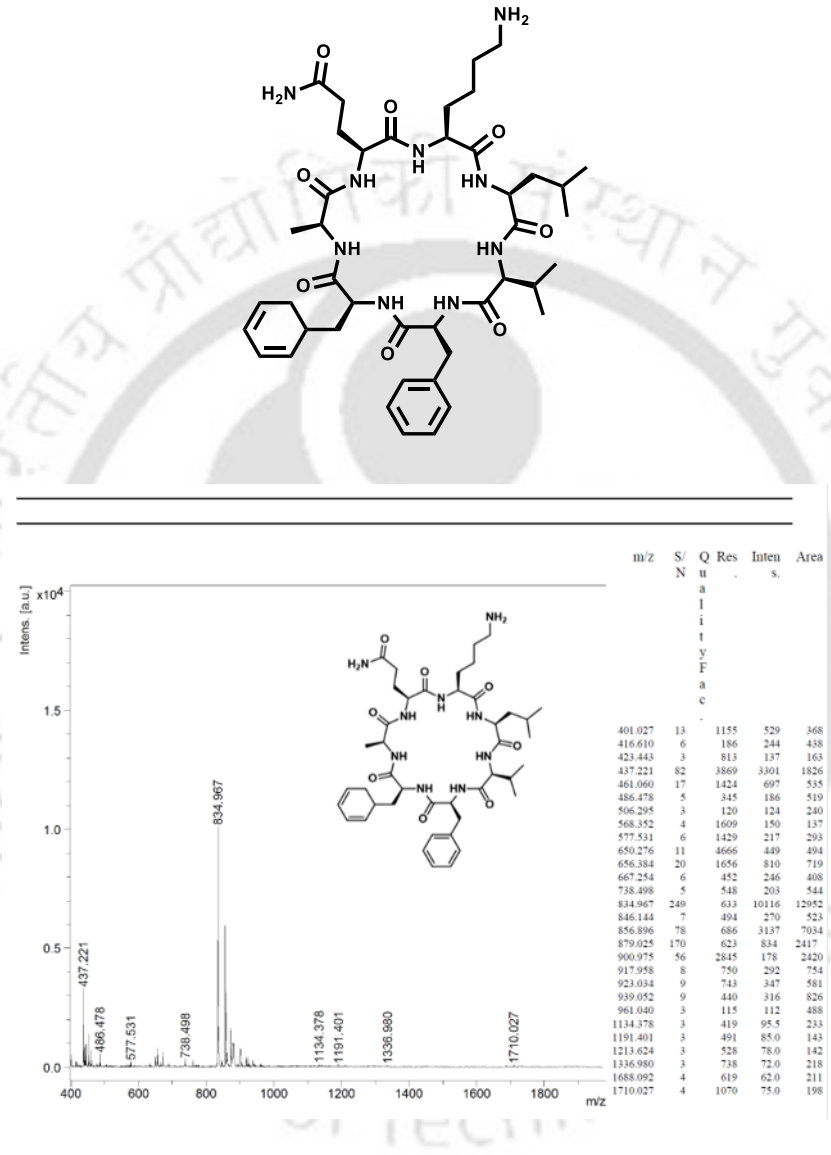

Figure 5.17. *MALDI-TOF mass spectrum of purified peptide T1.*

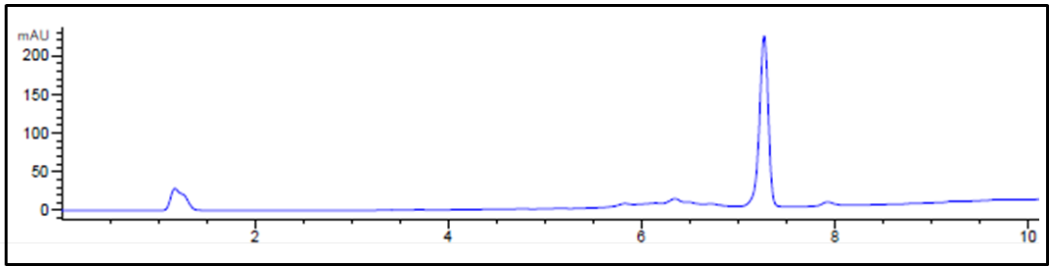

Figure 5.18. *HPLC profile of purified peptide T1.*

H_2N-A-L-V-F-F-A-Q-COOBn (A-LP1): (White fluffy powder, yield = 18.6 mg, 15% w.r.t the resin loading. Calculated mass is 884.479, observed mass is 908.172 $[M+Na+H]^+$, 925.174 $[M+K+2H]^+$. HPLC retention time (t_R) = 6.9 min).

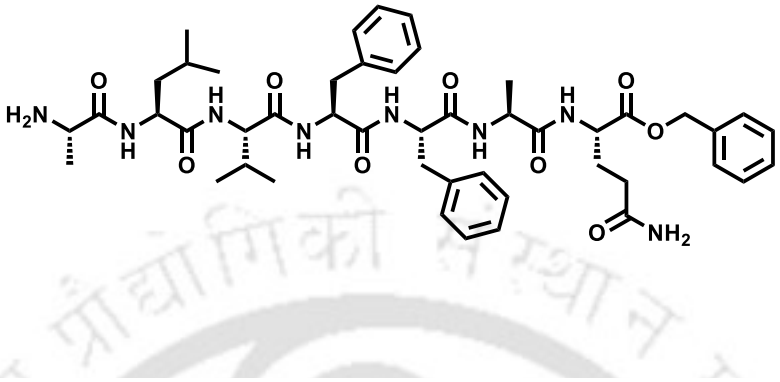

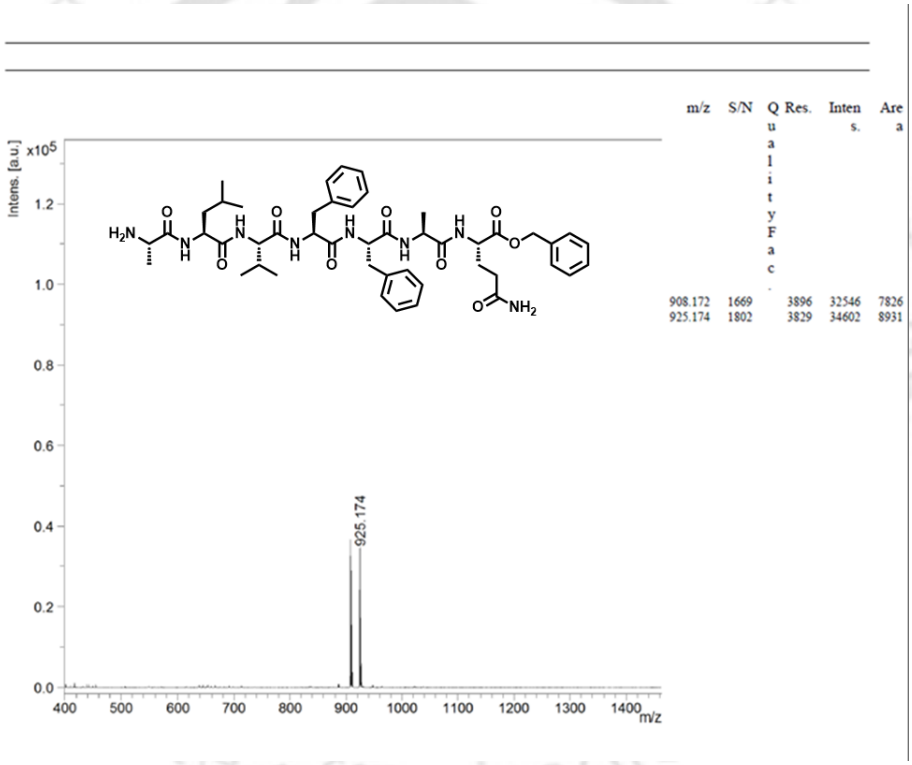

Figure 5.19. *MALDI-TOF mass spectrum of purified peptide A-LP1.*

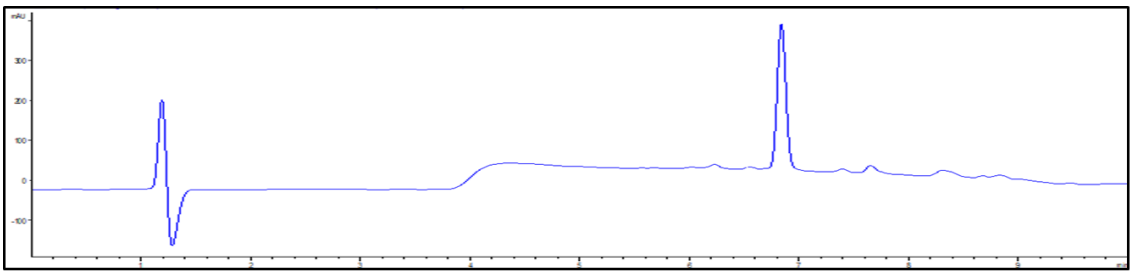

Figure 5.20. *HPLC profile of purified peptide A-LP1.*

H_2N-G-L-V-F-F-A-Q-COOBn (G-LP1): (White fluffy powder, yield = 20.2 mg, 16.5% w.r.t the resin loading. Calculated mass is 870.464, observed mass is 871.695 $[M+H]^+$, 893.706 $[M+Na]^+$, 909.721 $[M+K]^+$. HPLC retention time (t_R) = 6.9 min).

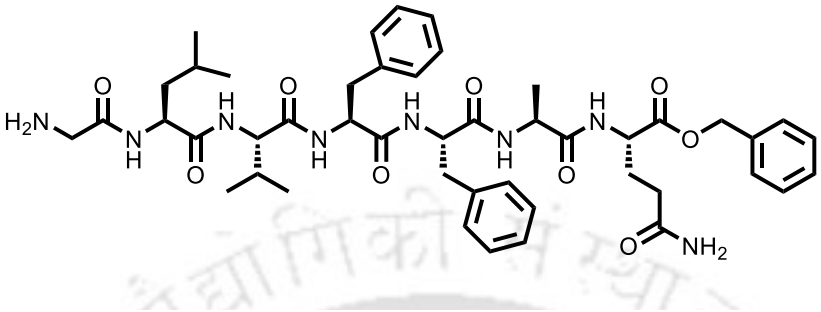

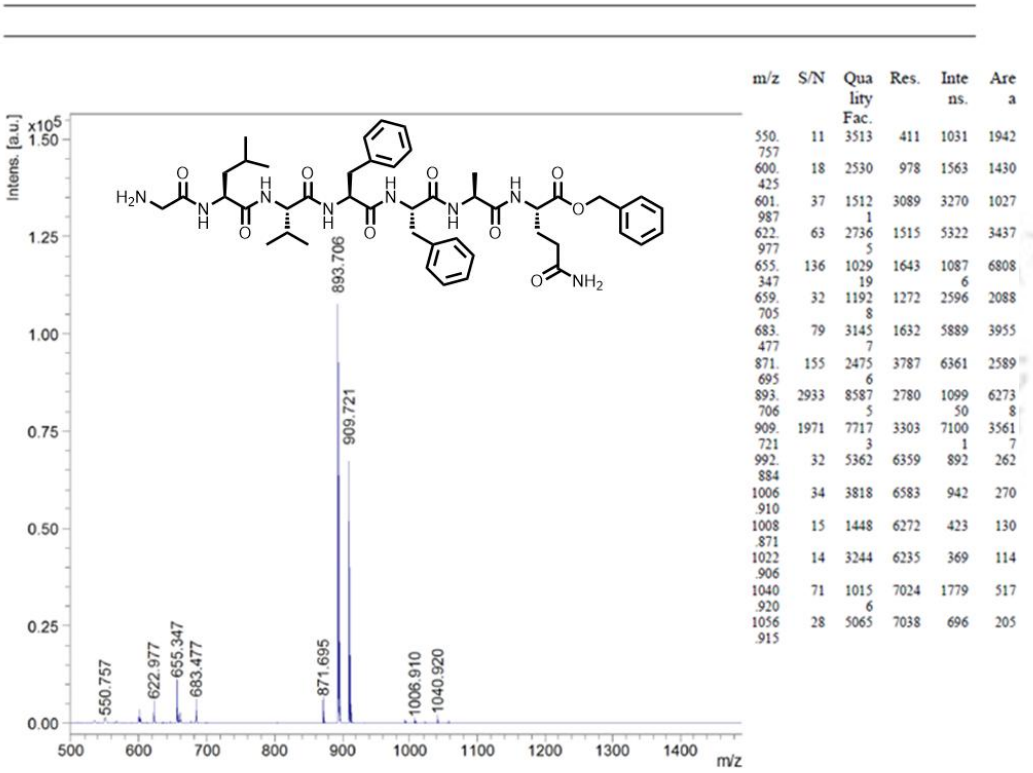

m/z	S/N	Quality Fac.	Res.	Intens.	Area
550.757	11	3513	411	1031	1942
600.425	18	2530	978	1563	1430
601.987	37	15121	3089	3270	1027
622.977	63	27365	1515	5322	3437
655.347	136	10291	1643	10876	6808
659.705	32	11928	1272	2596	2088
683.477	79	31457	1632	5889	3955
871.695	155	24756	3787	6361	2589
893.706	2933	85875	2780	10995	6273
909.721	1971	77173	3303	71001	35617
992.884	32	5362	6359	892	262
1006.910	34	3818	6583	942	270
1008.871	15	1448	6272	423	130
1022.906	14	3244	6235	369	114
1040.920	71	10156	7024	1779	517
1056.915	28	5065	7038	696	205

Figure 5.21. *MALDI-TOF mass spectrum of purified peptide G-LP1.*

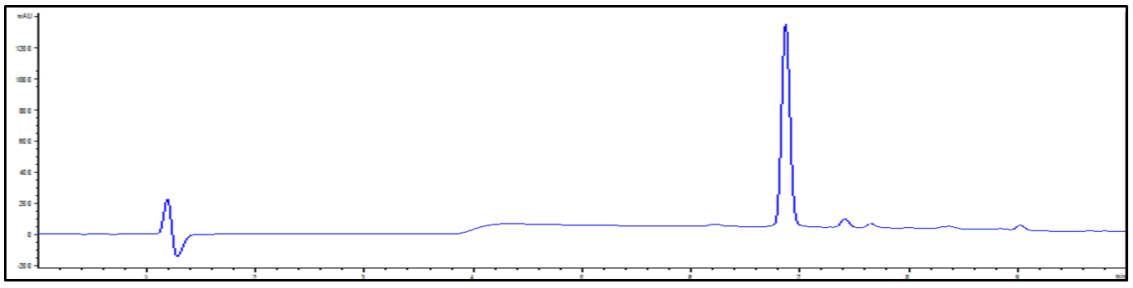

Figure 5.22. *HPLC profile of purified peptide G-LP1.*

5.11. References

1. Hill, T. A.; Shepherd, N. E.; Diness, F.; Fairlie, D. P. Constraining cyclic peptides to mimic protein structure motifs. *Angew. Chem. Int. Ed.* **2014**, *53*, 13020-13041.
2. Khatri, B.; Nuthakki, V. R.; Chatterjee, J. Strategies to enhance metabolic stabilities. *Methods Mol. Biol.* **2019**, 17-40.
3. Lee, D. H.; Granja, J. R.; Martinez, J. A.; Severin, K.; Ghadiri, M. R. A self-replicating peptide. *Nature* **1996**, *382*, 525-528.
4. Severin, K.; Lee, D. H.; Martinez, J. A.; Ghadiri, M. R. Peptide self-replication via template-directed ligation. *Chem. Eur. J.* **1997**, *3*, 1017-1024.
5. Saghatelian, A.; Yokobayashi, Y.; Soltani, K.; Ghadiri, M. R. A chiroselective peptide replicator. *Nature* **2001**, *409*, 797-801.
6. Yao, S.; Ghosh, I.; Zutshi, R.; Chmielewski, J. A pH-modulated, self-replicating peptide. *J. Am. Chem. Soc.* **1997**, *119* (43), 10559-10560.
7. Yao, S.; Ghosh, I.; Zutshi, R.; Chmielewski, J. A self-replicating peptide under ionic control. *Angew. Chem. Int. Ed.* **1998**, *37*, 478-481.
8. Rubinov, B.; Wagner, N.; Rapaport, H.; Ashkenasy, G. Self-replicating amphiphilic β-sheet peptides. *Angew. Chem.* **2009**, *121*, 6811-6814.
9. Nanda, J.; Rubinov, B.; Ivnitski, D.; Mukherjee, R.; Shtelman, E.; Motro, Y.; Ashkenasy, G. Emergence of native peptide sequences in prebiotic replication networks. *Nat. Commun.* **2017**, *8*, 434.
10. Tjernberg, L. O.; Näslund, J.; Lindqvist, F.; Johansson, J.; Karlström, A. R.; Thyberg, J.; Nordstedt, C. Arrest of-Amyloid Fibril Formation by a Pentapeptide Ligand. *J. Biol. Chem.* **1996**, *271*, 8545-8548.
11. Lührs, T.; Ritter, C.; Adrian, M.; Reik-Loher, D.; Bohrmann, B.; Döbeli, H.; Schubert, D.; Riek, R. 3D structure of Alzheimer's amyloid-β(1–42) fibrils. *Proc. Natl. Acad. Sci. USA*, **2005**, *102*, 17342.
12. Richman, M.; Wilk, S.; Chemerovski, M.; Warmlander, S. K.; Wahlstrom, A.; Graslund, A.; Rahimipour, S. In vitro and mechanistic studies of an antiamyloidogenic self-assembled cyclic D, L-α-peptide architecture. *J. Am. Chem. Soc*. **2013**, *135*, 3474-3484.
13. Soto, C.; Kindy, M. S.; Baumann, M.; Frangione, B. Inhibition of Alzheimer's amyloidosis by peptides that prevent β-sheet conformation. *Biochem. Biophys. Res. Commun*. **1996**, *226*, 672-680.
14. Dolai, G.; Shill, S.; Roy, S.; Mandal, B. Atomic Insight on Inhibition of Fibrillization of Dipeptides by Replacement of Phenylalanine with Tryptophan. *Langmuir* **2023**, *39* (27), 9367-9383.
15. Bera, S.; Jana, P.; Maity, S. K.; Haldar, D. Inhibition of fibril formation by tyrosine modification of diphenylalanine: crystallographic insights. *Cryst. Growth Des.* **2014,** *14*, 1032-1038.
16. von Kiedrowski, G. Minimal replicator theory I: Parabolic versus exponential growth. *Bioorg. Chem. Front.* **1993**, *3*, 113-146.
17. Dadon, Z.; Wagner, N.; Ashkenasy, G. The road to non-enzymatic molecular networks. *Angew. Chem. Int. Ed.* **2008**, *47* (33), 6128-6136.
18. Paul, A.; Sharma, B.; Mondal, T.; Thalluri, K.; Paul, S.; Mandal, B. Amyloid β derived switch-peptides as a tool for investigation of early events of aggregation: a combined experimental and theoretical approach. *MedChemComm* **2016**, *7* (2), 311-316.

19. Rosenheck, K.; Doty, P. The far ultraviolet absorption spectra of polypeptide and protein solutions and their dependence on conformation. *Proc. Natl. Acad. Sci. USA*, **1961**, *47* (11), 1775-1785.
20. Dawson, P. E.; Muir, T. W.; Clark-Lewis, I.; Kent, S. B. Synthesis of proteins by native chemical ligation. *Science* **1994**, *266*, 776-779.
21. Gless, B. H.; Schmied, S. H.; Bejder, B. S.; Olsen, C. A. Forster resonance energy transfer assay for investigating the reactivity of thioesters in biochemistry and native chemical ligation. *J. Am. Chem. Soc. Au.* **2023**, *3* (5), 1443-1451.
22. Yang, W.; Drueckhammer, D. G. Understanding the relative acyl-transfer reactivity of oxoesters and thioesters: computational analysis of transition state delocalization effects. *J. Am. Chem. Soc.* **2001**, *123* (44), 11004-11009.

Chapter 6

Tuning the Self-Replication of Cyclic Peptides through Backbone Stereochemical Modification

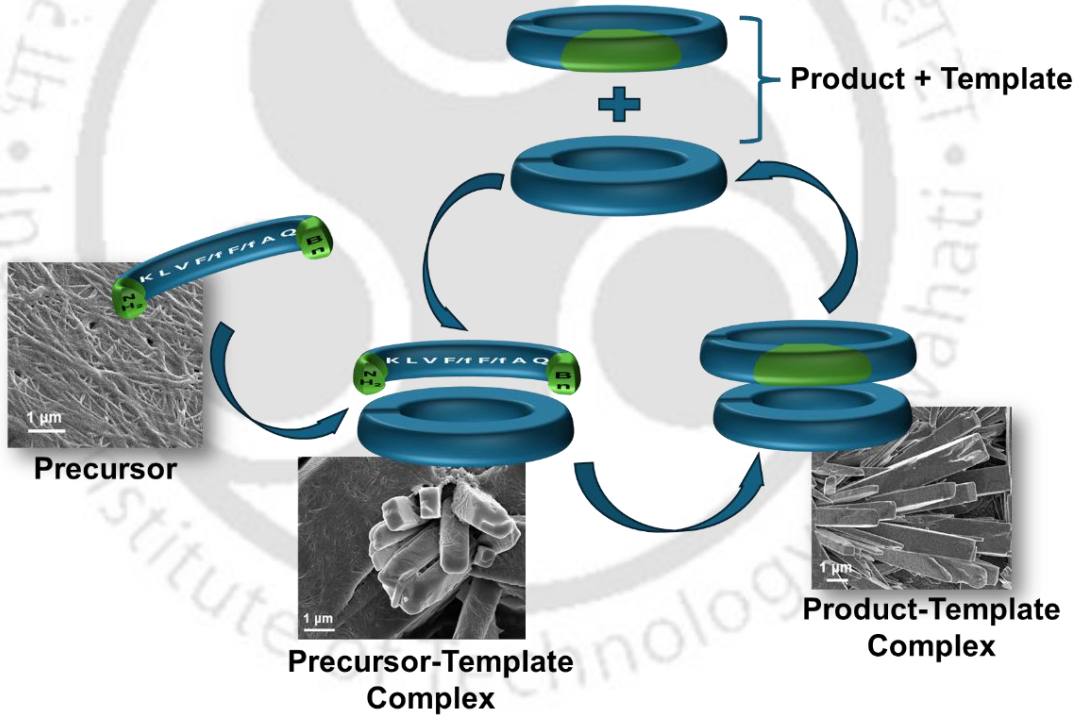

6.1. Background

In Chapter 5, we discussed about the first-ever design, synthesis, and self-replicating ability of a head-to-tail cyclic peptide (CP1) from its corresponding precursor molecule (LP1). The discussed self-replicating cyclic peptide did not possess a conventional secondary conformation for replication yet showed significant self-replication through a templated mechanism. In this chapter, we introduce two more heterochiral head-to-tail cyclic peptides and study their self-replicating efficacies. The difference between the earlier studied self-replicating cyclic peptides and these two designed cyclic peptides is that the previous one was homochiral (with all L-amino acids), and the newly designed cyclic peptides contain one D-amino acid each. Thus, in this chapter, through backbone stereochemical modification, we aim to achieve a more efficient cyclic peptide self-replicating model.

6.2. Proposed Hypothesis

As discussed in Chapter 5, our study leverages the self-assembling properties of the hydrophobic core motif of Aβ-peptide, and thereby, we design self-replicating cyclic peptides by incorporating D-amino acids. This is a well-established tactic in peptidomimetic and cyclic peptide design that the incorporation of a D-amino acid introduces a kink or turn in the peptide backbone, thereby bringing the N- and C-termini closer together in 3D space.[1,2] Using this tactic, we aim to construct highly efficient self-replicating cyclic peptides.

6.3. Design of the Cyclic Peptides

Similarly, as discussed in Chapter 5, the precursor molecules (LP2, LP3) were designed in such a way that their C-terminal is benzyl ester protected, and the N-terminal has a free -NH_2 group, i.e. the electrophilic and the nucleophilic site are located within the same molecule. As for the template molecules (T2, T3), were head-to-tail cyclized utilizing the synthetic procedure explained below. The precursor and the template molecules differ from the earlier discussed precursor (LP1) and template (T1) molecule only in the chirality of their diphenylalanine motif (Table 6.1). Thus, the introduction of the D-phenylalanine

reduces entropic penalties and increases effective molarity for cyclization, making the intramolecular cyclization reaction more favourable.[3,4]

Table 6.1. Sequence of the peptides synthesized along with their codes, molecular weights, and specific roles.[a]

Peptide code	Sequence	Mol. Wt.	Role
LP2	**H_2N-K(Ac)-L-V-f-F-A-Q-COOBn**	983.54	Precursor (Feed stock)
T2	**K-L-V-f-F-A-Q** **└HNOC┘**	833.48	Template (Self-replicator)
A-LP2	**H_2N-A-L-V-f-F-A-Q-COOBn**	884.47	Mutated precursor (Feed stock)
G-LP2	**H_2N-G-L-V-f-F-A-Q-COOBn**	870.46	Mutated precursor (Feed stock)
LP3	**H_2N-K(Ac)-L-V-F-f-A-Q-COOBn**	983.54	Precursor (Feed stock)
T3	**K-L-V-F-f-A-Q** **└HNOC┘**	833.48	Template (Self-replicator)
A-LP3	**H_2N-A-L-V-F-f-A-Q-COOBn**	884.47	Mutated precursor (Feed stock)
G-LP3	**H_2N-G-L-V-F-f-A-Q-COOBn**	870.46	Mutated precursor (Feed stock)

[a]*Standard amino acids are represented by their one-letter code, f= D-phenylalanine, Ac= acetyl group, Bn= benzyl group.*

6.4. Synthesis and Characterization of the Peptides

As described in Chapter 5, section 5.4.

6.5. Monitoring of the progress of self-replication reactions

Precursor, LP2 and LP3 (400 μM each) were prepared in PBS (50 mM) of pH 7.4. The prepared sample solutions were kept in incubation at 37 °C, and the intramolecular ligation reactions were monitored using analytical HPLC at different time intervals (Figure 6.1).

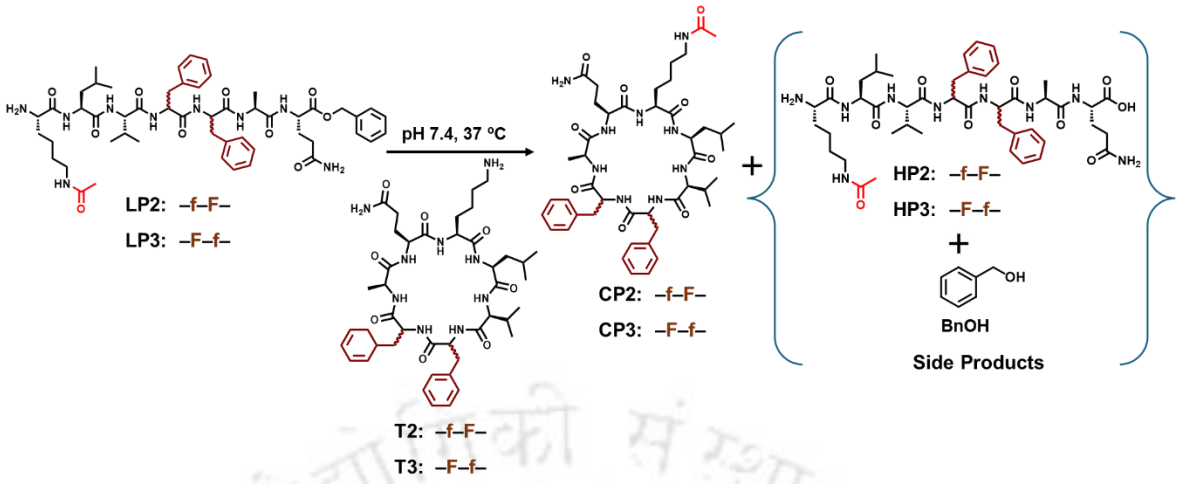

Figure 6.1. *Schematic representation of our designed cyclic peptide self-replicatory systems.*

6.5.1. Time-dependent RP analytical HPLC

The self-replicating abilities of CP2 and CP3 were then monitored in the absence and presence of different amounts of corresponding template molecules. The ligation reactions, monitored by analytical HPLC, revealed that in the absence of template molecules, the quantity of products formed (CP2 and CP3) was significantly lower compared to that formed under seeded conditions (Figure 6.2). The ligation reactions under seeded conditions proceeded efficiently, affording high yields of the desired products. The extent of product formation increases with an increase in template concentration, with the best condition being the precursor: product ratio in 1:0.5. The best ligating condition yielded ≈ 20-fold more product than that of the unseeded condition, with CP3 being produced faster and in slightly better amounts than that of CP2.

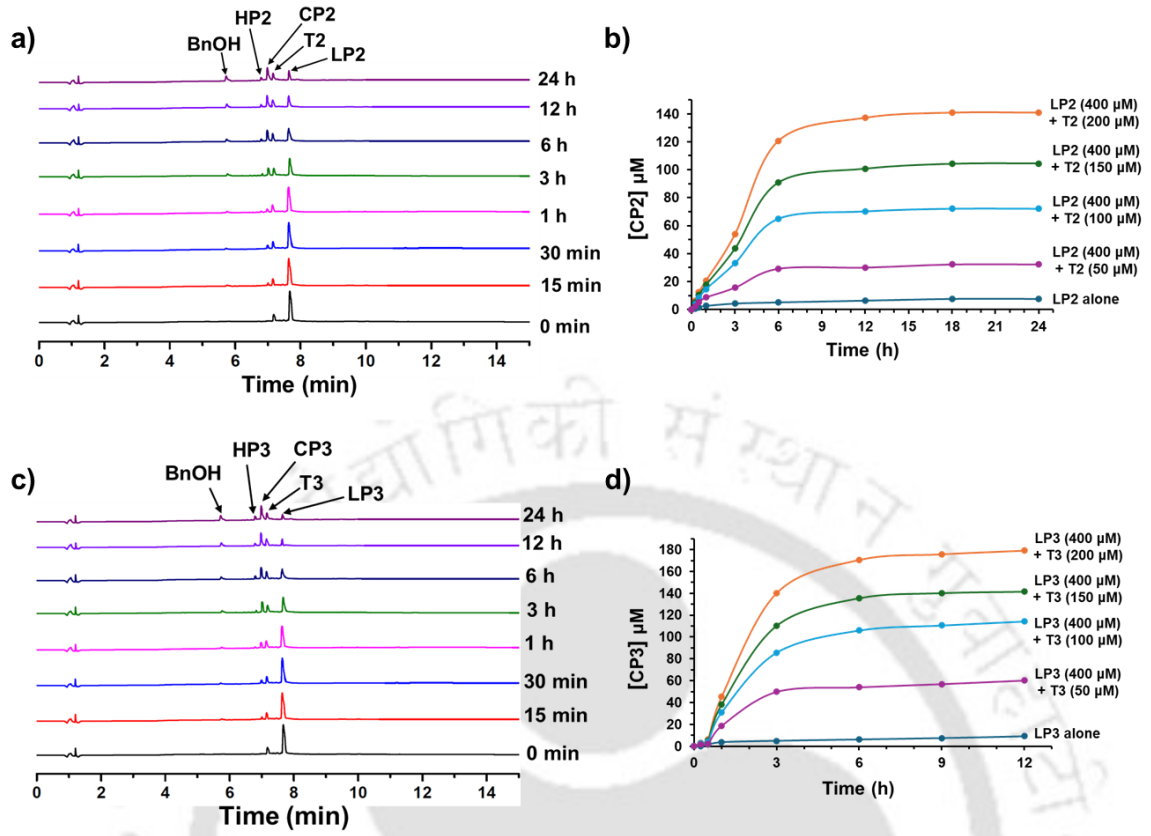

Figure 6.2. *Time-resolved HPLC chromatograms for the ligation reaction of a). LP2 c). LP3 (400 µM each) in the presence of T2 and T3 (200 µM each), respectively, monitored up to 24 h. Kinetic plots for the quantity of b). CP2 and d). CP3, produced over time in the presence and absence of different concentrations of template T2 and T3, respectively.*

A slightly better and faster production of CP3 compared to CP2 can be attributed to faster cyclization of LP3 due to the strain produced near the C-terminal region because of the presence of D-phenylalanine. This incorporation provided a faster route to cyclization rate due to conformational dynamics and aggregation-assisted folding.

Among the three self-replicating peptides, CP2 and CP3 showed superior replication yields compared to CP1 (discussed in Chapter 5), underscoring the beneficial impact of incorporating D-amino acids into their respective linear precursors (LP2 and LP3). A comparative plot for the amount of product formed through ligation of LP1 (from the previous Chapter 5), LP2, and LP3 in the presence (under the best seeded condition) and absence of respective templates is shown below (Figure 6.3a). Additionally, the decrease in the amount of side product formed in each case of ligation reactions, when seeded with different concentrations of template molecules, is also shown (Figure 6.3b) below.

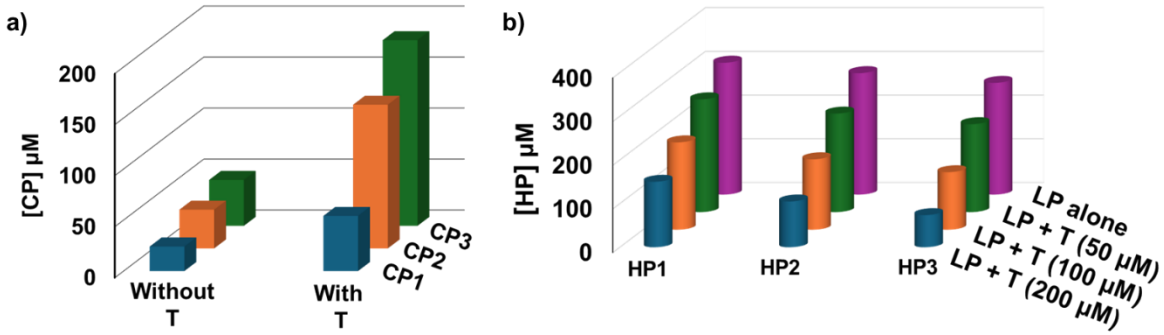

Figure 6.3. *a). Total amount of corresponding cyclic products formed in each cyclic peptide self-replicatory system in the absence of template and under best-seeded conditions. b). Quantity of hydrolyzed products (HPs) formed under different seeded conditions in each cyclic peptide self-replicatory system.*

6.6. Morphology & Conformational Analysis

Similarly, as discussed in Chapter 5, characterization of the precursor molecules (LP2 and LP3), template molecules (T2 and T3), and the product molecules (CP2 and CP3) revealed that the morphology of LP2 and LP3 is fibrillar in nature, whereas the template and product molecules displayed cuboidal rod-like morphology under both FESEM and FETEM. CD study reveals that the precursor molecules display a conformation largely containing a β-sheet structure, while T2, T3, and CP2, CP3 mostly exist in random coil conformations (Figure 6.4).

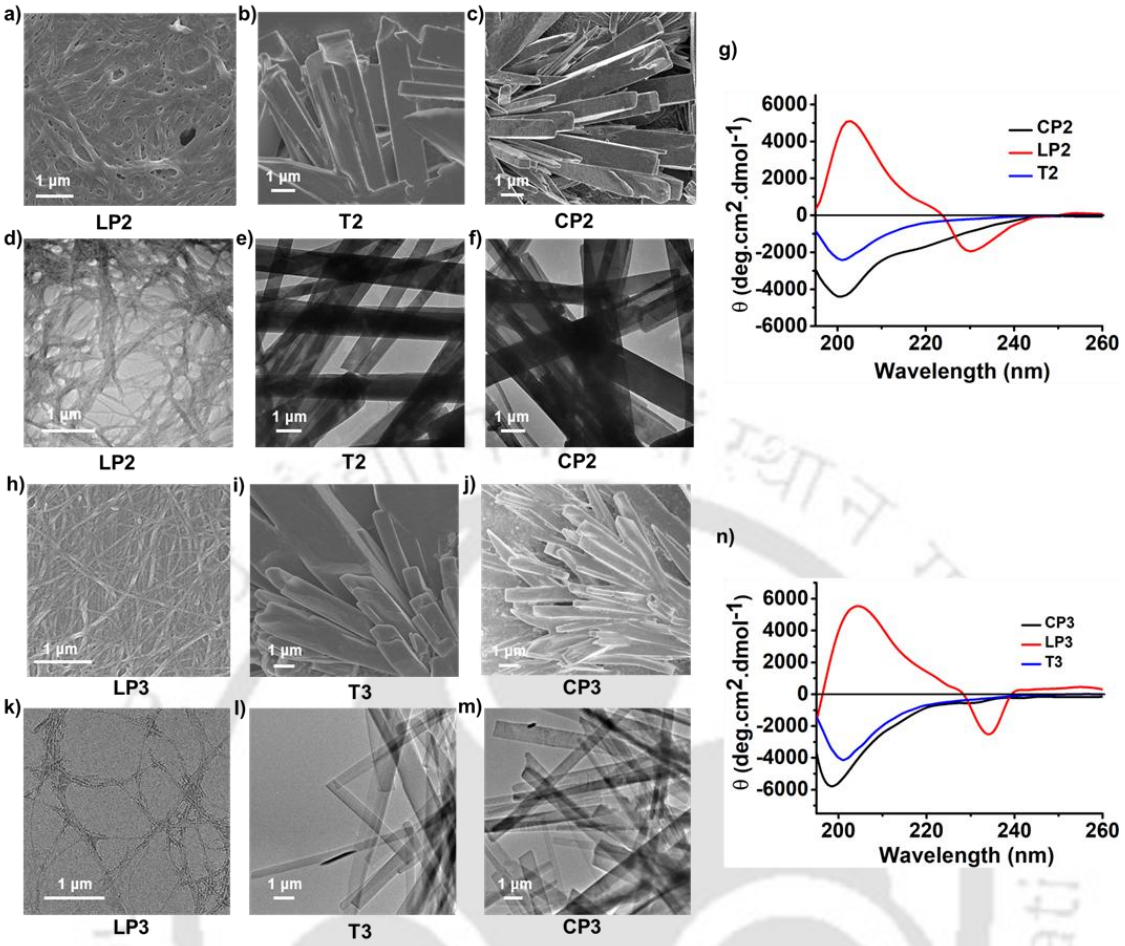

Figure 6.4. *a), b), c). FESEM images, d), e), f). FETEM images displaying morphologies, and g). CD spectra displaying the conformations of LP2, T2, and CP2. h), i), j). FESEM images, k), l), m). FETEM images displaying morphologies, and n). CD spectra displaying the conformations of LP3, T3, and CP3.*

6.7. Sequence and Spatio-chiro Selectivity

For sequence selectivity, when mutated LP2, i.e. A-LP2 and G-LP2 (400 μM each), in the presence of T2 (200 μM each), and mutated LP3, i.e. A-LP3 and G-LP3 (400 μM each), in the presence of T3 (400 μM each), were subjected to ligation reactions under the experimental conditions and procedure as mentioned earlier, an insignificant quantity of corresponding products was formed over the course of the reaction (Figure 6.5). This once again shows the importance of system specificity in the self-replication of the designed cyclic peptides.

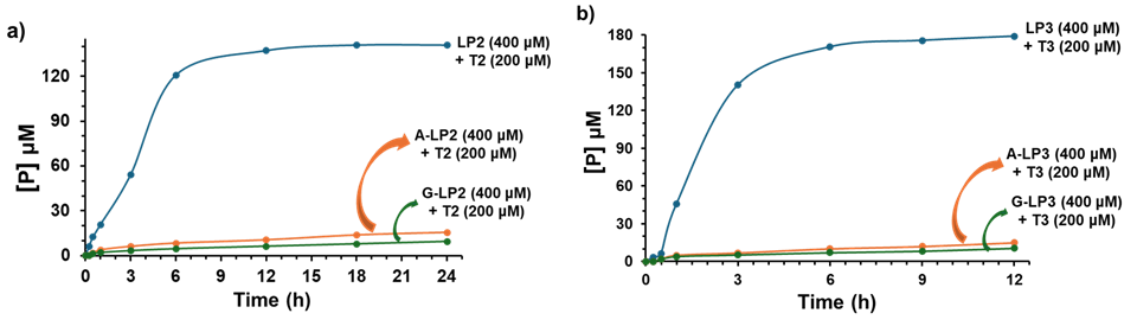

Figure 6.5. *Production of corresponding cyclic products (P) over time with mutated precursors a). A-LP2 and G-LP2 in the presence of T2. [Formation of P over time for LP2 + T2 is shown for comparison]. b). A-LP3 and G-LP3 in the presence of T3. [Formation of P over time for LP3 + T3 is shown for comparison].*

To investigate the spatio-chiroselectivity and directed evolution of products in a temporally changing environment, we designed an experimental system in which we mixed all three linear precursors, LP1 (discussed in the previous chapter), LP2, and LP3 at 200 µM each, along with template T3 (100 µM). These precursors have identical sequence except for the position of the chirality of their diphenylalanine residues: LP1 contains L-Phe-L-Phe, LP2 features D-Phe-L-Phe, and in LP3 the position of L- and D-phenylalanine was interchanged, i.e. L-Phe-D-Phe (see Table 5.1 and 6.1 for structural details). In the beginning, T3 selectively catalyse the ligation of LP3 from the mixture solution, leading to the exclusive formation of CP3. However, by 6 h, a small amount of CP2 was also detected, likely arising from autocatalytic amplification, cross-seeding or a combination of both. At this point, template T2 (100 µM) was introduced into the mixture, resulting in a significant increase in CP2 formation over the next 18 hours, driven by ligation of LP2. Similarly, by 24 hours, a small quantity of CP1 also emerged, presumably due to the reasons mentioned above. After 24 hours, the next template T1 (100 µM) was added to the above mixture solution, promoting the preferential formation of CP1 monitored up to 48 hours.

This study reveals the spatio-chiroselective nature of the designed cyclic peptide self-replicator, wherein even subtle differences in stereochemistry, such as a single chiral inversion within the precursor sequence, can be selectively recognized by the templated self-replication process. Among the structurally similar precursors, the template T3 selectively catalyzed the ligation of LP3 over LP1 and LP2. This selectivity persisted despite the presence of competing substrates, highlighting the system's remarkable ability to recognize and propagate stereochemical information. Temporal addition of templates T2 and T1 further enabled the system to switch product selectivity in a controlled manner,

leading to the sequential amplification of CP2 and CP1. These results demonstrate that conformationally guided, template-assisted self-replication can achieve highly selective molecular evolution in response to minute structural variations and dynamic environmental inputs (Figure 6.6).

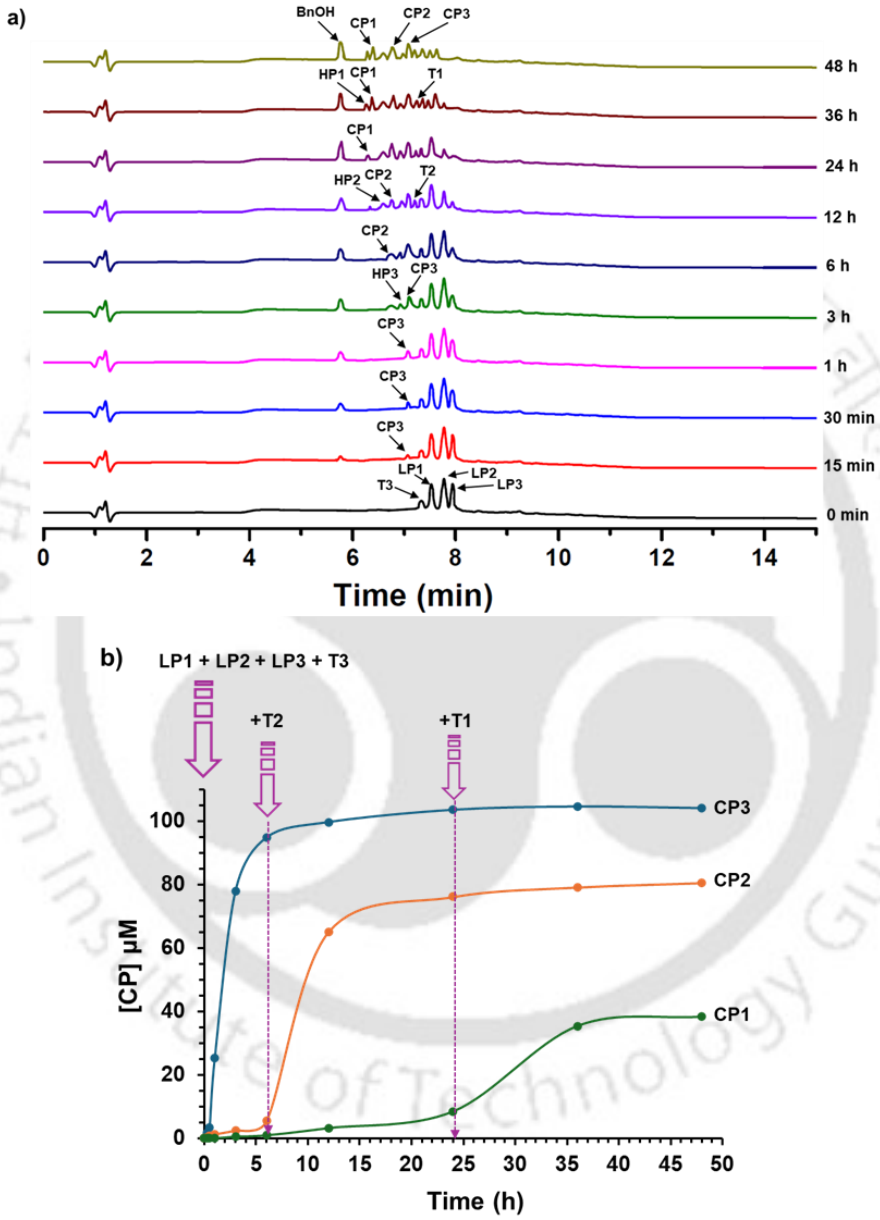

Figure 6.6. *a). Time-resolved HPLC chromatograms for ligation reaction of LP1+LP2+LP3 (200 µM each) with temporal addition of templates (100 µM). b) Kinetic plots for the quantity of cyclic products formed over time with the temporal addition of templates. [To identify the individual components, aliquots of the mixture solution were co-injected with individual reference solution of the known components. A selective increase in the absorbance intensity in one of the three peaks confirmed the identity of that specific component].*

6.8. Kinetic Study

The kinetics for the self-replicating systems and the probable mechanism can be understood from the discussion mentioned in Chapter 5, Section 4.8. However, a logarithmic plot of initial reaction rates against seeded template concentrations for the production of CP2 and CP3 reveals (Figure 6.7) a slightly better catalytic reaction order than that of CP1.

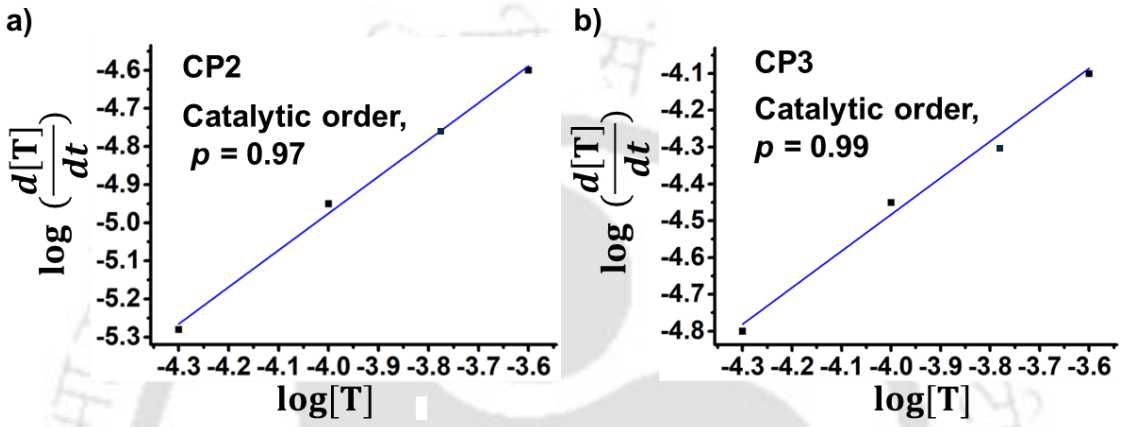

Figure 6.7. *a), b). Logarithmic plot of the initial rates extracted from the graph (Figure 6.2b, 6.2d), respectively, as a function of seeded template concentrations.*

6.9. Our Model of Minimalist Molecular Evolutionary Network

Our evolutionary design framework can be conceptualized as a temporal sequence of structural and chemical transitions within the peptide precursors (Figure 6.8). Initially, the system consists exclusively of unstructured precursor molecules exhibiting random-coil conformations. Some of these precursors undergo numerous conformational mutations (Path 1), but one of them becomes favoured by the local environment and adopts β–sheet–rich architectures in a self-replicatory manner, becoming stabilized by intermolecular hydrogen bonding, which subsequently evolves into fibrillar assemblies. In another pathway (Path 2), a fraction of the precursors undergoes chemical mutation through hydrolysis (not autocatalytic), generating fragments that also undergo similar conformational mutation and reorganise into β-sheet structures over time in a self-replicatory manner, displaying a similar fibrillar assembly at later stages.

In a distinct trajectory (Path 3), a portion of the precursor molecules undergoes a different kind of conformational mutation, which brings the reactive termini into close spatial

proximity, facilitating intramolecular cyclisation and leading to the specific chemical mutation. This process yields cyclic species that gradually self-replicate and assembles into rod-like nanostructures, representing a third accessible pathway within the system. All the above-mentioned conformational and chemical mutations initially occur as random events and are subsequently inherited through autocatalytic and template-directed propagation, giving rise to distinct self-replicating assembly lineages under the prevailing environmental conditions.

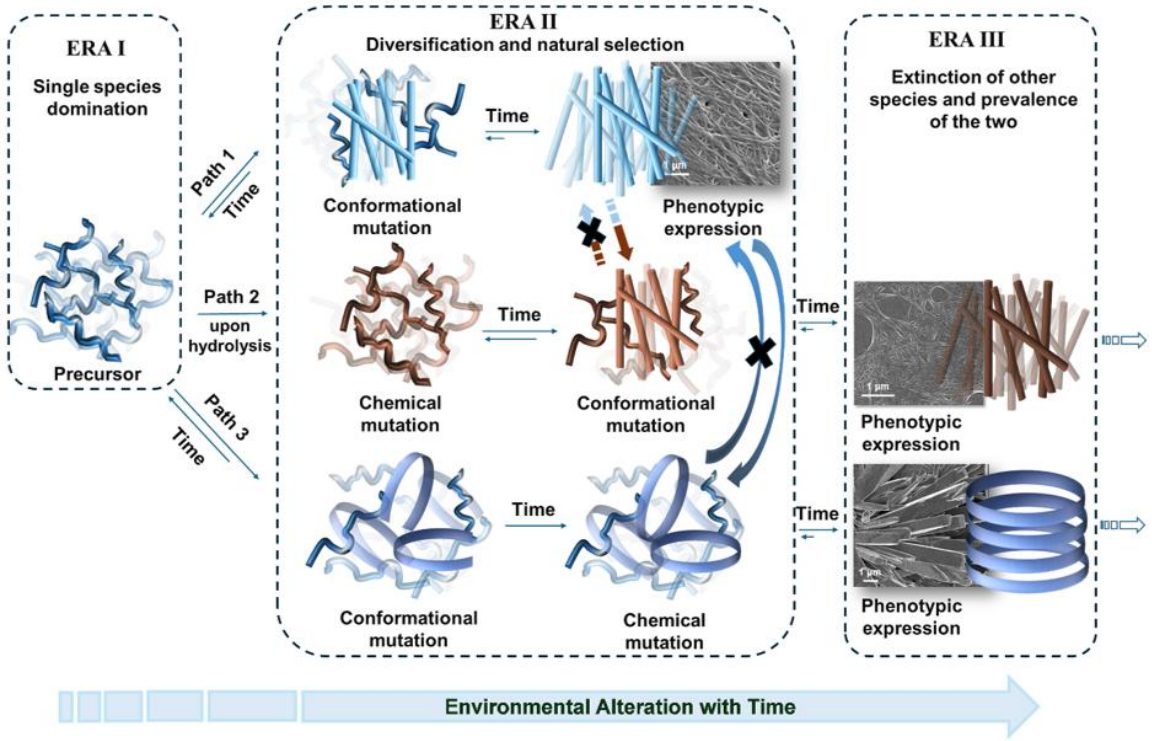

Figure 6.8. *Schematic representation of an open-ended model of molecular evolution.*

When viewed across temporal "eras," the system progresses from a homogeneous ensemble of unstructured precursors (Era I, single-species domination) to a diversified mixture containing both conformationally and chemically mutated species (Era II, diversification and natural selection). With continued evolution, only the hydrolyzed fibrillar products and cyclic rod-like assemblies persist as the most thermodynamically stable entities, marking the transition to Era III (Extinction of other species and prevalence of the two). Notably, even these stable species may undergo further structural or chemical transformations with time and under suitable conditions, suggesting that the system follows an open-ended model of peptide self-replication capable of continuous diversification and emergent evolutionary behaviour.

The predominance of either the hydrolyzed or cyclic products can be externally modulated. When the precursor transition pathway is seeded with preformed cyclic peptides serving as templates, the transformation of precursor molecules preferentially proceeds through the cyclization pathway (case 3), leading to a significant enrichment of cyclic products. On the other hand, in the absence of such templating influence, the system predominantly follows the hydrolytic pathway (case 2), yielding mainly hydrolyzed species that subsequently assemble into fibrillar structures.

Most previously reported self-replicating systems have been closed-ended, limited to the amplification of a single, template-defined product. The α-helical-based peptide self-replicator models by Ghadiri *et al.*[5-7] and Chmielewski *et al.*[8,9] exemplify efficient yet compositionally static autocatalysis. While Ashkenasy's peptide[10,11] networks introduced cross-catalytic interactions and Otto's[12,13] dynamic combinatorial systems exhibited adaptive selection, both remained confined to a finite chemical space. In contrast, our system enables both conformational and chemical mutations within the same precursor pool, producing structurally diverse assemblies that coexist and interconvert over time. This evolving molecular landscape establishes a mechanistic pathway toward open-ended peptide self-replication, where replication, diversification, and selection emerge spontaneously from the intrinsic chemistry of the system.

6.10. Conclusion

In summary, we have successfully introduced a new class of self-replicating cyclic peptides that operate through templated autocatalysis while adopting random-coil conformations rather than conventional β-sheet or helical motifs. These replicators exhibit unique morphological transitions from fibrous precursors to rod-like architectures and display exceptional fidelity, with strict sequence and stereoselectivity. Together, these findings demonstrate that efficient, selective self-replication can emerge from noncanonical conformations, thereby expanding the structural and mechanistic space available to synthetic replicators. By bridging molecular simplicity with life-like selectivity and adaptability, this work provides new design principles for advancing molecular evolution in peptide-based systems.

6.11. Characterization data

Prior to the synthesis of the peptides, Fmoc-Glu-OMe and Fmoc-Glu-OBn were first synthesized (as discussed in Chapter 5) and anchored to Rink Amide resin through their side chain to obtain the linear and cyclic peptides.

H_2N-K(Ac)-L-V-f-F-A-Q-COOBn (LP2): (White fluffy powder, yield = 15.8 mg, 11.5% w.r.t the resin loading. Calculated mass is 983.548, observed mass is 1007.105 $[M+Na+H]^+$, 1023.130 $[M+K+H]^+$. HPLC retention time (t_R) = 6.9 min).

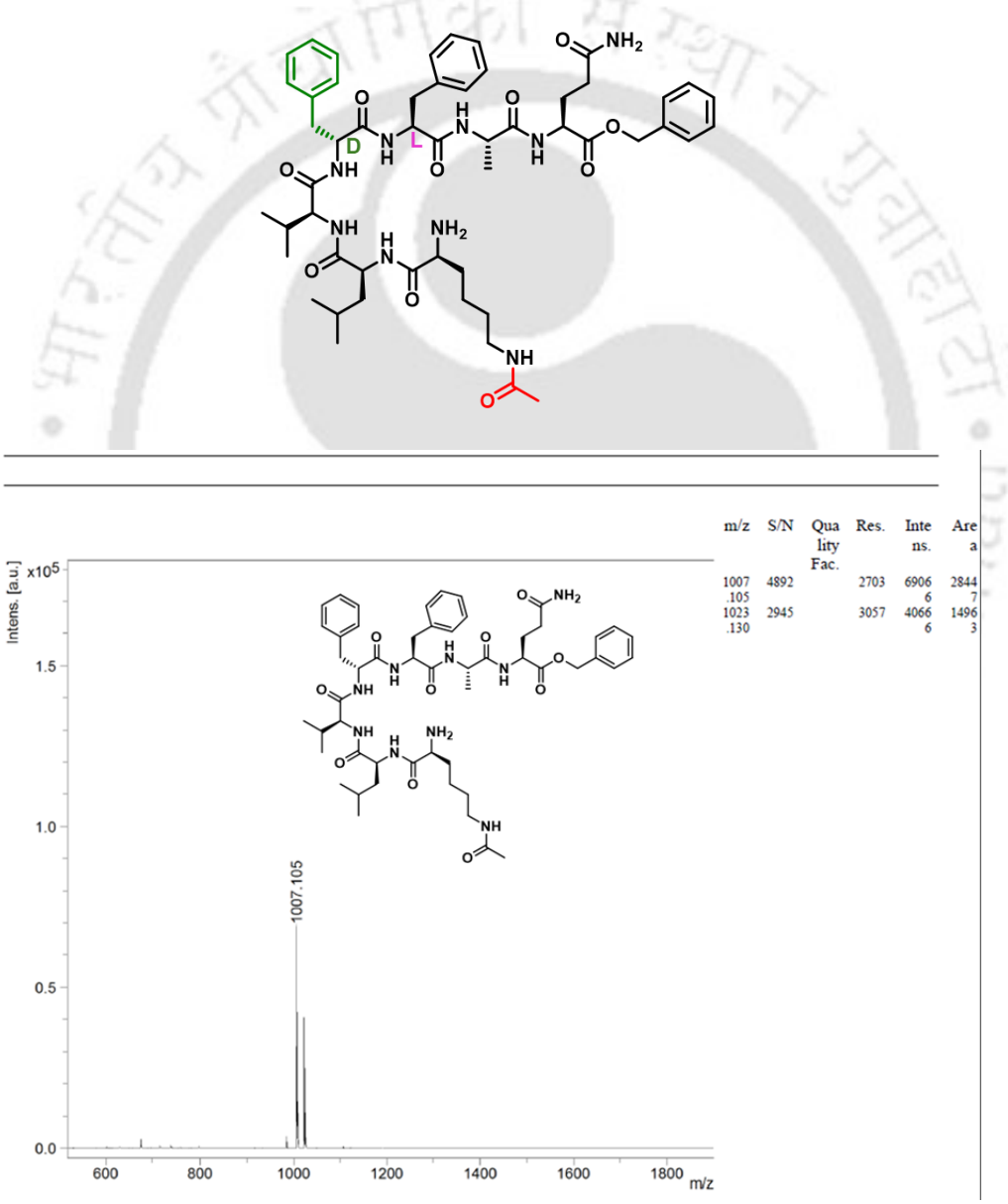

Figure 6.9. *MALDI-TOF mass spectrum of purified peptide LP2.*

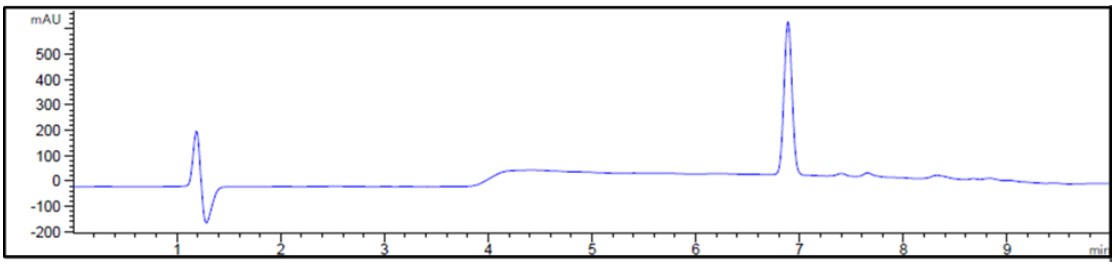

Figure 6.10. *HPLC profile of purified peptide LP2.*

K-L-V-f-F-A-Q
HNOC
(T2) **:** (White fluffy powder, yield = 10 mg, 8.6% w.r.t the resin loading. Calculated mass is 833.480, observed mass is 834.604 $[M+H]^+$, 856.798 $[M+Na]^+$, 873.120 $[M+K]^+$. HPLC retention time (t_R) = 7.4 min).

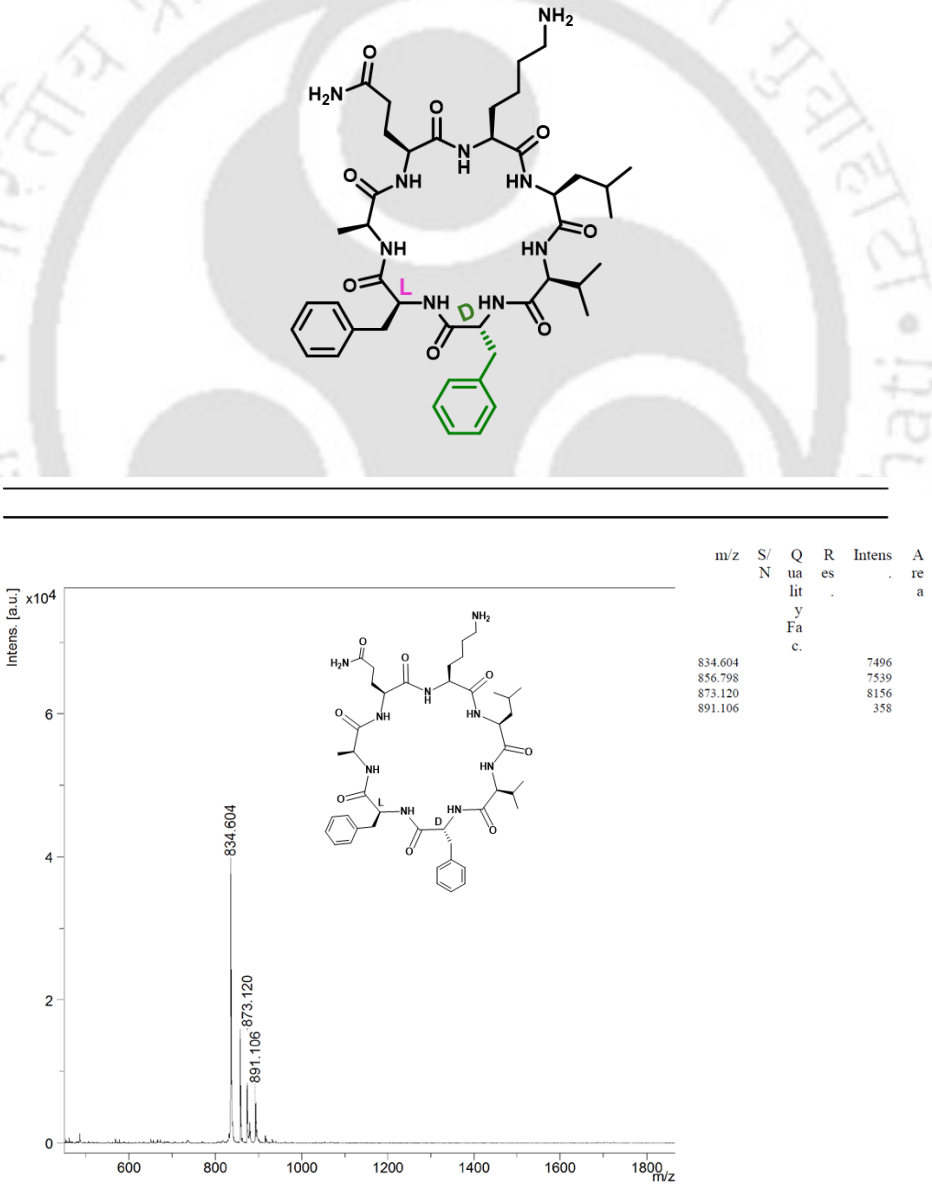

Figure 6.11. *MALDI-TOF mass spectrum of purified peptide T2.*

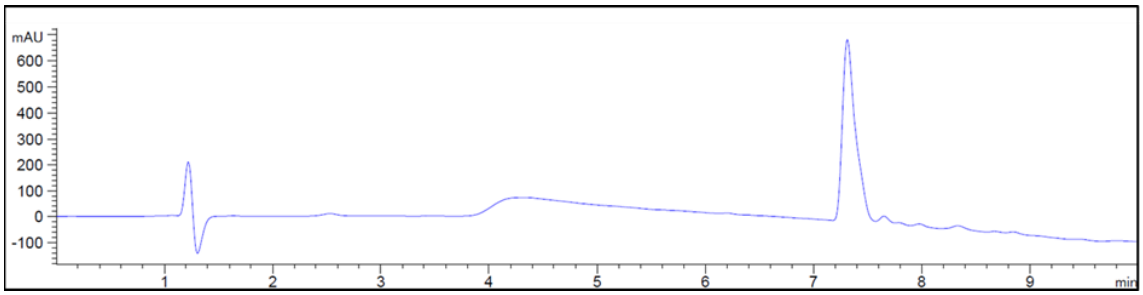

Figure 6.12. *HPLC profile of purified peptide T2.*

H_2N-A-L-V-f-F-A-Q-COOBn (A-LP2): (White fluffy powder, yield = 17.8 mg, 14.4% w.r.t the resin loading. Calculated mass is 884.479, observed mass is 907.753 $[M+Na]^+$, 923.795 $[M+K]^+$. HPLC retention time (t_R) = 6.9 min).

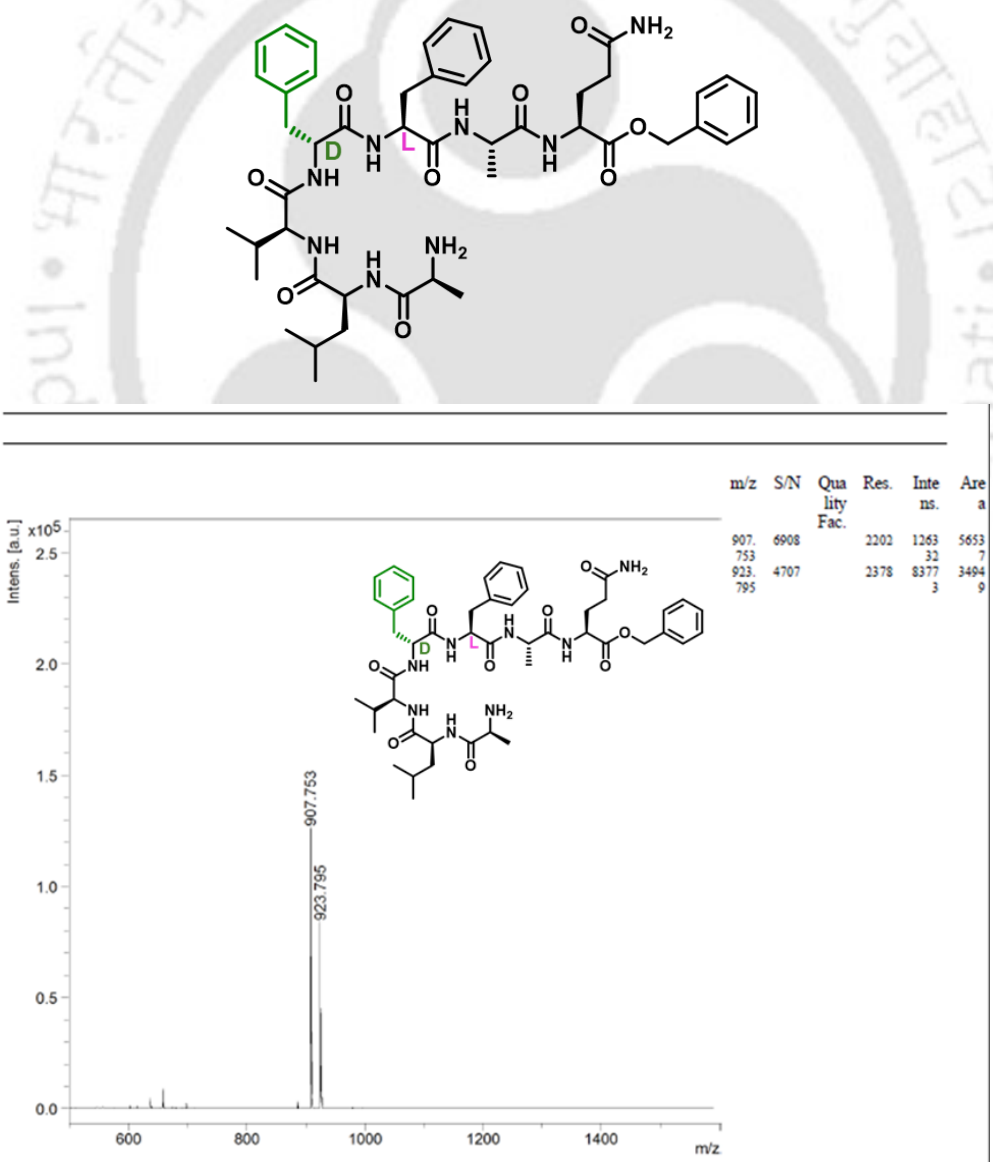

Figure 6.13. *MALDI-TOF mass spectrum of purified peptide A-LP2.*

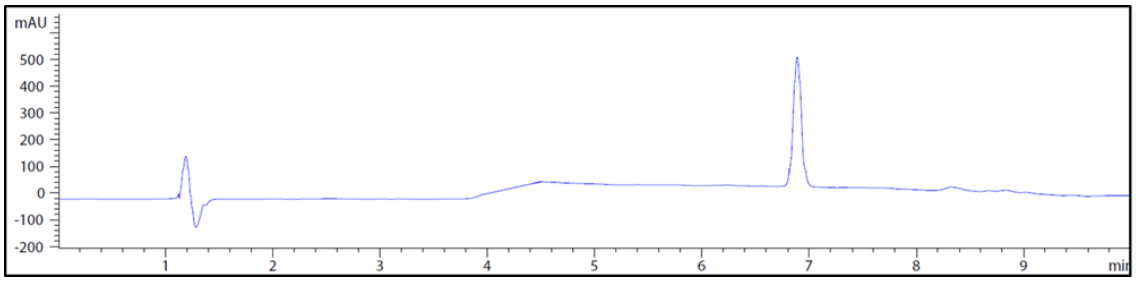

Figure 6.14. *HPLC profile of purified peptide A-LP2.*

H_2N-G-L-V-f-F-A-Q-COOBn (G-LP2): (White fluffy powder, yield = 20 mg, 16.4% w.r.t the resin loading. Calculated mass is 870.464, observed mass is 872.756 $[M+2H]^+$, 894.619 $[M+Na+H]^+$, 9011.721 $[M+K+2H]^+$. HPLC retention time (t_R) = 6.9 min).

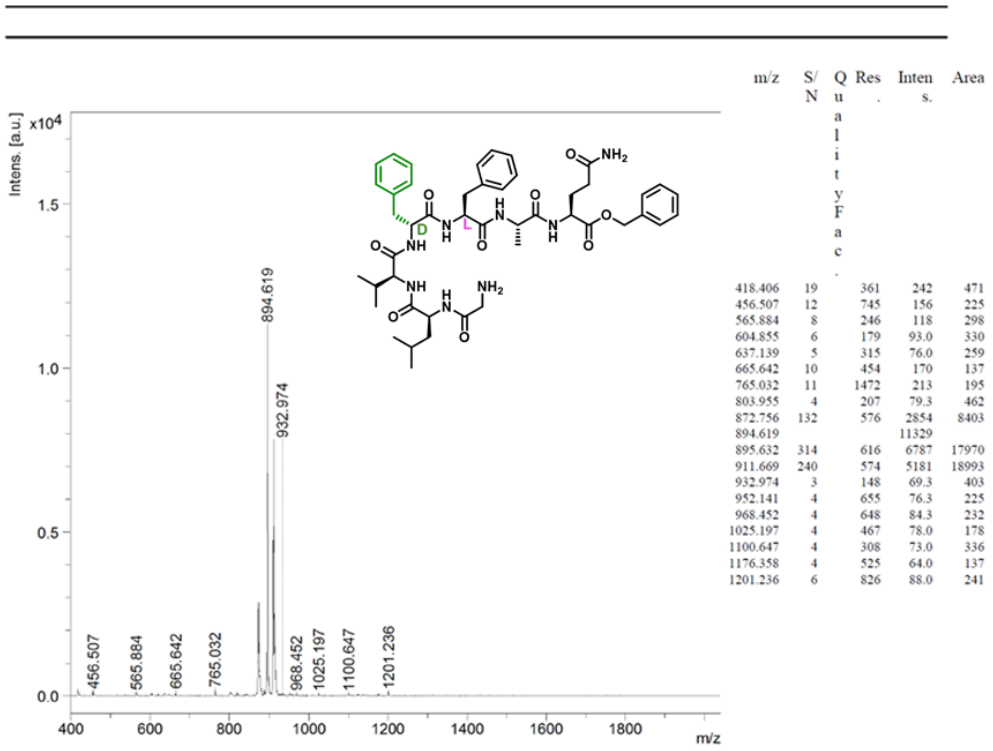

m/z	S/N	Quality Fac.	Res.	Intens.	Area
418.406	19		361	242	471
456.507	12		745	156	225
565.884	8		246	118	298
604.855	6		179	93.0	330
637.139	5		315	76.0	259
665.642	10		454	170	137
765.032	11		1472	213	195
803.955	4		207	79.3	462
872.756	132		576	2854	8403
894.619				11329	
895.632	314		616	6787	17970
911.669	240		574	5181	18993
932.974	3		148	69.3	403
952.141	4		655	76.3	225
968.452	4		648	84.3	232
1025.197	4		467	78.0	178
1100.647	4		308	73.0	336
1176.358	4		525	64.0	137
1201.236	6		826	88.0	241

Figure 6.15. *MALDI-TOF mass spectrum of purified peptide G-LP2.*

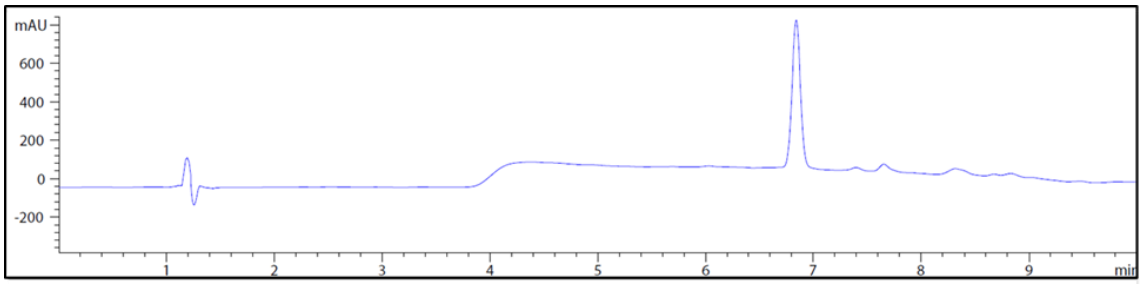

Figure 6.16. *HPLC profile of purified peptide G-LP2.*

H_2N-K(Ac)-L-V-F-f-A-Q-COOBn (LP3): (White fluffy powder, yield = 15.6 mg, 11.3% w.r.t the resin loading. Calculated mass is 983.548, observed mass is 985.752, $[M+2H]^+$, 1008.685 $[M+Na+2H]^+$, 1024.716 $[M+K+2H]^+$. HPLC retention time (t_R) = 6.9 min).

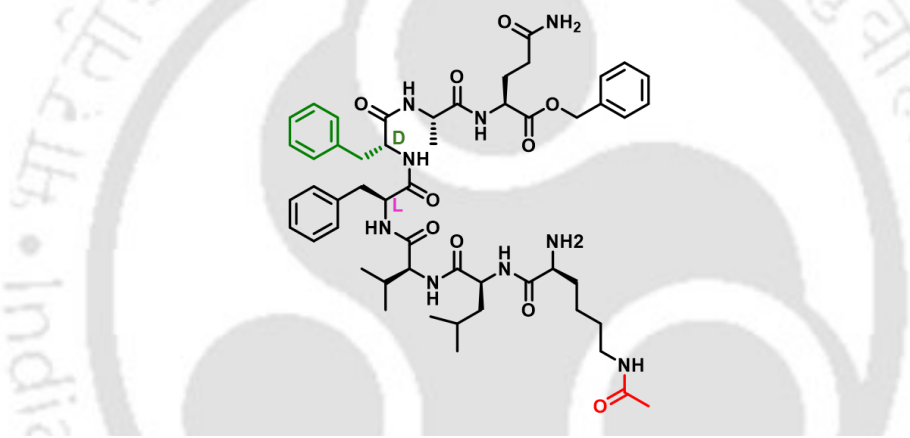

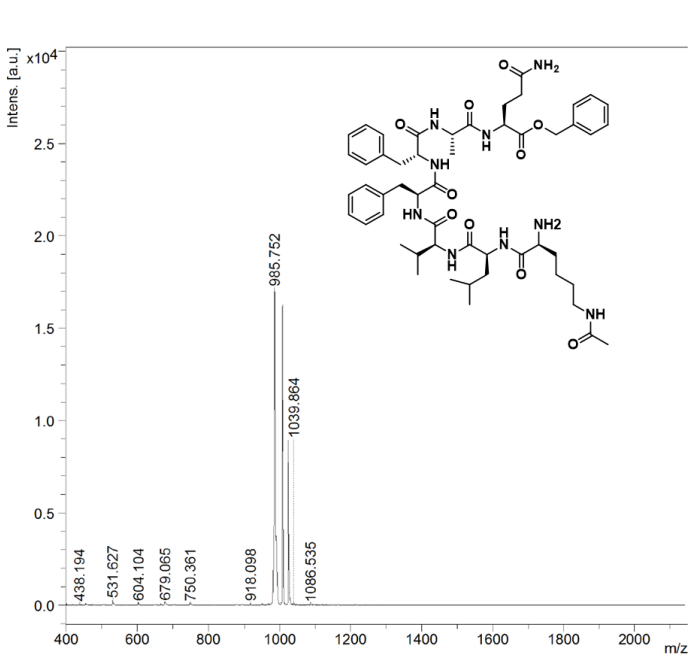

m/z	S/N	Quality Fac.	Res.	Intens.	Area
417.387	4	1175	46.0	45.6	
438.194	8	195	91.0	63.8	
503.517	3	67.1	35.0	109	
531.627	13	416	156	613	
604.104	6	472	67.0	301	
651.219	5	338	63.0	150	
679.065	8	131	107	575	
750.361	6	364	96.0	461	
918.098	6	704	113	138	
950.305	5	629	96.0	225	
967.723	4	137	76.0	353	
985.752	952	572	17171	60501	
1008.685	632	645	11332	26158	
1024.716	329	666	5856	15416	
1039.864	8	728	142	277	
1047.996	3	475	54.0	108	
1086.535	3	503	51.0	134	

Figure 6.17. *MALDI-TOF mass spectrum of purified peptide LP3.*

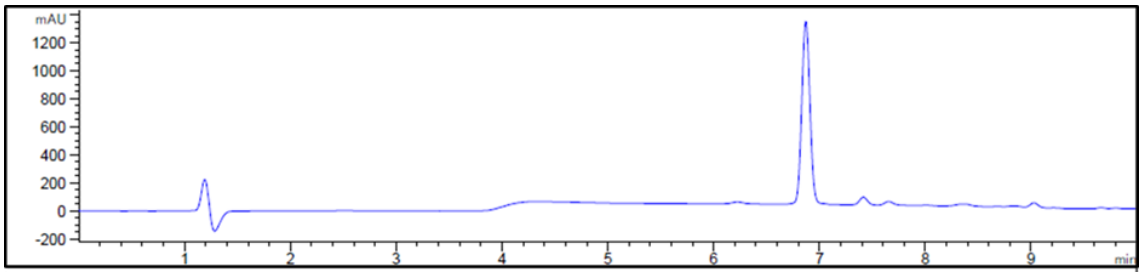

Figure 6.18. *HPLC profile of purified peptide LP3.*

K-L-V-F-f-A-Q
HNOC
(T3)

: (White fluffy powder, yield = 12.2 mg, 10.5% w.r.t the resin loading. Calculated mass is 833.480, observed mass is 834.991, $[M+H]^+$, 856.929 $[M+Na]^+$, 872.944 $[M+K]^+$. HPLC retention time (t_R) = 7.4 min).

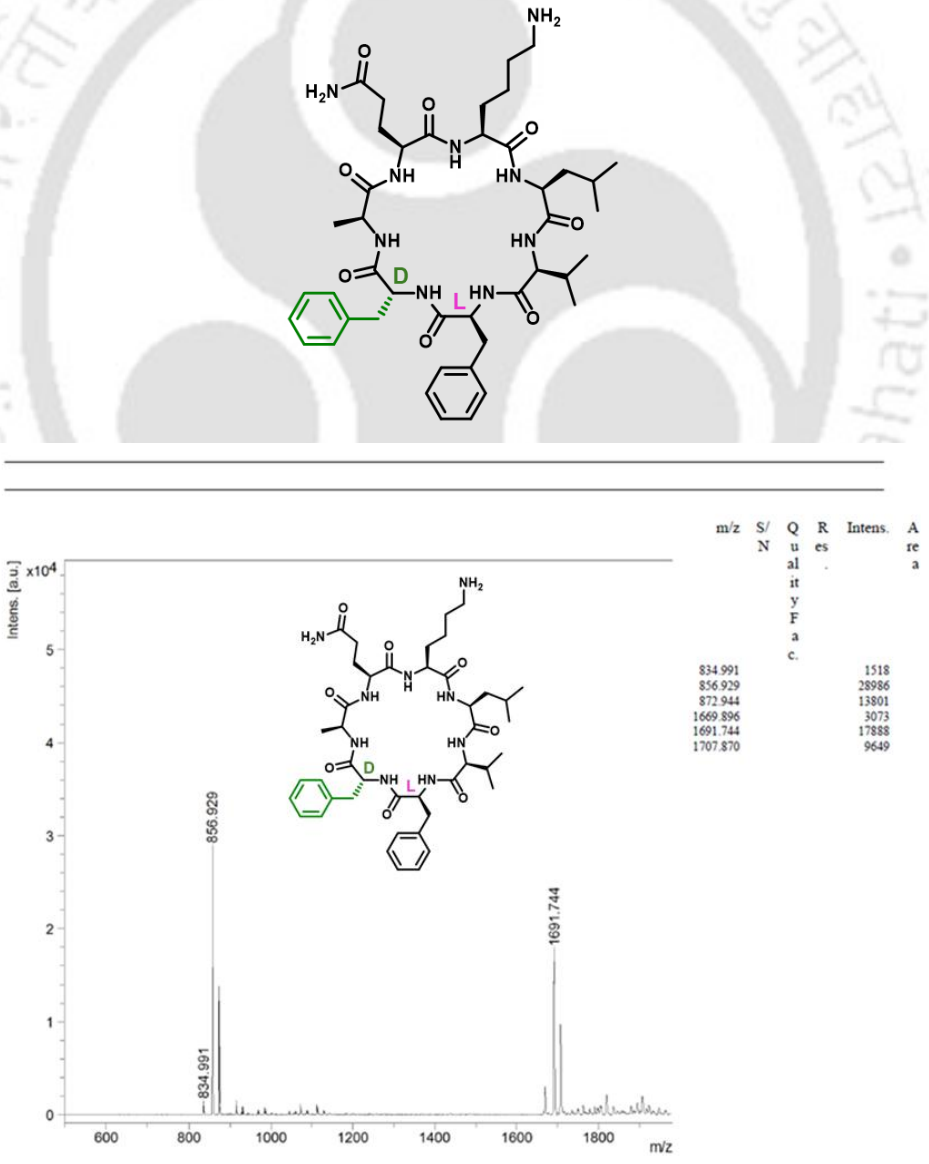

Figure 6.19. *MALDI-TOF mass spectrum of purified peptide T3.*

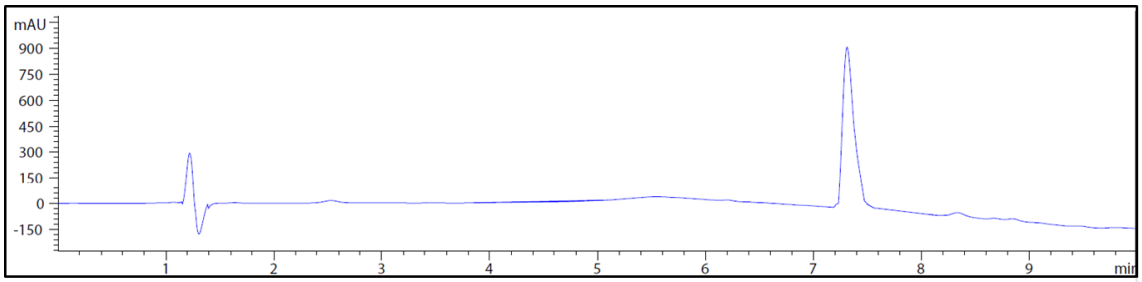

Figure 6.20. *HPLC profile of purified peptide T3.*

H_2N-A-L-V-F-f-A-Q-COOBn (A-LP3): (White fluffy powder, yield = 17.6 mg, 14.2% w.r.t the resin loading. Calculated mass is 884.479, observed mass is 886.995 $[M+2H]^+$, 909.684 $[M+Na+2H]^+$, 925.917 $[M+K+2H]^+$. HPLC retention time (t_R) = 6.9 min).

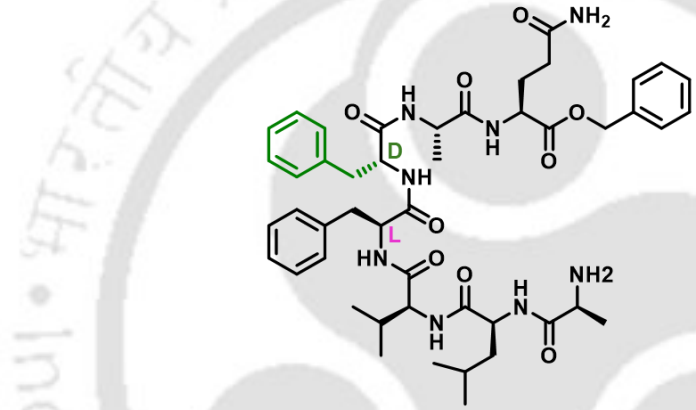

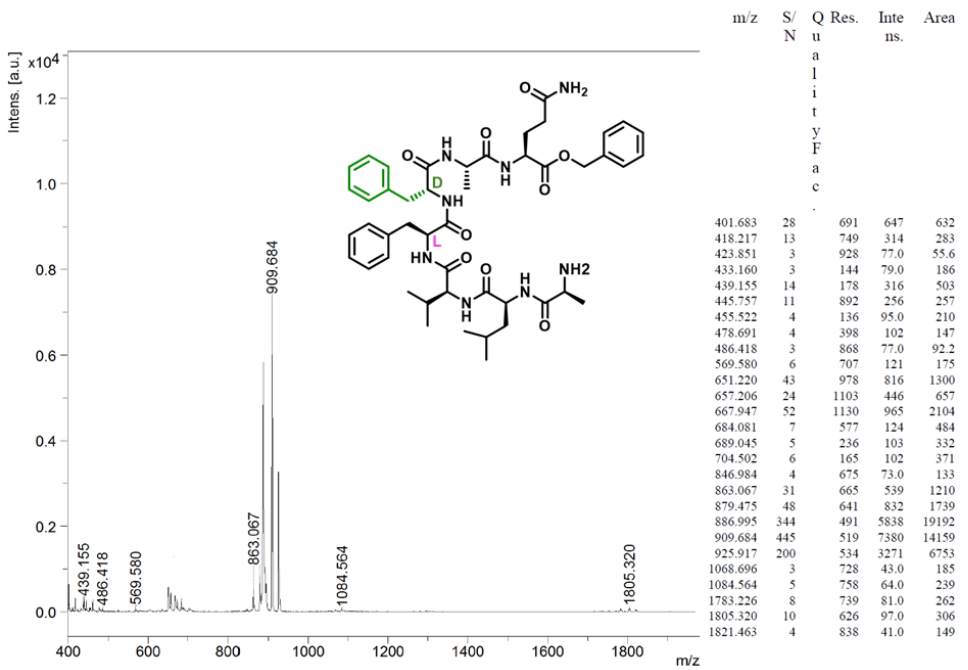

m/z	S/N	Quality Fac.	Res.	Intens.	Area
401.683	28		691	647	632
418.217	13		749	314	283
423.851	3		928	77.0	55.6
433.160	3		144	79.0	186
439.155	14		178	316	503
445.757	11		892	256	257
455.522	4		136	95.0	210
478.691	4		398	102	147
486.418	3		868	77.0	92.2
569.580	6		707	121	175
651.220	43		978	816	1300
657.206	24		1103	446	657
667.947	52		1130	965	2104
684.081	7		577	124	484
689.045	5		236	103	332
704.502	6		165	102	371
846.984	4		675	73.0	133
863.067	31		665	539	1210
879.475	48		641	832	1739
886.995	344		491	5838	19192
909.684	445		519	7380	14159
925.917	200		534	3271	6753
1068.696	3		728	43.0	185
1084.564	5		758	64.0	239
1783.226	8		739	81.0	262
1805.320	10		626	97.0	306
1821.463	4		838	41.0	149

Figure 6.21. *MALDI-TOF mass spectrum of purified peptide A-LP3.*

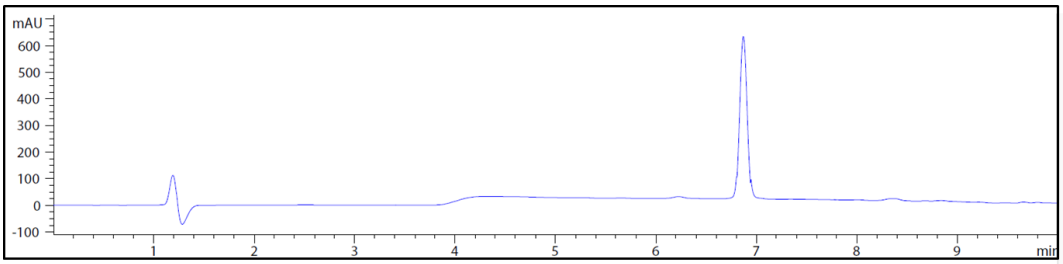

Figure 6.22. *HPLC profile of purified peptide A-LP3.*

H_2N-G-L-V-F-f-A-Q-COOBn (G-LP3): (White fluffy powder, yield = 18.5 mg, 15.2% w.r.t the resin loading. Calculated mass is 870.464, observed mass is 872.835 $[M+2H]^+$, 895.500 $[M+Na+2H]^+$, 910.894 $[M+K+H]^+$. HPLC retention time (t_R) = 6.9 min).

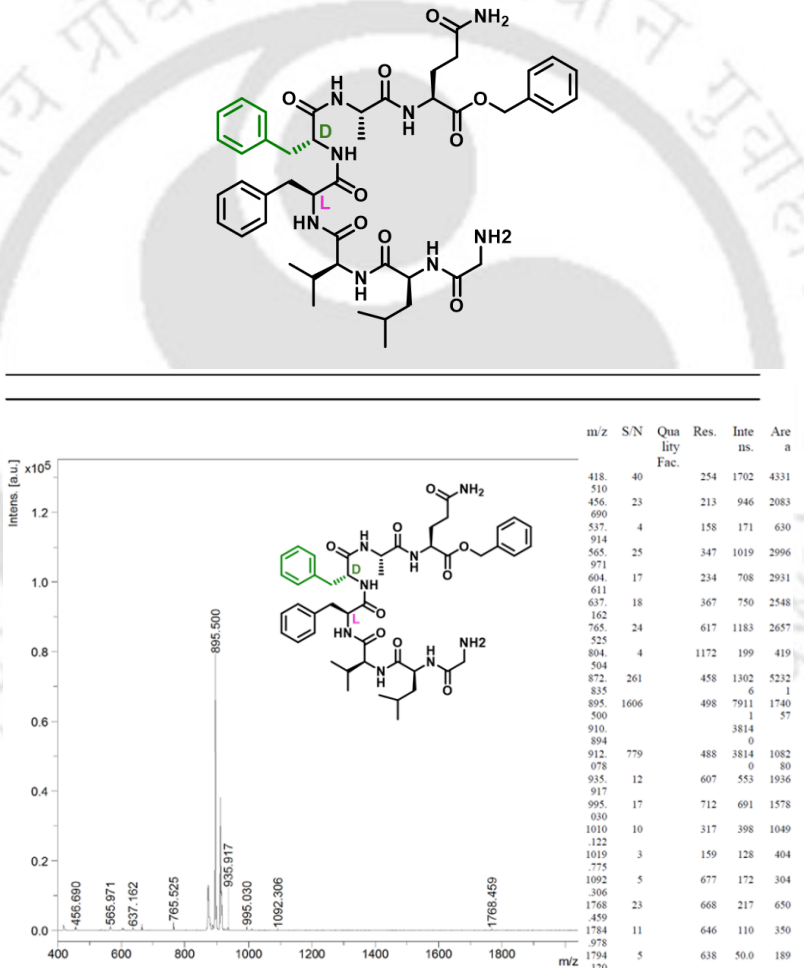

m/z	S/N	Quality Fac.	Res.	Intens.	Area
418.510	40		254	1702	4331
456.690	23		213	946	2083
537.914	4		158	171	630
565.971	25		347	1019	2996
604.611	17		234	708	2931
637.162	18		367	750	2548
765.525	24		617	1183	2657
804.504	4		1172	199	419
872.835	261		458	13026	52321
895.500	1606		498	79111	174057
910.894				38140	
912.078	779		488	38140	10828
935.917	12		607	553	1936
995.030	17		712	691	1578
1010.122	10		317	398	1049
1019.775	3		159	128	404
1092.306	5		677	172	304
1768.459	23		668	217	650
1784.978	11		646	110	350
1794	5		638	50.0	189

Figure 6.23. *MALDI-TOF mass spectrum of purified peptide G-LP3.*

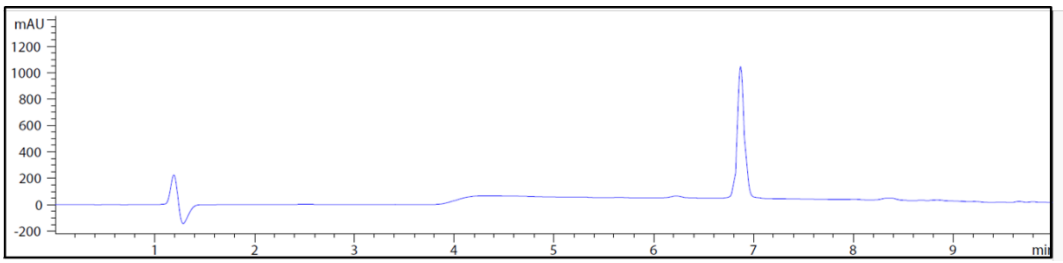

Figure 6.24. *HPLC profile of purified peptide A-LP3.*

6.12. References

1. Smith, J. A.; Pease, L. G.; Kopple, K. D. Reverse turns in peptides and protein. *Crit. Rev. Biochem.* **1980**, *8*, 315-399.
2. Varughese, K. I.; Kartha, G.; Kopple, K. D. Crystal structure and conformation of cyclo-(glycyl-D-leucyl-L-leucyl) 2. *J. Am. Chem. Soc.* **1981**, *103*, 3310-3313.
3. Kessler, H. Conformation and biological activity of cyclic peptides. *Angew. Chem., Int. Ed. Engl.* **1982**, *21*, 512-523.
4. Tran, H. L.; Lexa, K. W.; Julien, O.; Young, T. S.; Walsh, C. T.; Jacobson, M. P.; Wells, J. A. Structure–activity relationship and molecular mechanics reveal the importance of ring entropy in the biosynthesis and activity of a natural product. *J. Am. Chem. Soc.* **2017**, *139*, 2541-2544.
5. Lee, D. H.; Granja, J. R.; Martinez, J. A.; Severin, K.; Ghadiri, M. R. A self-replicating peptide. *Nature* **1996**, *382*, 525-528.
6. Severin, K.; Lee, D. H.; Martinez, J. A.; Ghadiri, M. R. Peptide self-replication via template-directed ligation. *Chem. Eur. J.* **1997**, *3*, 1017-1024.
7. Saghatelian, A.; Yokobayashi, Y.; Soltani, K.; Ghadiri, M. R. A chiroselective peptide replicator. *Nature* **2001**, *409* (6822), 797-801.
8. Yao, S.; Ghosh, I.; Zutshi, R.; Chmielewski, J. A pH-modulated, self-replicating peptide. *J. Am. Chem. Soc.* **1997**, *119*, 10559-10560.
9. Yao, S., Ghosh, I.; Zutshi, R.; Chmielewski, J. A self-replicating peptide under ionic control. *Angew. Chem. Int. Ed.* **1998**, *37*, 478-481.
10. Rubinov, B.; Wagner, N.; Rapaport, H.; Ashkenasy, G. Self-replicating amphiphilic β-sheet peptides. *Angew. Chem.* **2009**, *121*, 6811-6814.
11. Nanda, J.; Rubinov, B.; Ivnitski, D.; Mukherjee, R.; Shtelman, E.; Motro, Y.; Ashkenasy, G. Emergence of native peptide sequences in prebiotic replication networks. *Nat. Commun.* **2017**, *8*, 434.
12. Carnall, J. M.; Waudby, C. A.; Belenguer, A. M.; Stuart, M. C.; Peyralans, J. J. P.; Otto, S. Mechanosensitive self-replication driven by self-organization. *Science* **2010**, *327*, 1502-1506.
13. Frederix, P. W.; Idé, J., Altay, Y.; Schaeffer, G.; Surin, M.; Beljonne, D.; Marrink, S. J. Structural and spectroscopic properties of assemblies of self-replicating peptide macrocycles. *ACS nano* **2017**, *11*, 7858-7868.

Conclusions and Future Directions

Conclusions

The work presented in this thesis focuses deeply on supramolecular self-assembly of peptides, with particular emphasis on self-replication of cyclic peptides. Till date all previously reported studies on peptide self-replication were based on linear peptides, and no pure cyclic peptide-based model self-replicators have been studied. Additionally, in this thesis we have delved into self-assembly of small peptides such as di- and tri- peptides and their importance and implications for both fundamental science and practical applications. The overview of the thesis work has been illustrated in Scheme1 below.

In chapter 1, we have discussed the general overview of amino acids, peptides, proteins, and their levels of organization. We have also explored supramolecular self-assembly of small peptides and their implications. Moreover, we have examined self-replicating materials and the pioneering work in this area and reviewed reported literature on self-replication of peptides highlighting the limitations of existing work and potential avenues for improved designs. We planned our objective to address the drawbacks of previous work.

In chapter 3, we investigated the binding behaviour of Thioflavin T (ThT), a widely employed amyloid-specific fluorophore, with well-ordered spherical aggregates formed by supramolecular self-assembly of the designed dipeptides utilizing diverse array of analytical techniques, including spectroscopic methods and theoretical calculations. This intriguing phenomenon challenges the conventional understanding of ThT's binding properties and opens new avenues for exploring its interactions with diverse molecular structures beyond traditional amyloid fibrils.

In chapter 4, we investigated the morphological transformation of the designed tripeptides from nano-sphere to rod-like architecture with time. These self-assembled tripeptides are porous in nature and have significant N_2 adsorption capacity. Furthermore, they can encapsulate curcumin, a powerful hydrophobic fluorescent drug, and upon treatment with KCl, the self-assembled architecture holding the drug molecule inside gets disrupted and thus release the entrapped curcumin molecules. Therefore, understanding the dynamics of these interactions and their impact on peptide morphology is crucial for harnessing their functional diversity in applications such as drug delivery, tissue engineering, etc.

In chapter 5, we reported on the design, synthesis, and characterization of a new class of self-replicating material, i.e. cyclic peptide. The head-to-tail cyclic peptide was derived from the hydrophobic core of the Aβ peptide. Unlike traditional peptide-based self-replicators that rely heavily on structured motifs such as helical coiled coil and β-sheet assemblies, the designed self-replicating cyclic peptides exist predominantly in random coil conformations and also exhibit remarkable morphological transitions from fibrous precursors to rod-like architectures. We have also successfully implemented a new ligating strategy by using benzyl-ester mediated amide bond formation. The designed self-replicating system is highly efficient with a catalytic reaction order equal to unity, indicating its potential for Darwinian-like evolutionary dynamics. These findings contribute to a broader understanding of molecular self-organization and highlight the roles of supramolecular assembly, intermolecular recognition, and environmental conditions in the development of minimalist systems with life-like properties.

In chapter 6, we have tuned the self-replicating ability of the previously discussed cyclic peptide by introducing D-amino acid in the backbone of the peptide sequence. Thus, in this chapter, we reported two more head-to-tail cyclic peptide (heterochiral) having enhanced self-replicating ability. The designed self-replicating cyclic peptides exhibit exceptional molecular selectivity, such as sequence selectivity where sequence fidelity is strictly required between the precursor and the template for effective self-recognition and templated replication. Even a single point mutation is sufficient to disrupt the critical interactions required for successful templating. In addition to sequence-specificity, these self-replicating systems exhibit pronounced spatio-chiroselectivity, where the presence of a single mismatched chiral centre between the interacting components can be sensed, hampering effective templated interactions. The designed peptidic self-replicatory system represents a minimalist, continuous, and Darwinian-like evolutionary system that can be perturbed by manipulating the environmental composition as desired, thereby expanding the scope for further modification of the system to incorporate novel features.

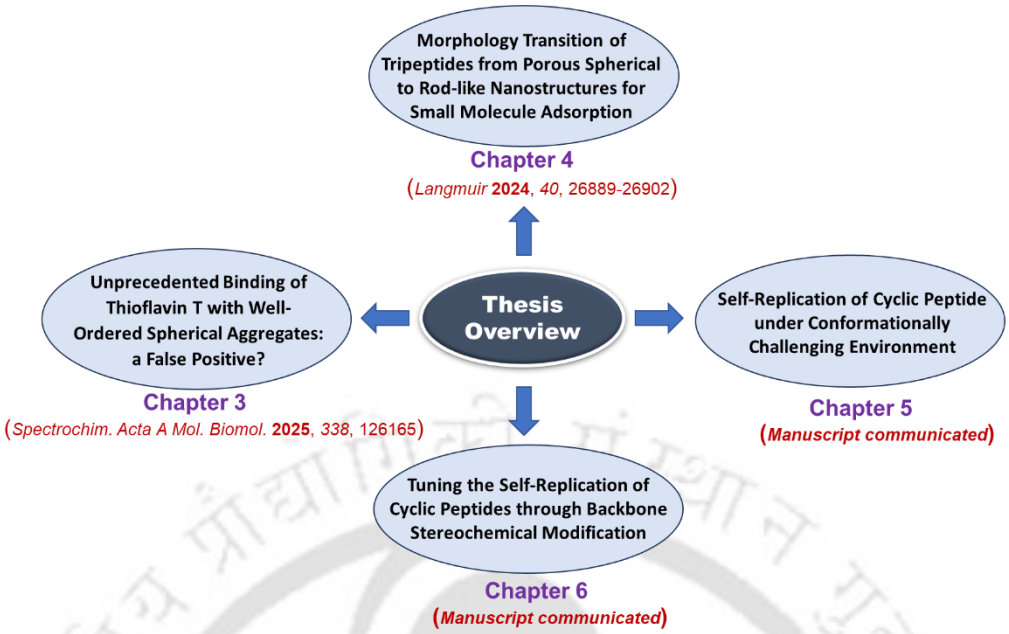

Scheme 1. Thesis overview

Future Directions

Throughout my doctoral research, I have worked on the self-assembly of small peptides and their diverse applications. In one of the works, we observed and established unprecedented binding of Thioflavin T with self-assembled dipeptides with spherical morphologies. This is a rare phenomenon, and such unusual binding of ThT to different architectures apart from amyloids challenges the conventional understanding of ThT's binding properties and opens new avenues for exploring its interactions with diverse molecular structures. Thus, understanding the unique binding mechanism between ThT and the designed dipeptides with well-ordered spherical morphology helps innovate its applications in biomaterials, diagnostics, and drug development. Moreover, we have also designed tripeptides that could transform their morphology with time through self-assembly. The ability to engineer and control peptides with such properties opens avenues for developing time-responsive biomaterials and applications in drug delivery.

We have also designed and developed novel cyclic peptide-based self-replicators and their ability to self-propagate without well-defined secondary structures. Thus, the findings state that self-replication can be done efficiently from unconventional conformations. It also broadens the structural and mechanistic space available to synthetic replicators. This work provides new design principles for advancing molecular evolution in peptide-based systems by bridging molecular simplicity with life-like selectivity and adaptability.

Research Outcome

Publications:

1. **Shill, S**.; Sarkar, A.; Biswas, T. K. Mandal, B. Directed Evolution in Cyclic Peptide Self-Replicatory Systems: Navigating Conformational Challenges towards Structural Transformation. (**Manuscript communicated**)
2. **Shill, S**.; Changmai, R. R.; Dolai, G.; Sarma. M.; Mandal, B. Unprecedented binding of Thioflavin T with well-ordered spherical aggregates: A false positive? *Spectrochim. Acta A Mol. Biomol.* **2025**, *338*, 126165
3. **Shill, S**.; Dolai, G.; Sarkar, A.; Mandal, B. Morphology Transition of Tripeptides from Porous Spherical to Rod-like Nanostructures for Small-Molecule Adsorption. *Langmuir* **2024**, *40*, 26889-26902.
4. Roy, S.; Giri, R. S.; Dolai, G.; **Shill, S**.; Baite, T. N.; Mandal, B. Self-Assembly of Enantiomeric Helical Dipeptides into Vesicles: Applications. Langmuir **2026**, *42*, 15620-15634.
5. Sarkar, A.; **Shill, S**.; Roy, S.; Mandal, B. Influence of Chirality in Supramolecular Self-assembly of α/β-Hybrid Dipeptides. *J. Mol. Struct.* **2025**, *1352*, 144545.
6. Dolai, G.; **Shill, S**.; Roy. S.; Mandal, B. Atomic Insight on Inhibition of Fibrillization of Dipeptides by Replacement of Phenylalanine with Tryptophan. *Langmuir* **2023**, *39*, 9367-9383.
7. Kalita, S.; Kalita, S.; Kawa, A. H.; **Shill, S**.; Gupta, A.; Kumar, S.; Mandal, B. Copper chelating cyclic peptidomimetic inhibits Aβ fibrillogenesis. *RSC Med. Chem.* **2022**, *13*, 761-774.

Conferences and Workshops:

Conferences:

1. **S. Shill** and B. Mandal* "Atomic Insight on Inhibition of Fibrillization by Dipeptides Upon Replacing Phenylalanine with Tryptophan." **Research and Industrial Conclave- Integration' 2024**, 9th- 11th August 2024, Students' Academic Board, IIT Guwahati and IIT Guwahati Research Park. (Poster Presentation).
2. **S. Shill** and B. Mandal* "Cyclic Peptidomimetic with Copper Chelating Ligand Inhibits Fibrillogenesis of Amyloid-β." **Research and Industrial Conclave-**

Integration' 2023, 14th- 16th May 2023, Students' Academic Board, IIT Guwahati and IIT Guwahati Research Park. (Poster Presentation).

3. **S. Shill**, and B. Mandal* "Novel Cyclic Peptidomimetic with Attached Copper Chelating Ligand Inhibits Aβ Fibrillogenesis." **International conference on Emerging Trends in Chemistry (ICETC-2023)**, 16th- 17th March 2023, Department of Chemistry, Assam Don Bosco University in collaboration with the Department of Chemistry, Pandu College. (Oral Presentation).
4. **S. Shill**, and B. Mandal* "Novel Cyclic Peptidomimetic with Attached Copper Chelating Ligand Inhibits Aβ Fibrillogenesis." **Frontiers In Chemical Sciences (FICS-2022)**, 2nd- 4th December 2022, Department of Chemistry, IIT Guwahati. (Poster Presentation).

Workshops:

1. **"Scanning Electron Microscopy: Technique and its Applications"** organized by North East Centre for Biological Sciences and Healthcare Engineering (NECBH), Indian Institute of Technology Guwahati, Assam in collaboration with Zeiss India, on 29th- 30th July, 2021.
2. **"Nuclear Magnetic Resonance: Technique and its Application"** organized by North East Centre for Biological Sciences and Healthcare Engineering (NECBH), Indian Institute of Technology Guwahati, Assam in collaboration with Bruker, India, on 23rd- 24th August, 2021.

Sukesh Shill

Personal Information:

Date of Birth: 12th March 1992
Father's Name: Samarendra Shill
Nationality: Indian
Religion: Hindu
Gender: Male
Tel no. +91-8638487708
Email: sukesh.shill25@gmail.com/ s.shill@iitg.ac.in

Present Address:

Senior Research Fellow, C/O: Prof. Bhubaneswar Mandal, Laboratory of Peptide & Amyloid Research, Department of Chemistry, IIT Guwahati, Guwahati, Assam, India-781039.

Permanent Address:

Rohinibill, Thelamara (Sonitpur), Assam, India-784149.

Academic Qualification

07/2019–Present	**Ph.D. in Chemistry (CPI 8.75 out of 10)** Indian Institute of Technology Guwahati, Assam, India-781039 Thesis: **Investigation on Molecular Self-Organisation in Peptide Systems: from Functional Assembly to Autonomous Replication** Thesis advisor: Prof. Bhubaneswar Mandal
2015–2017	**M.Sc. in Chemistry (CPI 7.49 out of 10)** Cotton University, Guwahati, Assam, India-781001 Thesis: **Ion Adsorption Using Humic Acid and Vermiculite** Thesis advisor: Prof. Kalyan Raidongia
2012–2015	**B.Sc. in Chemistry Honours (66.9%, First Class) with Physics and Mathematics** Arya Vidyapeeth College, Gauhati University, Assam, India-781014 Thesis: **Extraction of Components from "*Cynodon dactylon*" Using Chromatographic Techniques** Thesis advisor: Dr. Pankaj Kalita

2009–2011	**Higher Secondary Examination (AHSEC) (79.2%, First Division, star) with Physics, Chemistry, Mathematics, Biology, English, and Alternative English** Lokanayak Omeo Kumar Das College, Assam, India
2009	**High School Examination (SEBA) (77.1%, First Division, Star) with Hindi, English, Mathematics, Science, Social Science, and Advanced Maths** Vinoda Academy, Assam, India

Achievements and Awards

- Qualified National Eligibility Test (CSIR-UGC NET), December-2017 (LS rank-42) in Chemical Science, India.
- Qualified Graduate Aptitude Test (GATE), February 2018 (rank-1589), 2019 (rank-1310) in Chemistry, organized by the Ministry of Human Resource Development (MHRD), Government of India.
- Received Best Oral Presentation Award ICETC-2023: International conference on Emerging Trends in Chemistry, 16th- 17th March 2023, Department of Chemistry, Assam Don Bosco University in collaboration with the Department of Chemistry, Pandu College.

Research Experience

- During my Ph.D. tenure, I have worked on self-assembly of small peptides and their diverse applications. I have also learned and gained experiences working on self-replication of peptides and also designed and developed novel cyclic peptide-based self-replicators and their ability to self-propagate.
- I have expertise in peptide synthesis including both solution phase and solid phase peptide synthesis (SPPS). I find myself efficient in synthesizing “cyclic peptides”, “long chain peptides” having difficult or un-natural amino acid moieties.
- I have operated and have expertise in various instrumental techniques like HPLC, MALDI-TOF, CD, FT-IR, Optical Microscopy, Fluorescence, UV-Vis, *etc.*
- In parallel, I have worked on mechanistic insight of amyloid inhibition by our designed peptidomimetics using various analytical techniques and also developed scale-up synthesis of a novel and recyclable coupling reagent, invented in our lab, Ethyl 2-cyano-2-(2-nitrobenzenesulfonyloxyimino) acetate (*o*-NosylOXY) and its utilization in peptide synthesis.

Academic and Professional Skills

- **Laboratory and Instrumentation:** Familiar with Synthetic Organic Chemistry, peptide synthesis (proficiently solid phase and solution phase) and purification, Mass spectrometry (ESI), MALDI-TOF, HPLC, Fluorescence spectroscopy, UV-Visible spectroscopy, Circular Dichroism, Infrared spectroscopy, NMR spectroscopy, Optical Polarisable Microscopy, TGA-DSC, DLS, FETEM, and FESEM.
- **Software:** Familiar with Origin, Adobe Illustrator, MS-office, ChemDraw, MassHunter, and Mestrenova software.
- **Instrumental Experience:** Selected as an authorized operator for MALDI-TOF instrument at CIF, IIT Guwahati, April 2021-June 2025.
- **Teaching Experience:** Worked as a Teaching Assistant (TA) in B.Tech class and at IIT Guwahati, India.
- **Work Experience:** Worked as a member on an industry-level project "*Prototype Development for Scale-Up and Commercialization of o-NosylOXY: The Recyclable Coupling Reagent for Reducing Cost and Waste Generation in the Pharmaceutical Industry*" during 2020-2021 in the Department of Chemistry, funded by NewGen IEDC, IIT Guwahati
- **Language:** Assamese, Bengali, Hindi, and English.

Research Interests

- Protein and Peptide chemistry
- Peptide self-assembly and supramolecular chemistry
- Self-replication and origin of life studies
- Alzheimer's and other protein aggregating diseases